MODELLING SATURATED TEARING MODES IN TOKAMAKS

by

Willem Stephanus Mc Loud

This thesis is submitted in partial fulfilment of the requirements for the degree of Doctor of Philosophy at the University of Natal.

Fusion Studies Group
PELINDABA
December 1992

I dedicate this thesis to

my wife Marthé

and my daughter Lindi.

ACKNOWLEDGEMENTS

First and foremost I would like to thank my supervisors Dr Dave Sherwell and Prof Manfred Hellberg, who have been a constant source of help and encouragement, and with whom I have had innumerable discussions on many topics.

I also would like to thank Dr Ted Roberts for many helpful discussions on the experimental program and results. Also the advice of Dr Johan Neethling on the numerical iteration schemes, is gratefully acknowledged.

Then I would like to thank all my colleagues for their support. This includes Mr D F B Louw, Mr G van Vuuren, Mr J Fletcher and Mr J Venter with the computer programs used, Dr G Nothnagel for discussions, Dr J A M de Villiers for various forms of support for the theoretical programme and Mrs Tillie Kloppers for the typing of the thesis.

The AEC's consent to do this study and for the use of all the facilities needed, is thankfully acknowledged.

Finally, I would like to thank my God for assisting me through all these years of study. Time and again He made the impossible possible.

ABSTRACT

In this thesis a model for saturated tearing mode islands is developed. The equations for the mode amplitudes are essentially those of R B White et al., after a pertubation expansion has been made. It is well known that these equations are not then analytic at the mode rational surface. In our model this problem is overcome when a suitable choice of the **axisymmetric** current density perturbation is added to the unperturbed equilibrium current density profile. The modelled axisymmetric current density perturbation flattens the unperturbed profile locally at the rational surface and is sufficient to induce an island. No modelling in the interior of the island is necessary.

The axisymmetric perturbation has a free variable which adjusts the amount of local flattening. However, when the boundary conditions are taken into account, this free parameter is determined, and the problem becomes an eigenvalue problem. The boundary condition thus determines the amount of local flattening at the rational surface.

The **saturated** island widths are determined using a $\Delta'(W)$ criterion. The model allows for non–axisymmetric plasma surface in a simple way, requiring careful choice of $\Delta'(W)$. The different criteria are compared to establish the validity of the use of such criteria for perturbed boundaries.

In the cylindrical approximation, one or two modes may be included in the model. In the case of two modes, non–linear coupling via the current density profile is introduced. Toroidal coupling between modes can also be simply introduced. Two modes that are toroidally coupled are considered, but mode–mode coupling is ignored.

The emphasis falls in large part on the boundary conditions. Various boundary conditions can be considered because distortion of the plasma surface can be fixed by wall effects, plasma rotation, external DC coil currents, plasma rotation with external coil currents, etc. Of particular interest is the case of toroidally coupled modes, coupled in turn to these external conditions as this is the first study of such a nature.

Results flowing from the study include among others that:

- for the special case of circular boundaries the model agrees reasonably with the results of R B White et al.

- No significant difference was found between the $\Delta'(W)$ criterion of P H Rutherford, which is valid for circular boundaries, and that of A H Reiman, which is also valid for perturbed boundaries, when the boundary is perturbed significantly.

- Toroidally coupled islands do not increase in size if the boundary condition of that particular mode is not changed. If a coil current of particular helicity is switched on, it will only affect the mode of that particular helicity.

- Toroidally induced sideband islands have approximately the same width as natural tearing islands when the size of the natural island is large.

CONTENTS

CONTENTS

CONTENTS

CONTENTS

CONTENTS

CHAPTER 1

INTRODUCTION

1.1 General Introduction

The study of tearing modes has been going on for many years. It originated when instabilities other than ideal MHD instabilities were observed in magnetic confinement devices. The theoretical ground work for the study of these modes was laid in 1963 by Furth, Killeen and Rosenbluth [1]. They also developed a stability criterion. Only the first phase in the development of tearing modes was studied at this stage within linear theory and lead to estimates of exponential growth rates.

In 1973 Rutherford [2] extended this work to include the next phase in the tearing mode development. In quasi–linear theory the exponential growth changes to algebraic growth when the tearing island reaches the size of the so–called resistive layer – a region defined in the linear theory in which resistivity is of importance. This work was then built upon by White et al. [3] in 1977 when they studied small saturated islands which exceed the size of the resistive layer. For the first time it was possible to model saturated tearing modes as observed on Tokamaks.

In parallel with the analytic modelling of tearing modes, time dependant numerical codes were developed. They were used to study coupling between modes and mode overlapping and proved the validity of the theory. Important Tokamak phenomena were also investigated like the major and minor disruptions.

Another field of interest that was studied over the last few years, is the effect of boundary conditions on the tearing modes. External coils (both AC and DC) were installed on many Tokamaks to do experiments in this regard. This thesis will, among other things, concentrate on the effect of boundary conditions as this is relevant to the Tokoloshe experiment on which low m–number DC coils have been installed. This experiment will be much used in this thesis.

1.2 The Tokoloshe experiment

Tokoloshe is a medium sized Tokamak with major radius of 48 cm and a minor radius of 24 cm. Although fusion–like parameters cannot be obtained on such a small machine, relevant experiments can be done to investigate phenomena that are observed on all machines. In particular the physics of the tearing mode, the minor and major disruptions, the internal kink mode and edge phenomena were studied in the last few years.

In an attempt to influence the behaviour of the tearing modes, coils of similar helicity were installed on the outside of the vacuum chamber. Experiments with DC coil currents were performed with m=3,2 and 1 helicity coils.

An interesting feature of Tokoloshe is that it has a very large inverse aspect ratio (minor over major radius) of about 0.5. This however, makes it very difficult to use perturbation theory to study the physics on Tokoloshe. In this study we will assume a larger aspect ratio than that of Tokoloshe which will thus only enable us to do a qualitative study of Tokoloshe phenomena.

1.3 An Overview of this Thesis

We will now present a summary of the chapters. In chapter 2 the relevant literature on tearing modes is reviewed. This includes linear and non–linear tearing mode theory, equilibrium studies, numerical analysis and the studies on the effects of external conditions. Of particular interest to our studies are the time–independent reduced MHD equations which are used to do non–linear equilibrium studies with saturated tearing modes embedded in the plasma in the presence of a variety of different boundary conditions.

In chapter 3 the toroidal reduced MHD equations are derived following Izzo [4]. From these the cylindrical equations are deduced for Cartesian, cylindrical and helical coordinates. Finally the time independent equations are presented. In the case of one mode in the cylindrical approximation the flow automatically disappears from the magnetic flux equation. This simplifies the modelling of one tearing mode significantly. For two modes the parameter $S = \tau_R/\tau_A$ (τ_R is the resistive time scale and τ_A the Alfen time scale) has to be set to ∞ to exclude flows from the magnetic flux equation.

The case of one mode in cylindrical coordinates is discussed in chapter 4. A new model is developed in which the **axi–symmetric perturbed** current is modelled. The model is based on the work of White et al. [3] and that of Sykes and Wesson [5]. Our approach resembles that of Sykes and Wesson in the modelling of a flat region at the position of the saturated island, and also resembles White et al. [3] who expressed the perturbed current density inside the island as a function of the helical magnetic flux. Advantages of our model include the fact that no assumptions are made about the final current density profile in the island which can in principle be found accurately depending on the number of terms in the perturbation expansion

that is included. Another advantage is that no complicated inner or outer island regions are specified – the island in the plasma automatically arises by allowing for non–axisymmetric boundary perturbations.

Chapter 5 deals with the boundary conditions for cylindrical tokamaks. Boundary conditions are derived for the case of

- A non–conducting wall at the plasma edge surrounded by vacuum or a coil in the vacuum.

- An infinitely fast rotating plasma with a resistive wall, or superconducting wall. A vacuum region can be included between the plasma and the wall.

- A rotating plasma with a vacuum region outside the resistive wall.

- A rotating plasma with an external coil in the vacuum region outside the resistive wall.

(A constant frequency is assumed for a particular situation to allow for our time–independent treatment). Only the last case appears to be new.

When the model of chapter 4, for one saturated tearing mode in a plasma, is coupled to the various external situations described in chapter 5, it is possible to generate results. These are presented in chapter 6.

An eigenvalue problem for the free parameters of the model arises. The external situation thus self–consistently determines the degree of local flattening of the unperturbed axisymmetric current profile at the rational surface. When the $\Delta'(W)$ criteria are included in the problem it is possible to fix the saturated island width as well as the perturbation of the boundary.

In chapter 7 we expand the cylindrical model of chapter 4 to include two toroidally coupled modes. The boundary conditions developed in chapter 5 were found to be valid in this case too.

The model of chapter 7 enables us to study a situation similar to that on Tokoloshe where both a (2,1) and (3,1) mode are present. With the correct boundary conditions the interaction of these modes with external coils can now be studied. It is the first time that toroidally coupled modes have been studied in conjunction with such a variety of boundary conditions.

Finally in chapter 8 we present the results of the toroidal model. The effects of toroidal coupling, plasma rotation and external coils are studied for a Tokoloshe relevant profile. The relation of a natural (3,1) tearing island to a toroidally induced one is also studied as a case of particular interest on Tokoloshe.

In summary, we have developed both a cylindrical and toroidal model of saturated tearing modes, coupled to a variety of external situations. The model enabled us to do a qualitative study of Tokoloshe phenomena which could not be studied with the normal linear theory. It is thus of particular relevance to the Tokoloshe experiment.

CHAPTER 2

2. AN OVERVIEW OF TEARING MODES IN PLASMAS

2.1 Introduction

The purpose of this chapter is to give a *broad* overview of the work that has been done in the field of tearing modes. Linear and non–linear tearing mode theory, equilibrium studies, numerical analysis and studies on the effect of external conditions are reviewed.

2.2 Ideal MHD–theory

The phenomena taking place in a plasma can be divided into those taking place on a small scale (e.g. microscopic collisions described by kinetic theory) and those taking place over larger scales (e.g. macroscopic fluid type behaviour described by hydromagnetic (MHD) theory). Macroscopic phenomena are of great importance in plasma confinement because they can cause a dramatic loss of the plasma out of the confinement device.

The first and most obvious approach in understanding the macroscopic behaviour of plasmas, is to consider the high electrical conductivity limit (resistivity $\rightarrow 0$). This is called the ideal MHD approach.

If a plasma in equilibrium is displaced with a small perturbation, it will either return to the original or some other equilibrium (be stable), or keep growing (become unstable). In 1958 Bernstein et. al. [6] derived an energy principle which can distinguish between stable and unstable plasma equilibria. According to this

principle, a system is stable if a certain energy integral $W(\xi)$ is positive for every displacement ξ satisfying the boundary conditions, and unstable (ideal instabilities will grow) if there exists a ξ for which $W(\xi)$ is negative.

The energy integral is given by

$$W(\xi) = \tfrac{1}{2}\int d^3x \{Q^2 + \underline{J}.\xi \wedge Q + (\nabla.\xi)\xi.\nabla P + \gamma P(\nabla.\xi)^2\} \qquad (2.1)$$

where $Q = \nabla\wedge(\xi\wedge\underline{B})$, γ the specific heat, $\underline{J}$ the plasma current density, $\underline{B}$ the magnetic field strength and P a scalar plasma pressure. The most straightforward way of applying the energy principle is to impose a conveniently chosen normalization condition on ξ and then to minimize $W(\xi)$ with respect to ξ; the system is then stable if the minimum value is positive and unstable if it is negative.

If the energy integral $W(\xi)$ can be minimized with respect to ξ_θ and ξ_z, where (r,θ,z) are cylindrical coordinates, W can be reduced to a one–dimensional form

$$W(\xi) = \pi/2 \int_a^b r\, dr\ \wedge(\xi, \frac{d\xi}{dr}), \qquad (2.2)$$

where ξ is an abbreviation for the radial component ξ_r and $\wedge$ is a certain quadratic form in ξ and $d\xi/dr$ with m and k as parameters. It is assumed that ξ_r, $i\xi_\theta$ and $i\xi_z$ are real functions of r in cylindrical geometry multiplied by $\exp i(m\theta + kz)$, k the wavenumber of the mode in the z–direction. This important work was done by Newcomb [7].

Equation (2.2) can be integrated by parts to give

$$W(\xi) \quad = \quad \pi/2 \int_a^b dr\, [f(\frac{d\xi}{dr})^2 + g\xi^2], \tag{2.3}$$

where f and g are functions with m and k as parameters. The function that minimizes this integral, is given by the Euler–Lagrange equation

$$\frac{d}{dr}(f\frac{d\xi}{dr}) - g\xi = 0. \tag{2.4}$$

This equation has a singular point wherever f vanishes, which happens when

$$kr\, B_z + mB_\theta \quad = 0. \tag{2.5}$$

This will be important below.

From equation (2.4) it is possible to derive Suydam's stability condition [7,8]:

$$-\frac{dP}{dr} < \frac{r}{8}\frac{B_z^2}{\mu_0}(\frac{1}{q}\frac{dq}{dr})^2 \tag{2.6}$$

where q is called the safety–factor and is just $\frac{2\pi}{\iota}$ where ι is the rotational transform, i.e. the angle moved through in one toroidal circuit of the magnetic field as it encircles the cylinder. In the cylinder it can be written as

$$q \quad = \quad \frac{r}{R}\frac{B_z}{B_\theta} \tag{2.7}$$

which reduces to q=m/n at the rational surface, i.e. where equation (2.5) is valid. We now assume a large aspect ratio "tokamak" where $kz = n\varphi$, i.e. φ periodic and the ends of the cylinder are identified.

According to equation (2.6) the configuration is stable with respect to high–m interchange instabilities if $\frac{dq}{dr}$ is big enough. This change in the helicity of the magnetic field with radius is called shear.

2.3 Tearing Modes

An important result of early fusion research was that instabilities were observed in configurations where the ideal hydromagnetic theory predicted stability. To gain insight into this problem we follow Bateman [9]: Define $B_*(x) = B(x) - B_{q=m/n}(x)$ where for simplicity we work in a cartesian coordinate system. Assume the mode rational surface (i.e. where equation (2.5) is valid) to be at $x=0$ and use a series expansion of B_{*y} in the neighbourhood of this surface

$$B_{*y}(x) = B'_{*y}x \ldots . \tag{2.8}$$

Now include only one harmonic of the magnetic field perturbation in the x–direction

$$B_x^1(x,y) = B_x^1 \sin k_y y . \tag{2.9}$$

It is now possible to describe the total magnetic field by a flux function $\psi(x,y)$ which ensures $\nabla.B = 0$

$$B_x = -\frac{\partial \psi}{\partial y}, \qquad B_y = \frac{\partial \psi}{\partial x}, \tag{2.10}$$

$$\psi = \psi_0 + \tfrac{1}{2} B'_{*y}\, x^2 + (B_x^1/k_y) \cos k_y y . \tag{2.11}$$

This can be illustrated as follows:

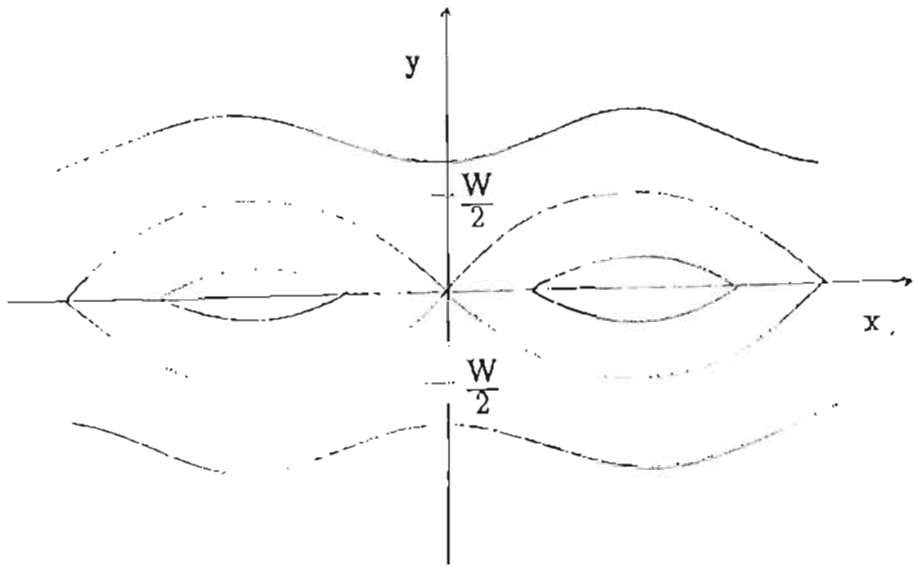

FIGURE 2.1 The combination of B_* and B_x leads to the formation of an island structure. Contours of constant magnetic field are shown. W denotes the island width.

Taking this approach of Bateman a little further, the following formulae for the island width can be derived:

$$W = 4r_s \left| \frac{B_{1r}}{m B_{\theta_0}} \frac{q}{r_s q'} \right|^{\frac{1}{2}}, \qquad (2.12)$$

with B_{1r} the perturbed radial magnetic field.

Bateman and Morris [10] showed that this expression is valid for large island widths in Tokamaks. They found a 2 % deviation for $W/a = 0.2$ and 4 % for $W/a = 0.3$, with a the minor radius of the Tokamak.

The flux function defined in equation (2.10) is proportional to the poloidal magnetic flux. The poloidal and toroidal flux can be written as follows in toroidal geometry:

$$\psi_{tor} = \int_{S_{tor}} d\underline{S}.\underline{B} = \text{flux the long way round} \qquad (2.13)$$

$$\psi_{pol} = \int_{S_{pol}} d\underline{S}.\underline{B} = \text{flux the short way round .} \qquad (2.14)$$

The subscripts denote the toroidal and poloidal directions.

With this in mind we can see that Figure 2.1 implies that the flux–surfaces (and thus also the magnetic field lines) on tokamaks are designed to have the same topology which are *broken* in the sense that their topology has changed because of disconnection and reconnection [11]. The perturbation (2.9) thus predicts a magnetic structure in which the magnetic field lines tear. In the ideal MHD case the field and fluid are coupled, and it is impossible to disconnect it. Finite conductivity (resistivity) can be included in the MHD theory to allow for this disconnection, and the formation of a tearing mode.

The above discussion suggests the possible occurrence of other instabilities (called resistive instabilities) not found in the ideal fluid description of a plasma. Apart from the tearing mode (from the tearing of the magnetic field lines into islands) which was discussed above, there are also the rippling and gravitational (interchange) modes [1] which will not be discussed further in this study. Prior to this study of reconnection in magnetic confinement devices, resistive studies had been made in relation to the earth's magnetosphere, most significantly by Sweet [12], Parker [13] and Petschek [14].

The reconnection rate is defined as the time rate of change of the magnetic flux, $\dot{\psi}$, at the X–point (the point where the magnetic islands are the narrowest) and is given by (see e.g. [15])

$$\dot{\psi}_s \sim \eta^{(1-t)/(2-t)} . \tag{2.15}$$

The Sweet–Parker model assumes t=0 ($\dot{\psi}_s \sim \eta^{\frac{1}{2}}$) and the Petschek model t=1 ($\dot{\psi}_s \sim \eta^0$) [15]. In the case of the tearing mode, reconnection initially occurs at the rate $\eta^{-3/5}$ when the island is small, but then slows down to [16]

$$\dot{\psi}_s \sim \eta , \tag{2.16}$$

when the island size gets large.

During the linear phase, the growth rate of the tearing instability increases with magnetic shear, i.e.

$$\gamma \sim (q'/q)^{2/5} , \tag{2.17}$$

with γ the growth rate. The magnetic shear that stabilizes the ideal MHD instabilities (equation (2.6)), destabilizes the tearing mode!

2.4 Linear Tearing Mode Theory

Although resistive modes had been investigated by Dungey [17], Murty [18], Aithen et al. [19] and Kadomtsev et al. [20] prior to 1963, the first complete discussion of the linear theory of resistive modes was published in that year by Furth, Killeen and Rosenbluth [1]. They separated the plasma into two regions:

(1) a narrow central region around the rational surface where finite conductivity permits relative motions of field and fluid; and where geometric curvature may be neglected;

(2) an outer region, where field and fluid are coupled as in the infinite conductivity case, and where generalizations to non–planar geometry can be introduced as desired.

In this approach it is assumed that resistivity is only important in the vicinity of the rational surface where the resistive mode can grow and therefore where the field lines must be allowed to reconnect. Only in this small region around the rational surface is resistivity included in the MHD equations. Manheimer et al. [21] derived this set of two second order differential equations in a very elegant way, following the approach of Coppi et al. [22]. Across the boundaries these equations are then matched with the ideal MHD equations which are valid in the outer region further away from the rational surface.

An important result obtained by Furth et al. [1] was a stability criterion for tearing modes. This is defined as

$$\Delta' = \frac{1}{\psi_p(r_s)} \left[\frac{d\psi_p}{dr} \Big/_{r_s+\epsilon} - \frac{d\psi_p}{dr} \Big/_{r_s-\epsilon} \right] < 0 \qquad (2.18)$$

where ψ_p is a perturbed magnetic flux function, r_s the radius of the rational surface and 2ϵ the width of the resistive layer. If Δ' is greater than zero, the perturbation will grow and form a tearing mode. The marginally stable tearing mode is defined by $\Delta' = 0$.

Manheimer et al. [21] have given a physical interpretation of Δ' as follows. The power per unit area released in the outer region is given by

$$P = \frac{\gamma}{4\pi k^2} | B_x (x=0) |^2 \Delta' + \text{constant}, \qquad (2.19)$$

from which it can be seen quite easily that there will only be energy available to be released if $\Delta' > 0$. In the formation of the tearing mode, this energy released in the outer region is dissipated by Ohmic heating in the inner region. Alternatively the energy released can also result in the acceleration of electrons [23,24,25] (an electron inertia–driven tearing mode) or be dissipated by viscous dissipation, i.e. without resistivity. It is thus possible to get reconnection without resistivity also.

When the calculation of tearing modes is extended to the collisionless regime (recognizing that fusion and magnetospheric plasmas were likely to be virtually collision–free) and electron and ion gradient drifts are included, the theory leads to the drift–tearing mode [26]. When Hazeltine et al. [27] unified all the previous calculations (electron inertia, gradient drifts) by carrying out a kinetic theory approach including the full electron–electron and electron–ion collision operators, they found that the tearing mode could also be driven unstable by temperature gradients [28].

From the *infinite–conductivity equation* [1]

$$\frac{d}{dr}\left(H \frac{d\psi_p}{dr}\right) - \psi_p \left[\frac{g}{F^2} + F^{-1} \frac{d}{dr}\left(H \frac{dF}{dr}\right)\right] = 0 , \qquad (2.20)$$

$$F = \underline{k}.\underline{B} = kB_z + \frac{m}{r} B_\theta ,$$

$$H = r^3/(k^2r^2 + m^2) ,$$

$$g = \frac{(m^2-1)rF^2}{k^2r^2 + m^2} + \frac{k^2r^2}{k^2r^2 + m^2}\left[2\frac{dP}{dr} + rF^2 + F\frac{2(krB_z - mB_\theta)}{k^2r^2 + m^2}\right] ,$$

valid in the outer region, an energy integral can be formulated [29]:

$$W_T = \int_a^b dr[H(\frac{d\psi_p^2}{dr})^2 + \psi_p^2 (g/F + F' \frac{d}{dr} H \frac{dF}{dr})] \qquad (2.21)$$

$$= W_\infty - \lim_{\epsilon \to 0} \left[\frac{H}{F}\frac{dF}{dr} \Big|_{r_s-\epsilon}^{r_s+\epsilon} \right] \psi_p^2 (r_s) , \qquad (2.22)$$

where $F^2H = f$, $W_\infty = \frac{2}{\pi} W(\xi)$, $\xi = \psi_p/F$ and f, $W(\xi)$, ξ are defined in equation (2.3). Note that F^{-1} occurs in W_T. We have pointed out above that $F(r_s) = 0$, indicating a singularity in W_T.

The integrals are to be interpreted in the sense

$$\int_0^b = \lim_{\epsilon \to 0} \left[\int_0^{r_s-\epsilon} + \int_{r_s+\epsilon}^b \right] . \qquad (2.23)$$

The point b represents a perfectly conducting outer wall. The quantity $-W_T$, given by $-W_T = H(r_s)\psi_p^2 (r_s)\, \Delta'$, represents the magnetic driving energy of the tearing mode (it is similar to (2.19)). The *infinite conductivity equation* (hereafter called ICE) derived by Furth et al. [1] and the Euler equation (2.4) is the same except that the one derived by Furth et al. [1] is in terms of ψ_p rather than ξ.

To determine tearing–mode stability, the ICE can be solved for the functions $\psi_1(r)$ and $\psi_2(r)$ in the respective ranges $0 < r < r_s$ and $r_s < r < b$, and with the respective boundary conditions $\psi_1 \to r^{m-1}$ at $r = 0$, $\psi_1(r_s) = \psi_2(r_s)$, $\psi_2(b) = 0$. In general, the derivative ψ_p' will be discontinued at r_s, and by evaluating Δ' it will be clear whether a tearing mode will grow or not [29]. Robinson [30] rewrites the ICE as follows:

$$\frac{d\psi_p^2}{dr^2} + A\psi_p = 0 \qquad (2.24)$$

by defining $\psi_p = \frac{r^{\frac{3}{2}} b_r(r)}{(m^2+k^2r^2)^{\frac{1}{2}}}$ where b_r is the perturbed radial magnetic field and A is a function of r, m and k and is singular at $r=r_s$. Equation (2.24), also called the tearing mode equation, need not only be derived in the process of searching for the perturbation which minimizes the magnetic potential energy of the system; it can also be calculated from pressure balance considerations as Ellis did [31]. We will return to consider this equation below as it applies to the equilibrium of a perturbed system.

2.5 Non–linear Theory

In 1973 Rutherford [2] showed that, as the island edge approaches the boundary of the tearing layer in its linear growth phase, non–linear effects become important. Sizeable non–linear eddy currents arise, producing forces which oppose the growth of the mode and which quickly assume the role played in the linear theory by the inertia. At this point the exponential growth in time is replaced by algebraic growth on a much slower time scale.

In Figure 2.2 [9] the magnetic field, longitudinal current density, and flow pattern of a tearing mode are shown together with the separatrix of the induced magnetic island. It can be seen that the velocity field can drive a second order contribution $V_y^1 B_x^1$ to the electric field, which, in turn, can drive a second order current density along the magnetic islands. This current $(J_z^{(2)})$ produces a new $J_z^{(2)} B_x'$ force which opposes the V_y^1 flow everywhere [9].

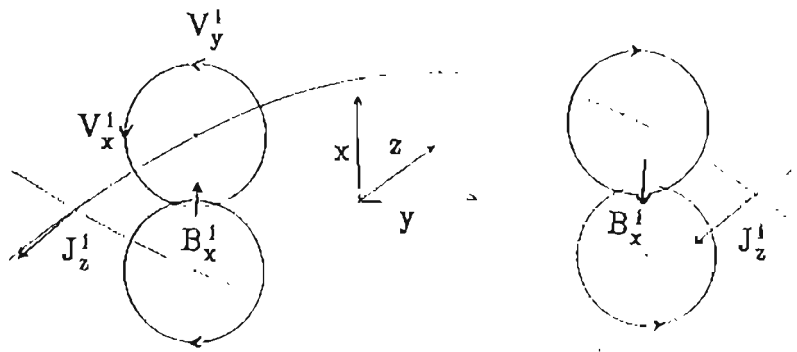

FIGURE 2.2 The magnetic field, current density and flow pattern of a tearing island are shown [9].

The growth of the tearing mode is now given by

$$\frac{dW}{dt} \simeq \eta \Delta' \qquad (2.25)$$

where W is the island width.

In 1977 White, Monticello, Rosenbluth and Waddell [3] made a quasi–linear extension of the work of Rutherford. They noted from numerical analysis that the current inside the island (J_b) can be modelled accurately by a linear function of ψ

(with $\underline{B}_\perp = \nabla\psi \wedge \hat{z} - kr/m\ \underline{B}\hat{\theta}$) within the island, written as

$$J_b(\psi) = a + b\ \psi(r,\theta) .$$

The work of White et al. [3] will be discussed in more detail in chapter 4, but we may note for future reference the use of a model for non–axisymmetric perturbed current in the island.

Together with a perturbation expansion of the current in terms of the fundamental harmonic on the *outside* of the island, they found

$$\frac{dW}{dt} = 1.66\ \eta(r_s)\ [\Delta'_1(W) - \alpha W] . \qquad (2.26)$$

In this equation they used

$$\Delta'_1(W) = (\psi'_{1+} - \psi'_{1-}) / \psi_1(r_s) , \qquad (2.27)$$

where ψ_1 is the first harmonic of the perturbed ψ and the $+,-$ refers to the island edges. The α–term in equation (2.26) is a numerical constant depending on the resistivity profile. It is practically negligible if the resistivity profile is increasing radially with a scale length given by the minor radius [32]. For typical resistivity profiles the mode saturates approximately when $\Delta'_1(W)$ vanishes, and the saturated island width can be determined by a numerical evolution of $\Delta'_1(W)$. Generally we can thus write

$$\frac{dW}{dt} \simeq 1.66\ \eta(r_s)\ \Delta'_1(W) . \qquad (2.28)$$

This is in agreement with the linear theory where the energy available in the outer region for island formation is given by equation (2.19). If all the available energy is dissipated P must vanish, and this implies that Δ'_1 must go to zero.

Numerical codes have confirmed this relation (2.26) for islands up to about $\frac{W}{a} = 0.2$ (a the minor radius) [3] and for experimentally relevant q profiles the results agree within 20 % [33].

Kutvitskii and Yurchenko [34] derived a result very similar to equation (2.26). They found

$$\frac{dW}{dt} = 1.24\,(\Delta' + 0.4\,u_0 u_j W\,\ell n\,(4/W))\,, \qquad (2.29)$$

where u_0 and u_j are the components of the velocity of the resonant magnetic surface which results from the gradients of the conductivity and of the current, respectively. Equation (2.29) is only valid for narrow islands. It is, according to the authors, an improvement on (2.26) since (2.26) cannot explain the effect of the conductivity profile on the island growth because it was derived assuming that the *equilibrium* current is steady and is thus applicable only in the case of an ohmic equilibrium, $J_0(r) \sim \frac{1}{\eta_0(r)}$.

The Δ' criterion is affected by pressure–gradient and toroidal–curvature effects [35,36], radial flow [37,38] and viscosity [39]. Equilibrium shear flow also has an effect on the Δ' criterion. When the flow shear is larger than the magnetic shear of the magnetic null plane, the flow freezes the magnetic field and stabilizes the tearing mode [40]. Inclusion of finite Larmor radius effects does not change the saturation width but causes a mode rotation at the diamagnetic frequency [41,42].

In their analytic modelling Hahm and Kulsrud [16] were able to follow the development of a tearing mode through its different phases providing a smooth transition from the linear to the non–linear theory for the case of a perturbed boundary.

These results were all remarkably successful [32,33]. Present work focuses on the boundary conditions and other effects like toroidicity.

2.6 Equilibrium Studies

In 1957–59 Grad [43], Shafranov [44] and Lüst and Schlüter [45] derived an equation describing the equilibrium for a axisymmetric toroid. This is called the Grad–Shafranov equation. By specifying the pressure ($P = P(\psi)$) and flux ($I = I(\psi)$) functions, together with boundary conditions or externally imposed constraints on ψ, the equilibrium flux function can be derived.

When a plasma possesses a nearby state of lower magnetic energy which is inaccessible without magnetic reconnection, the asymmetric ideal magneto–hydrodynamic equilibrium with magnetic surfaces consisting topologically of nested tori, will go to that lower–energy state which possesses one or more magnetic islands [11]. Kotschensreuther et al. [36] were able to modify the Grad–Shafranov equation to describe the MHD equilibrium with small magnetic islands present.

On tokamaks it was found that the characteristic linear and non–linear growth times are often much smaller than the time scale for changes in the general equilibrium. The tearing instabilities will thus be saturated and their time development will be determined by changes in the general equilibrium. Such an approach was taken by Sykes and Wesson [5]. They included a flat in the equilibrium conductivity profile, simulating a saturated tearing island. This has the effect of removing the singularity in the equations. A relaxation procedure was then used to find the final island width.

In section 2.5 on the non–linear work, we referred to the work of White et al. [3]. When $\frac{dW}{dt}$ is put to zero, the equation they derived (equation (2.26)) describes the time–independent situation of a saturated island. They studied the island size as a function of various current density profile types. In Figure 2.3 we present one of their graphs in which a peaked profile ($q(r) = C(1 + r^2/r_s^2)$ was used. We will use a profile very similar to this in our study.

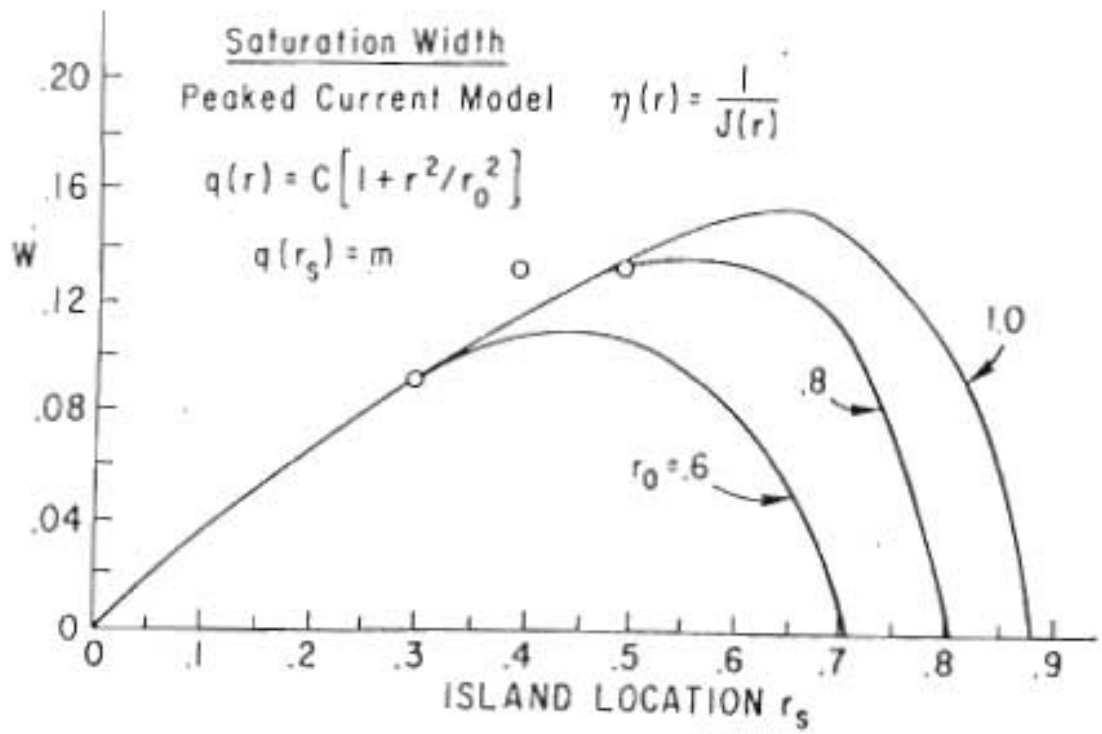

FIGURE 2.3 Saturation width predicted using the quasilinear model for m=2. The points are results of time stepping the full non–linear code [3].

Carreras et al. [46] later showed that their results do not differ very much from the simple time independent Rutherford equation (equation (2.25) with $\frac{dW}{dt} = 0$).

2.7 Numerical Analysis

Although the full three–dimensional set of resistive MHD equations had been solved numerically [47,48,49], a more common approach to the problem was, and is, to solve a reduced set of equations. In 1974 White et al., proposed a set of numerical techniques for investigating the full non–linear unstable behaviour of low–m kink modes of given helical symmetry in tokamaks [50]. When the equations are expanded in the inverse aspect ratio ($\epsilon = {}^{a}/R_0$ – the minor over the major radius), the terms can be ordered to exclude higher order terms. The equations were reduced to helical coordinates by Rosenbluth et al. [51] and cartesian coordinates by Strauss [52] (which made it applicable to non–circular cross–sections). In 1983 Holmes et al. [53] compared the full and reduced sets of magnetohydrodynamic equations for resistive tearing modes in cylindrical geometry and found good agreement. A comparison for the m=2 magnetic island width, using these different equations, is shown in Figures 2.4 and 2.5. A profile of the form $q = q_0[1 + (r/r_0)^{2\lambda}]^{\frac{1}{\lambda}}$ was used. We note the good agreement for **saturated** island sizes with small $\epsilon \lesssim 0.5$ and peaked profiles ($\lambda = 3.5$).

Since 1975 the reduced set of equations has been used extensively to study plasma phenomena. When Kadomtsev and Pogutse [54] proposed that major disruptions (an experimentally observed phenomenon in which plasma can be lost from the confinement device) were a consequence of the non–linear development of ideal kink modes, these *vacuum bubbles* were indeed found, but it was shown that when magnetic shear is included, the modes were stabilized [51,55]. The interaction of modes of different helicity has been studied by many people [56,33]. When modes overlap a stochastic region is formed resulting in fast plasma transport to the outer region. The possibility of this being the reason for the major disruption has been studied extensively [33,57,58,59]. When Goeler [60] and Kadomtsev [61] suggested

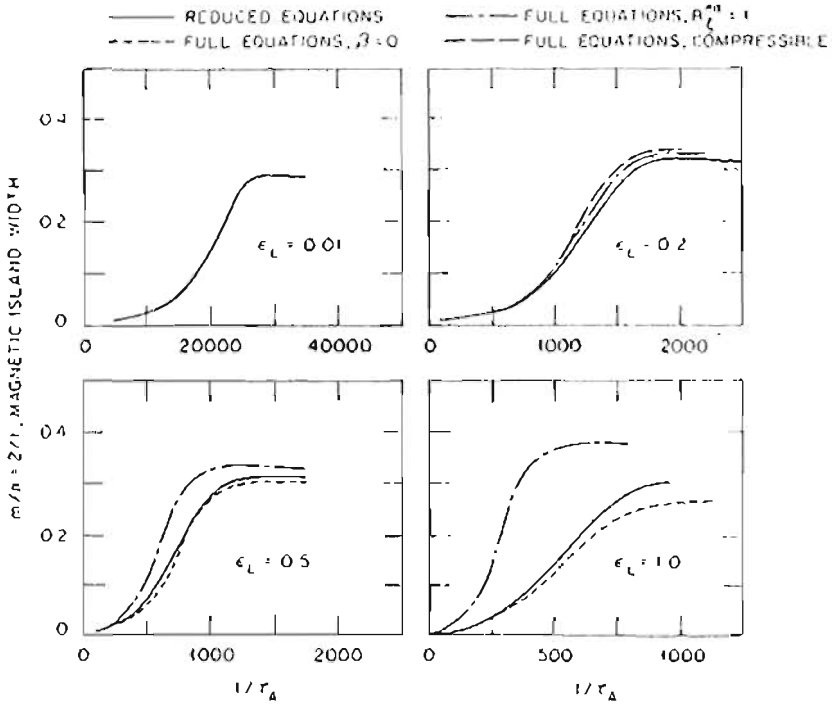

FIGURE 2.4 The (2,1) island width versus time for single–helicity non–linear calculations with $S = 10^5$, $\lambda = 3.5$, $q_0 = 1.08$ [53].

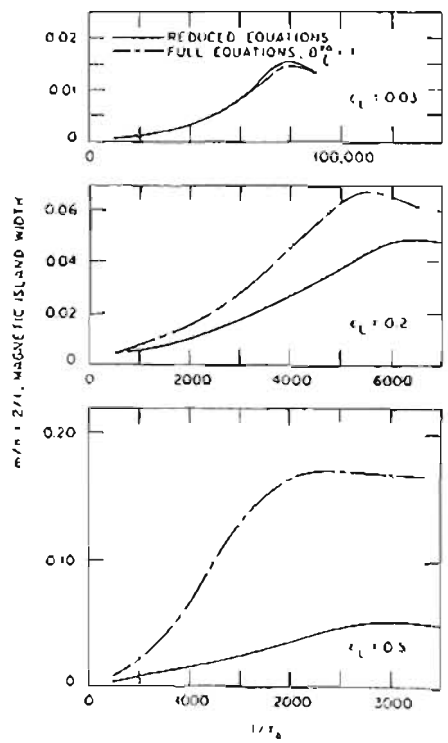

FIGURE 2.5 The (2,1) island width versus time for single–helicity non–linear calculations with $S = 10^5$, $\lambda = 1$, $q_0 = 1.08$ [53].

that the disruption is caused by the m=1 instability, it was investigated using the reduced MHD equations [62]. The effects of toroidicity and finite pressure have also been looked into [63].

Although plasma pressure has been found to have little effect on the linear growth rates of tearing modes, the non–linear aspects are affected severely. The pressure has an effect on the current–driven tearing modes as well as on the pressure–driven ballooning mode. Because of the lack of appropriate physical damping mechanisms in the reduced tokamak equations, the saturation of the pressure–driven modes was found to be very difficult [64]. These modes can be eliminated by excluding pressure perturbations for all harmonics. If equilibrium pressure is included [65] it is found that the saturation level of the non–linear harmonics increases monotonically with the pressure for the otherwise equal equilibria. The stochastic magnetic field region at the saturation time increases with pressure. The entire plasma region can be stochastic if the pressure is large enough. When the plasma resistivity is small, the stochastic field region is not large and the m=2 tearing island increases monotonically with the plasma pressure.

The drawback of the non–linear tearing mode theory is that it is derived for small islands. In solving the reduced MHD equations it is possible to look into the behaviour of large islands. Carreras et al. [66] have confirmed that the m=2 island width grows slowly (algebraically) from the time it exceeds the tearing layer width until it saturates, irrespective of the value of $S = \tau_R/\tau_A$ – as the non–linear theory predicts. (τ_R is the resistive time–scale and τ_A the Alvén time–scale). The island they looked at obtains a maximum width of 0.48a, relaxes, and eventually saturates at 0.37a (a = minor radius).

In chapter 3 we discuss the reduced MHD equations in more detail.

2.8 Toroidicity

Toroidicity has been included in the reduced MHD equations by various authors [4,67]. They found that the m=1, n=1 mode can strongly destabilize the m=2, n=1 and m=3, n=1 modes [63], that the size of the m=2, n=1 saturated island is reduced (by approximately 12 %) [4], that an m=2, n=1 mode can drive an m=3, n=1 mode in equilibria that could not otherwise support an m=3, n=1 island [10] among other results. Bateman and Morris [10] studied the following: (1) the breadth of the global current profile, (2) local peaking or suppression of current within the magnetic island being considered, (3) toroidal aspect ratio, (4) elongation of the plasma cross–section, (5) harmonic coupling caused by toroidicity and elongation, and (6) the influence of multiple magnetic islands on each other through the background current profile [10].

A toroidal Δ'–criterion was proposed by Connor et al. [68] and Zakharov et al. [69], given by

$$\Delta'_{mn} = \lim_{\epsilon \to 0} \left[(\psi'_1/\psi_1)\Big|_{r=r_m+\epsilon} - (\psi'_1/\psi_1)\Big|_{r=r_m-\epsilon} \right] ,$$

with ψ_1 the perturbed flux function. Conner et al. [70] showed that the MHD equations do not specify any particular set of Δ_{mn}, only a relation between them given as

$$|E - \Delta| = 0 ,$$

with E a matrix. Just as the single quantity Δ' contains all the information needed from the ideal MHD solution in order to determine the eigenvalue of the full problem in the cylinder, so the E matrix contains all the information needed in a torus [70].

2.9 Boundary Conditions

The external conditions can vary from a superconducting wall or a resistive wall with some form of plasma rotation, to the inclusion of external coils. The effects of plasma rotation on island stabilization have been studied by Gimblett [71] and others. Persson and Bondeson [72,73,74] were especially interested in the effect of wall stabilization on the major disruption.

Any perturbed magnetic field at the boundary can have an effect on the plasma, being able to force reconnection from outside. This phenomenon, where tearing mode stable equilibria $(\Delta' < 0)$ can be driven unstable from outside (using external coils) was studied by Reiman [75], Ellis [31], Lee et al. [76] and others. In such a case the energy needed for island formation is not released in the outer region as is the case with a natural island, but is made available from outside the plasma. This can be expressed as [75]

$$\Delta'_{\epsilon_1}(W) = \Delta'(W) - \frac{\epsilon_1}{\psi_1(r_s)}\,\delta'(W) \qquad (2.30)$$

where $\Delta'_{\epsilon_1}(W)$ is the Δ'-criterion with an external perturbation ϵ_1, $\Delta'(W)$ is the same criterion when $\epsilon_1 = 0$ and $\delta'(W)$ is a function of solutions of the tearing mode equation. The term $\frac{\epsilon_1}{\psi_1(r_s)}\,\delta'(W)$ now expresses the extra energy made available from outside.

Such a perturbed magnetic field can be caused by gaps in the conducting shell, coils, errors in the installation of coils or by external helical coils installed for this purpose. To illustrate island formation using external coils we follow an explanation of Karger [77]. On the rational surface field lines close on each other after rotating

around the torus a number of times. The field lines just outside a rational surface have a rotational transform ι which is just bigger than that of a field line on the rational surface because it encircles the torus a little slower. The line would thus tend to move downward on a surface which is just outside the previous rational surface. This is illustrated in Figure 2.6. The opposite would be true on the inside of the rational surface.

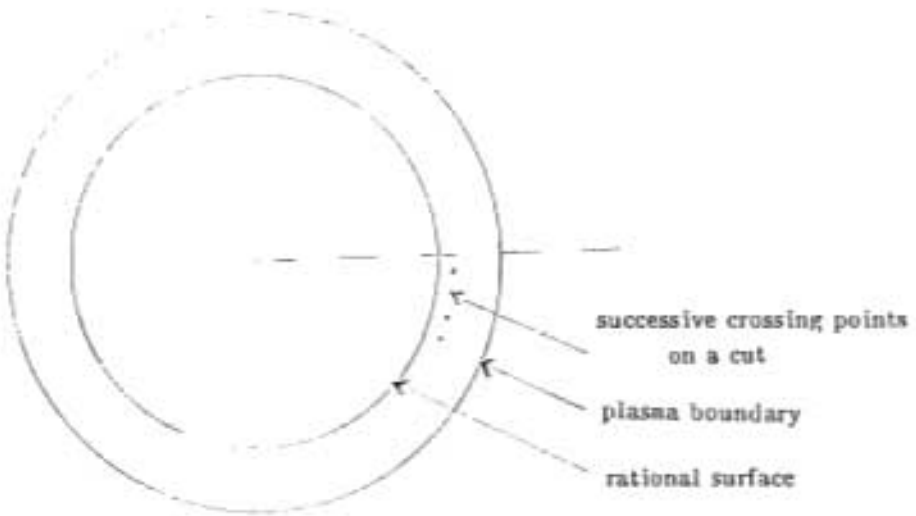

FIGURE 2.6 A graph showing the successive crossing points on a cut in the torus.

Now an external winding can be added and the field lines followed. Start on the inside of the rational surface. The next time the field line crosses the cut in the torus, it would not only be above the previous crossing but also a little to the right because of the field component of the external coil on the right side of the torus as shown in Figure 2.7. If this procedure is continued, the field line will eventually cross the rational surface. This time the next crossing would be below the previous one, but still shifted to the right. The end result is an island formed around the rational surface.

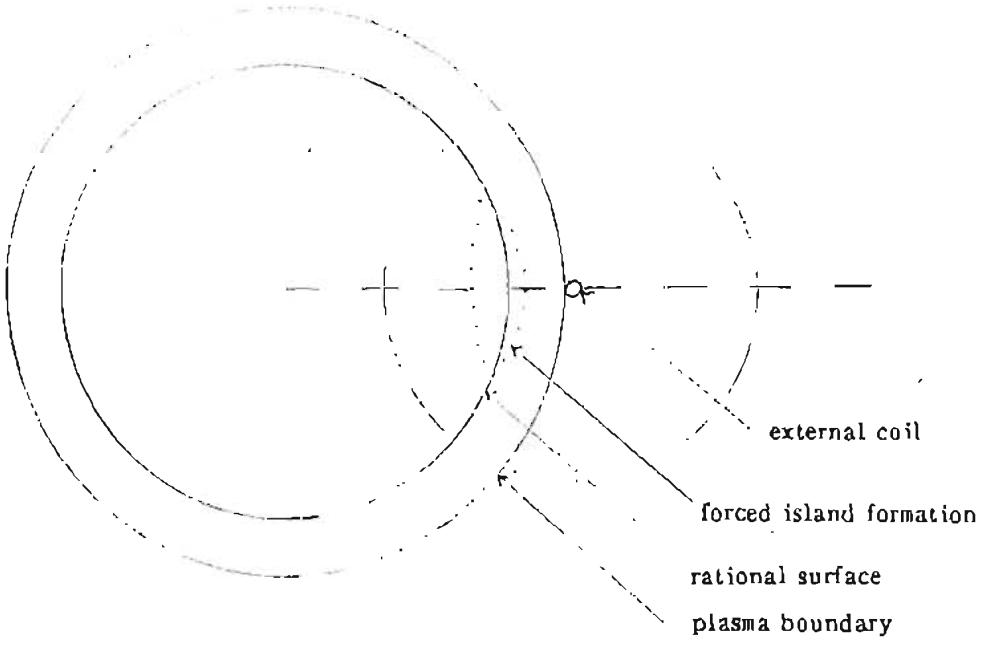

FIGURE 2.7 An external coil causes the formation of a magnetic island.

When Park et al. [15] modelled external coil driven reconnection, they found a finite jump in B_φ at the rational surface accompanied by a sharp current spike. The reconnection rate was found to satisfy the modified Sweet–Parker scaling:

$$\dot{\psi}_s \simeq K \eta^{\frac{1}{2}} (1 + \mu/\eta)^{-\frac{1}{4}},$$

with μ the viscosity and K a constant. No quasi–steady state was found for $\eta \gg \mu$, but for $\eta \ll \mu$ it was found that

$$\dot{\psi}_s \simeq \eta^{\frac{1}{2}} (\eta/\mu)^{\frac{1}{4}}, \qquad (2.31)$$

which is slightly different from the natural tearing mode case, i.e. $\eta^{3/5}$ as was discussed before (before equation (2.16)).

The MHD–equations can be adapted to include external windings by merely changing the boundary conditions. In this case the internal perturbed magnetic field includes the external induced field as well as the plasma response.

In 1985 J J Ellis [31] used the pressure balance equation

$$j \wedge B - \nabla p = 0$$

to derive equation (2.24). He dealt with the steady state phenomena, looking at an equilibrium which is perturbated by the magnetic islands induced from outside. He also looked into the time dependent situation (following Dibiase [78,30]) and showed the equilibrium of the time independent steady case is the same as when the external field has fully penetrated the plasma.

Using equation (2.28) makes it possible to calculate the width of the tearing island if the perturbed equilibrium is tearing mode unstable ($\Delta' > 0$). In this case it is assumed that the island will grow until $\Delta' = 0$ and that the field line topology outside the island is not changed in the process. Figure 2.8 illustrates this method:

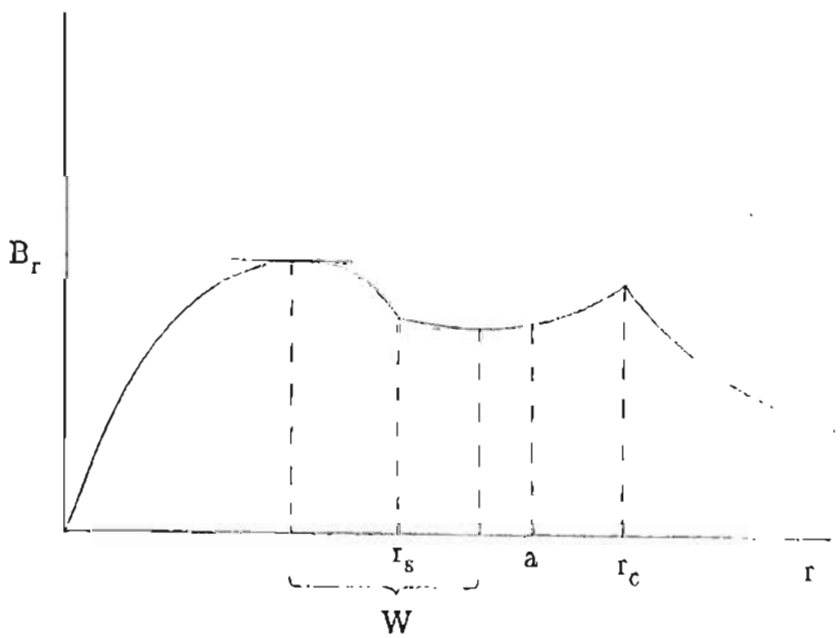

FIGURE 2.8 The plasma response when an external coil is included. Outward iteration (from $r = r_s$) is used to find the island edge where $B'_{1r}\Big|_{-} = B'_{1r}\Big|_{+}$.

In 1992 Hansen et al. [79] used the abovementioned method to study the effects of external coils on the Tokoloshe tokamak. Some of their findings were that the (2.1)–mode is not really affected by the external coils, whereas the locking of the (3,1)–mode (using a resonant external coil) does not lead to saturation of this mode. Both these results were observed on Tokoloshe – the last one in the form of minor disruptions. Similar work has been done elsewhere by Yamada et al. [80].

An important contribution of Hansen et al. is the derivation of a stability criterion for equilibria with external coils. The equilibria are stable to tearing modes when

$$\left[\frac{B_{1r}(r_s)}{B_{vac}(r_s)}\right]\left[\frac{B_{1r}(r_c)}{B_{vac}(r_c)}\right] > 0\,, \tag{2.32}$$

with r_c the coil radius, and subscript vac denoting vacuum magnetic fields.

Experimental studies on the effect of external DC coil currents were performed by several groups. The effect on plasma stability has been studied, among others, by Karger et al. [81], McCool et al. [82] and Roberts et al. [83,84].

The effect of external AC coils on the plasma was studied theoretically by various authors including Hender et al. [85] and Nave and Wesson [86]. Feedback loops had also been proposed by some authors [87,88] and can be used to reduce islands [89] in experiment.

2.9 Conclusions

We will build upon various aspects of tearing mode studies that have been reviewed in this chapter. The non–linear and equilibrium studies are of major importance and provide a theoretical framework for the study of saturated tearing modes. The $\Delta'(W)$ criteria will be used extensively.

The equations to be used will be based on the reduced MHD equations which will be discussed in more detail in the next chapter. Boundary conditions for these equations have to some extent been developed by the various authors that have been referred to under the section on external conditions. We have developed some for our specific application on Tokoloshe.

CHAPTER 3

THE REDUCED MHD EQUATIONS

3.1 Introduction

Since Strauss [52] and Rosenbluth et al. [51] derived the reduced MHD equations, they have been used extensively by many authors. In this chapter we will present the derivation of the more general reduced equations of Izzo et al. [4] in toroidal geometry. From these the Strauss and Rosenbluth equations can be derived. There is nothing new in this chapter. It is only included for completeness forming an important foundation for the rest of the thesis. We will use the reduced MHD equations in cylindrical as well as toroidal geometry. In cylindrical coordinates we include one mode in the plasma, ignoring all coupling. This introduces a model and is done in chapter 4. In chapter 7 we use the toroidal reduced equations when two modes are included in the plasma. In this case we use the model to consider toroidal coupling between these modes.

In these equations it is assumed that the inverse aspect ratio, $\epsilon = {}^{a}/R_0$, is much smaller than one (a is the minor plasma radius and R_0 the major radius of the device). This is not really the case on Tokoloshe where $\epsilon \simeq 0.5$. With nothing better available, we decided to use it while keeping this limitation in mind.

Another important feature of the equations that we are going to use, is that a low–beta tokamak ordering is assumed, i.e. the pressure is small ($O(\epsilon^2)$). We will ignore the effect of pressure in this study.

3.2 Deriving the Reduced MHD Equations in a Torus

In this section we will follow the approach of Izzo et al. [4] in the derivation of the reduced MHD equations.

Begin with the resistive MHD equations in rationalized electromagnetic units:

$$\frac{\partial \rho}{\partial t} = -\rho \nabla . \underline{V} + \underline{V} . \nabla \rho \tag{3.1}$$

$$\rho \frac{\partial \underline{V}}{\partial t} = -\nabla P + \underline{J} \wedge \underline{B} \tag{3.2}$$

$$\frac{\partial \underline{B}}{\partial t} = -\nabla \wedge \underline{E} \tag{3.3}$$

$$\frac{dP}{dt} = -\gamma P \nabla . \underline{V} \tag{3.4}$$

$$\underline{E} = \eta \underline{J} - \underline{V} \wedge \underline{B} \tag{3.5}$$

$$\underline{J} = \nabla \wedge \underline{B} \tag{3.6}$$

where

$$\frac{d}{dt} \equiv \frac{\partial}{\partial t} + \underline{V} . \nabla ,$$

and ρ is the mass density, $\underline{V}$ is the fluid velocity, $\underline{J}$ is the plasma current, $\underline{B}$ is the magnetic field, P is the thermodynamic scalar pressure, γ is the ratio of specific heats, and η is the plasma resistivity.

Use the inverse aspect ratio, $\epsilon \sim a/R_0 << 1$, as an expansion parameter, where a is the minor plasma radius and R_0 the major radius of the torus.

The following ordering is assumed:

$$\rho,\ B_\varphi,\ \nabla_\perp \sim O(\epsilon^0)$$

$$V_\perp,\ B_\perp,\ \frac{\partial}{\partial t},\ B.\nabla,\ 1/R \sim O(\epsilon)$$

$$P,\ V_\varphi,\ (1/R)\nabla(RB_\varphi),\ \nabla.V_\perp \sim O(\epsilon^2)$$

where the subscript $\perp$ denotes components perpendicular to φ, working in a cylindrical coordinate system (R,φ,z). Third order terms will be neglected.

Assume a perturbation of the toroidal magnetic field of order ϵ^2. The toroidal field can thus be written as

$$B_\varphi = I/R = (I_0 + \tilde{I})/R, \tag{3.7}$$

with I_0 constant (of $0(\epsilon^{-1})$) and $\tilde{I} \sim \epsilon^2 I_0$.

The perpendicular magnetic field can be written as the cross product of two Euler potentials [90]:

$$\underline{B}_\perp = R_0 \nabla\psi \wedge \nabla\varphi \tag{3.8}$$

or written in terms of a stream function ψ as

$$\underline{B}_\perp = R_0/R\ \nabla\psi \wedge \hat{\varphi},$$

with

$$\hat{\varphi} = R\nabla\varphi. \tag{3.9}$$

Thus,

$$\underline{B} = R_0/R\,\nabla\psi \wedge \hat{\varphi} + (I_0 + \tilde{I})\,\nabla\varphi . \tag{3.10}$$

Using

$$\nabla\psi = \frac{\partial\psi}{\partial R}\hat{R} + 1/R\,\frac{\partial\psi}{\partial\varphi}\hat{\varphi} + \frac{\partial\psi}{\partial z}\hat{z} ,$$

we get

$$\nabla\psi \wedge \hat{\varphi} = \frac{\partial\psi}{\partial R}\hat{z} - \frac{\partial\psi}{\partial z}\hat{R} . \tag{3.11}$$

Now, using equations (3.11) and (3.7) in (3.10), we get

$$\underline{B} = R_0\Big[\,1/R\,(-\frac{\partial\psi}{\partial z}\hat{R} + \frac{\partial\psi}{\partial R}\hat{z})\,\Big] + R\,B_\varphi\,\nabla\varphi . \tag{3.12}$$

Now using this, it is possible to derive the current density components from equation (3.6):

$$\underline{J} = \nabla\wedge\underline{B} = {}^{R_0}/_{R}\Big[\,\hat{R}\,(\frac{\partial}{\partial\varphi}\frac{1}{R}\frac{\partial\psi}{\partial R}) - \Big[\,\frac{\partial}{\partial R}(\frac{1}{R}\frac{\partial\psi}{\partial R}) + \frac{\partial}{\partial z}(\frac{1}{R}\frac{\partial\psi}{\partial z})\,\Big]\,R\hat{\varphi}$$

$$+ 1/R\,\frac{\partial}{\partial\varphi}\frac{\partial\psi}{\partial z}\hat{z}\,\Big] + \nabla(RB_\varphi) \wedge \nabla\varphi .$$

because $\nabla\wedge(\psi\nabla\varphi) = \nabla\psi \wedge \nabla\varphi$ giving $\nabla \wedge (RB_\varphi)\nabla\varphi = \nabla(RB_\varphi) \wedge \nabla\varphi$.

But $\frac{\partial}{\partial\varphi}\Big[\,1/R\,\frac{\partial\psi}{\partial R}\hat{R} + 1/R\,\frac{\partial\psi}{\partial z}\hat{z}\,\Big] \sim 0(\epsilon^3)$.

The resulting current density is

$$\underline{J} = {}^{-R_0}/_{R}\,\Delta^*\psi\hat{\varphi} + \nabla(RB_\varphi)\wedge\nabla\varphi \tag{3.13}$$

with $\Delta^* \equiv R\,\frac{\partial}{\partial R}(\frac{1}{R}\frac{\partial}{\partial R}) + \frac{\partial^2}{\partial z^2}$.

Thus

$$J_\varphi = -R_0/R\Delta^*\psi \tag{3.14}$$

and

$$\underline{J}_\perp = \nabla(RB_\varphi)\wedge\nabla\varphi = 1/R\nabla(RB_\varphi)\wedge\hat{\varphi}\,. \tag{3.15}$$

Substituting equation (3.10) into Faraday's law (3.3) gives

$$\frac{\partial\underline{B}}{\partial t} = -\nabla\wedge\eta\underline{J} + \nabla\wedge(\underline{V}\wedge\underline{B})$$

or

$$R_0/R\,\nabla\frac{\partial\psi}{\partial t}\wedge\hat{\varphi} + \frac{1}{R}\frac{\partial I_0}{\partial t}\hat{\varphi} + \frac{1}{R}\frac{\partial\tilde{I}}{\partial t}\hat{\varphi} = -\nabla\wedge\eta\underline{J} + \nabla\wedge(\underline{V}\wedge\underline{B}) + \nabla\wedge\nabla\phi\,,$$

with $\nabla\wedge\nabla\phi = 0$ and ϕ a scalar.

Using the fact that I_0 is constant and $\frac{1}{R}\frac{\partial\tilde{I}}{\partial t} \lesssim 0(\epsilon^3)$, this equation can be written as

$$R_0/R\,\nabla\wedge\frac{\partial\psi}{\partial t}\hat{\varphi} = -\nabla\wedge\eta\underline{J} + \nabla\wedge(\underline{V}\wedge\underline{B}) + \nabla\wedge\nabla\phi\,,$$

using $\nabla\psi\wedge\hat{\varphi} = \nabla\wedge\psi\hat{\varphi}$.

This reduces to

$$\nabla\wedge(R_0/R)\frac{\partial\psi}{\partial t}\hat{\varphi} = -\nabla\wedge\eta J + \nabla\wedge(\underline{V}\wedge\underline{B}) + \nabla\wedge\nabla\phi\,, \tag{3.16}$$

where terms of $O(\epsilon^3)$ have been dropped.

From equation (3.16) we get

$$R_0/R\frac{\partial\psi}{\partial t}\hat{\varphi} = -\eta\underline{J} + \underline{V}\wedge\underline{B} + \nabla\phi\,. \tag{3.17}$$

If the cross product with $\hat{\varphi}$ is taken

$$R_0/R \frac{\partial \psi}{\partial t} \hat{\varphi} \wedge \hat{\varphi} = -\eta \underline{J} \wedge \hat{\varphi} + (\underline{V} \wedge \underline{B}) \wedge \hat{\varphi} + \nabla \phi \wedge \hat{\varphi}$$

we are left with

$$0 = -\eta \underline{J} \wedge \hat{\varphi} + (\underline{V} \wedge \underline{B}) \wedge \hat{\varphi} + \nabla \phi \wedge \hat{\varphi} .$$

But $\underline{J} \wedge \hat{\varphi} = -J_z \hat{R} + J_R \hat{z}$.

resulting in $\|J \wedge \hat{\varphi}\| = \|J_\perp\|$ where $\|A\|$ denotes the magnitude of the vector $\underline{A}$.

Using the ordering of terms, we get from

$$\underline{J}_\perp = 1/R \nabla (RB_\varphi) \wedge \hat{\varphi} \sim O(\epsilon^2) ,$$

that

$$\underline{J} \wedge \hat{\varphi} \sim O(\epsilon^2) .$$

If we assume $\eta \leq O(\epsilon)$, we get

$$\eta \underline{J} \wedge \hat{\varphi} \leq O(\epsilon^3) .$$

Now we are left with

$$0 = (\underline{V} \wedge \underline{B}) \wedge \hat{\varphi} + \nabla \phi \wedge \hat{\varphi} \qquad (3.18)$$

which is valid if we are away from the rational surface where the effect of resistivity is negligible.

Further,

$$(\underline{V}\wedge\underline{B})\wedge\hat{\varphi} = -(V_z B_\varphi \hat{z} + V_R B_\varphi \hat{R})$$

$$= -\underline{V}_\perp B_\varphi$$

reduces equation (3.18) to

$$0 \approx -\underline{V}_\perp B_\varphi + \nabla\phi \wedge \hat{\varphi} . \tag{3.19}$$

If we assume that

$$\phi = B_0 U \quad (B_0 = {}^{I_0}/_{R_0}) , \tag{3.20}$$

equation (3.19) changes to

$$\underline{V}_\perp B_\varphi = \nabla B_0 U \wedge \hat{\varphi} .$$

From

$$B_\varphi = (I_0 + \tilde{I})/R \quad , \quad \tilde{I} \sim \epsilon^2 I_0$$

we have

$$\underline{V}_\perp ({}^{I_0}/_R + {}^{\tilde{I}}/_R) = \nabla {}^{I_0}/_{R_0} U \wedge \hat{\varphi} . \tag{3.21}$$

But

$$\underline{V}_\perp {}^{\tilde{I}}/_R \sim O(\epsilon^3) \text{ if } I_0 \sim O(\epsilon^{-1}) .$$

Now we have from equation (3.21) that

$$\underline{V}_{\perp}\,(I_0/R) \;=\; \nabla\frac{I_0 U}{R_0}\wedge\tilde{\varphi}$$

or

$$\underline{V}_{\perp} \;=\; R^2/R_0\,\nabla U\wedge\nabla\varphi\,. \tag{3.22}$$

It is thus clear that U is a flow potential.

If equations (3.10), (3.20) and (3.22) are substituted into the φ–component of equation (3.17) we get

$$\frac{R_0}{R}\frac{\partial\psi}{\partial t} \;=\; -\eta J_{\varphi} + (\underline{V}\wedge\underline{B})_{\varphi} + \nabla_{\varphi}B_0 U\,. \tag{3.23}$$

The term $(\underline{V}\wedge\underline{B})_{\varphi}$ can be written as

$$\Big[\,(\underline{V}_{\perp}+\underline{V}_{\varphi})\wedge(\underline{B}_{\perp}+\underline{B}_{\varphi})\,\Big]_{\varphi} \;=\; (\underline{V}_{\perp}\wedge\underline{B}_{\perp})_{\varphi}\,.$$

Now, after using equations (3.22) and (3.8) in the above expression, we get

$$\begin{aligned}(\underline{V}_{\perp}\wedge\underline{B}_{\perp}).\tilde{\varphi} \;&=\; \Big[\Big[R/R_0\nabla U\wedge\tilde{\varphi}\Big]\wedge\Big[R_0/R\nabla\psi\wedge\tilde{\varphi}\Big]\Big].\tilde{\varphi}\\ &=\; \Big[\nabla U.(\tilde{\varphi}\wedge\tilde{\varphi})\nabla\psi - \nabla U.(\tilde{\varphi}\wedge\nabla\psi)\tilde{\varphi}\Big].\tilde{\varphi}\\ &=\; \nabla\psi\wedge\tilde{\varphi}.\nabla U\,,\end{aligned} \tag{3.24}$$

changing equation (3.23) to

$$R_0/R\,\frac{\partial\psi}{\partial t} = -\eta J_\varphi + \nabla\psi \wedge \hat{\varphi}.\nabla U + \nabla_\varphi B_0 U$$

$$= -\eta J_\varphi + \nabla\psi \wedge \hat{\varphi}.\nabla U + (B_0/R)\,\frac{\partial U}{\partial \varphi}. \qquad (3.25)$$

When equation (3.14) is substituted into this, it results in

$$\frac{\partial\psi}{\partial t} = (R/R_0)\left[\left[\nabla\psi\wedge\hat{\varphi}.\nabla\right]U + B_0/R\;\frac{\partial U}{\partial\varphi} - \eta J_\varphi\right]$$

$$= (R/R_0)\left[\left[\nabla\psi\wedge\hat{\varphi} + B_0\hat{\varphi}\right].\nabla U + \eta\Delta^*\psi\right]. \qquad (3.26)$$

This is one of two important equations that are derived in this chapter. It gives an expression for the magnetic flux ψ.

To proceed further we multiply the momentum equation (3.2) by R^2 and then we take the $\hat{\varphi}$–component of the curl:

$$\underbrace{\hat{\varphi}.\nabla \wedge R^2\rho\,\frac{d\underline{V}}{dt}}_{A} = \hat{\varphi}.\nabla \wedge R^2(-\nabla P + \underline{J}\wedge\underline{B})$$

$$= \underbrace{-\,\hat{\varphi}.\nabla\; R^2\;\nabla P}_{B} + \underbrace{\hat{\varphi}.\nabla\wedge(R^2\underline{J}\wedge\underline{B})}_{C}. \qquad (3.27)$$

Term A can be written as

$$B^2\hat{\varphi}.\nabla\wedge\rho\,\frac{d\underline{V}}{dt} - 2R\,\rho\,\frac{dV_z}{dt}, \qquad \left(\nabla R^2\wedge\rho\,\frac{d\underline{V}}{dt}.\hat{\varphi} = -2R\rho\,\frac{dV_z}{dt}\right)$$

$$= -\rho R^2\,(R/R_0)\left[\frac{D}{dt}\nabla^2 U - 2/R_0\,\frac{\partial U}{\partial z}\nabla^2 U\right] - 2R\rho\,\frac{dV_z}{dt} \qquad (3.28)$$

from Appendix A. Note that

$$\frac{D}{dt} = \frac{\partial}{\partial t} + \underline{V}_{\perp}.\nabla .$$

Term B reduces to

$$-R^2\hat{\varphi}.\nabla \wedge \nabla P - \hat{\varphi}.\nabla R^2 \wedge \nabla P$$

$$= -2R\hat{\varphi}.\nabla R \wedge \nabla P . \qquad (3.29)$$

Term C can be analyzed as follows:

Recall from equations (3.10), (3.7) and (3.13) that

$$\underline{J} = -(R_0/R)\Delta^*\psi\hat{\varphi} + \nabla(RB_\varphi) \wedge \hat{\varphi}/R$$

$$\underline{B} = (R_0/R)\nabla\psi \wedge \hat{\varphi} + ({}^I/R)\hat{\varphi} .$$

Now we get

$$\underline{J}\wedge\underline{B} = \left[-(R_0/R)\Delta^*\psi\,(R_0/R)\frac{\partial\psi}{\partial R} - {}^I/R^2\,\frac{\partial}{\partial R}(RB_\varphi) \right] \hat{R}$$

$$- \left[-\frac{\partial B_\varphi}{\partial z}(R_0/R)\frac{\partial\psi}{\partial R} + R_0/R^2\,\frac{\partial\psi}{\partial z}\frac{\partial}{\partial R}(RB_\varphi) \right] \hat{\varphi}$$

$$+ \left[-\frac{\partial B_\varphi}{\partial z}({}^I/R) - R_0^2/R^2\,\frac{\partial\psi}{\partial z}\Delta^*\psi \right] \hat{z}$$

$$= -({}^I/R^2)\nabla_\perp(RB_\varphi) - R_0^2/R^2\Delta^*\psi\,\frac{\partial\psi}{\partial R}\hat{R} + \frac{\partial B_\varphi}{\partial z}R_0/R\,\frac{\partial\psi}{\partial R}\hat{\varphi}$$

$$- R_0/R^2\,\frac{\partial\psi}{\partial z}\frac{\partial}{\partial R}(RB_\varphi)\hat{\varphi} - R_0^2/R^2\,\frac{\partial\psi}{\partial z}\Delta^*\psi\,\hat{z} , \qquad (3.30)$$

using

$$\underline{J}_{\perp} = 1/R\left[-\frac{\partial}{\partial z}(RB_{\varphi})\hat{R} + \frac{\partial}{\partial R}(RB_{\varphi})\hat{z}\right]$$

and

$$\underline{B}_{\perp} = R_0/R\left[-\frac{\partial\psi}{\partial z}\hat{R} + \frac{\partial\psi}{\partial R}\hat{z}\right].$$

When equation (3.30) is substituted into term C, it results in

$$\hat{\varphi}.\nabla\wedge R^2(\underline{J}\wedge\underline{B}) = R_0^2\left[\frac{\partial}{\partial R}\left(\frac{\partial\psi}{\partial z}\Delta^*\psi\right) - \frac{\partial}{\partial z}\left(\frac{\partial\psi}{\partial R}\Delta^*\psi\right)\right]$$

$$= -RR_0\underline{B}.\nabla(\Delta^*\psi). \qquad (3.31)$$

From equations (3.28), (3.29) and (3.31) we get

$$-\rho R^2(R/R_0)\left[\frac{D}{dt}\nabla^2U - 2/R_0\frac{\partial U}{\partial z}\nabla^2U\right] - 2R\rho\frac{dV_z}{dt}$$

$$= -2R\hat{\varphi}.\nabla R\wedge\nabla P - RR_0\underline{B}.(\nabla\Delta^*\psi).$$

If we allow $R^2\rho = R_0^2\rho_0$, we get

$$\rho_0\left[\frac{D}{dt}\nabla^2U - 2/R_0\frac{\partial U}{\partial z}\nabla^2U\right] = 2/R_0\hat{\varphi}.\nabla R\wedge\nabla P + (\underline{B}.\nabla)\Delta^*\psi. \qquad (3.32)$$

The term

$$2\rho\, R_0/R^2\frac{dV_z}{dt} \sim O(\epsilon^4) \text{ and can be neglected.}$$

If the pressure is neglected we get (from equations (3.32) and (3.26))

$$\rho_0 \left(\frac{D}{dt} \nabla^2 U - 2/R_0 \frac{\partial U}{\partial z} \nabla^2 U\right) = {}^{R_0}/_{R} (\nabla\psi \wedge \hat{\varphi} + B_0\hat{\varphi}).\nabla\Delta^*\psi \,, \tag{3.33}$$

the velocity equation, and

$$\frac{\partial \psi}{\partial t} = {}^{R}/_{R_0} \left[(\nabla\psi \wedge \hat{\varphi} + B_0\hat{\varphi}).\nabla U \right] + \eta\Delta^*\psi \,, \tag{3.34}$$

the magnetic flux equation.

These are the final equations as derived by Izzo et al. [4]. The important feature of these equations in common with reduced MHD equations in general, is that only two independent variables, ψ and U, are involved.

For high beta equations where only terms of order $O(\epsilon)$ are included, the Pressure is included explicitly [64,65]. Equations (3.32) and (3.34) are used in Appendix B to derive the total energy of the plasma column in a toroidal configuration. We will make use of this energy in section 5.10.

3.3 The Reduced MHD Equations in the Cylindrical Approximation

The cylindrical reduced MHD equations will now be derived from the toroidal equations.

The cylindrical coordinate system describing the above toroidal configuration can be written as

$$R = R_0 + r\cos\theta$$

$$z = r\sin\theta$$

$$\varphi = s/R \,,$$

where s is the toroidal arc length.

Make the substitution

$$x = r\cos\theta\,,\quad y = r\sin\theta\,.$$

The result is

$$R = R_0 + x$$

$$z = y$$

$$\varphi = s/R\,.$$

We want to look at the simplified case of a cylinder. To do this we re–order the terms as follows:

$$1/R \sim O(\epsilon)\ (R \sim R_0 \sim O(\epsilon^{-1}))\ \text{ with }\ R_0 >> x.$$

$$\frac{\partial}{\partial x}\,,\ \frac{\partial}{\partial y} \sim O(1)\ (x,y \sim O(1))$$

$$\frac{\partial}{\partial s}\,,\ \frac{\partial}{\partial t} \sim O(\epsilon)\,.$$

From this we get

$$1/R = \frac{1}{(R_0 + x)} = 1/R_0 - x/R_0^2 + \ldots\,.$$

We can now write

$$\nabla_R^2 \equiv \frac{1}{R}\frac{\partial}{\partial R}\,R\,\frac{\partial}{\partial R} = \left(\frac{1}{R_0} - \frac{x}{R_0^2}\right)\left(\frac{\partial}{\partial x} + (R_0 + x)\,\frac{\partial^2}{\partial x^2}\right)$$

and

$$\Delta^* = R\,\frac{\partial}{\partial R}\,\frac{1}{R}\,\frac{\partial}{\partial R} + \frac{\partial^2}{\partial z^2}$$

$$= (R_0 + x)\left[-\,{}^{1}/R_0^2\,\frac{\partial}{\partial x} + \left({}^{1}/R_0 - {}^{x}/R_0^2\right)\frac{\partial^2}{\partial x^2}\right] + \frac{\partial^2}{\partial y^2}\,.$$

Now equations (3.33) and (3.34) become

$$\rho_0 \left[\frac{d}{dt}\left(\frac{\partial^2 U}{\partial x^2} + \frac{\partial^2 U}{\partial y^2}\right) \right] = (\nabla\psi \wedge \hat{s} + B_0\hat{s}).\nabla\left(\frac{\partial^2\psi}{\partial x^2} + \frac{\partial^2\psi}{\partial y^2}\right) \qquad (3.35)$$

$$\frac{\partial\psi}{\partial t} = (\nabla\psi \wedge \hat{s} + B_0\hat{s}).\nabla U + \eta\left(\frac{\partial^2\psi}{\partial x^2} + \frac{\partial^2\psi}{\partial y^2}\right), \qquad (3.36)$$

where

$$\nabla_\varphi = 1/R\,\frac{\partial}{\partial\varphi} = \frac{\partial}{\partial s} = \nabla_s\,,\ \hat{s} = \hat{\varphi}$$

and the following was assumed (as before):

$$\nabla\psi \sim O(\underline{B}_\perp) \sim O(\epsilon)\,,\ \nabla U \sim O(\underline{V}_\perp) \sim O(\epsilon)\,,\ \eta \sim O(\epsilon)\,,\ B.\nabla \sim O(\epsilon)\,.$$

Terms of $O(\epsilon^3)$ were dropped in these equations. It can be noted that all toroidal effects have been removed and that these equations are thus valid for a straight cylinder.

Equations (3.35) and (3.36) can be rewritten as

$$\rho_0 \frac{d}{dt}\nabla^2 U = (\nabla\psi\wedge\hat{s} + B_0\hat{s}).\nabla\nabla^2\psi \qquad (3.37)$$

$$\frac{\partial\psi}{\partial t} = (\nabla\psi\wedge\hat{s} + B_0\hat{s}).\nabla U + \eta\nabla^2\psi \qquad (3.38)$$

where ∇^2 is in the (x,y,s) coordinate system. The definitions of $\underline{B}$, $\underline{V}$ and J_z can now be adapted to

$$\underline{B} = \nabla\psi \wedge \hat{s} + B_0\hat{s}$$

$$\underline{V}_\perp = \nabla U \wedge \hat{s}$$

$$J_z = -\nabla_\perp^2\psi\,.$$

3.4 The Strauss Equations [52]

If the resistivity is neglected in equations (3.37) and (3.38), we get the ideal three–dimensional, non–linear approximate tokamak equations of motion in cartesian coordinates, first derived by Strauss [52]:

$$\rho \frac{d}{dt} \nabla^2 U = (\nabla\psi \wedge \hat{z} + B_0\hat{z}).\nabla\nabla_\perp^2\psi \tag{3.39}$$

$$\frac{d\psi}{dt} = (\nabla\psi \wedge \hat{z} + B_0\hat{z}).\nabla U \tag{3.40}$$

or, as he gave them

$$\frac{\partial \nabla_\perp^2 U}{\partial t} = -\underline{V}.\nabla\, \nabla_\perp^2 U + \underline{B}.\nabla\nabla_\perp^2 A \ , \ \rho = 1 \tag{3.41}$$

$$\frac{\partial A}{\partial t} = \underline{B}.\nabla U \tag{3.42}$$

where $s \rightarrow z$ in equations (3.39) and (3.40) with $\psi = A$.

3.5 The Equations of Rosenbluth et al. [51]

Rosenbluth et al. [51] derived these reduced MHD equations in helical geometry. This will now be discussed.

Equations (3.42) can be written as

$$\frac{\partial A}{\partial t} = \underline{B}_\perp.\nabla_\perp U + B_z.\nabla_z U$$

$$= -\underline{V}.\nabla A + B_z \frac{\partial U}{\partial z}.$$

or

$$\frac{\partial A}{\partial t} + \underset{\sim}{V}.\nabla A = B_z \frac{\partial U}{\partial z} . \qquad (3.43)$$

Equations (3.41) and (3.43) can be simplified if helical symmetry is assumed. Let

$$\tau = m\theta - kz \ , \ k = n/R .$$

Now m and n are the mode numbers of the original perturbation, which has the form $f(r)\exp[i(m\theta - kz)]$. For τ = constant we get

$$m d\theta = k dz$$

or

$$\frac{\partial}{\partial z} = \frac{k}{m}\frac{\partial}{\partial \theta} ,$$

using (r,θ,z) instead of (x,y,z) as coordinate system.

Equation (3.43) becomes

$$\frac{dA}{dt} = B_z \frac{k}{m}\frac{\partial U}{\partial \theta}$$

$$= \frac{B_z k}{2m} \underset{\sim}{V}.\nabla r^2 , \qquad (3.44)$$

from $\underset{\sim}{V}.\nabla r^2 = 2r\underset{\sim}{V}.\nabla r = 2rV_r$

$$= 2r(\nabla U \wedge \hat{z})_r$$

$$= 2\frac{\partial U}{\partial \theta} .$$

Substituting $\hat{\psi} = A - B_z kr^2/2m$ into equation (3.44) we get

$$\frac{\partial \hat{\psi}}{\partial t} + \underline{V}.\nabla\hat{\psi} = 0$$

or

$$\frac{D\hat{\psi}}{dt} = 0 ,$$

where B_z is just B_{z0}. (3.45)

When $\hat{\psi}$ is substituted into the expression for $\underline{B}$, now given by

$$\underline{B} = \nabla A \wedge \hat{z} + B_z\hat{z} ,$$

we get

$$B_r = \frac{1}{r}\frac{\partial \hat{\psi}}{\partial \theta}, \quad B_\theta = -\frac{\partial \hat{\psi}}{\partial r} - \frac{kr}{m}B_z .$$

These equations satisfy $(B.\nabla)\hat{\psi} = 0$ implying that $\hat{\psi}$ is a flux function.

Equation (3.41) can be written as

$$\frac{d}{dt}\nabla_\perp^2 U = \underline{B}.\nabla\nabla_\perp^2 A . \tag{3.46}$$

But

$$\nabla_\perp^2 A = \nabla_\perp^2\hat{\psi} + \frac{B_{z0}k}{2m}\nabla_\perp^2 r^2$$

$$= \nabla_\perp^2\hat{\psi} + \frac{2k}{m}B_{z0} \qquad (\text{from } \frac{1}{r}\frac{\partial}{\partial r}(\frac{1}{r}\frac{\partial}{\partial r}r^2) = 4) . \tag{3.47}$$

When equation (3.47) is substituted into (3.46), we get

$$\frac{d}{dt}\nabla_\perp^2 U = \underline{B}.\nabla(\nabla_\perp^2\hat{\psi})$$

$$= B_z\frac{\partial}{\partial z}(\nabla_\perp^2\hat{\psi}) + (\nabla A \wedge \hat{z}).\nabla_\perp(\nabla_\perp^2\hat{\psi})$$

$$= B_z\frac{\partial}{\partial z}(\nabla_\perp^2\hat{\psi}) - \frac{B_z kr}{m}\frac{1}{r}\frac{\partial}{\partial\theta}(\nabla_\perp^2\hat{\psi}) + (\nabla\hat{\psi}\wedge\hat{z}).\nabla_\perp(\nabla_\perp^2\hat{\psi}) , \qquad (3.48)$$

using $(\hat{r}\wedge\hat{z}).\nabla_\perp \equiv -\frac{1}{r}\frac{\partial}{\partial\theta}$.

Equation (3.48) can now be written as

$$\frac{d}{dt}\nabla_\perp^2 U = (\nabla\hat{\psi}\wedge\hat{z}).\nabla_\perp(\nabla_\perp^2\hat{\psi})$$

$$= \nabla(\nabla_\perp^2\hat{\psi}) \wedge \nabla\hat{\psi}.z , \qquad (3.49)$$

using the identity $(\underline{A}\wedge\underline{B}).\underline{C} = (\underline{C}\wedge\underline{A}).\underline{B}$.

In summary, equations (3.45) and (3.49) can be written as

$$\frac{D\psi}{dt} = 0 \qquad (3.50)$$

$$\frac{\partial}{\partial t}\nabla_\perp^2 U = -\underline{V}.\nabla(\nabla_\perp^2 U) + \nabla\nabla_\perp^2\hat{\psi}\wedge\nabla\hat{\psi}.\hat{z} . \qquad (3.51)$$

These are the same equations that were originally derived by Rosenbluth et al. [51] in helical symmetry.

3.6 The Equations of Waddell et al. [57]

If resistivity is included in equations (3.41) and (3.42) (using equations (3.37) and (3.38)), we get

$$\frac{\partial}{\partial t}\nabla_\perp^2 U = \underline{B}.\nabla\,\nabla_\perp^2 A\,,\ \rho = 1 \tag{3.52}$$

$$\frac{\partial A}{\partial t} = \underline{B}.\nabla U + \eta\,\nabla_\perp^2 A\,. \tag{3.53}$$

Using equation (3.47) in the expression for the current, i.e.,

$$J_z = -\nabla_\perp^2 A$$

gives

$$J_z = \nabla^2\dot{\psi} - {}^{2k}/_{m\,B_{z0}}\,. \tag{3.54}$$

When the transformations

$$\begin{aligned}
\bar{t} &= {}^{t}/_{\sqrt{\rho}\,m/(B_z k))} \\
\bar{A} &= A/(kr_w^2\,B_z/m\sqrt{\rho}) \\
\bar{r} &= {}^{r}/_{r_w} \\
\bar{\psi} &= \hat{\psi}/(kr_w^2\,B_z/m)\,,
\end{aligned}$$

are used in equations (3.52), (3.53) and (3.54), and the bars are dropped, these equations can be written as

$$D\psi/dt = -\eta J_z$$

$$\frac{D}{dt}\nabla^2 U = -\nabla_\perp\psi \wedge \nabla_\perp(\nabla_\perp^2\psi)$$

$$J_z = -\nabla^2\psi - 2\,,$$

where r_w is the wall radius.

It is convenient to replace ψ by $\psi - Et$ where E is the constant electric field at the wall, so that the boundary condition on ψ becomes $\psi(r_w,\theta,z,t) = 0$. Then we get

$$\frac{D\psi}{dt} = -\eta J_z + E \tag{3.55}$$

$$\frac{D}{dt}\nabla^2 U = -\nabla_\perp \psi \wedge \nabla_\perp(\nabla_\perp^2 \psi) \tag{3.56}$$

$$J_z = -\nabla^2\psi - 2\,, \tag{3.57}$$

which are the equations used by Carreras et al. [66], White et al. [91] and Waddell et al. [57].

3.7 Rewriting the Reduced Toroidal Equations in (r,θ,φ) Coordinates

The reduced toroidal equations were derived in section 3.2 and are given below.

$$\rho_0\left(\frac{D}{dt}\nabla^2 U - 2/R_0\,\frac{\partial U}{\partial z}\nabla^2 U\right) = {}^{R_0}/_{R}(\nabla\psi \wedge \hat{\varphi} + B_0\hat{\varphi}).\nabla\Delta^*\psi + \frac{2\nabla R \wedge \nabla P}{R_0}\cdot\hat{\varphi} \tag{3.32}$$

$$\frac{\partial\psi}{\partial t} = {}^{R}/_{R_0}\left[(\nabla\psi \wedge \hat{\varphi} + B_0\hat{\varphi}).\nabla U\right] + \eta\Delta^*\psi\,. \tag{3.34}$$

It is interesting to note that equation (3.33) is an explicit function of the z coordinate in cylindrical geometry.

We use the following normalization, with a bar specifying the normalized value,

$$\nabla \equiv \frac{1}{a}\nabla$$

$$\eta \equiv \hat{\eta}\,\bar{\eta}\ (\hat{\eta} \text{ a typical resistivity})$$

$$t \equiv \tau_R\,\bar{t} \text{ with } \tau_R = a^2/\hat{\eta} \text{ the resistive time scale}$$

$$\psi \equiv a\,B_0\,\bar{\psi}\,,$$

$$B \equiv B_0\,\bar{B}\,,$$

$$J \equiv B_0/a\,\bar{J}\,,$$

$$U \equiv \hat{\eta}\,\bar{U}$$

$$\Delta^* \equiv 1/a^2\,\bar{\Delta}^*\,,$$

$$P \equiv B_0^2\,\bar{P}/2$$

$$R \equiv \bar{R}\,a\,,$$

$$R_0 \equiv \bar{R}_0\,a\,,$$

$$z \equiv a\,\bar{z}\,,$$

with a the minor plasma radius.

Now, dropping the bars, the equations can be rewritten as

$$\frac{\partial}{\partial t}\nabla^2 U + \underline{V}.\nabla(\nabla^2 U) - 2\epsilon\frac{\partial U}{\partial z}\nabla^2 U = S^2/h(\nabla\psi\wedge\hat{\varphi}+\hat{\varphi}).\nabla\Delta^*\psi + \epsilon S^2\,\nabla R\wedge\nabla P\,.\,\hat{\varphi} \tag{3.58}$$

$$\frac{\partial\psi}{\partial t} = h[(\nabla\psi\wedge\hat{\varphi}+\hat{\varphi}).\nabla U] + \eta\Delta^*\psi \tag{3.59}$$

with

$$h = R/R_0 = 1 + \epsilon r\cos\theta$$

$$S = \tau_R/\tau_A\,,\ \tau_A^2 = a^2\rho/B_0^2\,,$$

$$\epsilon = 1/R_0\,,$$

τ_A the Alfven time scale. In these equations we have two variables ψ and U (η and P to be prescribed) and two explicit parameters ϵ and S.

In this study we will use the time independent equations to study saturated islands in the equilibrium. These are given by

$$\underline{V}.\nabla\,\nabla^2 U - 2\epsilon\,\frac{\partial U}{\partial z}\,\nabla^2 U \;=\; S^2/h\;(\nabla\psi\wedge\hat{\varphi}+\hat{\varphi}).\nabla\Delta^*\psi + \epsilon S^2\nabla R\wedge\nabla P.\hat{\varphi} \qquad (3.60)$$

$$h(\nabla\psi\wedge\hat{\varphi}+\hat{\varphi}).\nabla U + \eta\Delta^*\psi \;=\; 0\,. \qquad (3.61)$$

These equations are in the (R,φ,z)-system. The relation with the (r,θ,φ)-system, shown in Figure 3.1, is given by

$$\begin{aligned} R &= R_0 + r\cos\theta \\ z &= r\sin\theta \\ \varphi &= \varphi \end{aligned}$$

with

$$\sin\theta \;=\; z/r\,.$$

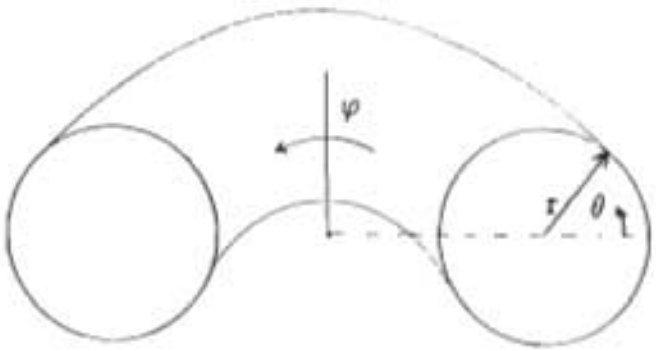

FIGURE 3.1 The (r,θ,φ) coordinate system.

We need the following to do the transformation between systems:

$$\frac{\partial r}{\partial z} = \sin\theta \tag{3.62}$$

$$\frac{\partial r}{\partial R} = \cos\theta \tag{3.63}$$

$$\frac{\partial \theta}{\partial z} = \frac{1}{r}\cos\theta \tag{3.64}$$

$$\frac{\partial \theta}{\partial R} = -\frac{1}{r}\sin\theta \ . \tag{3.65}$$

Further,

$$\Delta^*\psi = R\frac{\partial}{\partial R}\left(\frac{1}{R}\frac{\partial \psi}{\partial R}\right) + \frac{\partial^2 \psi}{\partial z^2}$$

$$= -2/R\frac{\partial \psi}{\partial R} + \nabla_\perp^2 \psi \tag{3.66}$$

$$\frac{\partial \psi}{\partial R} = \frac{\partial \psi}{\partial r}\frac{\partial r}{\partial R} + \frac{\partial \psi}{\partial \theta}\frac{\partial \theta}{\partial R}$$

$$= \cos\theta\frac{\partial \psi}{\partial r} - \frac{1}{r}\sin\theta\frac{\partial \psi}{\partial \theta} \tag{3.67}$$

$$\nabla^2\psi = \frac{1}{R}\left[\frac{1}{r}\frac{\partial}{\partial r}\left(r\,R\frac{\partial \psi}{\partial r}\right) + \frac{1}{R}\frac{\partial^2 \psi}{\partial \varphi^2} + \frac{1}{r^2}\frac{\partial}{\partial \theta}\left(R\frac{\partial \psi}{\partial \theta}\right)\right]$$

$$\nabla_\perp^2\psi = \frac{1}{r}\frac{\partial}{\partial r}\left(r\frac{\partial \psi}{\partial r}\right) + \frac{1}{r^2}\frac{\partial^2 \psi}{\partial \theta^2} + \frac{1}{R}\left(\cos\frac{\partial \psi}{\partial r} - \frac{1}{r}\sin\theta\frac{\partial \psi}{\partial \theta}\right) \ . \tag{3.68}$$

Thus, substituting equation (3.67) in equation (3.66), and writing $\nabla_\perp^2$ in coordinates (r,θ,φ), using equation (3.68), we get

$$\Delta^*\psi = -2/R\,(\cos\theta\,\frac{\partial\psi}{\partial r} - \frac{1}{r}\sin\theta\,\frac{\partial\psi}{\partial\theta}) + \frac{1}{r}\frac{\partial}{\partial r}(r\,\frac{\partial\psi}{\partial r}) + \frac{1}{r^2}\frac{\partial^2\psi}{\partial\theta^2}$$

$$+ \frac{1}{R}(\cos\theta\,\frac{\partial\psi}{\partial r} - \frac{1}{r}\sin\theta\,\frac{\partial\psi}{\partial\theta})$$

$$= -\epsilon/h\,(\cos\theta\,\frac{\partial\psi}{\partial r} - \frac{1}{r}\sin\theta\,\frac{\partial\psi}{\partial\theta}) + \frac{1}{r}\frac{\partial}{\partial r}(r\,\frac{\partial\psi}{\partial r}) + \frac{1}{r^2}\frac{\partial^2\psi}{\partial\theta^2}\,. \qquad (3.69)$$

Using equations (3.62) and (3.64) we find

$$\frac{\partial U}{\partial z} = \frac{\partial U}{\partial r}\frac{\partial r}{\partial z} + \frac{\partial U}{\partial\theta}\frac{\partial\theta}{\partial z} = \sin\theta\,\frac{\partial U}{\partial r} + \frac{1}{r}\cos\theta\,\frac{\partial U}{\partial\theta}\,. \qquad (3.70)$$

Another quantity in equation (3.60) is

$$\nabla R\wedge\nabla P = -\frac{\partial P}{\partial z}\,\hat{\varphi}\,.$$

$$= -(\sin\theta\,\frac{\partial P}{\partial r} + \frac{1}{r}\cos\theta\,\frac{\partial P}{\partial\theta})\,\hat{\varphi}\,. \qquad (3.71)$$

The perpendicular velocity is

$$\underline{V}_\perp = {}^{R}/_{R_0}\,\nabla U\wedge\hat{\varphi} = h(\frac{1}{r}\frac{\partial U}{\partial\theta}\,\hat{r} - \frac{\partial U}{\partial r}\,\hat{\theta})\,,$$

giving

$$\underline{V}.\nabla = V_\varphi\frac{1}{R}\frac{\partial}{\partial\varphi} + h\,\frac{1}{r}\frac{\partial U}{\partial\theta}\frac{\partial}{\partial r} - h\,\frac{\partial U}{\partial r}\frac{1}{r}\frac{\partial}{\partial\theta}\,. \qquad (3.72)$$

We can also write

$$\underline{V}.\nabla(\nabla^2 U) = h\,\frac{1}{r}\frac{\partial U}{\partial\theta}\frac{\partial}{\partial r}(\nabla^2 U) - h\,\frac{\partial U}{\partial r}\frac{1}{r}\frac{\partial}{\partial\theta}(\nabla^2 U) \qquad (3.73)$$

because

$$V_\varphi \frac{1}{R}\frac{\partial}{\partial\varphi} \sim O(\epsilon^3) \text{ and } \nabla^2 U \sim O(\epsilon) .$$

The Laplacian is now, using equation (3.68),

$$\nabla^2 U = \frac{1}{r}\frac{\partial}{\partial r}(r\frac{\partial U}{\partial r}) + \frac{1}{r^2}\frac{\partial^2 U}{\partial\theta^2} + (\epsilon/h)^2\frac{\partial^2 U}{\partial\varphi^2} + \epsilon/h(\cos\theta\frac{\partial U}{\partial r} - \frac{1}{r}\sin\theta\frac{\partial U}{\partial\theta}) . \tag{3.74}$$

Now the final time independent equations can be written in the (r,θ,φ) coordinate system by substituting equations (3.73), (3.70), (3.69) and (3.71) into equations (3.60) and (3.61).

$$h\frac{1}{r}\frac{\partial U}{\partial\theta}\frac{\partial}{\partial r}(\nabla^2 U) - h\frac{\partial U}{\partial r}\frac{1}{r}\frac{\partial}{\partial\theta}(\nabla^2 U) - 2\epsilon(\sin\theta\frac{\partial U}{\partial r} + \frac{1}{r}\cos\theta\frac{\partial U}{\partial\theta})\nabla^2 U$$

$$= S^2/h(\frac{1}{r}\frac{\partial\psi}{\partial\theta}\frac{\partial}{\partial r}(\Delta^*\psi) - \frac{1}{r}\frac{\partial\psi}{\partial r}\frac{\partial}{\partial\theta}(\Delta^*\psi) + \epsilon/h\frac{\partial}{\partial\varphi}(\Delta^*\psi))$$

$$- \epsilon S^2(\sin\theta\frac{\partial P}{\partial r} + \frac{1}{r}\cos\theta\frac{\partial P}{\partial\theta}) \tag{3.75}$$

$$h(\frac{1}{r}\frac{\partial\psi}{\partial\theta}\frac{\partial U}{\partial r} - \frac{1}{r}\frac{\partial\psi}{\partial r}\frac{\partial U}{\partial\theta} + \epsilon/h\frac{\partial U}{\partial\varphi}) + \eta\Delta^*\psi = 0 . \tag{3.76}$$

where ∇^2 and Δ^* are given by (3.74) and (3.69) respectively.

When $\nabla^2 U$ and $\Delta^*\psi$ are substituted into the above equations, (using equations (3.74) and (3.69)), it is possible to see from inspection that

$$U(\theta,\varphi) = -U(-\theta,-\varphi) \tag{3.77}$$

$$\psi(\theta,\varphi) = \psi(-\theta,-\varphi) . \tag{3.78}$$

We can now expand (see Appendix C)

$$\psi = \sum_{\substack{m n \\ -\infty}}^{\infty} a_{mn} e^{i(m\theta - n\varphi)}$$

$$U = \sum_{\substack{m n \\ -\infty}}^{\infty} i\, b_{mn} e^{i(m\theta - n\varphi)} ,$$

where a Fourier expansion is done in θ and φ. These expressions can now be substituted into equations (3.75) and (3.76) to get a system of ordinary differential equations for a_{mn} and b_{mn}. This has been done in Appendix D.

3.8 The Cylindrical Reduced MHD Equations

Let

$$J_{mn} = a''_{mn} + \frac{1}{r} a'_{mn} - \frac{m^2}{r^2} a_{mn}$$

$$J'_{mn} = a'''_{mn} - \frac{1}{r^2} a'_{mn} + \frac{1}{r} a''_{mn} + 2\frac{m^2}{r^3} a_{mn} - \frac{m^2}{r^2} a'_{mn}$$

$$K_{mn} = b''_{mn} + \frac{1}{r} b'_{mn} - \frac{m^2}{r^2} b_{mn} .$$

After the Fourier expansions have been carried out (in Appendix D), we get

$$\sum_{mn} \left[\left[\sum_{kl} D_{klmn} \right] + A_{mn} \right] \cos(m\theta - n\varphi) = 0 ,$$

with

$$A_{mn} = \epsilon^2 n b_{mn} + \epsilon f J_{mn}$$

$$D_{klmn} = \frac{\epsilon^2}{r} \left(-(m-k)\, a_{m-k,n-l}\, b'_{kl} + k\, a_{m-k,n-l}\, b_{kl} \right)$$

for the magnetic flux equation, and

$$\sum_{mn} \left[\left[\sum_{kl} D_{klmn} \right] + A_{mn} \right] \sin (m\theta - n\varphi) = 0 ,$$

with

$$A_{mn} = -n\epsilon^2 S^2 J_{mn}$$

$$D_{klmn} = \frac{S^2}{r} \epsilon^2 \left[(m-k)\, a_{m-k,n-l}\, J'_{kl} - k a'_{m-k,n-l}\, J_{kl} \right]$$

$$+ \frac{\epsilon^2}{r} \left[(m-k)\, b_{m-k,n-l}\, K'_{kl} - k b'_{m-k,n-l}\, K_{kl} \right]$$

for the momentum equation. In all these coefficients the ϵ has been made explicit.

Let

$$\mathfrak{L}(x,y) \equiv (m-k)\, x_{m-k,n-l}\, y'_{kl} - k x'_{m-k,n-l}\, y_{kl} .$$

This gives

$$\sum_{mn} \left[\left[\sum_{kl} -\frac{\epsilon^2}{r} \mathfrak{L}(a,b) \right] + \epsilon^2 n b_{mn} + \epsilon f J_{mn} \right] \cos (m\theta - n\varphi) = 0$$

$$\sum_{mn} \left[\left[\sum_{kl} \frac{S^2\epsilon^2}{r} \mathfrak{L}(a,J) + \frac{\epsilon^2}{r} \mathfrak{L}(b,K) \right] - n\epsilon^2 S^2 J_{mn} \right] \sin (m\theta - n\varphi) = 0 ,$$

or, since sine and cosine are a complete linearly independent set,

$$n\epsilon b_{mn} - \sum_{k\,l} \frac{\epsilon}{r} \mathfrak{L}(a,b) = -fJ_{mn} \qquad \forall\ m,n \qquad (3.79)$$

$$n\epsilon J_{mn} - \sum_{k\,l} \frac{\epsilon}{r} \mathfrak{L}(a,J) = \sum_{k\,l} \frac{\epsilon}{r} S^{-2}\, \mathfrak{L}(b,K) \qquad \forall\ m,n \qquad (3.80)$$

$$= S^{-2}\, \mathbb{R}$$

with

$$\mathbb{R} = \sum_{k\,l} \frac{\epsilon}{r} \mathfrak{L}(b,K) \ .$$

The J_{mn} terms may be regarded as the mn Fourier coefficients of the current density, using equation (3.14) for J_φ. Equation (3.79) is the primary equation to determine b_{mn}, and equation (3.80) to determine a_{mn}.

3.9 Mode Coupling in the Equations

The $\sum_{k\,l}$ terms in equations (3.79) and (3.80) give the coupling between modes since they are quadratic in mode amplitudes. Let us, for reasons of simplicity, examine equation (3.79) further.

For any mode (m,n) this equation can be written as

$$fJ_{mn} + n\epsilon b_{mn} - \frac{\epsilon}{\rho} \sum_{k\,l} [(m-k)a_{m-k,n-l}\, b'_{kl} - ka'_{m-k,n-l}\, b_{kl}] = 0 \ , \qquad (3.81)$$

with ρ substituted for r.

To look at the coupling between the (m,n)–mode and the (m+r,n+s)–mode, we do the following substitution:

$$k = m+r \ ,$$
$$\ell = n+s \ .$$

Since $k = 0,1,2 \ldots$ we have $r = -m, -m+1, -m+2 \ldots$ (see Appendix C).

For s, just as for n, we have

$$s: [-\infty , \infty] \ .$$

By the symmetry defined in equations (3.77) and (3.78), we also have

$$a_{-m,-n} = a_{mn} \ , \quad b_{-m,-n} = -b_{mn} \ .$$

(This is done in Appendix C).

Using these relations in equation (3.81), gives

$$fJ_{mn} + n\epsilon b_{mn} + \frac{\epsilon}{\rho} \sum_{\substack{r=-m \\ s=-\infty}}^{\infty} \left[r a_{rs} \, b'_{m+r,n+s} + (m+r) \, a'_{rs} \, b_{m+r,n+s} \right] = 0 \ .$$

In this equation we get coupling of b_{mn} to $b_{m+r,n+s}$ through a_{rs}.

As a practical example, we can take the coupling between the (2,1) and (3,1) modes which are, together with the (1,1)–mode, the dominant modes in Tokoloshe. These two modes are coupled to a secondary mode – the (5,2)–mode. The equations for *these* modes are

$$fJ_{21} + \epsilon b_{21} + \frac{\epsilon}{\rho} \sum_{\substack{r=-2 \\ s=-\infty}}^{\infty} [r a_{rs}\, b'_{2+r,1+s} + (2+r)\, a'_{rs}\, b_{2+r,1+s}] = 0$$

$$fJ_{31} + \epsilon b_{31} + \frac{\epsilon}{\rho} \sum_{\substack{r=-3 \\ s=-\infty}}^{\infty} [r a_{rs}\, b'_{3+r,1+s} + (3+r)\, a'_{rs}\, b_{3+r,1+s}] = 0$$

$$fJ_{52} + 2\epsilon b_{52} + \frac{\epsilon}{\rho} \sum_{\substack{r=-5 \\ s=-\infty}}^{\infty} (r a_{rs}\, b'_{5+r,2+s} + (5+r)\, a'_{rs}\, b'_{5+r,2+s} = 0 .$$

Other modes have been neglected in these equations. The coupling term is the same for Ampere's Equation (3.80).

More generally, ranking the modes, we get

$$\begin{array}{lccccc} O(\epsilon) & {}^{1}/_{1} & {}^{2}/_{1} & {}^{3}/_{1} & & \\ O(\epsilon^2) & & {}^{3}/_{2} & {}^{5}/_{2} & {}^{7}/_{2} & \\ O(\epsilon^3) & {}^{4}/_{3} & {}^{5}/_{3} & {}^{7}/_{3} & {}^{8}/_{3} & . \end{array}$$

If terms of $O(\epsilon^3)$ are neglected, it is clear that the first five modes will be the ones observed in a Tokamak plasma, where the (4,1)–mode falls outside the Tokoloshe plasma when the safety factor at the boundary is less than 4.

Also note that the coupling of dominant modes to themselves gives coupling to a higher order harmonic of that mode. For example the (2,1)–mode would via itself couple to the (4,2)–mode.

3.10 Interpreting the Reduced Time Independent Equations

When the resistivity is dropped in the magnetic field equation, we get

$$n\epsilon b - \sum_{kl} \frac{\epsilon}{r} \mathfrak{L}(a,b) = 0 \qquad \forall\ m,n. \qquad \text{(from equation (3.79))}$$

This is exactly the same as

$$B.\nabla U = 0 . \tag{3.82}$$

as can be seen from equation (3.61), remembering that

$$B = \nabla\psi\wedge\hat{\varphi} + \hat{\varphi} .$$

We now introduce a function $\hat{\psi}$ which satisfies $B.\nabla\hat{\psi} = 0$. Then $\hat{\psi} = \text{const}$ defines the magnetic surfaces where they exist. The magnetic fieldlines are now on these surfaces.

Equation (3.82) is analogous to $B.\nabla\hat{\psi} = 0$. For $B.\nabla U = 0$, the streamlines would now also be on the magnetic surfaces. Equation (3.82) is thus telling us that the streamlines would be on magnetic surfaces if there is no resistivity, and that resistivity will brake this effect.

If $S^2 \to \infty$, equation (3.80) reduces to

$$n\epsilon J_{mn} - \sum_{kl} \frac{\epsilon}{r} \mathfrak{L}(a,J) = 0 .$$

This is exactly the same as

$$B.\nabla J = 0 \quad . \tag{3.83}$$

as can be seen from equation (3.60) with $P = 0$ and $-\Delta^*\psi = J_\varphi = J$.

Thus, as above, it is clear that the current stays on the magnetic surfaces, and that this relation is broken by the introduction of the magnetic Reynolds number, that is by finite resistivity. In the case of only one perturbed mode, equation (3.80) will automatically reduce to (3.83) because $b_{00} = 0$. Thus, for one dominant mode in the plasma, the current will follow flux surfaces, whether there is resistivity or not.

3.11 Conclusions

In this chapter we derived the toroidal reduced MHD equations following Izzo et al. [4]. From these equations it was possible to derive the cylindrical equations in helical, cartesian and cylindrical coordinates, with and without resistivity. We also discussed the effect of resistivity as well, as $\tau_R >> \tau_A$ i.e. $S \to \infty$.

When only one mode is included in the plasma, equation (3.83) describes the equilibrium physical situation with or without resistivity. This will be the topic of the next chapter. In chapter 7 we will use the toroidal rendering of equation (3.83) to describe the situation with two modes in the plasma.

CHAPTER 4

EQUATIONS FOR ONE TEARING MODE IN CYLINDRICAL GEOMETRY

4.1 Introduction

In this chapter we include one mode in cylindrical geometry in the time–independent reduced MHD equations. The reason for including only one mode is that the equations simplify significantly as was discussed in the previous chapter. Although the situation of one saturated mode in a perturbed plasma equilibrium has been discussed before [3] our work differs from earlier studies for the reason that a different model is developed. This model makes perturbation theory work in the vicinity of the rational surface. It is done by flattening the current profile in a way very similar to that used by Sykes and Wesson [5]. It differs from White et al. [3], because they only use perturbation theory outside the island, modelling the total current profile inside the island as a linear function of the magnetic flux. Further, we are going to apply it to Tokoloshe. To model the external windings on Tokoloshe, the model will be extended to include various boundary conditions (the topic of the next chapter).

The effect of the resistive profile will be discussed. A resistive profile of the form $\eta = \eta(r,\theta,\varphi) \propto 1/J_\varphi$ is used to exclude flow from the problem. A simple resistive profile of the form $\eta = \eta(r)$ is then discussed.

4.2 The Reduced Equations for One Mode

4.2.1 Basic expressions defined

Assume the following directions for quantities used in this chapter:

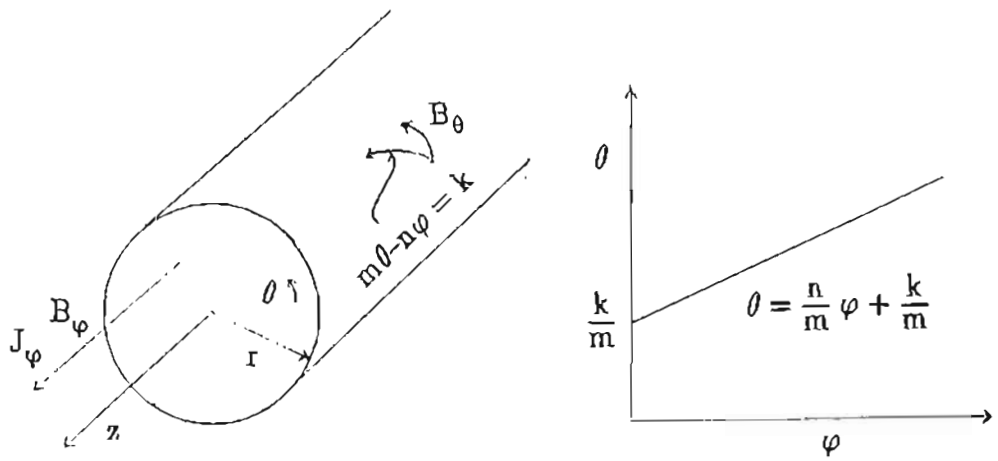

FIGURE 4.1 The directions of the important physical quantities are shown.

Let

$$\underline{B} = \nabla\psi \wedge \hat{\varphi} + \hat{\varphi} \tag{4.1}$$

with ψ of the form

$$\begin{aligned} \psi &= a_{00} + a_{mn} \cos mn \\ &= a_0(r) + a_1(r) \cos mn \,, \end{aligned} \tag{4.2}$$

where mn denotes $m\theta - n\varphi$.

The current $\underline{J} = J\hat{\varphi}$ can also be written as

$$\begin{aligned} J &= j_{00} + j_{mn} \cos mn \\ &= j_0(r) + j_1(r) \cos mn \,. \end{aligned} \tag{4.3}$$

From $\theta = \frac{n}{m}\varphi + \frac{k}{m}$ (using helical symmetry when only one mode is included) it is clear that $\Delta\theta = \frac{n}{m}\Delta\varphi$.

Thus

$$\frac{n}{m} = \frac{1}{q_{r_s}} = \frac{\Delta\theta}{\Delta\varphi}\Big|_{r_s} = \frac{d\theta}{d\varphi}\Big|_{r_s} = \frac{1}{\epsilon r} B_\theta\Big|_{r_s} = -\frac{1}{\epsilon r}\frac{\partial\psi}{\partial r}\Big|_{r_s},$$

where r_s denotes the rational surface, q the safety factor, and use is made of the field line equation

$$\frac{r\,d\theta}{B_\theta} = \frac{R_0\,d\varphi}{B_\varphi},$$

in the form $\frac{r\,d\theta}{B_\theta} = \frac{1}{\epsilon}\,d\varphi$ where $R_0 = \frac{1}{\epsilon}$ and $\underline{B}$ is normalized to $B_0 = B_\varphi\Big|_{r=0}$.

From the above we have

$$a_0'\Big|_{r_s} + \epsilon\, r_s \frac{n}{m} = 0 \qquad (4.4)$$

for an axisymmetric unperturbed equilibrium with $\frac{m}{n}$ the q–value at $r = r_s$. The derivative ($'$) denotes $\frac{d}{dr}$.

4.2.2 The helical equilibrium flux

Define a surface function $\hat{\psi}(r,\theta,\varphi)$ such that

$$\underline{B}.\nabla\hat{\psi} = 0, \qquad (4.5)$$

with

$$\hat{\psi} = \hat{\psi}_0 + \hat{\psi}_1 \cos mn\,. \qquad (4.6)$$

This $\hat{\psi}$ is not the same as the function ψ that was used to express the magnetic field in equation (4.1) and which is not in general a magnetic surface. When equation (4.1) is substituted into the above equation, we get

$$\hat{\psi}_0' = \hat{\psi}_1/a_1\,(a_0' + \epsilon r\,\frac{n}{m}) \qquad (4.7)$$

$$\hat{\psi}_1' = a_1'\hat{\psi}_1/a_1 \qquad \text{(first harmonic)}\,. \qquad (4.8)$$

For the axisymmetric unperturbed equilibrium we know that $B_{\theta_0} = \frac{-\partial\psi}{\partial r} = -\,a_0'$. At the rational surface we have $B_{\theta_0}\Big|_{r_s} = -\,a_0'\Big|_{r_s} = \frac{\epsilon r_s\, n}{m}$, from equation (4.4). Making these substitutions in equation (4.7) gives

$$\hat{\psi}_0' = -\,\hat{\psi}_1/a_1\,(B_{\theta_0} - B_{\theta_0}\Big|_{r_s})\,.$$

The equation for the first harmonic, given in equation (4.8), can be solved analytically, giving $\hat{\psi}_1 = \alpha\, a_1$. If α is chosen as 1, we get

$$\hat{\psi}_0' = a_0' + \epsilon r\frac{n}{m} \qquad (4.9)$$

$$\hat{\psi}_1' = a_1 \qquad (4.10)$$

and thus

$$\hat{\psi}_0' = -\,(B_{\theta_0} - B_{\theta_0}\Big|_{r_s})\,. \qquad (4.11)$$

This is just the helical magnetic flux for the unperturbed equilibrium [4]. This formula is also derived by an independent argument in Appendix E.

4.2.3 Rewriting the current density equation

As we have seen in Chapter 3, the equation

$$\underline{B}.\nabla J = 0 \qquad (4.12)$$

is valid when only one mode is included in the plasma, for any value of S.

Using the expressions for $\underline{B}$ and J (i.e. (4.1) – (4.3)) in equation (4.12) gives

$$-a_{mn}j'_{00} + a'_{00}\, j_{mn} + \epsilon r \frac{n}{m} j_{mn} = 0 . \qquad (4.13)$$

This is exactly the same as when one mode (m,n) is used with the zero–order equilibrium quantities in equation (3.80).

It will now be shown that, instead of using equation (4.12), we can just as well use the expression $J(\hat{\psi})$, where $\hat{\psi}$ is the helical magnetic flux.

Noting from equation (4.3) that equation (4.13) can be written as

$$j'_0 = j_1 (a'_0 + \epsilon \frac{n}{m} r) / a_1 \qquad (4.14)$$

and substituting equation (4.7) in here gives

$$j_1 = a_1 j'_0 / (a'_0 + \epsilon r \frac{n}{m})$$

$$= \hat{\psi}_1 j'_0 / \hat{\psi}'_0 . \qquad (4.15)$$

Using

$$j_0' = (dj_0/d\hat{\psi}_0)\hat{\psi}_0'$$

in equation (4.15) results in

$$j_1 = \hat{\psi}_1 \, dj_0/d\hat{\psi}_0 . \qquad (4.16)$$

We know from equation (4.12) that the current is along flux surfaces, which enables us to write $J = J(\hat{\psi})$. Let us now make a perturbation expansion of $J(\hat{\psi})$ about $J(\hat{\psi}_0)$. This gives

$$J(\hat{\psi}) = J(\hat{\psi}_0) + \hat{\psi}_1 \frac{dJ(\hat{\psi}_0)}{d\hat{\psi}_0} \cos mn + \ldots . \qquad (4.17)$$

When only the first harmonic is included, we get

$$J(\hat{\psi}) = j_0(r) + j_1(r) \cos mn .$$

This gives $j_1 = \hat{\psi}_1 \, dj_0/d\hat{\psi}_0$, just as in equation (4.16). Instead of equation (4.12) we can now use (4.17) to get the same result. Stating it differently: instead of using the equation $\underline{B}.\nabla J = 0$, we can just as well define $J = J(\hat{\psi})$, with $\hat{\psi}$ as in equation (4.6).

This result is not new, and was also stated by previous authors [5]. In the derivation of these equations, however, we did not follow any particular author.

4.2.4 A closed set of equations

The above discussion leaves us with the following equations:

$$a_0'' + \frac{1}{r} a_0' = -j_0 \tag{4.18}$$

$$a_1'' + \frac{1}{r} a_1' - \frac{m^2}{r^2} a_1 = -a_1 \frac{dj_0}{d\bar{\psi}_0} \tag{4.19}$$

$$\bar{\psi}_0' = a_0' + \epsilon r \frac{n}{m}, \tag{4.20}$$

with

$$\psi = a_0 + a_1 \cos(m\theta - n\varphi)$$

$$\hat{\psi} = \bar{\psi}_0 + a_1 \cos(m\theta - n\varphi)$$

$$J(\hat{\psi}) = J(\bar{\psi}_0) + \bar{\psi}_1 \frac{dJ(\bar{\psi}_0)}{d\bar{\psi}_0} \cos(m\theta - n\varphi)$$

$$= j_0 + a_1 \frac{dj_0}{d\bar{\psi}_0} \cos(m\theta - n\varphi).$$

Equations (4.18) and (4.19) are the same as (3.14) in cylindrical coordinates as was discussed at the end of section 3.3 and follow from $\nabla_\perp^2 \psi = -J(\hat{\psi})$. In the above equations the **axisymmetric current profile $j_0(r)$ is prescribed**. This leaves us with three equations and three unknowns (a_1, a_0, $\bar{\psi}_0$) to solve for. This enables us to determine a_0, and thus also $\bar{\psi}_0$. If $dj_0/d\bar{\psi}_0$ is known, a_1 can be solved for.

4.2.5 Problems of a perturbation expansion for $J(\hat{\psi})$

The problem with a first order perturbation expansion of $J(\hat{\psi})$ is that $dJ(\hat{\psi})/d\hat{\psi}_0\Big|_{r_s}$ blows up. This can easily be seen when equation (4.14) is written as

$$j_0' = \hat{\psi}_1 \frac{dj_0}{d\hat{\psi}_0}(a_0' + \epsilon \frac{n}{m} r) / a_1$$

$$= (a_0' + \epsilon \frac{n}{m} r) \frac{dj_0}{d\hat{\psi}_0}$$

$$= \frac{dj_0}{d\hat{\psi}_0} \hat{\psi}_0' , \qquad (4.21)$$

using equations (4.16), (4.10) and (4.9). We know that $\hat{\psi}_0'\Big|_{r_s} = 0$. For $j_0'\Big|_{r_s} \neq 0$, as is the case with any original unperturbed axisymmetric profile, $dj_0/d\hat{\psi}_0\Big|_{r_s} \to \infty$ in equation (4.21).

The behaviour of $J(\hat{\psi})$ at r_s can be illustrated with the following simple example: Let

$$J_\varphi = 1 - r^2 . \qquad (4.22)$$

Thus

$$a_0'' + \frac{1}{r} a_0' = -1 + r^2 . \qquad (4.23)$$

using equation (4.18).

Now we have

$$\frac{1}{r}\frac{d}{dr}\left(r\frac{d}{dr}a_0\right) = r^2 - 1$$

which we can integrate to give

$$a_0' = \frac{1}{4}r^3 - \frac{1}{2}r + K/r \quad . \tag{4.24}$$

The constant K is zero because $B_\theta = -a_0' \sim r^{m-1} \to 0$ as $r \to 0$.

When $\hat{\psi}_0' = a_0' + \epsilon r \frac{n}{m}$ is substituted in equation (4.24), we get

$$r^4 + 8\left(\epsilon\frac{n}{m} - \frac{1}{2}\right)r^2 + 16\left(k - \hat{\psi}_0\right) = 0 \quad . \tag{4.25}$$

This gives

$$r^2 = -4\left(\epsilon\frac{n}{m} - \frac{1}{2}\right) \pm 4\left[\left(\epsilon\frac{n}{m} - \frac{1}{2}\right)^2 - \left(k - \hat{\psi}_0\right)\right]^{\frac{1}{2}} . \tag{4.26}$$

When this is substituted into equation (4.22), we get

$$J_\varphi = -1 + 4\epsilon\frac{n}{m} \mp 4\left[\left(\epsilon\frac{n}{m} - \frac{1}{2}\right)^2 - \left(k - \hat{\psi}_0\right)\right]^{\frac{1}{2}} . \tag{4.27}$$

At $r = 0$ we have $\hat{\psi}_0 = k$ and at $r = 1$, $\hat{\psi}_0 = k + \frac{1}{2}\epsilon\frac{n}{m} - {}^3/_{16}$.

For $\hat{\psi}_0 = k + \frac{1}{2}\epsilon\frac{n}{m} - {}^3/_{16}$ we get

$$J_\varphi = 0 \text{ or } -2 + 8\frac{n}{m}\epsilon \, . \tag{4.28}$$

The rational surface r_s is where $\hat{\psi}_0' = 0$, resulting in

$$a_0'\Big|_{r_s} = -\epsilon\, r_s \frac{n}{m}$$

(using equation (4.4)).

Now we have, when this is substituted into equation (4.24),

$$-\epsilon\, r_s \frac{n}{m} = \frac{1}{4} r_s^3 - \frac{1}{2} r_s ,$$

giving

$$r_s = \sqrt{2 - 4\epsilon \frac{n}{m}} .$$

This gives, from equation (4.25),

$$\hat{\psi}_0\Big|_{r_s} = -\frac{1}{4} + \frac{n}{m}\epsilon - \left(\frac{n}{m}\epsilon\right)^2 + k .$$

Drawing J_φ as a function of $\hat{\psi}_0$, we get

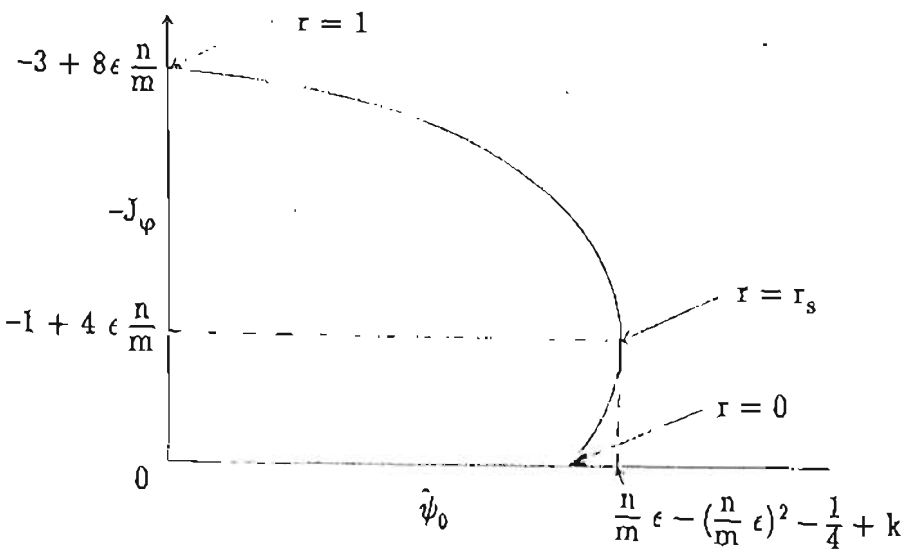

FIGURE 4.2 The graph of $-J_\varphi = r^2 - 1$ against $\hat{\psi}_0$.

From this graph it is clear that $\left.\frac{dJ}{d\hat{\psi}_0}\right|_{r_s} \to \infty$. It should be noted that J_φ is double valued for a range of $\hat{\psi}_0$ values. This behaviour is in general true for physical profiles.

4.3 Modelling a Perturbed Flattened Current Profile

4.3.1 Sykes and Wesson [5]

From equation (4.16) it is clear that $\left.\frac{dj_0}{d\hat{\psi}_0}\right|_{r_s} \to \infty$ is the same as $\left.j_1\right|_{r_s} \to \infty$ for a well–behaved $\hat{\psi}_1$. This divergence–problem is overcome in the linear theory of tearing modes where the equations are solved for $|r-r_s| > \epsilon$, ϵ the resistive layer width. They are then connected over the inner region using the Δ'–criterion. In this way the dynamics of the inner region are ignored. In the non–linear theory the $\Delta'(W)$–criterion is used instead [79].

If we take into account that the linear growth times are often substantially less than the time–scale for changes in the general equilibrium, it is expected that the tearing modes will be saturated most of the time. A possible approach is thus to ignore the first stages of tearing mode development, and to model the final saturated state by including a flat at the rational surface. Using energy relaxation, the saturation equilibrium can be determined. This approach has been used by Sykes and Wesson [5].

They used a conductivity profile σ of the form

$$\sigma = f\left(\frac{r}{a-w}\right) \qquad \text{in region i}$$

$$\sigma = f\left(\frac{r}{a-w}\right) \qquad \text{in region ii}$$

$$\sigma = f\left(\frac{r-w}{a-w}\right) \qquad \text{in region iii ,}$$

where f has the form $f = \sigma_0(1-x^2)^{\alpha}$,

and the regions are shown in Figure 4.3. The quantities a and w denote the minor radius and island width.

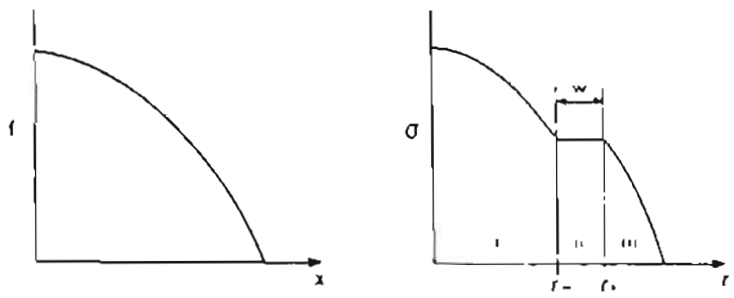

FIGURE 4.3 This graph is taken from Sykes and Wesson [5]. In (a) the typical form for $f(x)$ is shown and in (b) the typical conductivity profile for a plasma with a tearing mode present.

A relaxation procedure on a polar mesh was then used to solve the equilibrium equation

$$\nabla^2\hat{\psi} = -\sigma(\hat{\psi}) + 2 ,$$

with the functional form of the conductivity $\sigma(\hat{\psi})$ included in the equation. This equation is similar to equations (4.18) and (4.19), with (4.20) substituted therein.

White et al. [3] introduced another way to solve this problem. They assumed a linear form in $\hat{\psi}$ for the final flattened equilibrium profile inside the island modelled on numerical calculations. In introducing $J(\hat{\psi}) = a + b\,\hat{\psi}$, they were able to overcome the problems associated with the initial current profile as explained below.

4.3.2 The White et al. model [3]

White et al. [3] used the same approach as in the linear theory in distinguishing between an outer and an inner region. In the outer region they made use of the fact that the introduction of an island causes the current to change in two ways, that is because of the change in $\hat{\psi}$ and due to the change in the functional form of J itself. This gives $J(\hat{\psi}) = J_a(\hat{\psi}_0 + \Delta\hat{\psi}) + \Delta J(\hat{\psi}_0 + \Delta\hat{\psi})$, where $\hat{\psi}_0$ and J_a are the solutions of $\nabla^2\hat{\psi} = -J(\hat{\psi}) - 2$ in the absence of an island and ΔJ is the change in the functional form of J.

If a perturbation expansion is made in the outer region in terms of the fundamental harmonic $\hat{\psi}_1$, the following expressions are arrived at:

$$\hat{\psi} = \hat{\psi}_0(r) + \epsilon\,\hat{\psi}_1(r)\cos m\theta + \epsilon^2(\hat{\psi}_2\cos 2m\theta + \delta\hat{\psi}_0) + \ldots.$$

$$J = J_a(\hat{\psi}_0 + \Delta\hat{\psi}) + \epsilon\,\Delta J^{(1)}(\hat{\psi}_0 + \Delta\hat{\psi}) + \epsilon^2\Delta J^{(2)}(\hat{\psi}_0 + \Delta\hat{\psi}) + \ldots.$$

Substituting this in

$$\nabla^2\hat{\psi} = -J(\hat{\psi}) - 2 \qquad (4.29)$$

gives

$$\Delta J^{(1)} = 0$$

$$\nabla^2\hat{\psi}_1 = -(\partial J_a/\partial\hat{\psi})\hat{\psi}_1,$$

as usual.

This approach is not used in the inner region because of the fact that $\partial J_a/\partial\hat{\psi}\Big|_{r_s} \to \infty$ i.e. $J(\hat{\psi})$ is not analytic at the singular surface.

In the inner region, that is inside $\hat{\psi}_s$ (where $\hat{\psi}_s$ is the value of $\hat{\psi}$ on the separatrix), J is assumed to be $J_b(\hat{\psi})$. The motivation behind this functional dependence was discussed in section 4.2.3. They then proceeded to model $J_b(\hat{\psi})$. To quote them, "An N–parameter model of the current in the island interior, $J_b(\hat{\psi})$, along with a truncation of the harmonic expansion of $\hat{\psi}(r,\theta)$ with N harmonics then gives through equation (4.29) a set of N integral–differential equations for the harmonics $\hat{\psi}_n$, with the parameters of $J_b(\hat{\psi})$ serving as eigenvalues. Specifically, they take the form

$$\delta\hat{\psi}_0'' = -(\delta\hat{\psi}_0'/r) - \delta J_0 ,$$

$$\hat{\psi}_1 = (m^2/r^2)\hat{\psi}_1 - \frac{1}{r}\hat{\psi}_1' - J_1 ,$$

....

where the harmonics of the current are given by

$$J_0(r) = \frac{m}{\pi}\int_0^{\pi/m} d\theta\, J(\hat{\psi}) , \qquad (4.30)$$

$$J_1(r) = \frac{2m}{\pi}\int_0^{\pi/m} d\theta \cos m\theta\, J(\hat{\psi}) , \qquad (4.31)$$

and

$$\delta J_0 = J_0(r) - J_a(\hat{\psi}_0(r)) \qquad \text{"[3].} \qquad (4.32)$$

From numerical codes [3] they noted that the current $J_b(\hat{\psi})$ is accurately described by a linear function of $\hat{\psi}$.

For $\hat{\psi}(r,\theta)$, the flux function in the island interior, they used

$$\hat{\psi}(r,\theta) = \hat{\psi}_0(r) + \epsilon\hat{\psi}_1(r_x)\,(1 + sx)\cos m\theta \tag{4.33}$$

$$J_b(\hat{\psi}) = a + b\hat{\psi}(r,\theta)\,, \tag{4.34}$$

where $r = r_x + x$, where r_x is the position of the X–point, and s the slope of $\hat{\psi}_1(r)$ in the island interior given by $\hat{\psi}_1'(r_x)/\hat{\psi}_1(r_x)$. Their current profile is shown below.

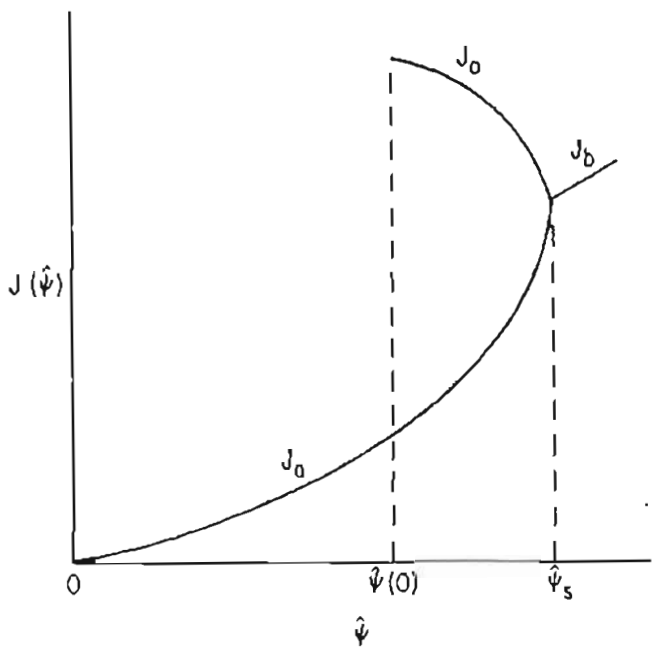

FIGURE 4.4 The current profile used by White et al. [3].

It should be stressed that they did not use perturbation theory in the inner region, and they therefore did not have the problem of singularities at the rational surface.

In their analytic work, they used the expression for Δ' to connect the inner and outer equations across the island. They also used

$$W = 4\,[-\hat{\psi}_1(r_s)/\hat{\psi}_0''(r_s)]^{\frac{1}{2}} \qquad \text{(the island width)},$$

to calculate

$$\frac{dW}{dt} = 1.66\,\eta(r_s)[\Delta'(W) - \alpha W]\,,$$

α a constant given by some expressions they derived.

4.4 An Alternative Approach

4.4.1 A new model

In our approach we do not distinguish between an inner and outer region of the plasma solving different equations in the different regions. The equations we solve are thus valid in the whole of the plasma region. We can do this since the definition of the inner region flows naturally from the problem. It is just the island interior.

As above, we carry out a Fourier expansion of the helical magnetic flux, given by

$$\hat{\psi} = \hat{\psi}_0(r) + \hat{\psi}_1(r)\cos(m\theta - n\varphi) \qquad (4.6)$$

where only one mode $\hat{\psi}_1$ is included in the plasma.

We then make a Taylor expansion about the perturbed current profile to give

$$J(\hat{\psi}) \quad = \quad J(\hat{\psi}_0) + \hat{\psi}_1 \cos(m\theta - n\varphi) \frac{dJ(\hat{\psi}_0)}{d\hat{\psi}_0} + \ldots ,$$

where $J(\hat{\psi}_0)$ is the first order axisymmetric part of the current. Now we will model $J(\hat{\psi}_0)$ such that $dJ(\hat{\psi}_0)/d\hat{\psi}_0$ is finite. This can be done by adding an axisymmetric perturbation δJ to the unperturbed axisymmetric profile $J_u(r)$ such that $J_u(r) + \delta J$ is analytic at the rational surface.

In the same way as the set of equations in 4.2.4 were derived, we can now derive

$$a_0'' + \frac{1}{r} a_0' = - J(\hat{\psi}_0) \tag{4.35}$$

$$a_1'' + \frac{1}{r} a_1' - \frac{m^2}{r^2} = - a_1 \frac{dJ(\hat{\psi}_0)}{d\hat{\psi}_0} \tag{4.36}$$

$$\hat{\psi}_0' = a_0' + \epsilon r \frac{n}{m} , \tag{4.37}$$

with

$$\psi = a_0 + a_1 \cos(m\theta - n\varphi) \tag{4.38}$$

$$\hat{\psi} = \hat{\psi}_0 + a_1 \cos(m\theta - n\varphi) \tag{4.39}$$

$$J(\hat{\psi}) \quad = \quad J(\hat{\psi}_0) + a_1 \frac{dJ(\hat{\psi}_0)}{d\hat{\psi}_0} \cos(m\theta - n\varphi) \tag{4.40}$$

$$= \quad j_0(r) + j_1(r) \cos(m\theta - n\varphi) . \tag{4.41}$$

In these equations $J(\bar{\psi}_0)$ is not the unperturbed axisymmetric profile $J_u(r)$, but a perturbed axisymmetric profile.

Recall $a_1 \dfrac{dJ(\bar{\psi}_0)}{d\bar{\psi}_0} = j_1$ as was derived in equation (4.16). The relation of our approach to that of White et al. is patent. Instead of their linear function for $J(\bar{\psi})$, we use a perturbation expansion for $J(\bar{\psi})$ in the expressions given by equations (4.30) and (4.31). This gives

$$J_0(r) = \frac{m}{\pi}\int_0^{\frac{\pi}{m}} d\theta\, J(\bar{\psi}) = J(\bar{\psi}_0) = j_0(r) \tag{4.42}$$

$$J_1(r) = \frac{2m}{\pi}\int_0^{\frac{\pi}{m}} d\theta \cos m\theta\, J(\bar{\psi}) = a_1 \frac{dJ(\bar{\psi}_0)}{d\bar{\psi}_0} = j_1(r)\,, \tag{4.43}$$

where $J_0(r)$ and $J_1(r)$ are their functions, and $j_0(r)$ and $j_1(r)$ our functions.

From equation (4.32) it is clear that

$$\begin{aligned} \delta J_0(r) &= J_0(r) - J_u(\bar{\psi}_0(r)) \\ &= J(\bar{\psi}_0) - J_u(r)\,, \end{aligned} \tag{4.44}$$

where $J_u(r)$ denotes the unperturbed axisymmetric original current profile. We now model δJ_0, and thus indirectly $J(\bar{\psi}_0)$, where White et al. [3] model $J(\bar{\psi})$. The perturbation δJ_0 will be modelled such that $\left.\dfrac{dJ(\bar{\psi}_0)}{d\bar{\psi}_0}\right|_{r_s} \neq \infty$, removing the difficulty at the rational surface. The reason for modelling $J(\bar{\psi}_0)$ instead of $J(\bar{\psi})$ is that no assumptions of the final functional form of the current density $J(\bar{\psi})$ have to be made.

It is important to note in our theory that the axisymmetric equilibrium quantities a_0, $\hat{\psi}_0$, $J(\hat{\psi}_0)$ do not refer to the unperturbed equilibrium as in section 4.2.4, but to an axisymmetric perturbed equilibrium. Further, it should be noted that $\delta J_0 \neq 0(\epsilon^2)$ and that it is not part of the perturbation expansion. If this perturbed axisymmetric current has $\left.\frac{dJ}{d\hat{\psi}_0}\right|_{r_s} \neq \infty$ these equations (4.35) – (4.37) can be solved without the singularities which are inherent in the unperturbed case. This can be assured by forcing $\left.\frac{dJ}{dr}\right|_{r_s} = 0$ in such a way that $J'/\hat{\psi}_0'$ is finite. This is immediately obvious from equation (4.21), where j_0 is now a perturbed axisymmetric current.

In solving the above equations, $J(\hat{\psi}_0)$ must be prescribed. Because $J(\hat{\psi}_0) = j_0(r)$, we can just as well prescribe $j_0(r) = J(r)$. This $J(r)$ we get by including a perturbation δJ on the unperturbed current profile, such that $\left.\frac{dJ}{dr}\right|_{r_s} = 0$. This will force $\frac{dJ}{d\hat{\psi}_0} \neq \infty$. With $J(r)$ known, $\frac{dJ}{dr}$ can be calculated and $\frac{dJ}{d\hat{\psi}_0} = \frac{dJ}{dr}/\hat{\psi}_0'$ can also be calculated easily. The given set of equations (4.35) – (4.37) can now be solved without problems.

It is important to note that the perturbation δJ_0 can cause $J(r)$ to be double valued in the island. In that case the radial points with equal $J(r)$ must also fall on equal values of $\hat{\psi}_0$ to keep $J = J(\hat{\psi}_0)$. This is not easily accomplished. For reasons of simplicity we decided not to allow $J(r)$ to be double valued in this model. To keep $J(r)$ from being double valued, we can just ensure that $J''|_{r_s} = 0$.

4.4.2 The effect of the higher order terms in $J(\hat{\psi})$

Instead of writing $J(\hat{\psi})$ as in equation (4.40), we could have included higher order terms to give

$$J(\hat{\psi}) = J(\hat{\psi}_0) + \hat{\psi}_1 \frac{dJ(\hat{\psi}_0)}{d\hat{\psi}_0} \cos mn + \hat{\psi}_1^2 \frac{d^2J(\hat{\psi}_0)}{d^2\hat{\psi}_0} \cos^2 mn + \dots \quad . \qquad (4.45)$$

In this expression the higher order derivatives of the current $J(\hat{\psi}_0)$ with respect to $\hat{\psi}_0$ are included. We can rewrite the n–th/order derivative of $J(\hat{\psi}_0)$ as

$$\frac{d^nJ(\hat{\psi}_0)}{d\hat{\psi}_0^n} = \frac{d^{n-1}}{d\hat{\psi}_0^{n-1}}[(\hat{\psi}')^{-1}J']$$

$$= \frac{\partial^{n-2}}{\partial\hat{\psi}_0^{n-2}}[(\hat{\psi}_0')^{-1}\{(\hat{\psi}_0')^{-1}J'\}']$$

$$= ((\hat{\psi}_0')^{-1}\dots((\hat{\psi}_0')^{-1}\{(\hat{\psi}_0')^{-1}[(\hat{\psi}_0')^{-1}J'^{(1)}]'^{(2)}\}'^{(3)})'^{(4)}\dots)'^{(n)}/\hat{\psi}_0' \; . \qquad (4.46)$$

where $<i>$, $i = 1,2 \dots n$, denotes the order of the derivative.

If we take into account that

$[(\hat{\psi}_0')^{-1}J']$ has an order one pole

$(\hat{\psi}_0')^{-1}[(\hat{\psi}_0')^{-1}J']'$ has an order three pole

$(\hat{\psi}_0')^{-1}\{(\hat{\psi}_0')^{-1}[(\hat{\psi}_0')^{-1}J']'\}'$ has an order five pole,

it is clear that the term $\dfrac{d^n J(\hat{\psi}_0)}{d\hat{\psi}_0^n}$ has a pole of order 2n–1.

We can thus write the term with the highest order pole on the right–hand side of equation (4.46) as

$$\frac{J'}{(\hat{\psi}_0')^{2m+1}} f(\hat{\psi}_0'', \hat{\psi}_0'', \ldots, J'', J''', \ldots) ,$$

with $m = n-1$.

Assuming $J'\Big|_{r_s} = 0$, we can apply L'Hospital's rule to this term, getting

$$f \lim_{r \to r_s} \frac{J'}{(\hat{\psi}_0')^{2m+1}} = \frac{(2m+1) f J'' \hat{\psi}_0''}{(\hat{\psi}_0')^{2m}} .$$

If we want to proceed using L'Hospital's rule, we must have $J''\Big|_{r_s} = 0$. In that case we can define a new function f_1 which contains poles of order less than 2m and write

$$f_1 \lim_{r \to r_s} \frac{J''}{(\hat{\psi}_0')^{2m}} = \frac{2m J''' \hat{\psi}_0'' f_1}{(\hat{\psi}_0')^{2m-1}} .$$

Other terms of similar form are grouped together and handled in similar fashion. If this process is repeated $2(n-1)+1$ times, making all the derivatives of J up to the $2(n-1)+1$ th one zero, we can remove all the poles. It is thus always possible to get a non–divergent value for the n–th derivative of $J(\hat{\psi}_0)$ to $\hat{\psi}_0$, if L'Hospital's rule can be applied $2(n-1)+1$ times.

If all the derivatives of J are made zero at the rational surface, all the higher order terms of $J(\hat{\psi})$ will be zero at $r = r_s$ and thus well behaved. Sykes and Wesson [5] managed to define exactly such a profile by including an absolute flat for the inner region in their profile.

4.5 Resistivity

4.5.1 Resistivity as a function of r

If the resistivity is included as a function of r, $\eta = \eta(r)$, we can get an expression for the perturbed velocity potential b_1 from equation (3.61), which is the same as $B.\nabla U = \eta J$ in the cylindrical approximation. This gives

$$b_1 = \frac{r}{m} \eta \, j_1 / \hat{\psi}_0' \, . \tag{4.47}$$

from the definitions of $\underline{B}$ and $\underline{U}$ as given at the end of section 3.7.

From this it is clear that $b_1\Big|_{r_s} \to \infty$ if $j_1\Big|_{r_s} \neq 0$. To keep b_1 finite, j_1 must be zero at the rational surface. For j_1 to be zero at r_s, $dj_0/d\hat{\psi}_0$ must be zero at r_s [using (4.16)]. It is thus clear that $dj_0/d\hat{\psi}_0$ must not only be finite (as was discussed in section 4.2.5) but zero if velocity perturbations are included as well as $\eta(r)$. This result is not stated in previous work as far as we are able to determine, and is compatible with the White et al. [3] model in which $j_1(r_s)$ was zero and $\eta = \eta(r)$.

Applying L'Hospital's rule to

$$\frac{dj_0}{d\hat{\psi}_0} = \frac{j_0'}{\hat{\psi}_0'},$$

we get

$$\lim_{r \to r_s} \frac{j_0''}{\hat{\psi}_0''} = 0 .$$

With $\hat{\psi}_0''\Big|_{r_s} \neq 0$, it is clear that $j_0''\Big|_{r_s}$ must be zero to have $dj_0/d\hat{\psi}_0$ zero at the rational surface.

We noted previously that

$$\frac{dJ}{dr}\Big|_{r_s} \neq 0 \implies \frac{dJ}{d\hat{\psi}_0}\Big|_{r_s} \to \infty \text{ for the unperturbed profile}$$

$$\frac{dJ}{dr}\Big|_{r_s} = 0 \implies \frac{dJ}{d\hat{\psi}_0}\Big|_{r_s} \text{ is finite for a perturbed axisymmetric profile.}$$

Now we also have

$$\frac{d^2J}{dr^2}\Big|_{r_s} = 0 \implies \frac{dJ}{d\hat{\psi}_0}\Big|_{r_s} = 0 \text{ for a perturbed axisymmetric profile with } \eta(r).$$

It is now important that $\frac{dJ}{dr}\Big|_{r_s} = 0$ is not enough, but $\frac{d^2J}{dr^2}\Big|_{r_s} = 0$ is required to have a well behaved set of equations if flow perturbations are allowed, together with finite $\eta(r)$.

Lastly, we know that $\hat{\psi}_0' = a_0' + \epsilon r \frac{n}{m}$. Because $a_0' = -B_{\theta_0}$ and $B_{\theta_0} \to 0$ as $r \to 0$, it is clear that $\hat{\psi}_0'\Big|_0 = 0$. This implies that

$$\frac{dJ}{dr}\Big|_0 = 0, \tag{4.48}$$

using equation (4.21).

4.5.2 Resistivity depending on θ and φ

Let $\eta = \eta_0 + \eta_1 \cos(m\theta - n\varphi)$. This gives

$$b_1 = \frac{r}{m}(j_1 \eta_0 + \eta_1 j_0) / (a_0' + \epsilon r \frac{n}{m}) , \qquad (4.49)$$

using (3.61) in the cylindrical approximation. If $B.\nabla\eta = 0$ (just like $B.\nabla J = 0$), we get $\eta_1 = \tilde{\psi}_1 \eta_0' / \tilde{\psi}_0'$. This means that the resistivity is along flux surfaces, just like the current. A resistive profile of the form $\eta(r) \sim 1/J_0(r)$ is often used [4]. The form we specified allows for $\eta(\tilde{\psi}) \sim \frac{1}{J(\tilde{\psi})}$, following from equation (2.5) with no flow and constant E. Equation (4.49) can now be written as

$$b_1 = -\frac{r}{m}(\tilde{\psi}_1 \frac{dj_0}{d\tilde{\psi}_0} \eta_0 + \tilde{\psi}_1 \frac{d\eta_0}{d\tilde{\psi}_0} j_0) / \tilde{\psi}_0'$$

$$= -\frac{r}{m} \tilde{\psi}_1 \frac{d}{d\tilde{\psi}_0}(j_0 \eta_0) / \tilde{\psi}_0' . \qquad (4.50)$$

The only condition for finite b_1 in this case is that $\frac{d}{d\tilde{\psi}_0}(j_0\eta_0) = 0$ at r_s.

On the other hand, if $\left.\frac{dJ_0}{d\tilde{\psi}_0}\right|_{r_s} = 0$ and $\left.\frac{d\eta_0}{d\tilde{\psi}_0}\right|_{r_s} = 0$, b_1 will also be well behaved.

If $\eta_0 j_0 = \text{const}$, we get $b_1 = 0$ for all r. This is consistent with equation (3.5), where we get $E = \eta J$ for $\underline{V} \equiv 0$ (assuming E = constant).

We used both $\eta = \eta(r)$ and $\eta(r,\theta,\varphi)$ in our model.

4.5.3 Expected features of the plasma as time evolves

From the previous discussions, we can get some understanding of the plasma behaviour as time proceeds.

If the equilibrium is tearing mode unstable, and a tearing mode can evolve at a rational surface, the following features can be expected: The original unperturbed current profile j_0 has $j_0'\big|_{r_s} \neq 0$ which causes the perturbed current j_1 to grow very strongly. This can easily be seen from the relation $j_1 = \frac{dj_0}{d\hat{\psi}_0}\hat{\psi}_1$, and the fact that $dj_0/d\hat{\psi}_0\big|_{r_s} \to \infty$ for $j_0'\big|_{r_s} \neq 0$. If η is a function of r the fact that $j_1\big|_{r_s} \neq 0$ will cause a strong localized flow at r_s (from equation 4.47). As the current profile flattens ($j_0'\big|_{r_s} = 0$), the perturbed current will go to zero in the case where $\eta = \eta(r)$. The strong flow at r_s will then also disappear. In the case where $\eta = \eta(r,\theta,\varphi)$ the perturbed current j_1 will not necessarily go to zero, and if $\eta_0 = {const}/{j_0}$ there will be no flows.

4.6 Conclusions

A simple model for the case of one tearing mode in a cylindrical plasma has been developed. It is simple in the sense that first order perturbation theory is used. No difficult numeric schemes are needed to solve the equations. No model of the island shape is included, which follows of its own accord.

The model developed here has similarities with Sykes and Wesson [5] and White et al. [3]. It is similar to that of Sykes and Wesson in the sense that we also include a flattening of the profile and look only at time independent final saturated island

situations. It differs from them because we do not include an inner and outer region, instead only demanding a local flattening at r_s, and also, as we shall see, because our model reduces to an eigenvalue problem. This will be discussed in chapter 5. The model is similar to that of White et al. [3] in the sense that the perturbed current profile is modelled in the island region as a function of $\tilde{\psi}$ (the magnetic flux). It differs therein that theirs is an exact function of $\tilde{\psi}$ where ours is a Fourier series where only the first order perturbation has been included, making it an approximate function of $\tilde{\psi}$. If higher perturbations were included, it would be an exact function of $\tilde{\psi}$. Instead of using harmonic analysis as they do, we used a combination of harmonic analysis and perturbation theory. It differs from White et al. in the sense that we make perturbation theory work at the rational surface, whereas they only use perturbation theory outside the island. They also use an inner and an outer region, something we do not do. Although we do not have these different regions, we must still use a $\Delta'(W)$ criterion across the island. It should be noted that White et al. [3] did analytic work, whereas we only solve the equations numerically.

The model we developed will be used in conjunction with different boundary conditions discussed in the next chapter. The results of the model will be presented in chapter 6.

CHAPTER 5

BOUNDARY CONDITIONS

5.1 Introduction

In this chapter we discuss the boundary conditions for equations (4.35) to (4.37), i.e. for the new proposed model. The aim is to consider the effect of different physical situations, i.e.

- the plasma is locked and coupled to a vacuum region outside
- the plasma is locked and coupled to an external coil current in the vacuum region
- the plasma is rotating infinitely fast with a partly conducting wall or the wall is superconducting
- the plasma is rotating at some frequency and is coupled to an external vacuum region
- the plasma is rotating at some frequency and is coupled to an external coil current in the vacuum region.

In the first section (i.e. 5.2) the boundary conditions on the plasma edge are derived. These are totally general and will later be related to the outside conditions. An important parameter in these boundary conditions is δ, the surface deformation of the plasma edge. If $\delta = 0$, conventional tearing mode solutions are obtained, but $\delta \neq 0$ allows for the wide variety of situations mentioned above. This perturbation is chosen to be consistent with the internal mode, i.e. for an internal mode modelled by a perturbation $\psi_1 \cos(m\theta - n\varphi)$, a surface perturbation of $\delta \cos(m\theta - n\varphi)$ is assumed.

The first configuration discussed is for the plasma touching a non–conducting wall. A coil current can also be included in this configuration, placing it in the vacuum outside the wall. In such a situation the plasma boundary conditions are coupled to the solutions in vacuum across the wall. This coupling makes it possible to derive an expression for $\left.\frac{a_1}{a_1'}\right|_{\text{plasma boundary}}$ for the case of a locked mode (i.e. no time dependence is included) or for an infinitely fast rotating mode with a partly conducting wall, which is similar to a superconducting wall, in which case $\left.\frac{a_1}{a_1'}\right|_{\text{plasma boundary}} = 0$. This parameter $\left.\frac{a_1}{a_1'}\right|_{\text{plasma boundary}}$ is directly proportional to $B_r/B_{\theta_1}\Big|_{\text{plasma boundary}}$ and will be of major importance in the rest of the study.

When the rotation frequency is included explicitly, the configuration is changed slightly. A vacuum region is included inside the resistive wall. It is shown that this solution agrees with the previous one when this vacuum region is reduced in size. An external coil is also included with this configuration.

The work done in the first part of this chapter on boundary conditions is not new and has been done elsewhere [75,86]. The approach followed is not that of any author in particular. The results are given in a form which is compatible with our model. The work done in the last part of the chapter, where a rotational plasma is coupled to an external coil current, appears to be new.

5.2 Non–homogeneous Boundary Conditions

For equations (4.35) – (4.37) we need $a_0'\Big|_\partial$, $a_0\Big|_\partial$, $\hat{\psi}_0\Big|_\partial$, $a_1\Big|_\partial$, $a_1'\Big|_\partial$. The sign $\Big|_\partial$ denotes "at the boundary of the plasma".

The value of $a_0\Big|_{\partial}$ may be chosen freely because $\underline{B}_{\perp} = \nabla \psi \wedge \hat{\varphi}$ – allowing us to add any constant to a_0. We also know, from equation (4.9), that

$$\tilde{\psi}_0 = a_0 + \tfrac{1}{2} \epsilon \frac{n}{m} r^2 + k \qquad (5.1)$$

where k is a free constant.

From section 4.2.1 we know that

$$a_0' = -\epsilon r \frac{1}{q}.$$

in zeroth order.

Thus $a_0'\Big|_{\partial} = -\epsilon r/q\Big|_{\partial}$,
as was shown in equation (4.4).

With expressions for the boundary values for a_0', a_0 and $\tilde{\psi}_0$ known, we can proceed to get expressions for $a_1'\Big|_{\partial}$ and $a_1\Big|_{\partial}$. When a perturbation expansion is made about J_φ at the boundary, using the expression for the boundary,

$$r^{\partial} = r_0 + \delta \cos mn, \qquad (5.2)$$

we get to first order in δ

$$J_\varphi^{\partial} = j_0(r^{\partial}) + j_1(r^{\partial}) \cos mn \qquad \text{(from equation 4.3))}$$

$$= j_0(r_0) + \delta \cos mn\, j_0'(r_0) + j_1(r_0) \cos mn\,.$$

When $J_{\varphi}^{\partial} = 0$, and the coefficients of linearly independent functions are grouped together, we get

$$j_0(r_0) = 0 \qquad (\cos(0)) \qquad (5.3)$$

$$\delta\, j_0'(r_0) = -\, j_1(r_0) \qquad (\cos mn)\,. \qquad (5.4)$$

The second of these equations can be substituted into equation (4.14) giving

$$a_1(r_0) = -\,\delta\,(a_0'(r_0) + \frac{n\,\epsilon}{m}\, r_0)\,. \qquad (5.5)$$

The quantity $a_1'\Big|_{\partial} = B_{\theta_1}\Big|_{\partial}$ must be chosen such that $B_{\theta_1}\Big|_0 \to 0$ for modes with $m \geq 2$. This follows from the fact that $B_{\theta_1}\Big|_0 \sim r^{m-1}$. The notation $\Big|_0$ denotes "at $r = 0$ ".

If we carry out a Taylor expansion about any quantity of order δ (like a_1 or a_1') at the boundary, we get

$$A\Big|_{\partial} = A\Big|_{r_0} + \delta \cos mn\; A'\Big|_{r_0} + \ldots\,.$$

Dropping terms of $0(\delta^2)$ gives

$$A\Big|_{\partial} = A\Big|_{r_0}. \qquad (5.6)$$

If we remind ourselves that $r_0 = a$ (the plasma boundary), and r is normalized to a, we can replace r_0 with 1. In summary we get

$$a_0\Big|_1 = k \qquad \text{(arbitrary)} \tag{5.7}$$

$$\dot{\psi}_0\Big|_1 = k_1 \qquad \text{(using equation (5.1))} \tag{5.8}$$

$$a_0'\Big|_1 = -\epsilon \frac{1}{q_1} \qquad (q_1 = q\Big|_1) \tag{5.9}$$

$$a_1\Big|_1 = -\delta\,(a_0'\Big|_1 + \epsilon \frac{n}{m}) \tag{5.10}$$

$$a_1'\Big|_1 = \text{chosen (shooting value).} \tag{5.11}$$

Note that $B_r = \frac{1}{r}\frac{\partial \psi}{\partial \theta} = -\frac{m}{r} a_1 \sin(m\theta - n\varphi)$. If a_1 is known, B_r is known. Using $a_1\Big|_1 = f(\delta)$, we see that the perturbation of the boundary is directly related to the radial magnetic field on the boundary. It is also immediately clear that, because $B_{\theta_0}\Big|_1$ is included in the expression for $a_1\Big|_1$, this perturbed quantity is normalized if B_{θ_0} is normalized. These boundary conditions are thus non–homogeneous. Because of this fact, amplitudes are fixed, unlike the case of linear tearing mode theory.

These boundary conditions are completely general. They are valid for any δ. They are also valid for $\delta \to 0$. This follows from perturbation theory, δ being a perturbation of a circular boundary.

5.3 Effects of islands on the boundary shape

When an island is present in the plasma, there will be an accompanying perturbed magnetic field B_r – otherwise the fieldlines will be circular at any angle φ. This magnetic field would not be able to penetrate the wall if the plasma is rotating infinitely fast with a partly conducting wall or when the wall is superconducting.

Using the fact that $B_{r1} = B_{r2}$ where 1,2 stand for inside, outside [following from $(\underline{B}_{r2} - \underline{B}_{r1}).\underline{n} = 0$] it is immediately clear that $B_r\Big|_1$ is zero in these cases, agreeing with $\delta = 0$ as was discussed in the previous section. This means that the boundary is circular. It was assumed above that $r_w = 1$, i.e. that the plasma touches the wall at the wall radius r_w.

When the plasma is locked somehow, the perturbed field can penetrate the wall. In such a case $B_r\Big|_1$ is non–zero resulting in a perturbed boundary. This corresponds to the free–boundary situation which can be illustrated schematically as follows:

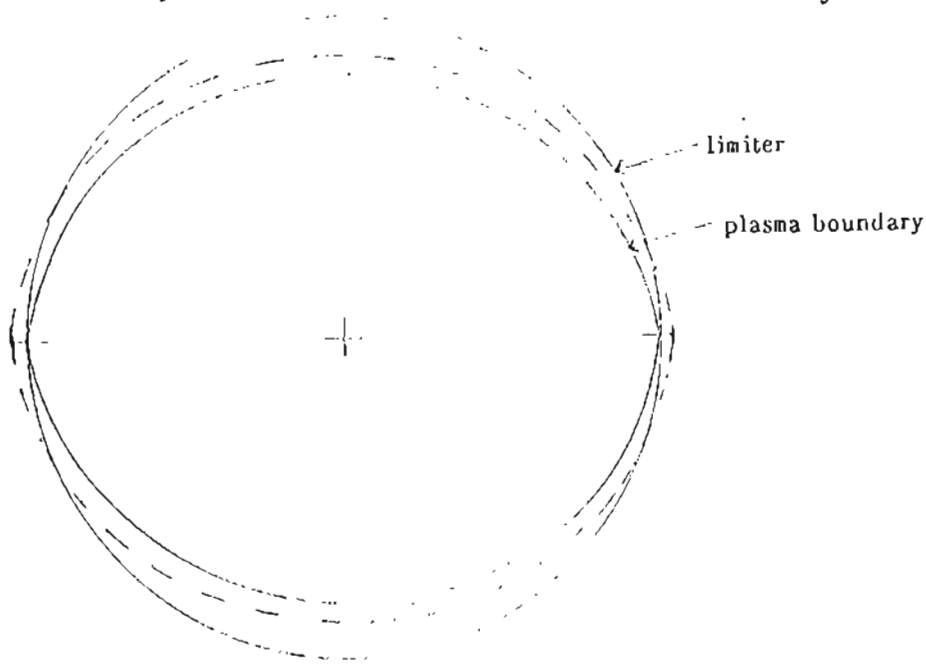

FIGURE 5.1 When $B_r\Big|_1 = 0$, the boundary will be circular. Otherwise it will be perturbed according to the internal mode.

In our approach we include a local axisymmetric flat in the current profile, and at the same time perturb the boundary in a resonant way. The flatness of the current profile, and ultimately the island width, can now be related to the external perturbed boundary, arising either because of a natural tearing island or because of an externally induced one (using external coils), or both.

On Tokoloshe we attempt to influence the natural tearing modes by an external coil current. This can be understood easily in the following way:

Assume the natural tearing mode (with mode numbers m,n) has a perturbation of the form

$$i\, B_r\, e^{i(m\theta - n\varphi)} .$$

Let $\chi = m\theta - n\varphi$ to get $\sin(m\theta - n\varphi) = \sin\chi$.

In the case of a cylinder, where no side bands are present, this tearing mode can be affected by a perturbation of the same form, resonating with the inside mode. This is possible if four windings are put helically around the cylinder as in Figure 5.2:

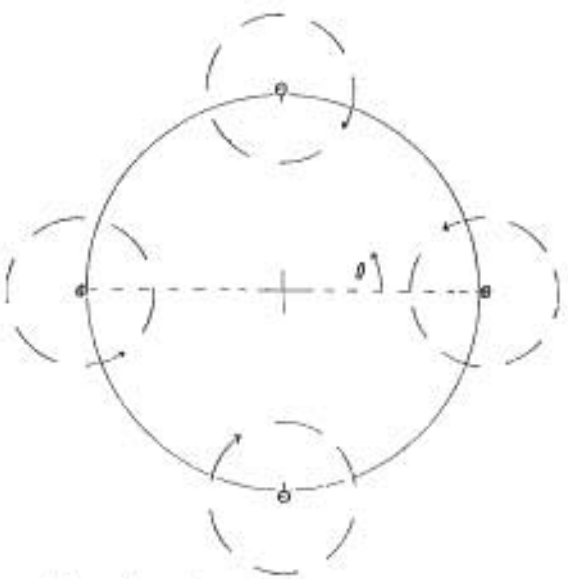

FIGURE 5.2 The configuration with a (2,1) external winding. The value of φ is taken to be zero for simplicity.

It is now easy to see that the form of B_r is approximately $K \sin \chi$, $K < 0$, when θ is varied at a specific r on the inside of the plasma in Figure 5.2.

The configuration of coils can be expressed as

$$\theta = \alpha\varphi + (k-1)\frac{\pi}{\ell}, \quad k = 1, 2 \ldots \ell,$$

with ℓ the polarity of the winding and α a constant.

The way to solve the tearing mode problem with external helical coil currents is to include these currents in the boundary conditions of the reduced MHD equations as will be discussed in the next section.

5.4 Including coil currents in the problem

Assume a configuration of the following form:

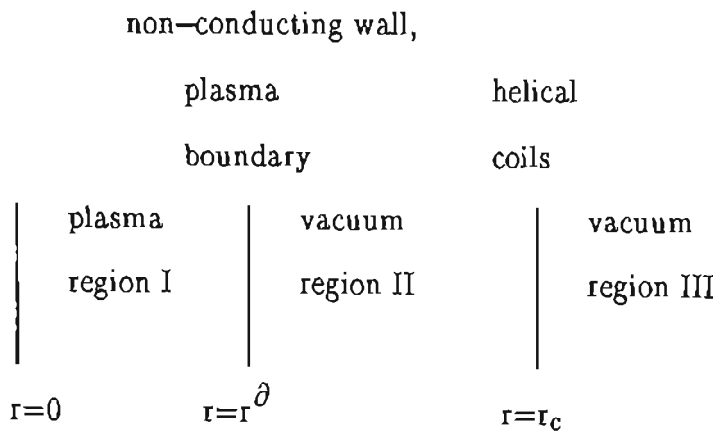

FIGURE 5.3 A configuration where the plasma boundary touches the wall. An external coil is applied in the vacuum region outside.

In region I equations (4.35) – (4.37) give the expressions for the magnetic field. Regions II and III are vacuum and therefore in these two regions,

$$\nabla \wedge \underline{B}_1 = 0 , \tag{5.12}$$

with $\underline{B}_1$ the perturbed magnetic field given by

$$\underline{B}_1 = (B_r(r)\hat{r} + B_{1\theta}(r)\hat{\theta} + B_{1z}(r)\,\hat{z})\, e^{i(m\theta - n\varphi)} .$$

Substituting this in equation (5.12) gives

$$\nabla \wedge B_1 = (\frac{im}{r} B_{1z} + in\epsilon B_{1\theta})\hat{r} - (B'_{1z} + i\epsilon n B_r)\hat{\theta}$$

$$+ (\frac{B_{1\theta}}{r} + B'_{1\theta} - \frac{im}{r} B_r)\hat{z}$$

$$= 0 ,$$

resulting in

$$B_{1\theta} = -\frac{m}{\epsilon n r} B_{1z} \tag{5.13}$$

$$B_r = -\frac{1}{i\epsilon n} B'_{1z} \tag{5.14}$$

$$\frac{B_{1\theta}}{r} + B'_{1\theta} = \frac{im}{r} B_r . \tag{5.15}$$

From

$\nabla . B_1 = 0$, we get

$$B'_r + \frac{1}{r} B_r + \frac{im}{r} B_{1\theta} - in\epsilon B_{1z} = 0 ,$$

or after using equations (5.13) – (5.15),

$$B''_{1z} + \frac{1}{r} B'_{1z} - \frac{m^2}{r^2} B_{1z} - (\epsilon n)^2 B_{1z} = 0 . \tag{5.16}$$

The general solution of this equation is

$$B_{1z} = C_1 I_m(\epsilon n r) + C_2 K_m(\epsilon n r) ,$$

giving (via equations (5.13) – (5.15))

$$-iB_r = C_1 I'_m(\epsilon n r) + C_2 K'_m(\epsilon n r) \tag{5.17}$$

$$-B_{1\theta} = \frac{m}{\epsilon n r}[C_1 I_m(\epsilon n r) + C_2 K_m(\epsilon n r)] \tag{5.18}$$

in region II (derivatives with respect to $\epsilon n r$), and

$$-iB_r = C_3 K'_m(\epsilon n r) \tag{5.19}$$

$$-B_{1\theta} = \frac{m}{\epsilon n r} C_3 K_m(\epsilon n r) \tag{5.20}$$

in region III because $I_m(\epsilon n r)$ and $I'_m(\epsilon n r)$ are divergent when $r \to \infty$.

Connecting these solutions, we get at the vacuum–plasma interface $(r = r^{\partial})$

$$-iB_r^{\partial} = C_1 I'_m(n\epsilon r^{\partial}) + C_2 K'_m(n\epsilon r^{\partial}) \tag{5.21}$$

$$-B_{1\theta}^{\partial} = \frac{m}{\epsilon n r}[C_1 I_m(n\epsilon r^{\partial}) + C_2 K_m(n\epsilon r^{\partial})] , \tag{5.22}$$

where $\underline{B}^{\partial}$ is the solution of the plasma equations (i.e. (4.35) to (4.37)) at the boundary (discussion in section 5.2).

At the coils we get

$$C_1 I'_m(n\epsilon r_c) + C_2 K'_m(n\epsilon r_c) = C_3 K'_m(n\epsilon r_c) ; \tag{5.23}$$

$$-\frac{m}{n\epsilon r_c} C_3 K_m(n\epsilon r_c) + \frac{m}{n\epsilon r_c}[C_1 I_m(n\epsilon r_c) + C_2 K_m(n\epsilon r_c)]$$

$$= j_z^{(m,n)} , \tag{5.24}$$

where use is made of

$$(B_r^{III} - B_r^{II})\Big|_{r_c} = 0 \tag{5.25}$$

$$(B_r^{II} - B_r^{I})\Big|_{r^{\partial}} = 0 \tag{5.26}$$

$$(B_{\theta_1}^{II} - B_{\theta_1}^{I})\Big|_{r^{\partial}} = 0 \tag{5.27}$$

$$(B_{\theta_1}^{III} - B_{\theta_1}^{II})\Big|_{r_c} = j_z^{(m,n)} \qquad (\text{from } \underline{n} \wedge (\underline{B}_2 - \underline{B}_1) = \underline{J}) , \tag{5.28}$$

and $j_z^{(m,n)}$ is the (m,n) fourier component of the surface current density of the coils.

From equations (5.23) and (5.24) we get

$$C_1 = -\frac{\epsilon n r_c}{m} j_z^{(m,n)} / \{[I'_m(\epsilon n r_c)/K'_m(\epsilon n r_c) - I_m(\epsilon n r_c)/K_m(\epsilon n r_c)]\, K_m(\epsilon n r_c)\} . \tag{5.29}$$

When substituted into equation (5.21) we get a relation between the magnetic field at the plasma boundary and the coil current.

We will first look at the situation with zero coil current. In such a situation it is only the constant C_2 that needs to be calculated. In the plasma we have

$$B_r = \frac{1}{r}\frac{\partial a_1}{\partial \theta} = \frac{mi}{r} a_1 \tag{5.30}$$

$$B_{1\theta} = -\frac{\partial a_1}{\partial r} = -a_1' . \tag{5.31}$$

In the vacuum (using the expression for $\underline{B}_1$ used in equation (5.12))

$$B_r = iC_2 K_m'(\epsilon n r) \tag{5.32}$$

$$B_{1\theta} = -\frac{m}{\epsilon n r} C_2 K'(\epsilon n r) . \tag{5.33}$$

Now we get

$$\left.\frac{B_r}{B_{1\theta}}\right|_{r^\partial} = \left.\frac{i\, m a_1}{-r a_1'}\right|_{r^\partial} = \left.\frac{i\ C_2 K_m'(\epsilon n r)}{-\frac{m}{\epsilon n r} C_2 K_m(\epsilon n r)}\right|_{r^\partial} \tag{5.34}$$

or

$$\left.\frac{a_1}{a_1'}\right|_{r^\partial} = r^\partial \frac{\epsilon n}{m^2} K_m'(\epsilon n r^\partial)/K_m(\epsilon n r^\partial) , \tag{5.35}$$

with $r^\partial = r_0 + \delta \cos \chi$.

If a Taylor expansion is done about r_0, we get

$$[a_1(r_0) + \delta \cos\chi\, a_1'(r_0)](K_m(\epsilon n r_0) + \delta \cos\chi\, K_m'(\epsilon n r_0))m^2$$

$$= \epsilon n(r_0 + \delta \cos\chi)[K_m'(\epsilon n r_0) + \delta \cos\chi\, K_m''(\epsilon n r_0)][a_1'(r_0) + \delta \cos\chi\, a_1''(r_0)] .$$

Terms of order ϵ yield

$$\frac{a_1(1)}{a_1'(1)} = \frac{\epsilon n}{m^2} K_m'(\epsilon n)/K_m(\epsilon n) \quad , \quad r_0 = 1 . \tag{5.36}$$

As an example we get (for $\epsilon = 0.1$)

$$\frac{a_1(1)}{a_1'(1)} = -0.501 \text{ when } (m,n) = (2,1) \tag{5.37}$$

and

$$\frac{a_1(1)}{a_1'(1)} = -0.3336 \text{ when } (m,n) = (3,1) .$$

Lazzaro and Nave [92] found a similar result given as $\left.\frac{a_1}{a_1'}\right|_1 = -1/m$. This is just the value found when only the first order terms in the series expansion of $K_m(\epsilon n r)$ is included. Their result is thus valid when $\epsilon << 1$.

For any perturbation δ_0, which agrees with a no–coil situation, C_2 can be calculated from equation (5.34) or $C_2 = -m\delta_0(\left.a_0'\right|_1 + \frac{\epsilon n}{m})/K_m'(\epsilon n)$.

5.5 Deriving expressions for $B_r\big|_1$ and $B_{1\theta}\big|_1$ with an external coil current

Equations (5.21) and (5.22) can be rewritten as

$$B_r\Big|_1 = i\,m a_1\Big|_1 = i\,[C_1 I'_m(\epsilon n) + C_2 K'_m(\epsilon n)] \tag{5.38}$$

$$B_{1\theta}\Big|_1 = -a'_1\Big|_1 = -\frac{m}{\epsilon n}[C_1 I_m(\epsilon n) + C_2 K_m(\epsilon n)]\,, \tag{5.39}$$

where use is made of the plasma solutions for B_r^{∂} and $B_{1\theta}^{\partial}$ i.e. equations (5.30) and (5.31). Equations (5.38) and (5.39) can now be rewritten as

$$\frac{m\,a\Big|_1}{K'_m(\epsilon n)} = C_1 \frac{I'_m(\epsilon n)}{K'_m(\epsilon n)} + C_2 \tag{5.40}$$

$$\frac{\epsilon\, n\; a'_1\Big|_1}{m}\,\frac{1}{K_m(\epsilon n)} = C_1 \frac{I_m(\epsilon n)}{K_m(\epsilon n)} + C_2\,. \tag{5.41}$$

Subtracting equation (5.41) from (5.40) gives

$$\frac{m\,a_1\Big|_1}{K'_m(\epsilon n)} - \frac{\epsilon n}{m}\,\frac{a'_1\Big|_1}{K_m(\epsilon n)} = C_1\left[\frac{I'_m(\epsilon n)}{K'_m(\epsilon n)} - \frac{I_m(\epsilon n)}{K_m(\epsilon n)}\right]. \tag{5.42}$$

When C_1 (i.e. equation (5.29)) is substituted in this equation, we get

$$\frac{m\,a_1\Big|_1}{K'_m(\epsilon n)} - \frac{\epsilon n}{m}\,\frac{a_1\Big|_1}{K_m(\epsilon n)} = -\frac{\epsilon n r_c}{m}\, j_z^{(m,n)}\,\frac{L(\epsilon n)}{L(\epsilon n r_c)}\,\frac{1}{K_m(\epsilon n r_c)}\,, \tag{5.43}$$

with

$$L(x) = \frac{I'_m(x)}{K'_m(x)} - \frac{I_m(x)}{K_m(x)} . \qquad (5.44)$$

Rewriting equation (5.43) results in

$$\left.\frac{a_1}{a'_1}\right|_1 = \frac{K'_m(\epsilon n)}{K_m(\epsilon n)} \frac{\epsilon n}{m^2} \left[1 - \frac{r_c j_z^{(m,n)}}{a'_1} \frac{L(\epsilon n)}{L(\epsilon r_c)} \frac{K_m(\epsilon n)}{K_m(\epsilon r_c)} \right] . \qquad (5.45)$$

When $j_z^{(m,n)} = 0$, we get

$$\left.\frac{a_1}{a'_1}\right|_1 = \frac{K'_m(\epsilon n)}{K_m(\epsilon n)} \frac{\epsilon n}{m^2} ,$$

which has been derived as equation (5.36) for the no–coil situation. The parameter $\left.\frac{a_1}{a'_1}\right|_1$ is of major importance in the rest of the study. It should be remembered that it is proportional to $B_r/B_{1\theta}\Big|_1$.

5.6 Deriving the coil current in the cylindrical approximation

On the cylinder we shall use the coil winding law [83]

$$\theta = \alpha z + (p-1)\,\pi/\ell , \quad p = 1, 2 \ldots , 2\ell \text{ with } \ell = \frac{m}{n} \qquad (5.46)$$

and let

$$\underline{J} = \underline{f}\,(r,\theta,z)\,\delta\,(r-r_c)\,\delta\,(\theta - \alpha z - (p-1)(\pi/\ell)) , \qquad (5.47)$$

where $\underline{f}(r,\theta,z)$ is to be determined.

On Tokoloshe tokamak, the windings are not perfectly helical, but have an additional term to account for the shift of field lines due to toroidicity. The general winding law is $\theta = \alpha\varphi + \Delta_\ell \sin\theta + \frac{\pi}{\ell}(p-1)$. The current density may be modelled in the present cylindrical case by [83]

$$\underline{J} = \underline{f}(r,\theta,z)\ \delta(r-r_c)\ \delta(\theta - \alpha z - (p-1)\tfrac{\pi}{\ell})\ . \tag{5.48}$$

The current in the coil is just

$$I_\ell = \int \underline{J}\ .\ d\underline{S}. \tag{5.49}$$

Any surface through which the whole current flows can be used in the above equation:

$$\begin{aligned} I_\ell &= \int J_z\, r\,dr\,d\theta \\ &= \int f_z\ \delta(r-r_c)\ \delta(\theta - g(z))\, r\,dr\,d\theta \\ &= r_c\, f_z\,(b,\ \theta = g(z),\ z) \end{aligned} \tag{5.50}$$

or $$\begin{aligned} I_\ell &= \int J_\theta\, dr\, dz \\ &= \int f_\theta\,(r_c,\theta,z)\ \delta\,(\theta - g(z))\, dz \end{aligned} \tag{5.51}$$

with $g(z) = \alpha z + (p-1)\pi/\ell$.

Let

$$g(z) = y\ . \tag{5.52}$$

Now we have, from equation (5.52),

$$\frac{\partial g}{\partial z}\,dz \;=\; dy \;\text{ or }\; \alpha\,dz = dy\,.$$

Equation (5.51) now becomes

$$\begin{aligned} I_\ell &= \int f_\theta\,(r_c,\theta,z)\;\delta\,(\theta - y)\,\frac{1}{\alpha}\,dy \\ &= f_\theta\,(r_c,\theta = y, z(y))/\alpha \quad (\delta(x) = \delta(-x))\;. \end{aligned} \tag{5.53}$$

From equations (5.50) and (5.53) we get $f_\theta = \alpha\, I_\ell$ and $f_z = I_\ell/r_c$. The current density can now be written as

$$\begin{aligned} \underline{J} &= (0,\alpha\, I_\ell,\, I_\ell/r_c)\;\delta\,(r-r_c)\;\delta\,(\theta - g(z)) \\ &= I_\ell\,(0,\alpha,(1/r_c))\;\delta\,(r-r_c)\;\delta\,(\theta - \alpha\, z - (p-1)\,\pi/\ell)\,. \end{aligned} \tag{5.54}$$

In the above calculations we used an external coil to generate a magnetic field which is of the same helicity as the tearing mode that we want to affect.

5.7 The (m,n) Fourier component of J_z

To be able to solve for B_r^{∂} (with coil current), we need the Fourier mode $j_z^{(m,n)}$ in equation (5.24).

Express J_z as a Fourier sum:

$$J_z = \sum_{n=-\infty}^{\infty} \sum_{m=0}^{\infty} \text{Real } (j_z^{(m,n)} e^{i(m\theta - n\varphi)}) .$$

We know that

$$j_z^{(m,n)} = \frac{1}{4\pi^2} \int_{\theta=0}^{2\pi} \int_{\varphi=0}^{2\pi} J_z e^{-i(m\theta - n\varphi)} d\theta d\varphi . \tag{5.55}$$

for $m,n \neq 0$.

Using equation (5.54) , we get

$$j_z^{(m,n)} = \frac{1}{4\pi^2} I_{\ell/r_c} \delta(r-r_c) \int_{\theta=0}^{2\pi} \int_{\varphi=0}^{2\pi} \delta(\theta - \alpha z - (p-1)\pi/\ell) e^{i(m\theta - n\varphi)} d\theta d\varphi$$

$$= \frac{1}{2\pi} I_{\ell/r_c} e^{-i(p-1)\frac{\pi}{\ell} m} \tag{5.56}$$

with $\alpha = \frac{k}{m}$, $z = R_0 \varphi$, k the wave number.

This is true if only one coil is used. In a situation like Tokoloshe, we have four coils for the $\ell=2$ case. The configuration was shown in Figure 5.2.

Now, with $I_{\ell_{tot}} = \sum_{p=1}^{4} (-1)^p I_\ell$, we get

$$j_z^{(m,n)} = \frac{I_\ell}{2\pi r_c} \sum_{k=1}^{2\ell} (-1)^k e^{-in(p-1)\pi} . \tag{5.57}$$

The sum in (5.57) gives 2ℓ if n is odd and zero if n is even. The resulting current density component is just

$$j_z^{(m,n)} = (-1)^{m-n1} \frac{I_\ell}{\pi r_c} \frac{m}{n} . \qquad (5.58)$$

When the $\Delta_\ell \sin \theta$ term (in equation (5.48)) is included in the calculations, an expression can be derived modelling the situation on a Tokamak (Appendix F). This was done by Hansen [79]. In that case the expression for $j_z^{(m,n)}$ is given by

$$j_z^{(m,n)} = (-1)^{m-n1} \frac{I_\ell}{\pi r_c} \frac{m}{n} J_{m-n1}(n\ell\Delta_\ell) , \qquad (5.59)$$

where J_{m-n1} is a Bessel function. In the case of the (2,1) coil the value of Δ_ℓ is about 48^0 and for the (3,1) coils it is 0^0, on Tokoloshe.

5.8 Including the rotational frequency in the boundary conditions

In the previous sections it was assumed that there was a non–conducting wall between the plasma and the vacuum. For such a configuration it was possible to derive an expression for $\left.\frac{a_1}{a_1'}\right|_1$ in the case of no external coil as well as when one was included. Both these calculations excluded time dependence, reducing it to a time independent situation, i.e. when the plasma is locked and non–rotating.

Another case that can be studied is the one where the plasma rotation frequency is infinite with a partly conducting wall or, equivalently, when a super–conducting wall is included. Then $\left.\frac{a_1}{a_1'}\right|_1 = 0$. This was discussed in section 5.3. No external coil is assumed to exist in this case.

When finite rotational frequency is included in the above case, where the plasma touches the non–conducting wall, difficulties arise [93]. However, when a vacuum region is included between the plasma and the wall, the expression derived by Gimblett [71] can be used at the wall. This is

$$\frac{i\omega\tau_w}{r_w} B_r = B_r' \Big|_{\text{inside}}^{\text{outside}} \tag{5.60}$$

$$B_r^{\text{inside}} = B_r^{\text{outside}}, \tag{5.61}$$

assuming a "thin" wall approximation, with ω the mode frequency, $\tau_w = r_w\delta_w/\eta_w$ the resistive wall time, and r_w the position of the resistive wall, δ_w the wall thickness and η_w the wall resistivity. The frequency can be written as $\omega_1 m - \omega_2 n$ where ω_1 is the poloidal rotation and ω_2 the toroidal rotation. This is found when $B_r e^{i(m\theta - n\varphi)}$ is used in $\frac{\partial B_r}{\partial t} = \eta_w \frac{\partial^2 B_r}{\partial r^2}$, and $\theta = \theta(t)$, $\varphi = \varphi(t)$. The following configuration is now assumed

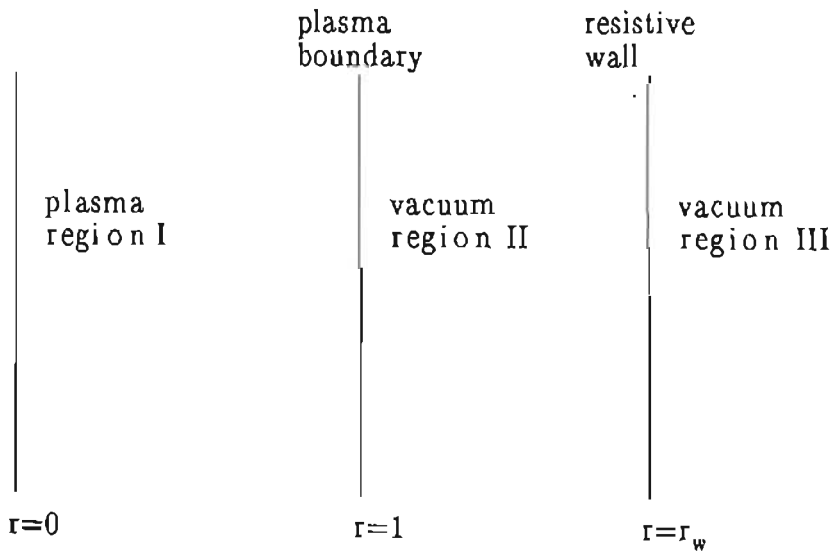

FIGURE 5.4 The configuration used when finite rotational frequency in included.

From the equations (5.17), (5.18), (5.30), (5.31) we have the following expressions

$$B_r^I = i\frac{m}{r}a_1$$

$$B_{1\theta}^I = -a_1'$$

$$B_r^{II} = i[C_1 I_m'(\epsilon n r) + C_2 K_m'(\epsilon n r)]$$

$$B_{1\theta}^{II} = -\frac{m}{\epsilon n r}[C_1 I_m(\epsilon n r) + C_2 K_m(\epsilon n r)]$$

$$B_r^{III} = i C_3 K_m'(\epsilon n r)$$

$$B_{1\theta}^{III} = -\frac{m}{\epsilon n r} C_3 K_m(\epsilon n r) .$$

Now we have

$$B_r^I\Big|_1 = B_r^{II}\Big|_1$$

$$B_{1\theta}^I\Big|_1 = B_{1\theta}^{II}\Big|_1$$

at the plasma edge and

$$B_r^{II}\Big|_{r_w} = B_r^{III}\Big|_{r_w}$$

$$\frac{i\omega\tau_w}{r_w} B_r^{III}\Big|_{r_w} = (B_r'^{III} - B_r'^{II})\Big|_{r_w}$$

at the thin wall.

Let $\omega\tau_w = \Omega$. Then, with a_1 and a_1' evaluated at $r=1$, we get

$$ma_1 = C_1 I_m'(\epsilon n) + C_2 K_m'(\epsilon n) \tag{5.62}$$

$$a_1' = \frac{m}{\epsilon n}(C_1 I_m(\epsilon n) + C_2 K_m(\epsilon n)) \tag{5.63}$$

$$C_1 I_m'(\epsilon n r_w) + C_2 K_m'(\epsilon n r_w) = C_3 K_m'(\epsilon n r_w) \tag{5.64}$$

$$\frac{i\Omega}{r_w} C_3 K_m'(\epsilon n r_w) = [C_3 K_m''(\epsilon n r_w) - C_1 I_m''(\epsilon n r_w) - C_2 K_m''(\epsilon n r_w)]\epsilon n . \tag{5.65}$$

This results in

$$\left.\frac{a_1}{a_1'}\right|_1 = \frac{C_1 I_m'(\epsilon n) + C_2 K_m'(\epsilon n)}{\frac{m^2}{\epsilon n}(C_1 I_m(\epsilon n) + C_2 K_m(\epsilon n))} \tag{5.66}$$

from equations (5.62) and (5.63).

From equation (5.64), we get

$$C_1 \frac{I_m'(\epsilon n r_w)}{K_m'(\epsilon n r_w)} + C_2 = C_3 . \tag{5.67}$$

Rewriting equation (5.65) results in

$$C_3 \left[\frac{i\Omega}{r_w \epsilon n} \frac{K_m'(\epsilon n r_w)}{K_m''(\epsilon n r_w)} - 1 \right] = -C_2 - C_1 \frac{I_m''(\epsilon n r_w)}{K_m''(\epsilon n r_w)} . \tag{5.68}$$

When equation (5.67) is substituted in this equation, we get

$$-C_1\left[\frac{I_m'(\epsilon n r_w)}{K_m'(\epsilon n r_w)}\left[\frac{i\Omega}{r_w \epsilon n}\frac{K_m'(\epsilon n r_w)}{K_m''(\epsilon n r_w)}-1\right]+\frac{I_m''(\epsilon n r_w)}{K_m''(\epsilon n r_w)}\right]=C_2\frac{\Omega i}{r_w \epsilon n}\frac{K_m'(\epsilon n r_w)}{K_m''(\epsilon n r_w)}$$

which can also be written as

$$\begin{aligned} C_2 &= -\frac{r_w \epsilon n}{i\Omega}\frac{K_m''(\epsilon n r_w)}{K_m'(\epsilon n r_w)}C_1\left[\frac{I_m'(\epsilon n r_w)}{K_m'(\epsilon n r_w)}\left[\frac{i\Omega}{r_w \epsilon n}\frac{K_m'(\epsilon n r_w)}{K_m''(\epsilon n r_w)}-1\right]+\frac{I_m''(\epsilon n r_w)}{K_m''(\epsilon n r_w)}\right] \\ &= A\,C_1, \end{aligned} \tag{5.69}$$

with

$$A = -\frac{r_w \epsilon n}{i\Omega}\frac{K_m''(\epsilon n r_w)}{K_m'(\epsilon n r_w)}\left[\frac{I_m'(\epsilon n r_w)}{K_m'(\epsilon n r_w)}\left[\frac{i\Omega}{r_w \epsilon n}\frac{K_m'(\epsilon n r_w)}{K_m''(\epsilon n r_w)}-1\right]+\frac{I_m''(\epsilon n r_w)}{K_m''(\epsilon n r_w)}\right]. \tag{5.70}$$

This results in

$$\left.\frac{a_1}{a_1'}\right|_1 = \frac{I_m'(\epsilon n) + A\,K_m'(\epsilon n)}{\frac{m^2}{\epsilon n}\,(I_m(\epsilon n) + A\,K_m(\epsilon n))}, \tag{5.71}$$

using equation (5.66).

Equation (5.71) can be rewritten as

$$\left.\frac{a_1}{a_1'}\right|_1 = \frac{B + iC}{D + iE}, \tag{5.72}$$

with

$$B = I_m'(\epsilon n) - \frac{I_m'(\epsilon n r_w)}{K_m'(\epsilon n r_w)}K_m'(\epsilon n)$$

$$D = \frac{m^2}{\epsilon n}\left[I_m(\epsilon n) - \frac{I'_m(\epsilon n r_w)}{K'_m(\epsilon n r_w)} K_m(\epsilon n) \right]$$

$$C = -\frac{\epsilon n r_w}{\Omega}\left[\frac{K''_m(\epsilon n r_w)}{K'_m(\epsilon n r_w)} \frac{I'_m(\epsilon n r_w)}{K'_m(\epsilon n r_w)} - \frac{I''_m(\epsilon n r_w)}{K'_m(\epsilon n r_w)} \right] K'_m(\epsilon n)$$

$$E = -\frac{m^2 r_w}{\Omega}\left[\frac{K''_m(\epsilon n r_w)}{K'_m(\epsilon n r_w)} \frac{I'_m(\epsilon n r_w)}{K'_m(\epsilon n r_w)} - \frac{I''_m(\epsilon n r_w)}{K'_m(\epsilon n r_w)} \right] K_m(\epsilon n) .$$

The magnitude of $\left.\frac{a_1}{a'_1}\right|_1$ is thus

$$\left.\frac{a_1}{a'_1}\right|_1 = \pm \sqrt{\frac{B^2 + C^2}{D^2 + E^2}} . \qquad (5.73)$$

In the case of $\Omega \to 0$, we get from equation (5.72)

$$\left.\frac{a_1}{a'_1}\right|_1 = \frac{\epsilon n}{m^2} \frac{K'_m(\epsilon n)}{K_m(\epsilon n)}$$

which was derived earlier for the case of a locked mode (i.e. equation (5.36)). When $\Omega \to \infty$, equation (5.73) reduces to $\left.\frac{a_1}{a'_1}\right|_1 = 0$ when $r_w \to 1$. This is in agreement with the situation where the mode is rotating infinitely fast and there is no vacuum on the inside of the resistive wall, i.e. when the wall is seen by the plasma as superconducting. This was discussed in section 5.3.

When $\Omega \to \infty$ and $r_w \neq 1$, we get

$$\left.\frac{a_1}{a'_1}\right|_1 = \frac{\epsilon n}{m^2} \frac{K'_m(\epsilon n)}{K_m(\epsilon n)} \frac{\left[\frac{I'_m(\epsilon n)}{K'_m(\epsilon n)} - \frac{I'_m(\epsilon n r_w)}{K'_m(\epsilon n r_w)} \right]}{\left[\frac{I_m(\epsilon n)}{K_m(\epsilon n)} - \frac{I'_m(\epsilon n r_w)}{K'_m(\epsilon n r_w)} \right]} , \qquad (5.74)$$

using equation (5.72).

When $r_w \to 1$, it reduces to $\left.\frac{a_1}{a_1'}\right|_1 = 0$, and when $r_w \to \infty$ we get

$$\left.\frac{a_1}{a_1'}\right|_1 = \frac{\epsilon n}{m^2}\frac{K_m'(\epsilon n)}{K_m(\epsilon n)},$$

as in the case of no wall. This result is arrived at when the asymptotic solutions of $I_m'(x)$ and $K_m'(x)$ are used and L'Hospital's rule is applied.

In the following table the values of $\left.\frac{a_1}{a_1'}\right|_1$ are tabled in the case of $\epsilon = 0.1$ and 0.5, (m,n) = (2,1) and with r_w(wall radius) = 1.1 and 1.01 where r=1 is the plasma radius.

	$\epsilon = 0.1$		$\epsilon = 0.5$	
Ω	$r_w = 1.1$	$r_w = 1.01$	$r_w = 1.1$	$r_w = 1.01$
0	–0.501	–0.501	–0.527	–0.527
1	–0.462	–0.447	–0.489	–0.474
2	–0.384	–0.353	–0.411	–0.377
5	–0.227	–0.185	–0.246	–0.2
10	–0.146	–0.104	–0.158	–0.106
20	–0.110	–0.05	–0.118	–0.054
∞	–0.094	–0.01	–0.1	–0.011

Table 5.1

It is also shown graphically in Figure 5.5.

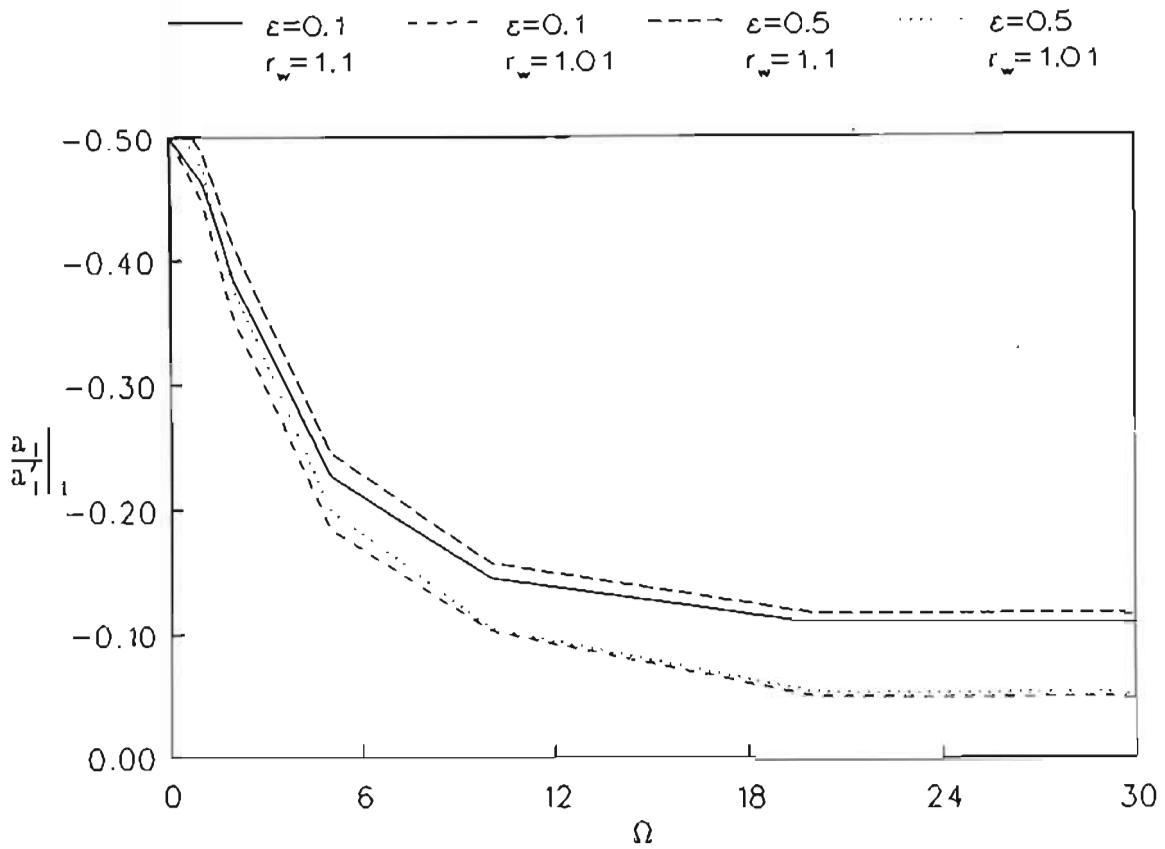

FIGURE 5.5 The graph of $\left.\frac{a_1}{a_1'}\right|_1$ against Ω for $r_w = 1.1$ and 1.01. When the distance between the plasma boundary and the wall increases, the value of $\left.\frac{a_1}{a_1'}\right|_1$ deviates further from zero.

The values of $\left.\frac{a_1}{a_1'}\right|_1$ increases in magnitude when the vacuum region between the plasma boundary and the wall is increased. The parameter ϵ does not have a significant effect.

Lazzaro and Nave [86] found a result similar to equation (5.73). They found, in the case of a resistive wall,

$$\left.\frac{a_1'}{a_1}\right|_1 = -\frac{m(1 + f(1/r_w)^{2m})}{(1 - f(1/r_w)^{2m})}, \qquad (5.75)$$

with

$$f = \frac{\omega^2\tau_v - im\omega\tau_v}{(\omega^2\tau_v^2 + m^2)},$$

$$\tau_v = \mu_0\sigma\delta_w r_w/2,$$

σ the vessel conductivity.

For a perfectly conducting wall they found (f=1)

$$\left.\frac{a_1'}{a_1}\right|_1 = -\frac{m(1 + (1/r_w)^{2m})}{(1 - (1/r_w)^{2m})}.$$

When $r_w = 1$ this reduces to $\left.\frac{a_1'}{a_1}\right|_1 = 0$. When r_w is shifted away from r=1, this value increases (with negative sign) as was shown in Figure 5.5. When f=0 (agreeing with $\Omega = 0$) in equation (5.75) we get $\left.\frac{a_1'}{a_1}\right|_1 = -1/m$, which agrees with our locked results. For different frequencies the value of $\left.\frac{a_1'}{a_1}\right|_1$ varies between these two extremes in a similar fashion to what has been shown in Figure 5.5.

5.9 Including an external coil with rotational frequency

When an external coil is included in the vacuum region outside the resistive wall in Figure 5.4, the following equations are valid in the different regions (with region IV on the outside of the coil):

$$B_r^I = i\frac{m}{r} a_1$$

$$B_{1\theta}^I = -a_1'$$

$$B_r^{II} = i[C_1 I_m'(\epsilon nr) + C_2 K_m'(\epsilon nr)]$$

$$B_{1\theta}^{II} = \frac{-m}{\epsilon n r}[C_1 I_m(\epsilon nr) + C_2 K_m(\epsilon nr)]$$

$$B_r^{III} = i[C_3 I_m'(\epsilon nr) + C_4 K_m'(\epsilon nr)]$$

$$B_{1\theta}^{III} = \frac{-m}{\epsilon n r}[C_3 I_m(\epsilon nr) + C_4 K_m(\epsilon nr)]$$

$$B_r^{IV} = i C_5 K_m'(\epsilon nr)$$

$$B_{1\theta}^{IV} = -\frac{m}{\epsilon n r} C_5 K_m(\epsilon nr) .$$

These equations can now be coupled across the different boundaries, giving

$$B_r^I\Big|_1 = B_r^{II}\Big|_1$$

$$B_{1\theta}^I\Big|_1 = B_{1\theta}^{II}\Big|_1$$

$$B_r^{II}\Big|_{r_w} = B_r^{III}\Big|_{r_w}$$

$$\frac{i\omega\tau_w}{r_w} B_r^{III}\Big|_{r_w} = (B_r'^{III} - B_r'^{II})\Big|_{r_w}$$

$$B_r^{III}\Big|_{r_c} = B_r^{IV}\Big|_{r_c}$$

$$B_{1\theta}^{III}\Big|_{r_c} - B_{1\theta}^{IV}\Big|_{r_c} = -j_z^{(m,n)},$$

which can be written as

$$m\, a_1 = C_1 I'_m(\epsilon n) + C_2 K'_m(\epsilon n) \tag{5.76}$$

$$-a'_1 = \frac{-m}{\epsilon n}\left[C_1 I_m(\epsilon n) + C_2 K_m(\epsilon n)\right] \tag{5.77}$$

$$C_1 I'_m(\epsilon n r_w) + C_2 K'_m(\epsilon n r_w) = C_3 I'_m(\epsilon n r_w) + C_4 K'_m(\epsilon n r_w) \tag{5.78}$$

$$\frac{i\omega\tau_w}{r_w}\left[C_1 I'_m(\epsilon n r_w) + C_2 K'_m(\epsilon n r_w)\right] = \Big\{\left[C_3 I''_m(\epsilon n r_w) + C_4 K''_m(\epsilon n r_w)\right] - C_1 I''_m(\epsilon n r_w) - C_2 K''_m(\epsilon n r_w)\Big\}\,\epsilon n \tag{5.79}$$

$$C_3 I'_m(\epsilon n r_c) + C_4 K'_m(\epsilon n r_c) = C_5 K'_m(\epsilon n r_c) \tag{5.80}$$

$$-C_3 I_m(\epsilon n r_c) - C_4 K_m(\epsilon n r_c) + C_5 K_m(\epsilon n r_c) = \frac{-\epsilon n r_c}{m} j_z^{(m,n)} . \tag{5.81}$$

The quantities a_1 and a'_1 are evaluated at $r=1$.

From equations (5.76) and (5.77)

$$\left.\frac{a_1}{a'_1}\right|_1 = \frac{C_1 I'_m(\epsilon n) + C_2 K'_m(\epsilon n)}{\frac{m^2}{\epsilon n}\left[C_1 I_m(\epsilon n) + C_2 K_m(\epsilon n)\right]} \tag{5.82}$$

From equation (5.78) we get

$$\frac{I'_m(\epsilon n r_w)}{K'_m(\epsilon n r_w)}\left[C_1 - C_3\right] = C_4 - C_2 . \tag{5.83}$$

Equation (5.79) can be written as

$$-\frac{i\Omega}{r_w \epsilon n}\left[C_1 \frac{I'_m(\epsilon n r_w)}{K''_m(\epsilon n r_w)} + C_2 \frac{K'_m(\epsilon n r_w)}{K''_m(\epsilon n r_w)}\right] = \frac{I''_m(\epsilon n r_w)}{K''_m(\epsilon n r_w)}[C_1 - C_3] + C_2 - C_4 \tag{5.84}$$

with

$\Omega = \omega T_w$ as before.

From equation (5.80) we get

$$C_3 \frac{I'_m(\epsilon n r_c)}{K'_m(\epsilon n r_c)} = C_5 - C_4 \tag{5.85}$$

and from equation (5.81)

$$-C_3 \frac{I_m(\epsilon n r_c)}{K_m(\epsilon n r_c)} = -\frac{\epsilon n r_c}{m} j_z^{(m,n)} / K_m(\epsilon n r_c) + C_4 - C_5 . \tag{5.86}$$

Now, if equations (5.85) and (5.86) are added, we get

$$C_3 \left[\frac{I'_m(\epsilon n r_c)}{K'_m(\epsilon n r_c)} - \frac{I_m(\epsilon n r_c)}{K_m(\epsilon n r_c)}\right] = -\frac{\epsilon n r_c}{m} \frac{j_z^{(m,n)}}{K_m(\epsilon n r_c)} . \tag{5.87}$$

If equations (5.84) and (5.83) are added in the same way, we get

$$(C_1 - C_3)\left[\frac{I'_m(\epsilon n r_w)}{K'_m(\epsilon n r_w)} - \frac{I''_m(\epsilon n r_w)}{K''_m(\epsilon n r_w)}\right] = \frac{i\Omega}{\epsilon n r_w}\left[C_1 \frac{I'_m(\epsilon n r_w)}{K''_m(\epsilon n r_w)} + C_2 \frac{K'_m(\epsilon n r_w)}{K''_m(\epsilon n r_w)}\right] . \tag{5.88}$$

When C_3 is substituted from equation (5.87) in here, we get

$$C_1\left[\frac{I'_m(\epsilon n r_w)}{K'_m(\epsilon n r_w)}-\frac{I''_m(\epsilon n r_w)}{K''_m(\epsilon n r_w)}-\frac{i\Omega}{r_w\epsilon n}\frac{I'_m(\epsilon n r_w)}{K''_m(\epsilon n r_w)}\right]+\frac{\epsilon n r_c}{m}\frac{j_z^{(m,n)}}{K_m(\epsilon n r_c)}\frac{1}{L(\epsilon n r_c)}\cdot$$

$$\left[\frac{I'_m(\epsilon n r_w)}{K'_m(\epsilon n r_w)}-\frac{I''_m(\epsilon n r_w)}{K''_m(\epsilon n r_w)}\right]$$

$$= C_2\frac{i\Omega}{\epsilon n r_w}\frac{K'_m(\epsilon n r_w)}{K''_m(\epsilon n r_w)}, \tag{5.89}$$

with

$$L(X) = \frac{I'_m(X)}{K'_m(X)}-\frac{I_m(X)}{K_m(X)}. \tag{5.90}$$

This can also be written as

$$C_2 = \frac{\epsilon n r_w}{i\Omega}\frac{K''_m(\epsilon n r_w)}{K'_m(\epsilon n r_w)}\left\{\left[S(\epsilon n r_w)-\frac{i\Omega}{\epsilon n r_w}\frac{I'_m(\epsilon n r_w)}{K''_m(\epsilon n r_w)}\right]C_1+\frac{\epsilon n r_c}{m}\frac{j_z^{(m,n)}}{K_m(\epsilon n r_c)}\cdot\right.$$

$$\left.\frac{S(\epsilon n r_w)}{L(\epsilon n r_c)}\right\}, \tag{5.91}$$

with

$$S(X) = \frac{I'_m(X)}{K'_m(X)}-\frac{I''_m(X)}{K''_m(X)}. \tag{5.92}$$

or

$$C_2 = A\,C_1 + B\,j_z^{(m,n)} \tag{5.93}$$

with

$$A = \frac{r_w\epsilon n}{i\Omega}\frac{K''_m(\epsilon n r_w)}{K'_m(\epsilon n r_w)}\left[S(\epsilon n r_w)-\frac{i\Omega}{\epsilon n r_w}\frac{I'_m(\epsilon n r_w)}{K''_m(\epsilon n r_w)}\right] \tag{5.94}$$

$$B = \frac{r_w \epsilon n}{i\Omega} \frac{K_m^n(\epsilon n r_w)}{K_m'(\epsilon n r_w)} \frac{\epsilon n r_c}{m} \frac{1}{K_m(\epsilon n r_c)} \frac{S(\epsilon n r_w)}{L(\epsilon n r_c)} . \tag{5.95}$$

We can also write equation (5.76) as

$$\frac{m a_1}{K_m'(\epsilon n)} = C_1 \frac{I_m'(\epsilon n)}{K_m'(\epsilon n)} + C_2 \tag{5.96}$$

and equation (5.77) as

$$\frac{\epsilon n}{m} \frac{a_1'}{K_m(\epsilon n)} = C_1 \frac{I_m(\epsilon n)}{K_m(\epsilon n)} + C_2 . \tag{5.97}$$

If equation (5.97) is subtracted from (5.96), it results in

$$\frac{m a_1}{K_m'(\epsilon n)} - \frac{\epsilon n}{m} \frac{a_1'}{K_m(\epsilon n)} = C_1 \left(\frac{I_m'(\epsilon n)}{K_m'(\epsilon n)} - \frac{I_m(\epsilon n)}{K_m(\epsilon n)} \right)$$

$$= L(\epsilon n)\, C_1 \tag{5.98}$$

or

$$\frac{a_1}{a_1'} - \frac{\epsilon n}{m^2} \frac{K_m'(\epsilon n)}{K_m(\epsilon n)} = \frac{K_m'(\epsilon n)}{m a_1'} L(\epsilon n)\, C_1 . \tag{5.99}$$

When equations (5.93) and (5.99) are substituted into (5.76), we get

$$m a_1 = C_1 I_m'(\epsilon n) + A\, C_1 K_m'(\epsilon n) + B\, j_z^{(m,n)} K_m'(\epsilon n)$$

$$= \frac{m a_1'}{K_m'(\epsilon n)} \frac{1}{L(\epsilon n)} \left(\frac{a_1}{a_1'} - \frac{\epsilon n}{m^2} \frac{K_m'(\epsilon n)}{K_m(\epsilon n)} \right) \left(I_m'(\epsilon n) + A\, K_m'(\epsilon n) \right)$$

$$+ B\, j_z^{(m,n)} K_m'(\epsilon n)$$

or

$$\frac{a_1}{a_1'} = \left(\frac{a_1}{a_1'} \frac{1}{K_m'(\epsilon n)} \frac{1}{L(\epsilon n)} - \frac{\epsilon n}{m^2} \frac{1}{K_m(\epsilon n)} \frac{1}{L(\epsilon n)} \right) \left(I_m'(\epsilon n) + A\, K_m'(\epsilon n) \right)$$

$$+ B\, j_z^{(m,n)}\, K_m'(\epsilon n) \frac{1}{m a_1'}$$

$$= \left(\frac{a_1}{a_1'} \frac{1}{K_m'(\epsilon n)} \frac{1}{L(\epsilon n)} - \frac{\epsilon n}{m^2} \frac{1}{K_m(\epsilon n)} \frac{1}{L(\epsilon n)} \right) \left(I_m'(\epsilon n) + A_1\, K_m'(\epsilon n) \right.$$

$$\left. \frac{r_w}{i\Omega} A_2\, K_m'(\epsilon n) \right) + \frac{r_w}{\Omega i} B_1 \frac{j_z^{(m,n)} K_m'(\epsilon n)}{m a_1'} \qquad (5.100)$$

with

$$A_1 = -\frac{I_m'(\epsilon n r_w)}{K_m'(\epsilon n r_w)}, \qquad A_2 = \epsilon n \frac{K_m''(\epsilon n r_w)}{K_m'(\epsilon n r_w)} S(\epsilon n r_w)$$

$$B_1 = \frac{(\epsilon n)^2}{m} r_c \frac{1}{K_m(\epsilon n r_c)} \frac{K_m''(\epsilon n r_w)}{K_m'(\epsilon n r_w)} \frac{S(\epsilon n r_w)}{L(\epsilon n r_c)}.$$

Now, rewriting (5.100) results in

$$\frac{a_1}{a_1'} - \left(\frac{a_1}{a_1'} \frac{1}{K_m'(\epsilon n)} \frac{1}{L(\epsilon n)} - \frac{\epsilon n}{m^2} \frac{1}{K_m(\epsilon n)} \frac{1}{L(\epsilon n)} \right) \left(I_m'(\epsilon n) + A_1\, K_m'(\epsilon n) \right)$$

$$= \frac{r_w}{i\Omega} \left[\left(\frac{a_1}{a_1'} \frac{1}{K_m'(\epsilon n)} \frac{1}{L(\epsilon n)} - \frac{\epsilon n}{m^2} \frac{1}{K_m(\epsilon n)} \frac{1}{L(\epsilon n)} \right) A_2\, K_m'(\epsilon n) \right.$$

$$\left. + B_1 \frac{j_z^{(m,n)}}{m a_1'} K_m'(\epsilon n) \right].$$

or

$$\frac{i\Omega}{r_w} = \left(\frac{a_1}{a_1'} \frac{1}{K_m'(\epsilon n)} \frac{1}{L(\epsilon n)} - \frac{\epsilon n}{m^2} \frac{1}{K_m(\epsilon n)} \frac{1}{L(\epsilon n)} \right) \epsilon n \frac{K_m^n(\epsilon n r_w)}{K_m'(\epsilon n r_w)} S(\epsilon n r_w) K_m'(\epsilon n)$$

$$+ \frac{(\epsilon n)^2}{m^2} r_c \frac{K_m'(\epsilon n)}{K_m(\epsilon n r_c)} \frac{K_m^n(\epsilon n r_w)}{K_m'(\epsilon n r_c)} \frac{S(\epsilon n r_w)}{L(\epsilon n r_c)} \frac{j_z^{(m,n)}}{a_1'}$$

$$\Big[\frac{a_1}{a_1'} \left(1 - \frac{1}{L(\epsilon n)} \frac{1}{K_m'(\epsilon n)} \left(I_m'(\epsilon n) - \frac{I_m'(\epsilon n r_w)}{K_m'(\epsilon n r_w)} K_m'(\epsilon n) \right) \right)$$

$$+ \frac{\epsilon n}{m^2} \frac{1}{K_m(\epsilon n)} \frac{1}{L'(\epsilon n)} \left((I_m'(\epsilon n) - \frac{I_m'(\epsilon n r_w)}{K_m'(\epsilon n r_w)} K_m'(\epsilon n) \right) \Big] . \tag{5.101}$$

Equation (5.101) can also be written as

$$\frac{i\Omega}{r_w} = \frac{\left.\frac{a_1}{a_1'}\right|_1 A + B + C \frac{j_z^{(m,n)}}{a_1'}}{\left.\frac{a_1}{a_1'}\right|_1 D + E} \tag{5.102}$$

or

$$\left.\frac{a_1}{a_1'}\right|_1 = \frac{B + C \frac{j_z^{(m,n)}}{a_1'} - iE \frac{\Omega}{r_w}}{i D \frac{\Omega}{r_w} - A} , \tag{5.103}$$

with

$$A = \frac{\epsilon n}{L(\epsilon n)} \frac{K_m^n(\epsilon n r_w)}{K_m'(\epsilon n r_w)} S(\epsilon n r_w)$$

$$B = -\left(\frac{\epsilon n}{m}\right)^2 \frac{K_m'(\epsilon n)}{K_m(\epsilon n)} \frac{1}{L(\epsilon n)} S(\epsilon n r_w) \frac{K_m^n(\epsilon n r_w)}{K_m'(\epsilon n r_w)}$$

$$C = \left(\frac{\epsilon n}{m}\right)^2 r_c \frac{K'_m(\epsilon n)}{K_m(\epsilon r_c)} \frac{K''_m(\epsilon r_w)}{K'_m(\epsilon r_w)} \frac{S(\epsilon r_w)}{L(\epsilon r_c)}$$

$$D = 1 - \frac{I'_m(\epsilon n)}{K'_m(\epsilon n)} \frac{1}{L(\epsilon n)} + \frac{I'_m(\epsilon r_w)}{K'_m(\epsilon r_w)} \frac{1}{L(\epsilon n)}$$

$$E = \frac{\epsilon n}{m} \frac{1}{L(\epsilon n)} \frac{K'_m(\epsilon n)}{K_m(\epsilon n)} \left[\frac{I'_m(\epsilon n)}{K'_m(\epsilon n)} - \frac{I'_m(\epsilon r_w)}{K'_m(\epsilon r_w)} \right].$$

The magnitude of $\left.\frac{a_1}{a'_1}\right|_1$ is thus

$$\left.\frac{a_1}{a'_1}\right|_1 = \pm \sqrt{\frac{\left(B + C \frac{j_z^{(m,n)}}{a'_1}\right)^2 + \left(E \frac{\Omega}{r_w}\right)^2}{\left(D \frac{\Omega}{r_w}\right)^2 + A^2}} \qquad (5.104)$$

where $\frac{j_z^{(m,n)}}{a'_1}$ has been treated as a real quantity, as was found in equation (5.45).

Now, using equation (5.103), we can test this result. When $\Omega = 0$, we get

$$\left.\frac{a_1}{a'_1}\right|_1 = -\frac{1}{A}\left(B + C \frac{j_z^{(m,n)}}{a'_1}\right)$$

$$= \frac{\epsilon n}{m^2} \frac{K'_m(\epsilon n)}{K_m(\epsilon n)} \left[1 - r_c \frac{K_m(\epsilon n)}{K_m(\epsilon r_c)} \frac{L(\epsilon n)}{L(\epsilon r_c)} \frac{j_z^{(m,n)}}{a'_1} \right],$$

as was found in equation (5.45). When $\Omega \to \infty$, we get

$$\left.\frac{a_1}{a'_1}\right|_1 = -\frac{E}{D} = \frac{\epsilon n}{m} \frac{K'_m(\epsilon n)}{K_m(\epsilon n)} \frac{\left[\frac{I'_m(\epsilon n)}{K'_m(\epsilon n)} - \frac{I'_m(\epsilon r_w)}{K'_m(\epsilon r_w)} \right]}{\left[\frac{I_m(\epsilon n)}{K_m(\epsilon n)} - \frac{I'_m(\epsilon r_w)}{K'_m(\epsilon r_w)} \right]},$$

as in equation (5.74), from which the case of no wall can be found directly. When $j_z^{(m,n)} = 0$, we get equation (5.72) as can be expected. Now, from equation (5.102), we get

$$\Omega = \pm r_w \left(\frac{B + C \dfrac{j_z^{(m,n)}}{a_1'} + A \left. \dfrac{a_1}{a_1'} \right|_1}{D \left. \dfrac{a_1}{a_1'} \right|_1 + E} \right) \tag{5.105}$$

Close examination of the equations of this section will show that the coil current and tearing island magnetic fields are considered to be in phase with each other. This means that the coil is rotating with the plasma which is not the situation we have on Tokoloshe, although it might be relevant to future work.

When the external coil is fixed in a certain configuration, and the plasma is rotating, the tearing island will move in and out of phase with the coil as it rotates. If we now assume that the tearing mode stays saturated during the rotation, this model gives an approximation to maximum island size when the island is in phase with the external coil. The model clearly breaks down when the rotation is slow because island oscillation can come into play.

Out of phase situations can also be considered by changing the sign of the current density of the coil current and gives an estimate of minimum island size. An arbitrary phase angle can also be included.

This is the first time as far as we were able to determine, that boundary conditions for the case of plasma rotation with an external DC coil current have been derived in the presence of a resistive wall.

5.10 Minimizing the Energy with respect to δ

It was thought that the energy of the equilibrium could be minimized with respect to δ and thus fix the value of δ. The energy can be expressed as

$$E = 1/2 \frac{a^2 B_0^2 R_0}{4\pi^2} \int_0^{2\pi} \int_0^{2\pi} \int_0^{r^\partial} \nabla_\perp \psi . \nabla_\perp \psi \, r \, dr \, d\theta d\varphi , \qquad (5.106)$$

as was shown in Appendix B (neglecting pressure and flows).

Let

$$A(r^\partial) = A(1) + \delta \cos mn \left.\frac{\partial A}{\partial r}\right|_1 + \frac{1}{2} \delta^2 \cos^2 mn \left.\frac{\partial^2 A}{\partial r^2}\right|_1 \qquad (5.107)$$

with

$$A(r) = \int_0^1 \nabla_\perp \psi . \nabla_\perp \psi \, r \, dr$$

and again using $mn \equiv (m\theta - n\varphi)$.

If δ is included explicitly in the expression for ψ, we get

$$\psi = a_0 + \delta a_1 \cos mn .$$

From

$$\nabla_\perp \psi = \frac{\partial \psi}{\partial r} \hat{r} + 1/r \frac{\partial \psi}{\partial \theta} \hat{\theta}$$

we get

$$\nabla_\perp \psi . \nabla_\perp \psi = (a_0' + \delta a_1' \cos mn)^2 + \frac{m^2}{r^2} a_1^2 \delta^2 \sin^2 mn .$$

This is now substituted into the expression for E, to get

$$E = K \int_0^{2\pi} \int_0^{2\pi} \Big[\int_0^1 r \Big[(a_0')^2 + \delta^2 (a_1')^2 \cos^2 mn + 2a_0' a_1' \delta \cos mn + \frac{m^2}{r^2} a_1^2 \delta^2 \sin^2 mn \Big] dr$$

$$+ [(a_0')^2 + 2a_0' a_1' \delta \cos mn] \Big|_1 \delta \cos mn$$

$$+ [(a_0')^2 + 2a_0' a_0'' r] \Big|_1 \delta^2 \cos^2 mn \Big] d\theta d\varphi , \qquad (5.108)$$

with K a normalization constant.

Thus the resulting energy is of the form

$$E = A + B \delta^2 .$$

To minimize E with respect to δ, we must have $\frac{\partial E}{\partial \delta} = 0$. The only solution is $\delta = 0$, which is not in general the case for situations considered here. Thus δ is to be determined in some other way. This is done in the next chapter.

5.11 Conclusions

Boundary conditions for the proposed model of chapter 4 were derived. It is now possible to have a saturated island with any of the situations of a locked or rotating plasma, with or without an external coil current, with or without a resistive wall.

The value of the basic model proposed in chapter 4, with respect to these different situations will now be studied in chapter 6.

CHAPTER 6

THE RESULTS OF THE ONE MODE MODEL

6.1 Introduction

In this chapter the axisymmetric perturbation δJ in the new proposed model of section 4.4 is modelled. An unperturbed current model which has been used with some success on the Tokoloshe tokamak [94] is used, together with two possible functional forms for δJ. No significant difference was found between the two models.

The width of the local flattening caused by δJ is specified by a parameter w. This parameter has very specific values for different boundary conditions – reducing the theoretical modelling to an eigenvalue problem. Boundary conditions considered are for a superconducting wall, no–wall and external coils. Findings are presented for (2,1) and (3,1) modes.

The parameters of the unperturbed current profile are changed allowing flattening or peaking of the overall profile. It is found that peaking of the profile can lead to a bifurcation where there are no tearing modes present when $B_r = 0$ at the boundary, but where a tearing mode does exist for some $B_r \neq 0$ at the boundary.

The first part of this chapter contains the general results for rotating or locked modes, i.e. with $B_r = 0$ at the boundary as well as $B_r \neq 0$ at the boundary. It does not include the effects of external coils, which are discussed in the last part of this chapter.

6.2 The Functional Form of $\delta J(r)$

In the consideration of possible functional forms for δJ, the following constraints need to be satisfied:

(a) The total current must stay unchanged. This condition can be expressed mathematically as

$$\int_0^1 \delta J \, dr = 0. \tag{6.1}$$

(b) If only the first term is included in the expansion for $J(\hat{\psi})$, that is $\hat{\psi}_1 \dfrac{dJ(\hat{\psi}_0)}{d\hat{\psi}_0} \cos mn$, it is clear from equation (4.21) that $J'(r)$ must be zero at $r = r_s$ to keep $\left.\dfrac{dJ}{d\hat{\psi}_0}\right|_{r_s}$ finite. (The prime denotes derivatives with respect to r and $J(r)$ denotes the modelled axisymmetric current profile $J(\hat{\psi}_0(r))$. To have $J(r)$ as a single valued function of $\hat{\psi}_0$, the second derivative of $J(r)$ must also be zero, as was discussed at the end of section 4.4.

A simple functional form that satisfies equation (6.1) if r_s is not too close to the wall, is

$$\delta J = g_1 p \, e^{-\left(\frac{p}{w}\right)^2}, \tag{6.2}$$

where

$$p = r - r_s + d,$$

with g_1, d and w parameters to be determined. This functional form allows for the position where $\delta J = 0$ to be shifted a distance d away from the rational surface as was found by White et al. [3]. Their form for δJ is shown in Figure 6.1.

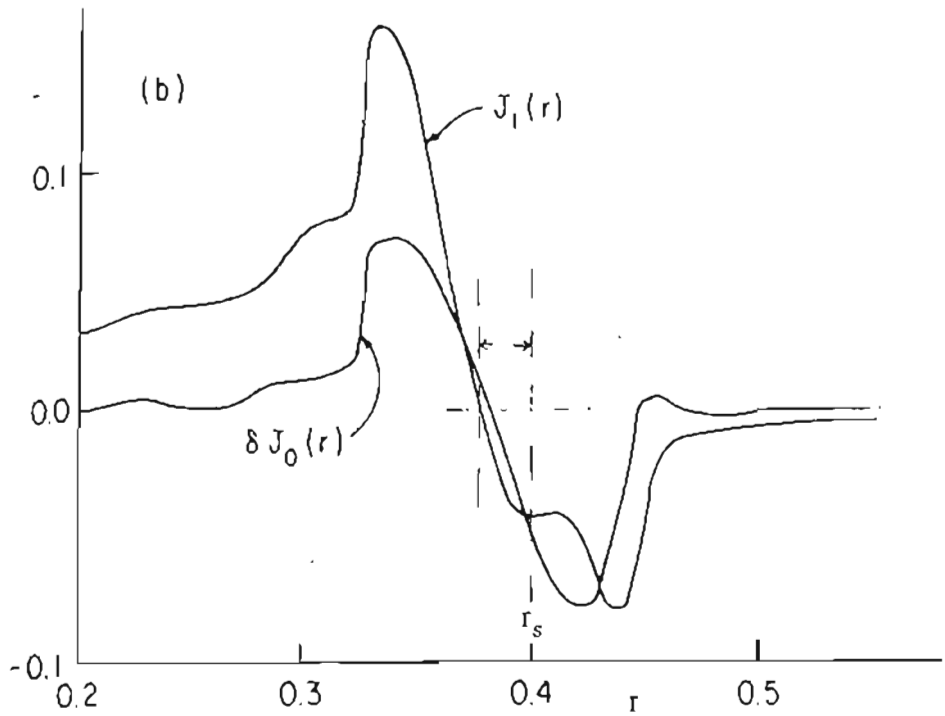

FIGURE 6.1 The functional forms of $\delta J(r)$ and $j_1(r)$ as was found by White et al. [3]. The point $\delta J(r) = 0$ is shifted a small distance from r_s.

In this chapter an unperturbed profile $J_u(r)$ of the form

$$J_u(r) = g_0(1-r^2)^b \tag{6.3}$$

is assumed. This is done because a similar profile has been used with some success on Tokoloshe, and we want to relate our results to experiment. The profile used on Tokoloshe is the one given in equation (6.3), but only valid from r=0 to r=t, where

t is chosen on the inside of r=1 (i.e. $t < 1$). From r=t to r=1 it is assumed that $J_u(r) = 0$ [94].

For the perturbed axisymmetric profile the values of g_1 and d will be fixed when the two equations flowing from $J'(r)\Big|_{r_s} = 0$ and $J''(r)\Big|_{r_s} = 0$ (constraint b above) are solved. From $J'(r)\Big|_{r_s} = 0$ we get

$$g_1 = 2\,b g_0\, r_s (1-r_s^2)^{b-1}$$

and from $J''(r)\Big|_{r_s} = 0$ we get

$$a_3 + a_2 d + a_1 d^2 + d^3 = 0\,,$$

with

$$a_1 = -\frac{1}{2} A \frac{w^2}{r_s}$$

$$a_2 = -\frac{3}{2} w^2$$

$$a_3 = A \frac{w^4}{4 r_s}$$

$$A = 2(b-1)\, r_s^2 \,(1-r_s^2)^{-1} - 1\,.$$

When the normal procedure to solve a cubic equation is followed, it is found that all three roots are real. One is always close to zero. Of these the only realistic current density profile is the one with negligible shift d. The other two result in $J'(r)$ becoming positive in the region to the right or left (depending on the root being positive or negative) of the rational surface. This can be illustrated by an example. For $r_s = 0.5$, $w = 0.05$ and $b = 2.6$ the following roots were found:

d = -0.0004

d = 0.0608

d = -0.0616 .

The only useful root is d = -0.0004. The different forms of the current profiles for different d's look as follows:

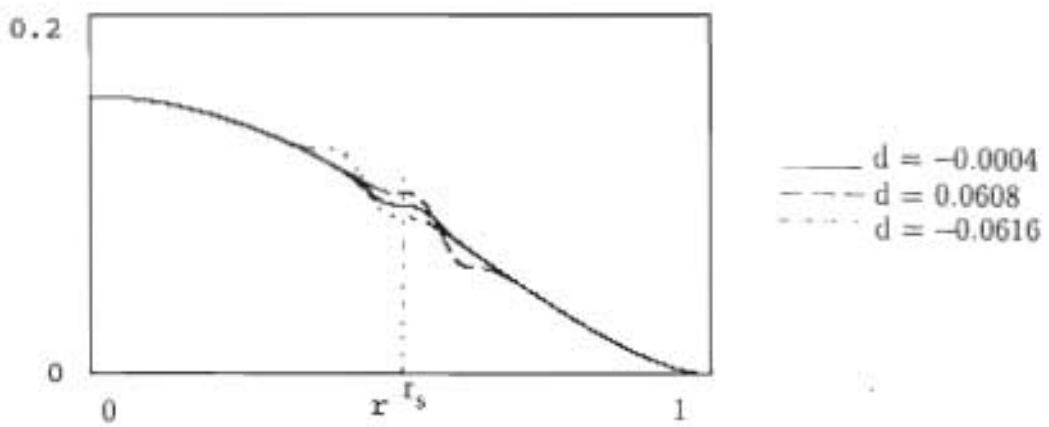

FIGURE 6.2 The three possible profiles agreeing with the three values of d for $r_s = 0.5$, $w = 0.05$ and $b = 2.6$.

As was shown in the above example, we found $d \sim 0.0$ for profiles of the form given in equation (6.3). There is thus no shift away from the rational surface in the position where $\delta J = 0$ as in the case of White et al. [3].

Another possible functional form for δJ is

$$\delta J = -[J_u(r) - J_u(r_s)]\, e^{-\left(\frac{r-r_s}{w}\right)^2} . \qquad (6.4)$$

For a current profile of the form given in equation (6.3), we get

$$\delta J = -g_0[(1-r^2)^b - (1-r_s^2)^b]e^{-\left(\frac{r-r_s}{w}\right)^2} . \qquad (6.5)$$

This profile also has the feature that the first and second derivatives are zero. The different forms of δJ given by equations (6.2) and (6.5) are shown in Figure 6.3 below. They are so similar that no differences can be detected. This also explains the fact that no significant difference was found between the results.

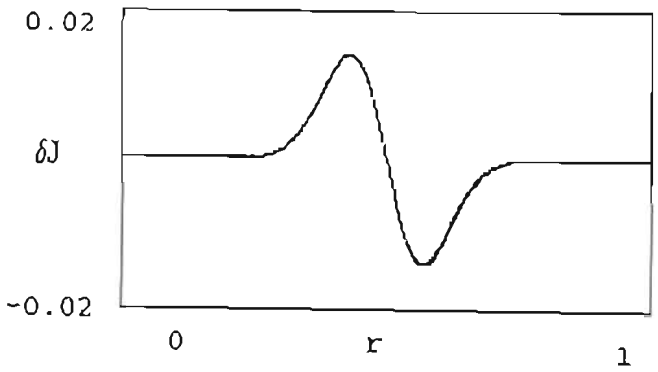

FIGURE 6.3 The forms of $\delta J(r)$ for equations (6.2) and (6.5) are indistinguishable.

6.3 Determining the Equilibrium and Perturbed Quantities

When either of these forms for δJ (equation (6.2) or (6.5)) is included in the prescribed profile, $J(r) = J_u(r) + \delta J(r)$, there are four unknowns that must be

determined, i.e. g_0, b, r_s, w. The first two are linked to the overall profile form (peaked, rounded, flat), the last one (i.e. w) is the eigenvalue of the problem giving the local flatness of the profile at the rational surface, and r_s is to be found iteratively.

It is easy to show that, for an unperturbed profile of the form given in equation (6.3), we have

$$g_0 = 2\epsilon/q\Big|_0 \tag{6.6}$$

and

$$b = (q|_1)/(q|_0) - 1 = q_1/q_0 - 1 , \tag{6.7}$$

where q is the safety factor given by

$$q = -\epsilon r/a_0' . \tag{6.8}$$

The notation $\Big|_0$ denotes "at r=0". For reasons of simplicity we write $q\Big|_0$ as q_0 and $q\Big|_1$ as q_1 in the case of the safety factor. This does not hold for other quantities where the "0" refers to equilibrium and the "1" to perturbed quantities.

The profile given in equation (6.3) has been used with some success on Tokoloshe. During a typical shot the plasma is first in the so–called *high MHD phase*, corresponding to $q_1 = 3.6$ and $1.3 \lesssim q_0 \lesssim 1.6$, and then reaches the so–called *low MHD phase*, corresponding to $q_1 = 3.6$ and $q_0 \lesssim 1$ (as signalled by the onset of sawteeth). In Figure 6.4 below it is shown how the plasma is first in the high MHD phase and then in the low MHD phase during the natural evolution, without external coils, as the current peaks.

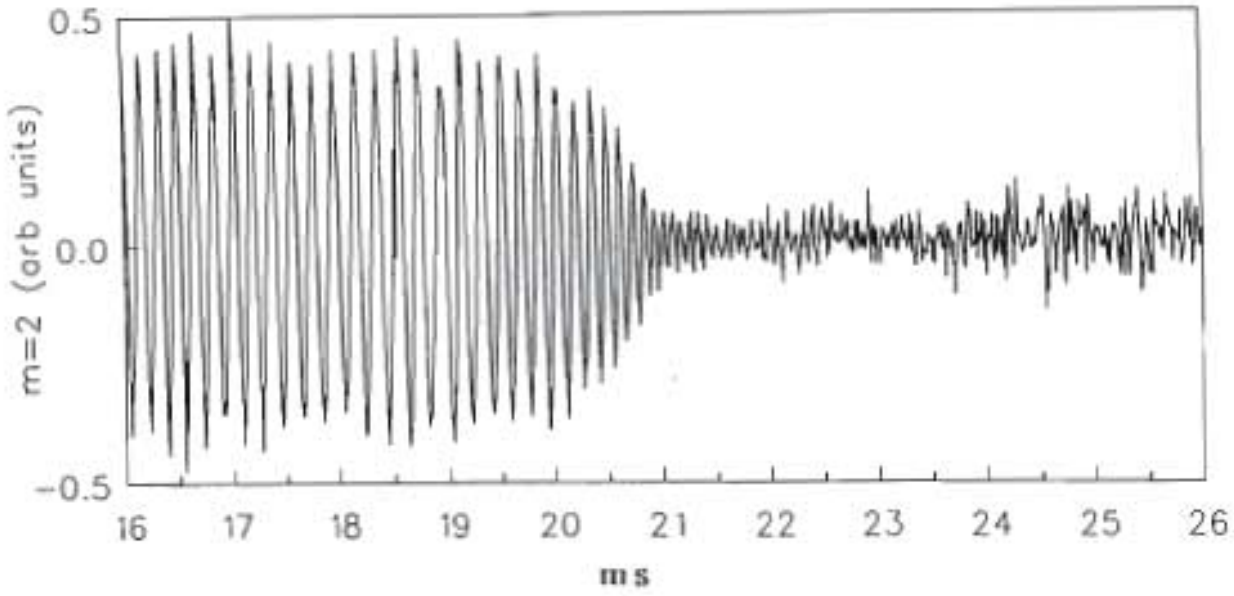

FIGURE 6.4 The typical evolution of a Mirnov signal through the high and low MHD phases.

When the perturbation δJ is added to $J_0(r)$ to give the perturbed axisymmetric current profile, the relations given by equations (6.6) and (6.7) do not hold any more.

As the total current is fixed, the q–value at the boundary must stay unchanged, as can be seen from the expression

$$1/q_1 = \left[\frac{1}{\epsilon r^2}\int_0^1 rJ(r)dr\right]\Big|_1 . \qquad (6.9)$$

After q_1 and q_0 are chosen, we use equation (6.7) to get the parameter b which specifies our profile type (peaked, rounded, flat). It is important to note that this is just a simple way to determine a useful b. The correct q_0 will be calculated later and q_1 is included implicitly via the boundary condition $a_0'\Big|_1 = -\epsilon r/q_1\Big|_1$, given in equation (5.9).

For any value of w, the profile would be fully specified once g_0 is known. To determine g_0 we make use of the fact that $B_{\theta_0}\Big|_0 = a_0'\Big|_0 = 0$ for $m \geq 2$. The parameter g_0 is now varied until this condition is satisfied. With g_0, q_1 and b known (for any value of w), we can calculate the corrected value of q_0 from equation (6.8).

We know that $\dot{\psi}_0'\Big|_{r_s} = 0$ (from equations (4.9) and (4.4)). Remember that $\dot{\psi}_0'$ is related to the helical magnetic flux. This enables us to determine the value of r_s. This value is adapted during every iteration in the process of finding g_0. Once g_0 is known, r_s is also known.

The final current profile can now be calculated for any value of w. It has the form shown in Figure 6.5.

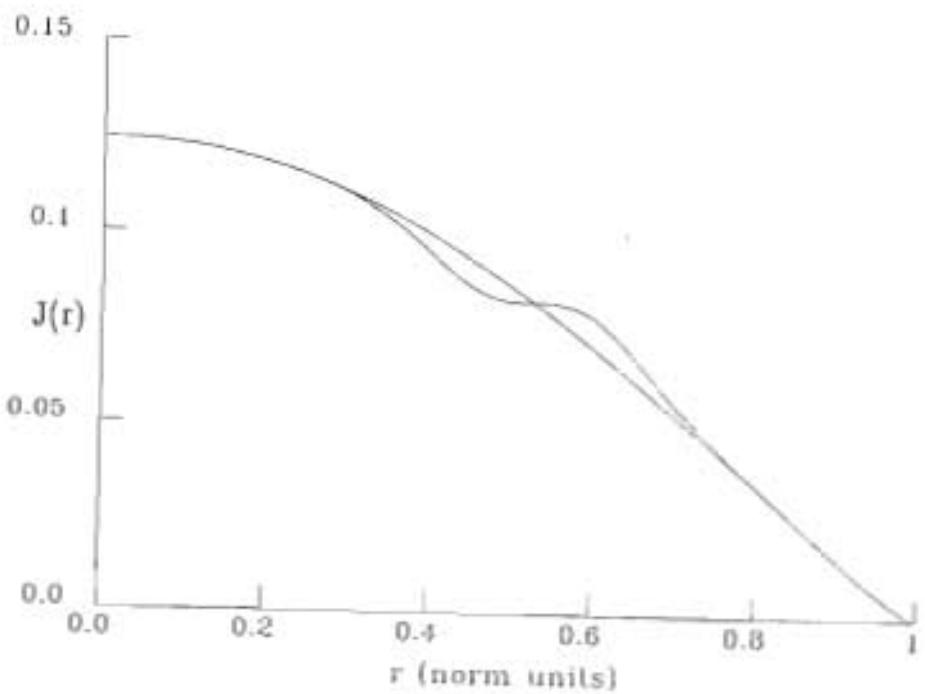

FIGURE 6.5 The forms of the perturbed and unperturbed axisymmetric current density profiles. For this graph we used the δJ specified in equation (6.5) with $w = 0.1128$, $b = 1.25$, $q_1 = 3.6$ and $q_0 = 1.6$.

Using this profile in equation (4.35) enables us to calculate a_0' and thus the helical magnetic flux $\tilde{\psi}_0$ (using equation (4.37)), which has the form given below. The graph of the safety factor for a perturbed and unperturbed profile is shown in Figure 6.7.

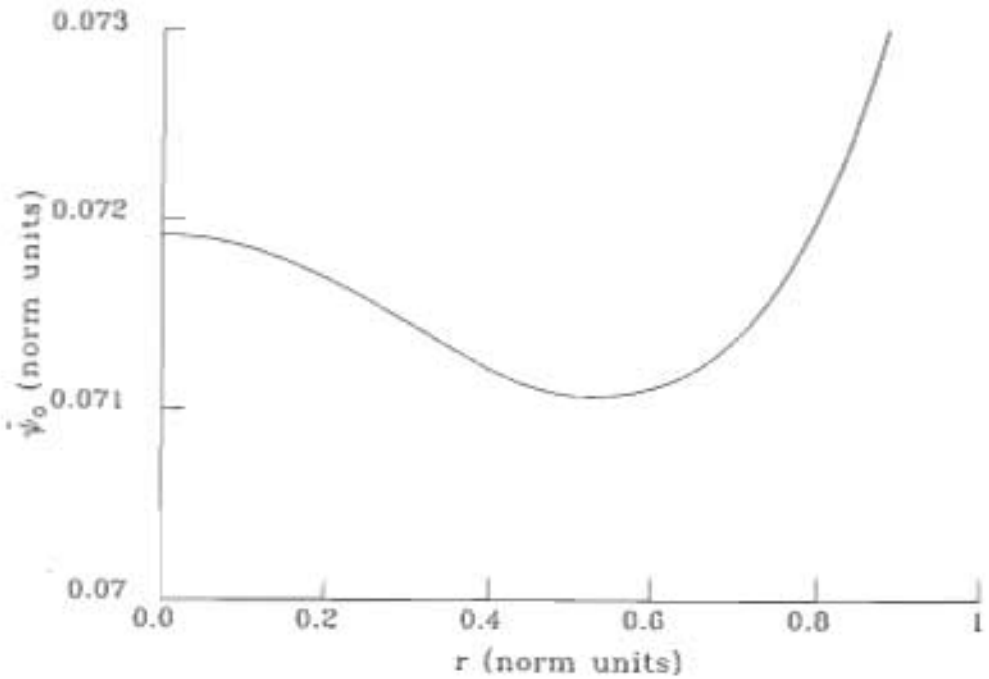

FIGURE 6.6 The graph of $\tilde{\psi}_0$ for $b = 1.25$ and $w = 0.1132$. The value of q_1 was 3.6 and q_0 was 1.6.

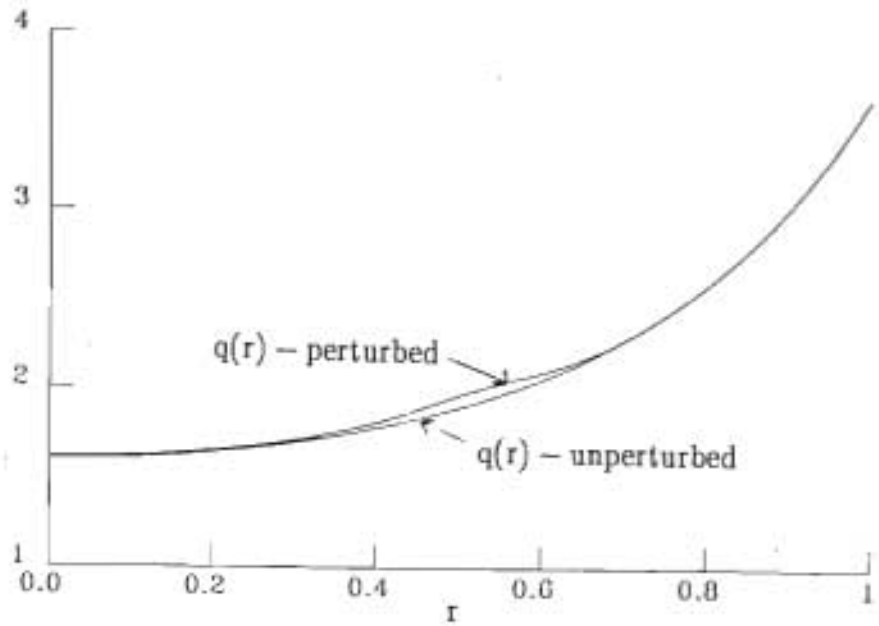

FIGURE 6.7 The graph of q for the perturbed and unperturbed axisymmetric current density profile. The parameters were $w = 0.1275$, $b = 1.77$, $q_1 = 3.6$ and $q_0 = 1.6$.

All the equilibrium quantities are now known. The next step is to calculate the perturbed quantities, a_1 and a_1'. This can be done using equation (4.36), but this requires the further axisymmetric quantity $dJ(\hat{\psi})/d\hat{\psi}_0$. This is rewritten as $J'/\hat{\psi}_0'$. Both these quantities (J' and $\hat{\psi}_0'$) are shown in Figure 6.8. In both these cases the unperturbed quantities are also shown. It is clear that the effect of δJ is to make J' zero at the rational surface. For these calculations the model specified in equation (6.5) is used.

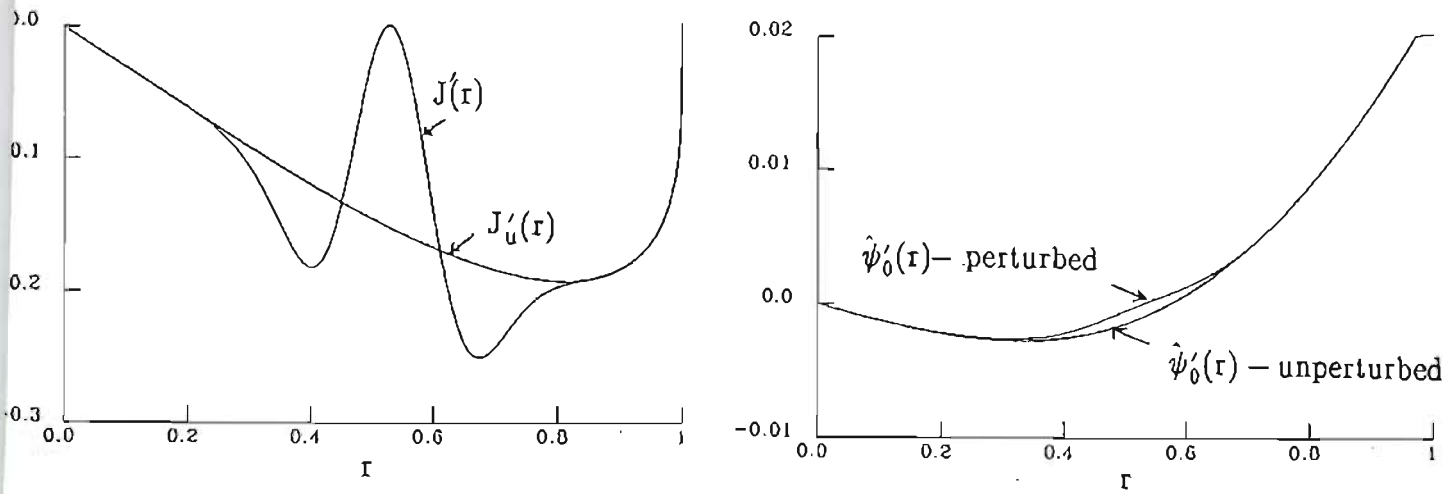

(a) (b)

FIGURE 6.8 (a) The graph of $J'(r)$ for both the perturbed and unperturbed axisymmetric profiles. (b) The graph of $\hat{\psi}_0'$ for both the perturbed and axisymmetric unperturbed profiles. The parameters are $w = 0.1275$, $b = 1.77$, $q_1 = 3.6$ and $q_0 = 1.6$.

The factor $dJ(\hat{\psi}_0)/d\hat{\psi}_0$ can now be constructed by dividing J' by $\hat{\psi}_0'$. For this factor to be well–behaved the rational surface must be calculated very accurately to ensure that both J' and $\hat{\psi}_0'$ are zero at r_s. If this is not the case the mentioned factor will blow up because $J'\Big|_{r_s} \neq 0$ will be divided by $\hat{\psi}_0'\Big|_{r_s} = 0$. From Figure 6.9 it is clear that it is indeed well–behaved.

Using the boundary conditions specified by equations (5.10) and (5.11), we can now solve equation (4.36) to get results for the (2,1) or (3,1) modes.

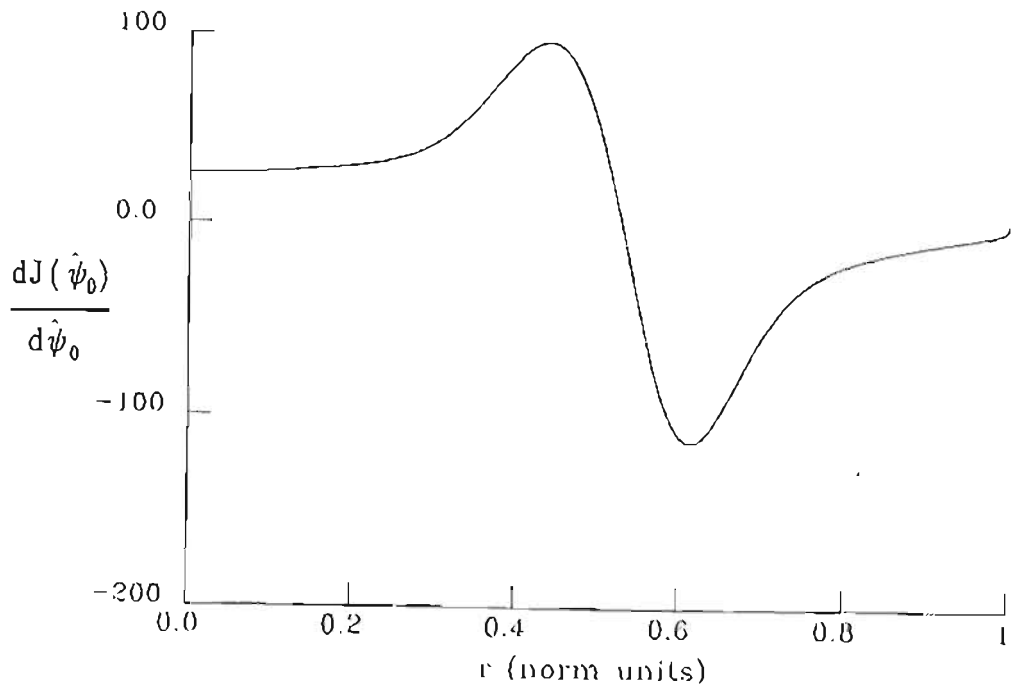

FIGURE 6.9 The graph of $dJ/d\hat{\psi}_0$. It is generated by dividing $J'(r)$ by $\hat{\psi}_0'$.

6.4 Solving for the eigenvalue of the problem

6.4.1 Determining the local flatness of the current density profile with a saturated tearing mode present

In this section we will show that the local flatness of the current density profile (at the rational surface) expressed in terms of the parameter w, is dependent on the quantity $\left.\frac{a_1}{a_1'}\right|_1$ which is proportional to $\left.\frac{B_r}{B_{1\theta}}\right|_1$. Every value of w can be related to a specific value of $\left.\frac{a_1}{a_1'}\right|_1$. It is now important to recall that different external physical situations, i.e. superconducting wall, partly conducting wall with a rotating plasma, no–wall, external coil etc. are related to different expressions for $\left.\frac{a_1}{a_1'}\right|_1$ as was discussed in chapter 5 (equations (5.36), (5.45), (5.71), (5.104)). This means that these different external situations are related to different values of w.

When $\left.a_1'/a_1\right|_1$ is plotted as a function of w, we get the graph in Figure 6.10 for a (2,1) tearing mode during the high MHD phase ($q_0 = 1.6$, $q_1 = 3.6$) on Tokoloshe. (The δJ perturbation used is given by equation (6.5)). Figure 6.11 illustrates a similar graph for the (3,1) mode with $q_0 = 2.0$ and $q_1 = 4.5$. In Figure 6.12 the (2,1) and (3,1) modes are compared for $q_0 = 1.75$ and $q_1 = 3.6$ i.e. during the high MHD phase. When b is changed and thus the functional form of the profile, the vertical asymptote is shifted to the left or right.

The value of w where the vertical asymptote occurs is much smaller for the (3,1) than for the (2,1) mode. This was generally found to be true for the overall current profile form of equation (6.3). It means that the (3,1) island size is much smaller than the (2,1) for this profile. (We will show later that $w \propto$ W(island size)).

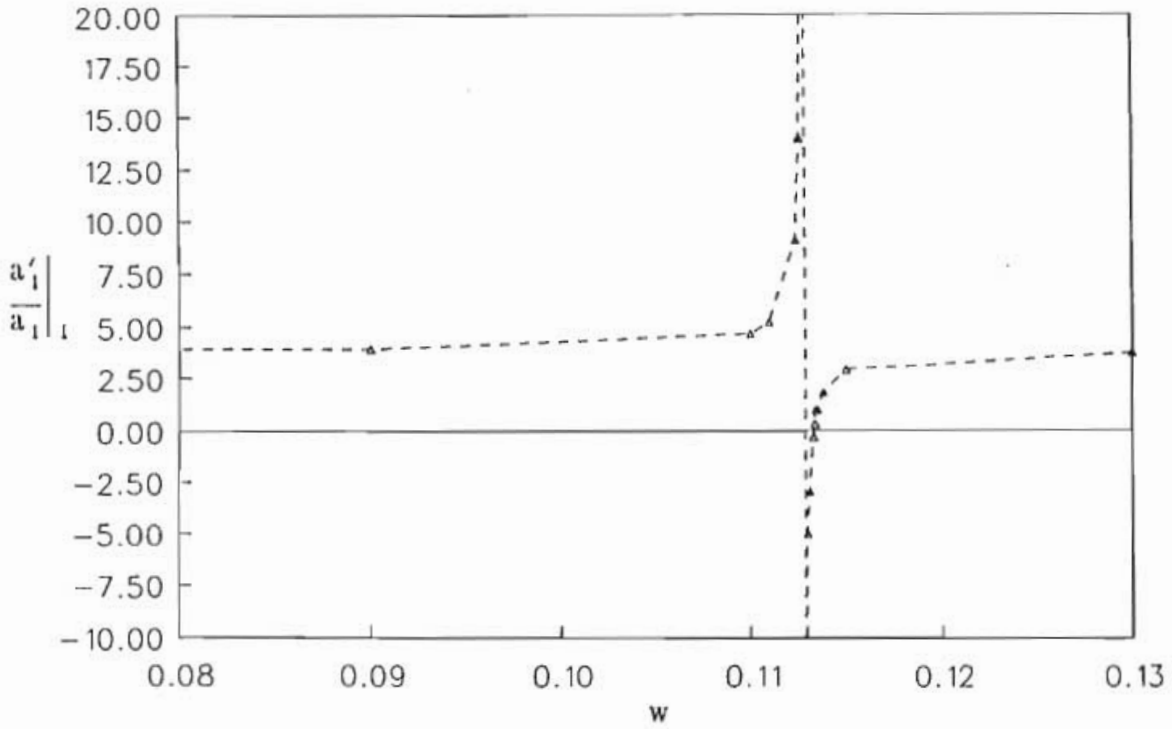

FIGURE 6.10 The graph of $a_1'/a_1\Big|_1$ against w for a (2,1) mode. It has an asymptotic behaviour about a certain w as well as a certain $\frac{a_1'}{a_1}\Big|_1$ value.

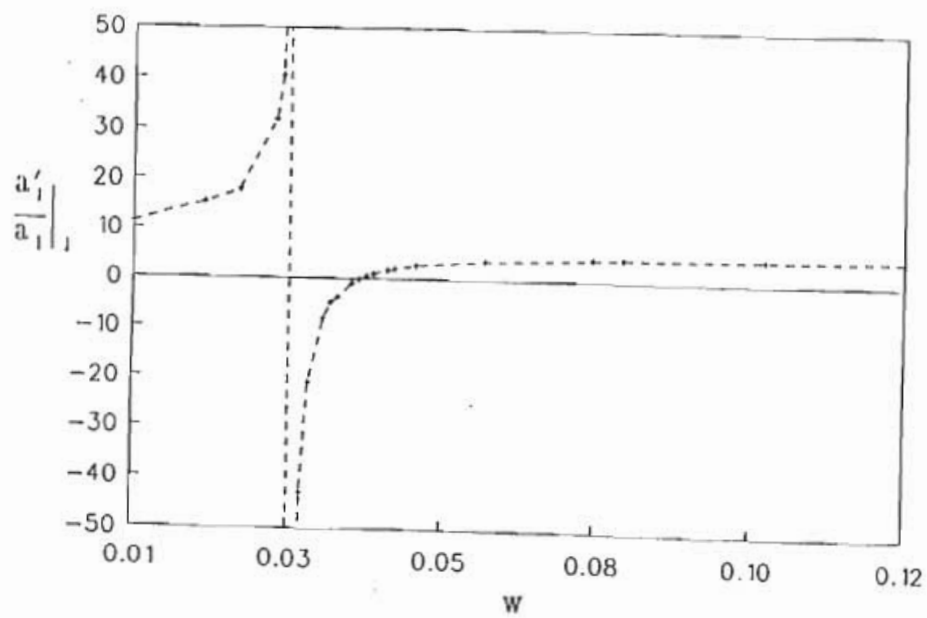

FIGURE 6.11 A graph similar to the previous one for the (3,1) mode.

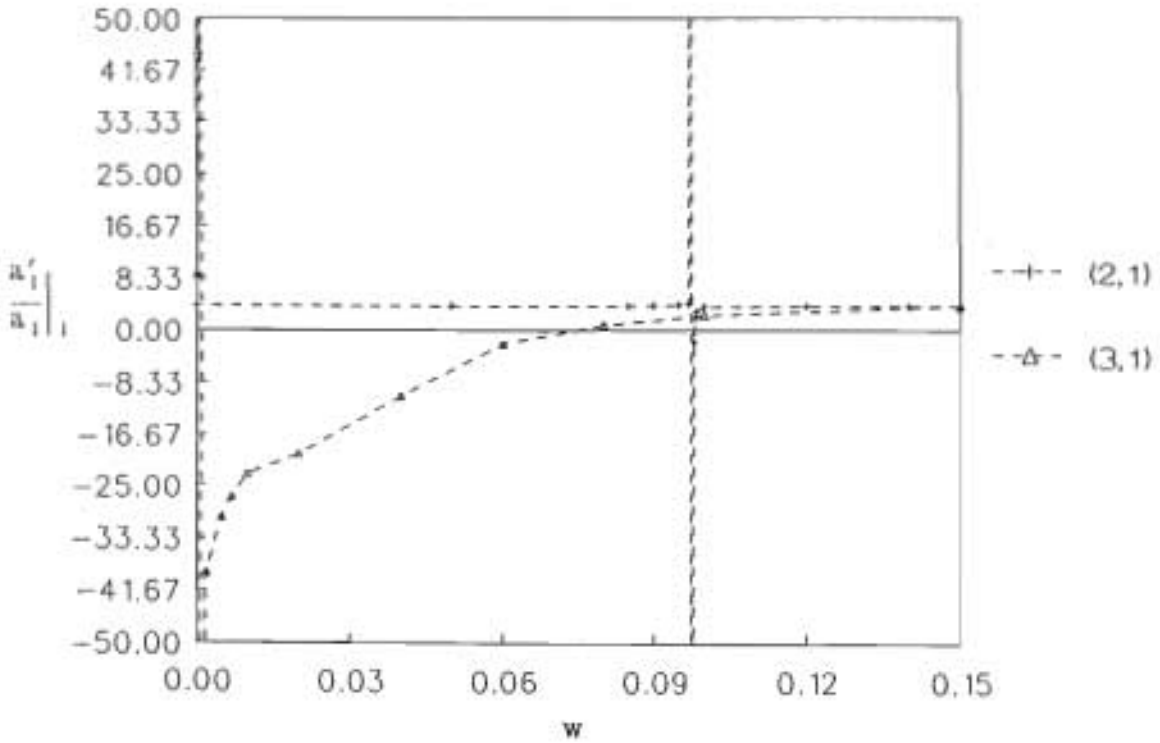

FIGURE 6.12 Both the (2,1) and (3,1) modes are shown on this graph for $q_1 = 3.6$ and $q_0 = 1.75$. The value of w about which the asymptote occurs is much larger for the (2,1) than for the (3,1) mode.

It is important to note that it has been found numerically that the graphs are independent of δ (the parameter of the boundary condition $r^{\partial} = 1 + \delta \cos mn$). This can be seen from the fact that a_1 is an explicit function of δ (from equation (5.10)). When δ and r are independent of each other, then a_1' would also be a function of δ. This is implicit here since we do not use an analytic expression for a_1' – it is a shooting value. From these arguments it is clear that $\left.\frac{a_1'}{a_1}\right|_1$ should be independent of δ.

For a certain value of δ the value of $a_1\Big|_1$ can immediately be calculated using equation (5.10). This will then give a graph of $a_1'\Big|_1$ or $a_1\Big|_1$ against w – enabling us to get a well–determined value of $a_1'\Big|_1$ for all w. The same reasoning is valid for ϵ. It was thus also found that the graph is independent of the value of ϵ.

We will now use Figure 6.10, which shows the general behaviour of $\frac{a_1'}{a_1}\Big|_1$ against w, to discuss the general features of the results. An interesting feature is that the top–left part and the bottom–right part have two different types of solutions for $a_1(r)$.

The solutions of $a_1(r)$ are shown in Figure 6.13, and are representative of the (2,1) or (3,1) mode. Solution Type I is presented in Figure 6.13(a) and Type II in Figure 6.13(b) and 13(c). In the case of solution II the value of $a_1'\Big|_1$ can be positive (Figure 6.13(b)) or negative (Figure 6.13(c)), giving rise to a slight difference in the form of the solution.

These solutions (Types I and II) agree with those found by Ellis [31], using linear perturbation theory as we do. Using the criterion developed by him and adapted by Hansen [79] (i.e. if the curve of a_1 cuts the $a_1 = 0$ line inside the plasma, the profile is unstable to tearing modes, otherwise it is stable), it is clear that the Type I solution corresponds to a tearing mode unstable situation. As w is increased, we go from a Type I (tearing mode unstable) to a Type II (tearing mode stable) solution. The effect of an increasing w is thus to drive an unstable equilibrium stable as was also found by Ellis [31]. Another feature of the graph shown in Figure 6.10, is that the point where the $a_1'/a_1\Big|_1 \to \pm\infty$, agrees with $a_1\Big|_1 = 0$ (i.e. $B_r\Big|_1 = 0$). The point where $a_1'/a_1\Big|_1 = 0$ corresponds to $a_1'\Big|_1 = 0$ (i.e. $B_{\theta_1}\Big|_1 = 0$).

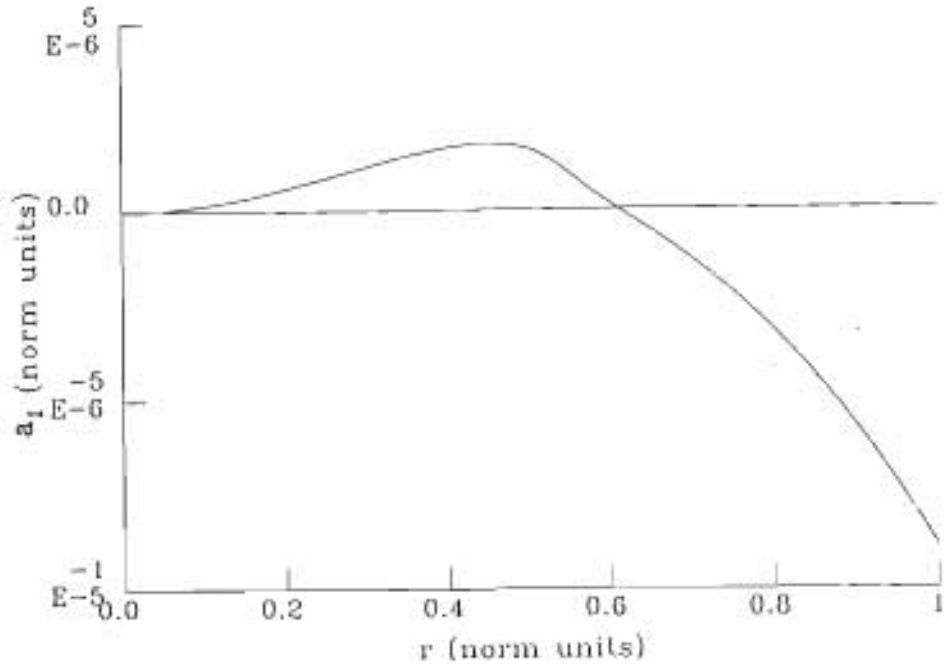

(a)

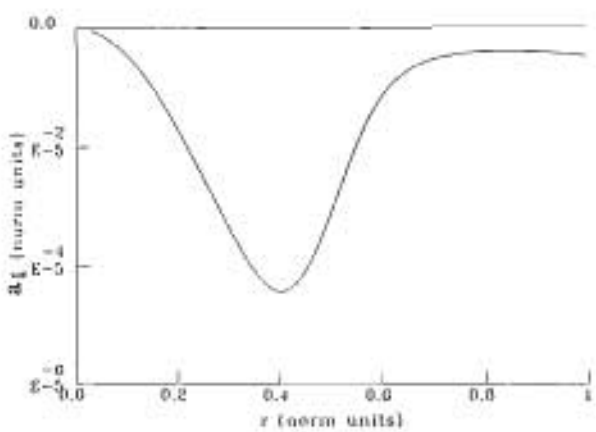

(b)

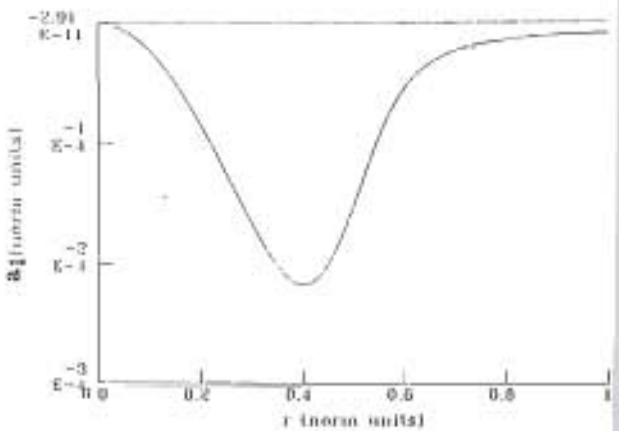

(c)

FIGURE 6.13 (a) Type I solution. This agrees with a tearing mode unstable situation which is found to the left of the vertical asymptote on Figure 6.10. (b) Type II solution with $a_1'\Big|_1$ positive. This is a tearing mode stable situation and is found to the right of the vertical asymptote. (c) Type II solution with $a_1'\Big|_1$ negative.

These results are totally general and any set of external conditions (like an external coil for example) can be coupled to $a_1'/a_1\Big|_1$.

When the plasma is rotating infinitely fast (the rotation frequency $\omega \to \infty$) and the wall is partly conducting or in the case of a superconducting wall, the radial magnetic field is not allowed to penetrate the wall, giving rise to $B_r\Big|_1 = 0$ when the plasma touches the wall. It is thus clear that the point where $a_1'/a_1\Big|_1 \to \pm\infty$ gives the eigenvalue w of the problem in such a case. The physical interpretation of this is that the local flatness of the current profile at $r = r_s$ (expressed mathematically as w) is now given for the case of a fast rotating plasma (or superconducting wall). This position on Figure 6.10 agrees with marginally stable equilibria – lying between the stable and unstable equilibria as was discussed in the previous paragraph.

In the case when the plasma is non–rotating – allowing B_r to fully penetrate the wall – the eigenvalue w will be determined by the external conditions, i.e. whether an external coil is switched on or not. In the case of $I_{\#} = 0$ we have $a_1/a_1'\Big|_1 = -0.501$ (for $\epsilon = 0.1$) for a (2,1) tearing mode as was shown in equation (5.37). When an external coil is switched on, $a_1/a_1'\Big|_1$ is dependent on the value of $j_z^{(m,n)}$ as was shown in equation (5.45)

We can now see why it is an eigenvalue problem. For any boundary condition $a_1'/a_1\Big|_1$ we have one discrete value of w. The boundary conditions thus determine the "eigenvalue" of the problem, i.e. what amount of local flattening at $r = r_s$ (described mathematically as w) is associated with that specific perturbation of the boundary.

Another important feature of Figure 6.10 is that this gives all the possible values of w for different $a_1'/a_1\Big|_1$ which can be associated with different degrees of flattening in the process of island growth. When growth occurs in an adiabatic way because of external perturbations (i.e. changing $a_1'/a_1\Big|_1$), this graph gives all the possible saturated islands associated with a particular overall current density profile.

There is a last point to mention. The vertical asymptotes occur at a much smaller w for the (3,1) mode than for the (2,1) mode as can be seen from Figure 6.12 for $q_0 = 1.75$, $q_1 = 3.6$. This was found to be a general feature of the profile defined in equation (6.3). For any value of $a_1'/a_1\Big|_1$ the value of w will thus be much smaller, meaning that the same outside physical situation will lead to a comparatively smaller (3,1) island (it will be shown that w ~ W(island size)). Because of this we will only focus on the (2,1) mode for the rest of this chapter, for which the current profile is ideally suited.

6.4.2 An analytic approach to the problem

The solution of the equation for the perturbed magnetic flux has been found numerically in the previous section. In this section we show that the same type of solution can be found when the factor $dJ(\tilde{\psi}_0)/d\tilde{\psi}_0$ is modelled, and the equation solved analytically. This serves as a check on the previous work.

The form of the factor $dJ(\tilde{\psi}_0)/d\tilde{\psi}_0$ is shown in Figure 6.9. This form can be modelled with three simple functions

$$p(r) = b \sin\left[\frac{r-r_s}{w_1}\right], \qquad r_s - x_1 < r < r_s + x_1$$

$$= [b_1 / (r_s - x_1)]r, \qquad r < r_s - x_1$$

$$= [b_1 / (1-(r_s+x_1))](r-1) \qquad r > r_s + x_1$$

with

$$x_1 = \frac{\pi w_1}{1.2}, \quad b_1 = b \sin\left[-\frac{x_1}{w_1}\right].$$

It is shown in Figure 6.14. (Only the first three terms of the expansion for $\sin(\frac{r-r_s}{w_1})$ have been included in the series).

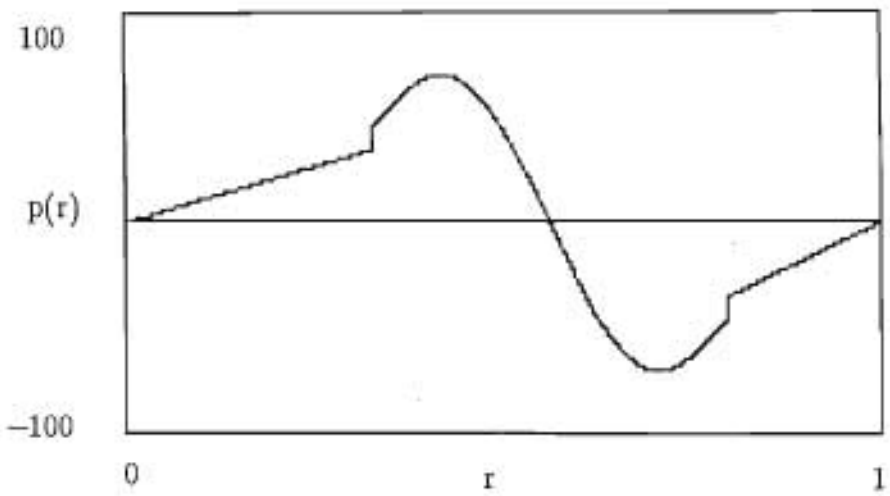

FIGURE 6.14 The graph of $^{dJ}/_{d\dot{\psi}_0}$ as modelled by $p(r)$.

These functions p(r) can now be substituted into equation (4.36) and solved analytically by the method of Frobenius assuming

$$a_1 = r^k \sum_{n=0}^{\infty} \gamma_n r^n ,$$

and $m=2$.

The solution in the region $r < r_s - x_1$ is

$$a_1 = \gamma_2[r^2 - \frac{x_3}{21} r^5 + \frac{x_3^2}{1260} r^8 - \dots] ,$$

with

$$x_3 = \frac{b_1}{r_s - x_1} ,$$

and the solution in the region $r > r_s + x_1$ is

$$a_1 = \gamma_2[r^2 + \frac{b_1}{21\ x_2} r^4 - \frac{b_1}{21\ x_2} r^5 - \frac{b_1^2}{384\ x_2^2} r^6 + \dots] ,$$

with

$$x_2 = 1 - (r_s + x_1) .$$

The solution of the middle part, which is more complicated than the solutions of the side parts, is given below:

$$a_1 = \gamma_2\Big[r^2 - (A_1/12)\, r^4 + (A_2/21)\, r^5 + \Big[\frac{A_1^2/2 - A_3}{32}\Big] r^6$$

$$+ \Big[\frac{-33}{252} A_1 A_2 + A_4\Big]/45\, r^7 +$$

$$\Big[- A_1 \Big[\frac{A_1^2/2 - A_3}{32}\Big] + A_2^2/21 + A_3 A_1/12 - A_5\Big]/60\, r^8$$

$$+ \quad \left[- A_1 \left[\frac{-33}{252} A_1 A_2 + A_4 \right] /45 + A_2 \left[A_1^2/2 - A_3 \right] /32 \right.$$

$$\left. - \quad A_2 A_3/21 - A_1 A_4/12 + A_6 \right] /77 \, r^9 \ ,$$

$$A_1 = - \frac{r_s}{w_1} + r_s^3/(3! w_1^3) - r_s^5/(5! w_1^5)$$

$$A_2 = - \frac{1}{w_1} + 3r_s^2/(3! w_1^3) - 5r_s^4/(5! w_1^5)$$

$$A_3 = \frac{3r_s}{3! w_1^3} - 10r_s^3/(5! w_1^5)$$

$$A_4 = \frac{1}{(3! w_1^3)} - 10r_s^2/(5! w_1^5)$$

$$A_5 = - \frac{5r_s}{(5! w_1^5)}$$

$$A_6 = - \frac{1}{(5! w_1^5)} \ . \qquad (6.10)$$

This solution is not matched smoothly to the one in $r > r_s + x_1$, because of the neglected higher order terms. However, it can be seen from Figure 6.15 that the solutions agree qualitatively with those found numerically. The marginally stable solution is found at $w_1 \simeq 0.133$. For $w_1 = 0.131$ the unstable solution (in qualitative agreement with Figure 6.13a)) is given in Figure 6.15a), and for $w_1 = 0.136$ the stable solution (in qualitative agreement with Figure 6.13b)) is given in Figure 6.15b).

This relatively direct way of obtaining analytic estimates for stability emphasizes the possible power of the model, and should be persued in the future.

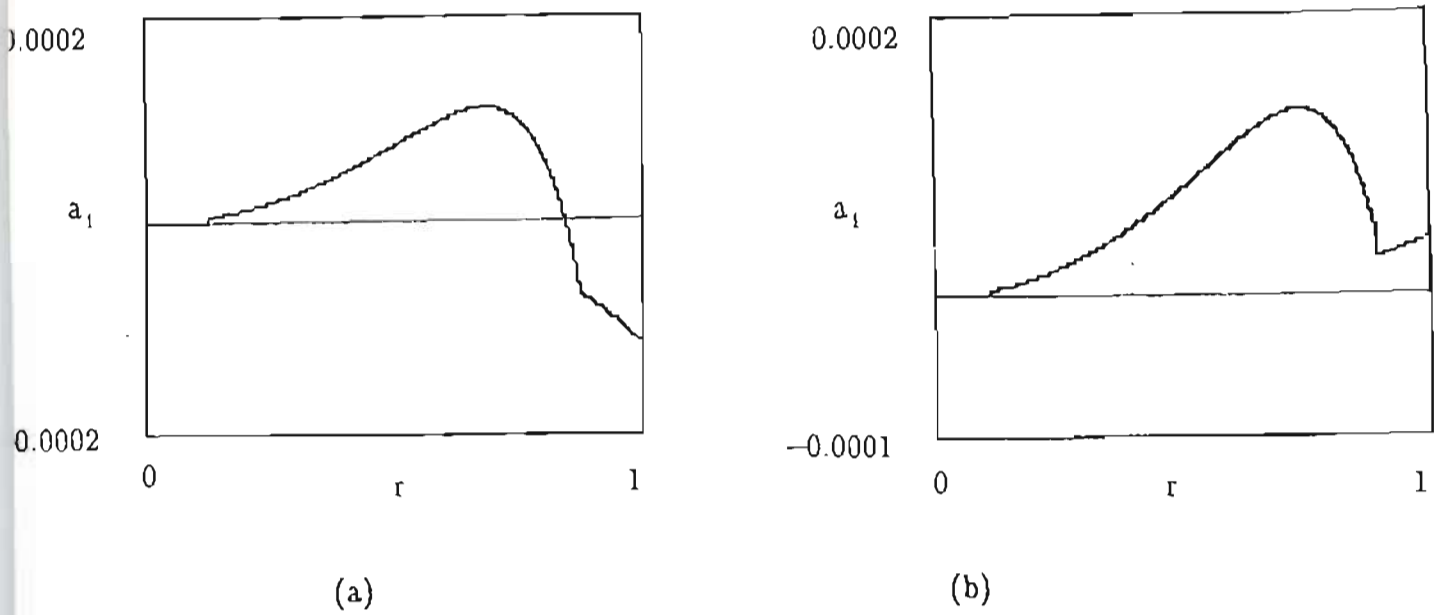

FIGURE 6.15 (a) The analytic solution $a_1(r)$ for $w_1 = 0.131$. This agrees with the unstable solution. (b) The analytic solution $a_1(r)$ for $w_1 = 0.136$. This agrees with the stable solution.

6.5 The Island Width

6.5.1 A method to determine the island width in general

In determining the width of the island, we make use of the fact that the helical magnetic flux will have the same value at both the X–point and at the island edge at the position of the O–point. This is the same assumption that has been used to determine the well–known approximate formula for the island width [3], i.e.

$$W = 4\left[-a_1(r_s)/\tilde{\psi}_0''(r_s)\right]^{\frac{1}{2}} . \qquad (6.11)$$

The total functions $\tilde{\psi}(r,\theta_1,\varphi_0)$ and $\tilde{\psi}(r,\theta_2,\varphi_0)$ can be drawn as functions of r, where θ_1 is the poloidal angle corresponding to the position of the X–point and θ_2 the poloidal angle at the O–point (φ_0 is any chosen toroidal angle, taken to be zero in

this case). These functions have a minimum at the radial point where the X–point occurs (in the case of $\hat{\psi}(r,\theta_1,\varphi_0)$) or at the radial point where the O–point occurs (in the case of $\hat{\psi}(r,\theta_2,\varphi_0)$). This is shown in Figure 6.16, where $\theta_1 = \frac{\pi}{2}$ and $\theta_2 = 0$.

Using the fact that $\hat{\psi}$(X–point) = $\hat{\psi}$(island edge in line with O–point), the island width (W) can easily be determined as shown in Figure 6.16.

The values of $\hat{\psi}$ at the O and X–points can be calculated. They are

$$\hat{\psi}_{\text{O-point}} = \begin{cases} (\hat{\psi}_0(r) + a_1(r))_{\min}, & a_1(r_s) < 0 \\ (\hat{\psi}_0(r) - a_1(r))_{\min}, & a_1(r_s) > 0 \end{cases}$$

$$\hat{\psi}_{\text{x-point}} = \begin{cases} (\hat{\psi}_0(r) + a_1(r))_{\min}, & a_1(r_s) > 0 \\ (\hat{\psi}_0(r) - a_1(r))_{\min}, & a_1(r_s) < 0 . \end{cases}$$

We assume that the island perturbation is of the same phase as the outer boundary ($r^{\partial} = 1 + \delta \cos(m\theta - n\varphi)$), as has been done by Reiman [75] and Hahm and Kulsrud [16]. AT the X–point the value of r^{∂} is just $r^{\partial} = 1-\delta$ (minimum) and at the O–point $r^{\partial} = 1 + \delta$ (maximum). It is now clear that the solution $a_1(r_s) < 0$ corresponds to $\delta > 0$, and $a_1(r_s) > 0$ to $\delta < 0$. When the sign of δ is changed, the value of $a_1\Big|_1$ changes sign and the solution also changes sign. A change in the sign of δ thus corresponds to changing the orientation of the island.

This method makes it unnecessary to go through the time–consuming process of fieldline tracing to calculate the island structure. When points of similar $\hat{\psi}$ are connected, a contour plot of $\hat{\psi}$ can be drawn showing the island structure clearly.

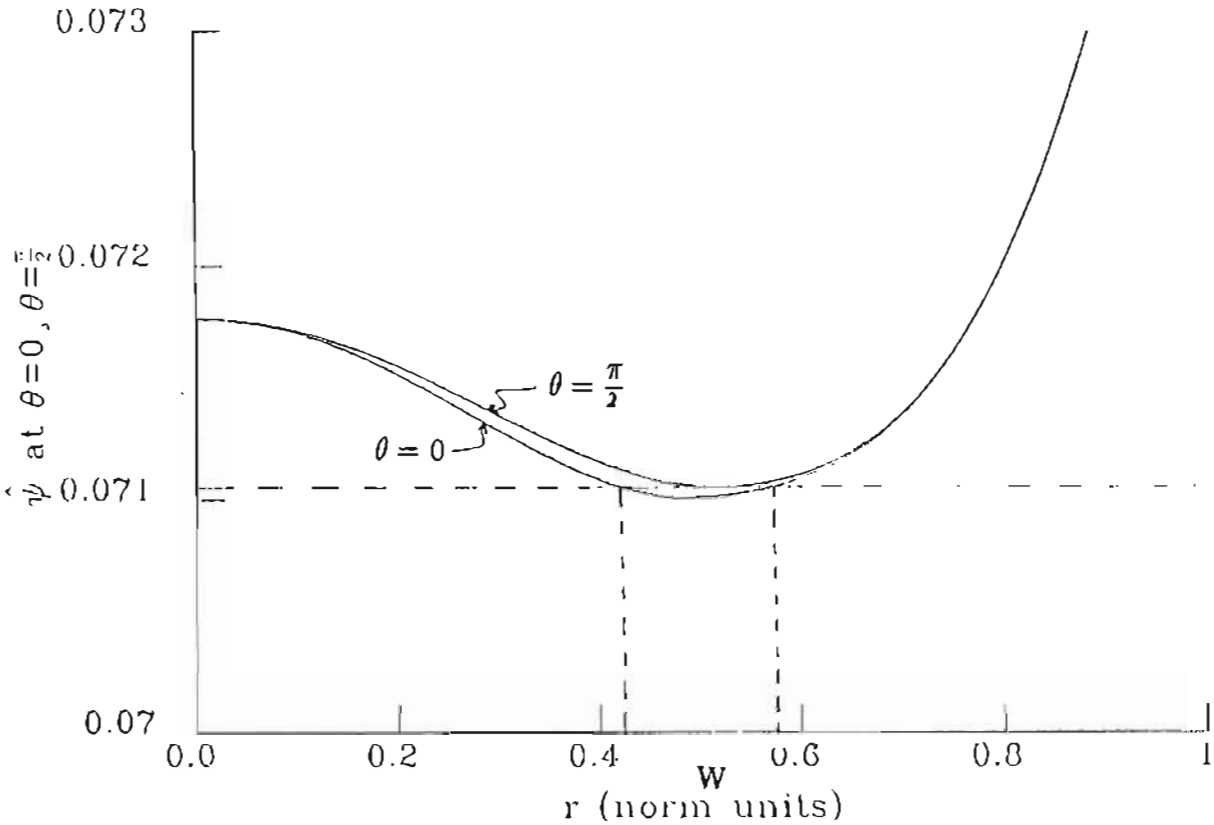

FIGURE 6.16 The graph of $\hat{\psi}$ at $\theta = \pi/2$ and $\theta = 0$ agreeing with the poloidal angles where the X–point and the O–point occur. The value of $\hat{\psi}$ at the X–point is the same as that of $\hat{\psi}$ at the island edge at the O–point. From this information it is possible to determine the island width (W) as shown.

This is done in the next section. Another point of interest is of course that the plama response is included in the calculations.

We can at this stage make some estimate of the errors involved in the calculation of the island size. Using the same method as was applied to calculate the island width formula, we can assume that the $W \sim (a_1\big|_{r_s})^{\frac{1}{2}}$ relationship will hold. We know that the error involved in our expressions is $O(\epsilon^3)$, i.e. one order smaller than a_1 which is $O(\epsilon^2)$. The error in W is thus $[O(\epsilon^3)]^{\frac{1}{2}}$, which is clearly small.

6.5.2 Using $\Delta'(W) = 0$ to calculate the saturation width

Although it is now possible to calculate the island width for any value of $B_r(r_s)$, it is still not clear what the final saturation width would be for a natural (or externally induced when $I_{\#} \neq 0$) island since δ remains undetermined. We now adopt the method of White et al. [3]. They found $\frac{dW}{dt} = 1.66\,\eta(r_s)[\Delta'(W) - \alpha W]$, with

$$\Delta'(W) = \frac{1}{\hat{\psi}_1(r_s)} \left[\hat{\psi}_1'\Big|_{w^+} - \hat{\psi}_1'\Big|_{w^-}\right], \tag{6.12}$$

where w^+ is the outer edge and w^- the inner edge of the island ($\hat{\psi}_1 = a_1$), and α a parameter depending on the resistive profile among other things. This $\Delta'(W)$ is calculated over the island width which is also their "inner region". Although we do not have an inner and outer region in our approach, we do have a saturated island in the plasma over which the abovementioned $\Delta'(W)$ can be calculated. Once the island is saturated ($\frac{dW}{dt} = 0$), their expression reduces to $\Delta'(W) - \alpha W = 0$.

When $\eta \sim 1/J$, the form of $\Delta'(W) - \alpha W$ is very similar to that of $\Delta'(W)$ [3]. This is shown in Figure 6.17 which is taken from their publication [3]. In another publication it was shown that the effect of α is indeed negligible [46]. This is shown in Figure 6.18. In a simple approach $\Delta'(W) = 0$ can thus be assumed for a saturated island, which is the form originally derived by Rutherford [2].

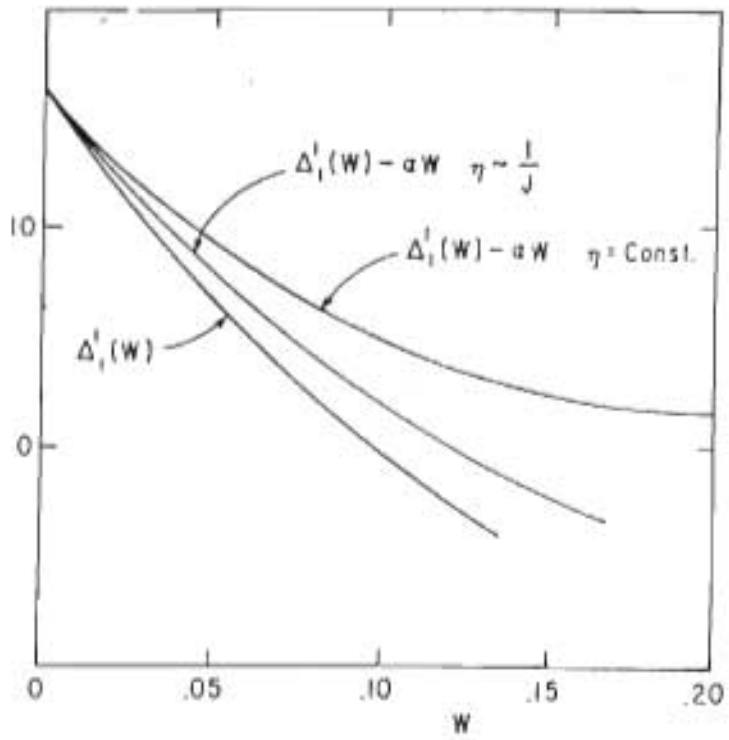

FIGURE 6.17 This is taken from White et al. [3]. The island growth rate in the Rutherford regime against width is shown.

The approach of White et al. is however, only valid when a superconducting wall is present. When a perturbed boundary is allowed, their formula has to be adapted. Reiman [75] defined a criterion that is slightly different from that of White et al. It is given as:

$$\Delta'_{\epsilon_1}(W) = [r_{w+}\,\hat{\psi}'_1(w_+) - r_{w-}\,\hat{\psi}'(w_-)]/(r_s\,\hat{\psi}_1(r_s)) . \tag{6.13}$$

It can also be written as [75]

$$\Delta'_{\epsilon_1}(W) = \Delta'(W) - [\epsilon_1/\hat{\psi}_1(r_s)]/\sigma'(W) , \tag{6.14}$$

where $\sigma'(W)$ is a function depending on W, $\epsilon_1 = \hat{\psi}_1(1)$, and $\Delta'(W)$ refers to $\Delta'_{\epsilon_1}(W)$ with $\epsilon_1 = 0$.

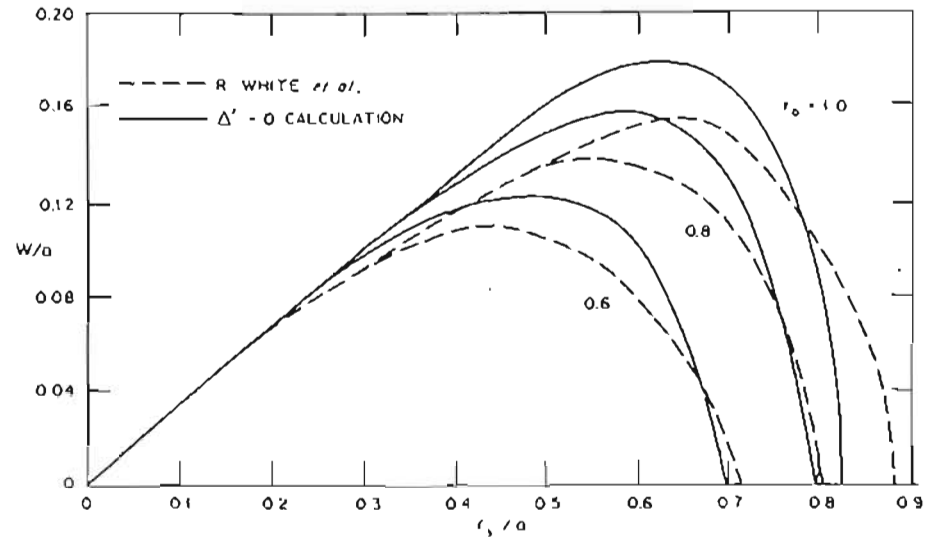

FIGURE 6.18 This is taken from Carreras et al. [45]. Their results are compared with that of White at al. [3] for their peaked model.

The following relations now hold [75]:

$$\lim_{\epsilon_1 \to 0} \Delta'_{\epsilon_1}(W) = \Delta'(W)$$

$$\lim_{W \to 0} \Delta'(W) = \Delta' , \qquad (6.15)$$

where Δ' is the linear rendering first derived by Furth et al. [1]. We will use this generalized form of $\Delta'_{\epsilon_1}(W)$ in our work which includes external perturbations.

We can now get important information from Figure 6.10. As was discussed earlier, the ratio $\left.\frac{a_1}{a'_1}\right|_1$ can be related to different external physical situations, i.e. superconducting wall, partly conducting wall with rotating plasma, no wall, external coils with a rotating or locked plasma. This was discussed in chapter 5. This value

of $\left.\frac{a_1}{a_1'}\right|_1$ can now be chosen according to the external situation, i.e. if the plasma is locked with no wall, $\left.\frac{a_1}{a_1'}\right|_1 = -0.5$ for a (2,1) mode (using equation (5.37)). When the physical situation has been chosen, there is a certain w value corresponding to it (from Figure 6.10).

The way to set–up the numerical program, is to define w as input parameter. There are then many possible values that δ (and thus $a_1\big|_1$ – using equation (5.10)) can have. We can now vary δ until $\Delta'_{\epsilon_1}(W) = 0$, which determines the δ corresponding to the saturated island width. Every value of w is thus related to a value of δ using the Δ'_{ϵ_1} criterion.

In some of the expressions of $\left.\frac{a_1}{a_1'}\right|_1$ the value of $a_1'\big|_1$ is also needed, i.e. equation (5.45), (5.71), (5.104). This is now known because $\left.\frac{a_1}{a_1'}\right|_1$ as well as $a_1'\big|_1$ is known. This is important because we are now able to determine $B_r\big|_1$ (from $a_1\big|_1$) as well as B_{θ_1} (from $a_1'\big|_1$) for a saturated island with a perturbed boundary. It is not straight forward to calculate both these quantities in other models.

We can now look at the effect of a change in boundary conditions. If δ is increased for some reason (not important for this discussion), the value of w will increase and with it the current profile would become more flattened. We will show that this corresponds to an increase in island size. Figure 6.10 thus gives all the possible islands (parameterized as w) for any boundary condition that a specific equilibrium current profile can have access to if changed in an adiabatic way, and assuming our model is valid. To our knowledge this concise picture has not been shown before.

Contour plots for $J(\hat{\psi})$ and $\hat{\psi}$ with a (2,1) tearing mode present are shown in Figures 6.19 and 6.20. The cases for a (3,1) mode are given in Figure 6.21 and 6.22. In these the island widths have been determined by varying δ (the edge perturbation) until $\Delta'_{\epsilon_1}(W) = 0$. The corresponding graphs for $\hat{\psi}(r)$ and $j_1(r)$ (and $\delta J(r)$) as a function of r are shown in Figures 6.23 and 6.24 in the case of a (2,1) mode present, and in Figures 6.25 and 6.26 in the case of a (3,1) mode. For the (2,1) mode the plasma parameters are $q_0 = 1.6$, $q_1 = 3.6$ and in the case of the (3,1) mode $q_0 = 2.0$ and $q_1 = 4.5$. The relation of $j_1(r)$ to $\delta J(r)$ is determined by the island width which is dependent on $a_1(r_s)$. When $a_1(r_s)$ increases, $j_1(r)$ will also increase because it is a function of $a_1(r_s)$, as was shown in equation (4.16).

6.5.3 The form of the total current $J(\hat{\psi})$ inside the island

In our model it was assumed that the total current J is a function of $\hat{\psi}$. This $J(\hat{\psi})$ function will now be discussed both inside and outside the island.

(a) Outside the island: On the outside of the island $J(\hat{\psi})$ is double valued, as was shown in Figure 4.2 for the case of no island. . Although it looks as if $J(\hat{\psi})$ has two values at the same $\hat{\psi}$, it is actually two values of $J(\hat{\psi})$ corresponding to two different flux surfaces having the same value of $\hat{\psi}$. This can be seen from the form of $\hat{\psi}$ in Figure 6.16.

(b) Inside the island: $J(r)$ has the same value at different r inside the island as is shown in Figure 6.27 for a (2,1) mode with $q_0 = 1.6$ and $q_1 = 3.6$. The two radial points at which $J(r)$ has the same value, correspond to the same flux surface, having the same value of $\hat{\psi}$. This means that $J(\hat{\psi})$ will be single valued inside the island as was shown in Figure 4.3.

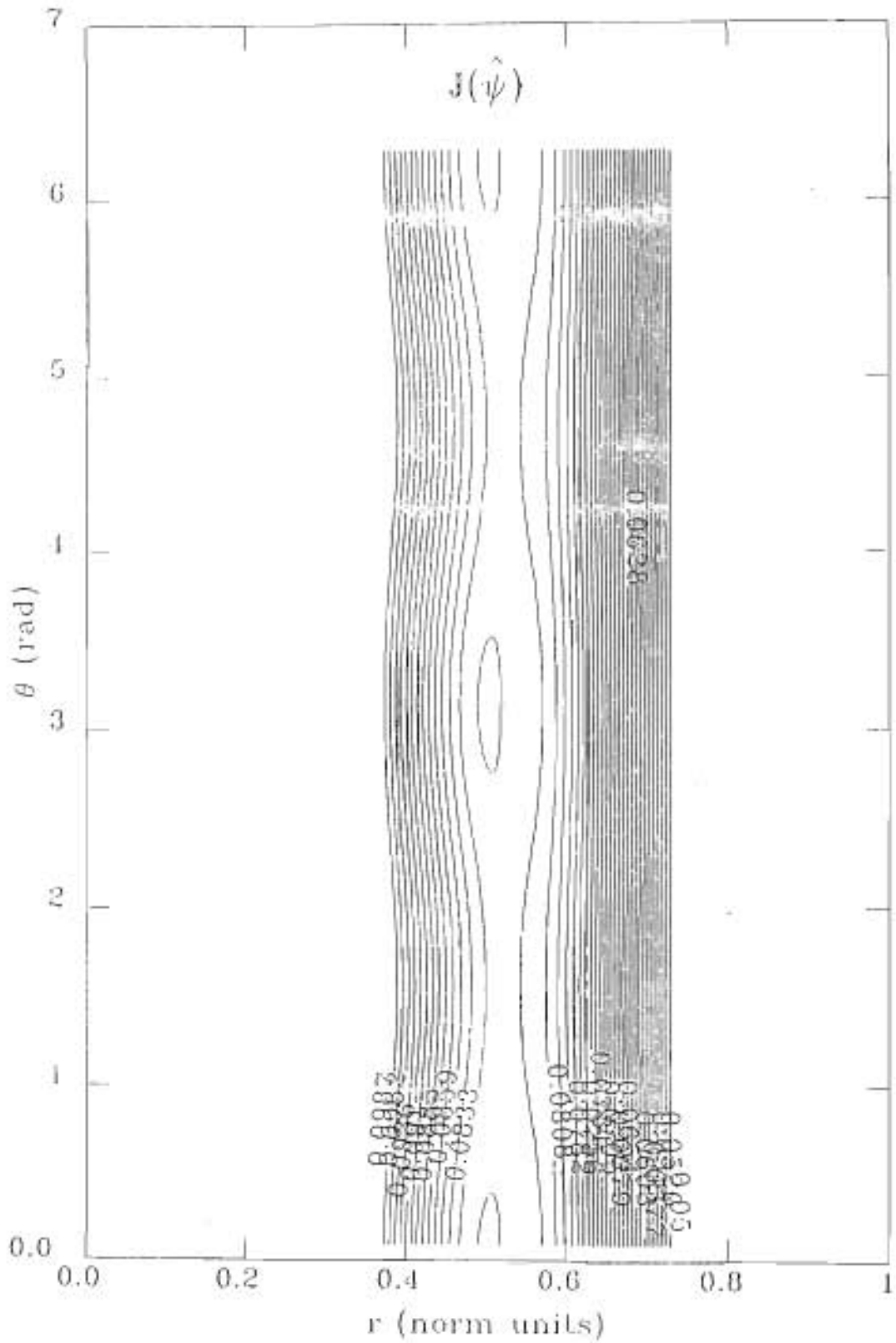

FIGURE 6.19 A contour plot of $J(\hat{\psi})$ with a (2,1) mode present. It is a saturated island with $q_0 = 1.6$, $q_1 = 3.6$.

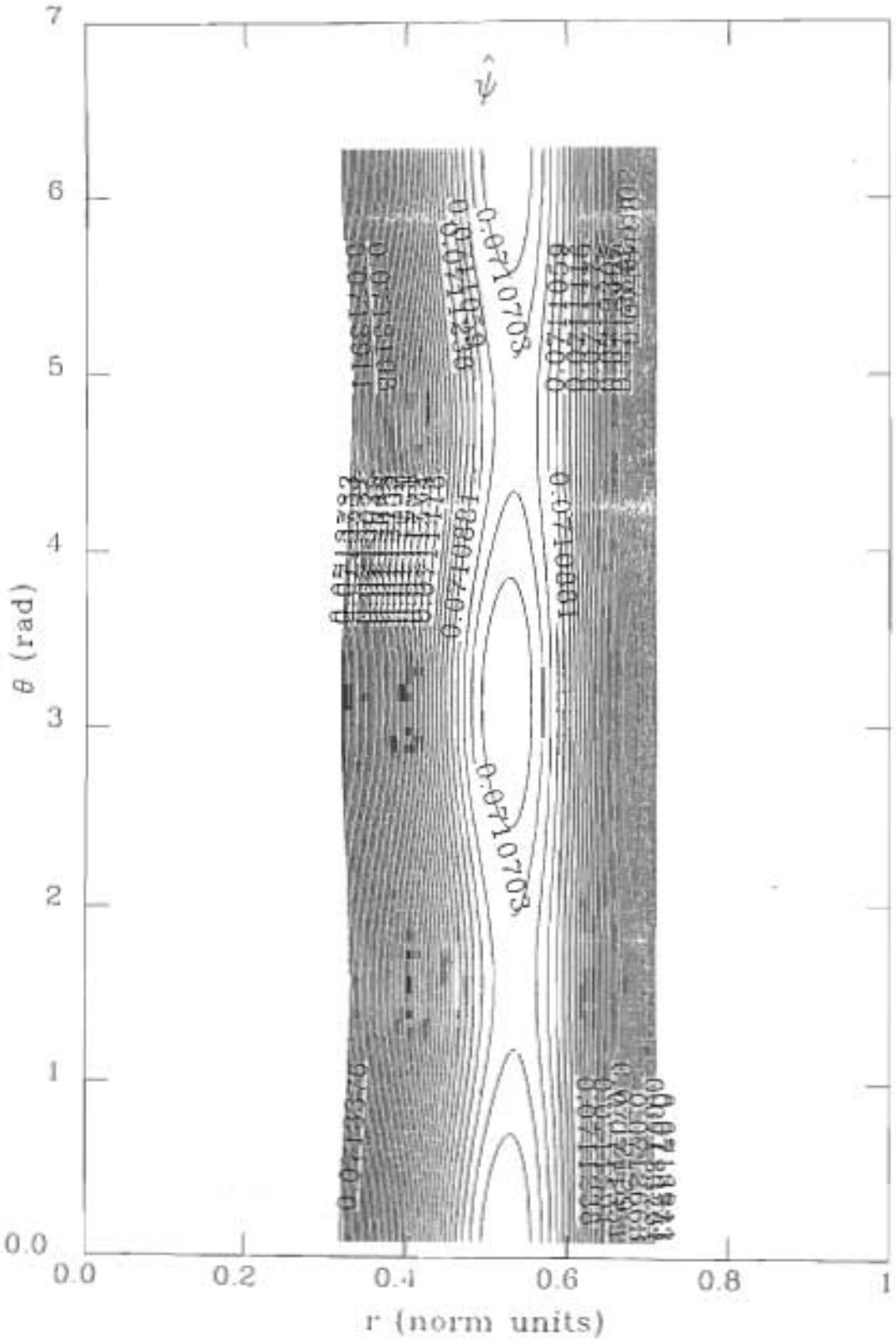

FIGURE 6.20 A contour plot of $\hat{\psi}$ with a (2,1) mode present.

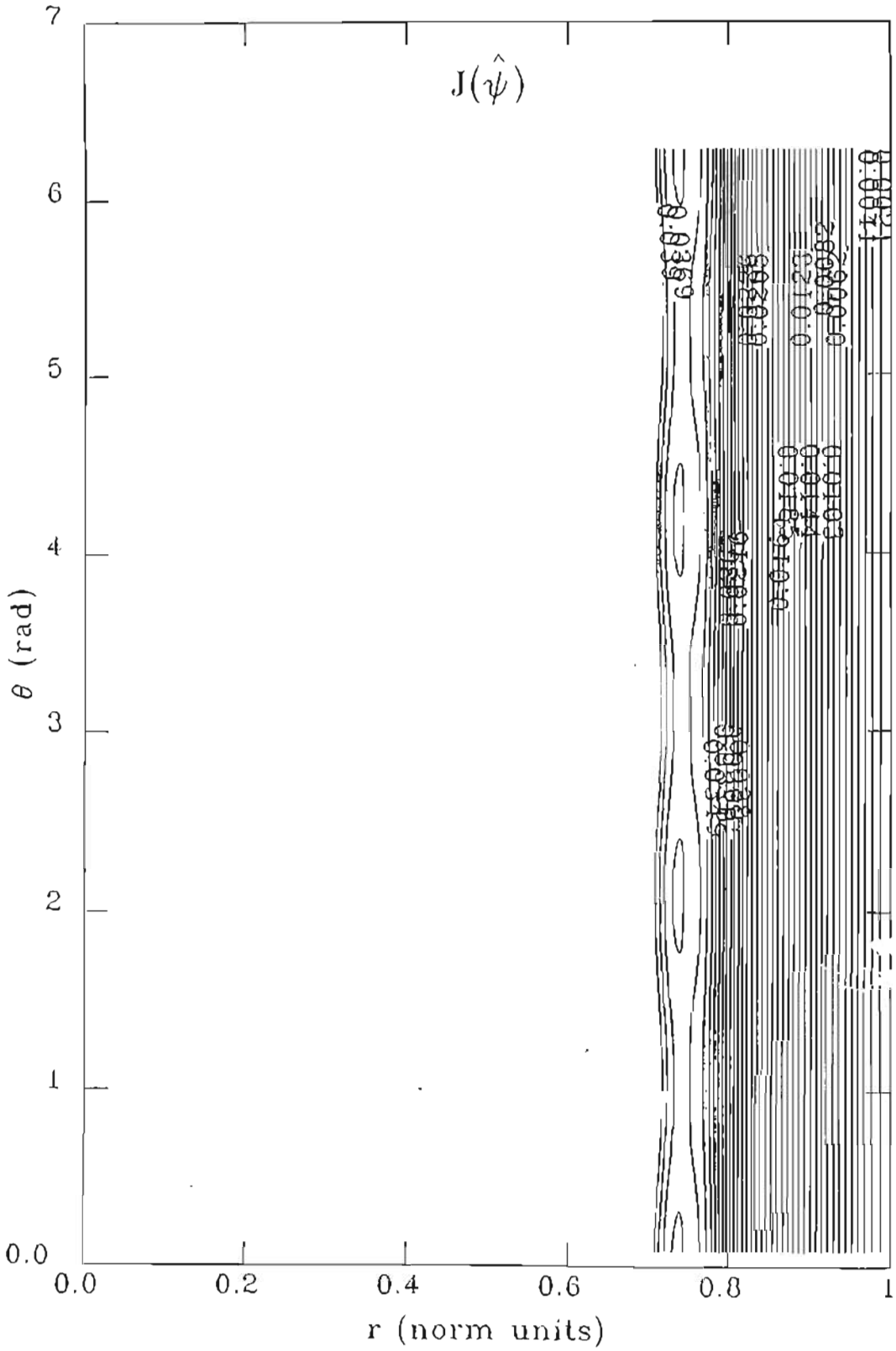

FIGURE 6.21 A contour plot of $J(\hat{\psi})$ with a (3,1) mode present. The island is saturated and the profile has $q_0 = 2.0$, $q_t = 4.5$.

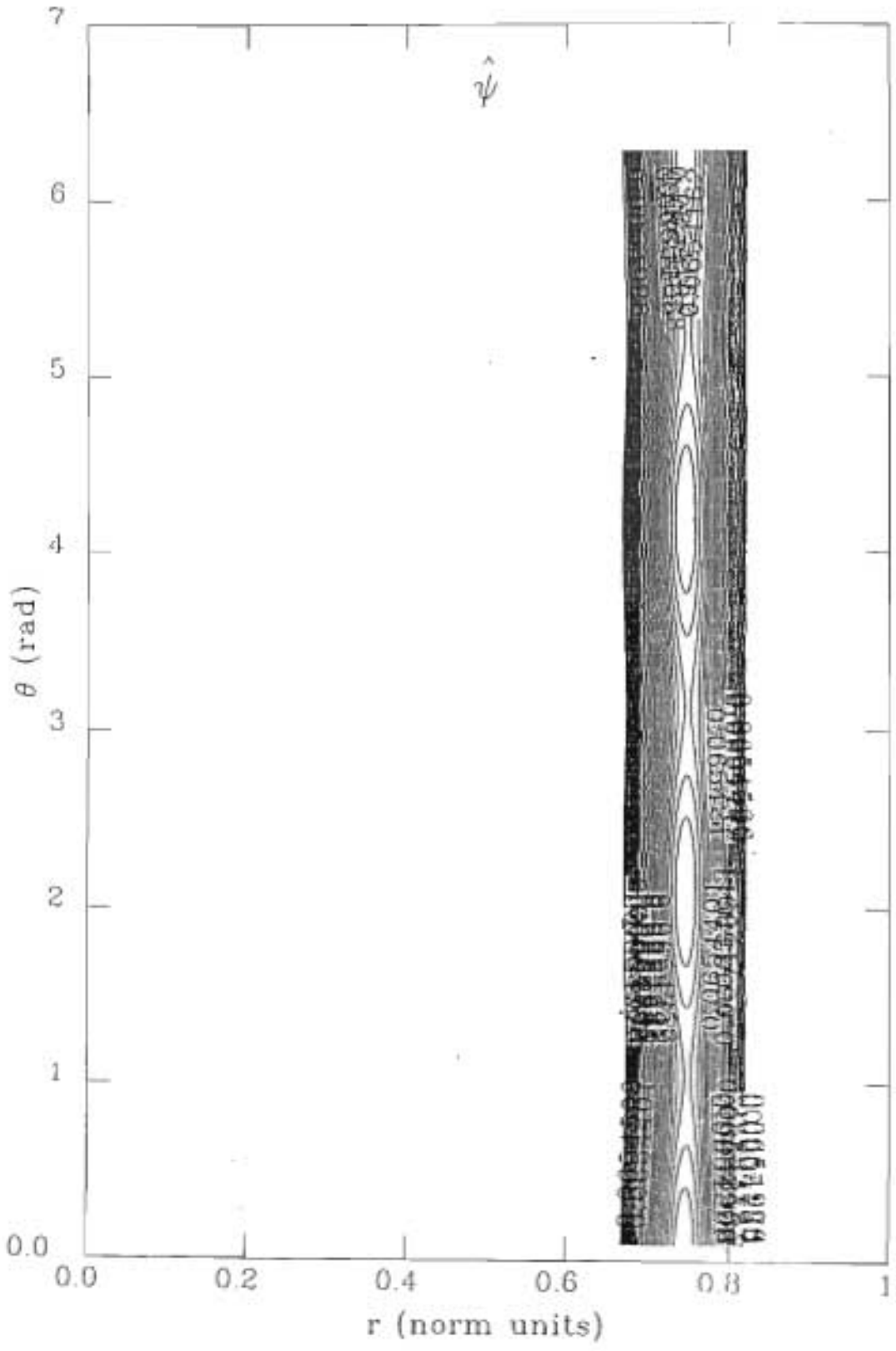

FIGURE 6.22 A contour plot of $\tilde{\psi}$ for a (3,1) mode present.

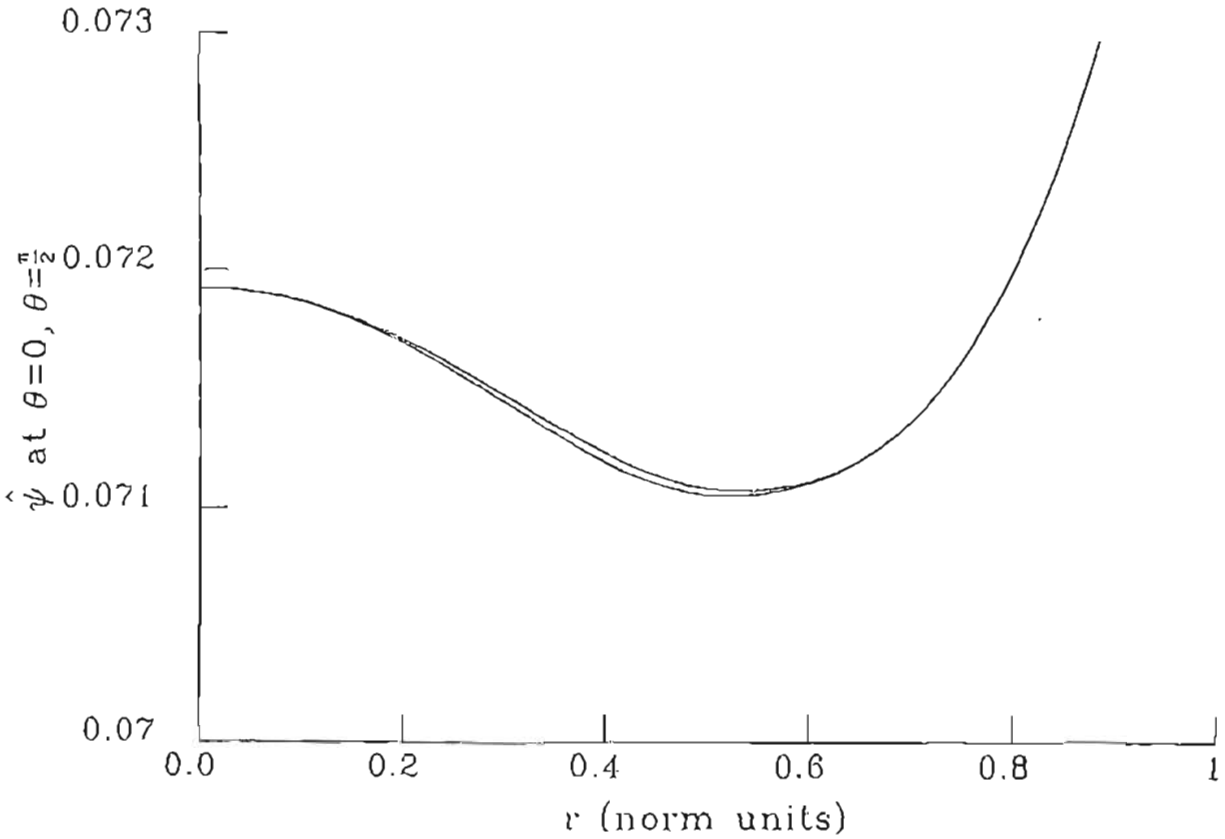

FIGURE 6.23 The graph of $\hat{\psi}$ at both the X and O—points. A (2,1) mode is present. As before $\hat{\psi}$ at the X—point is the upper of the graphs.

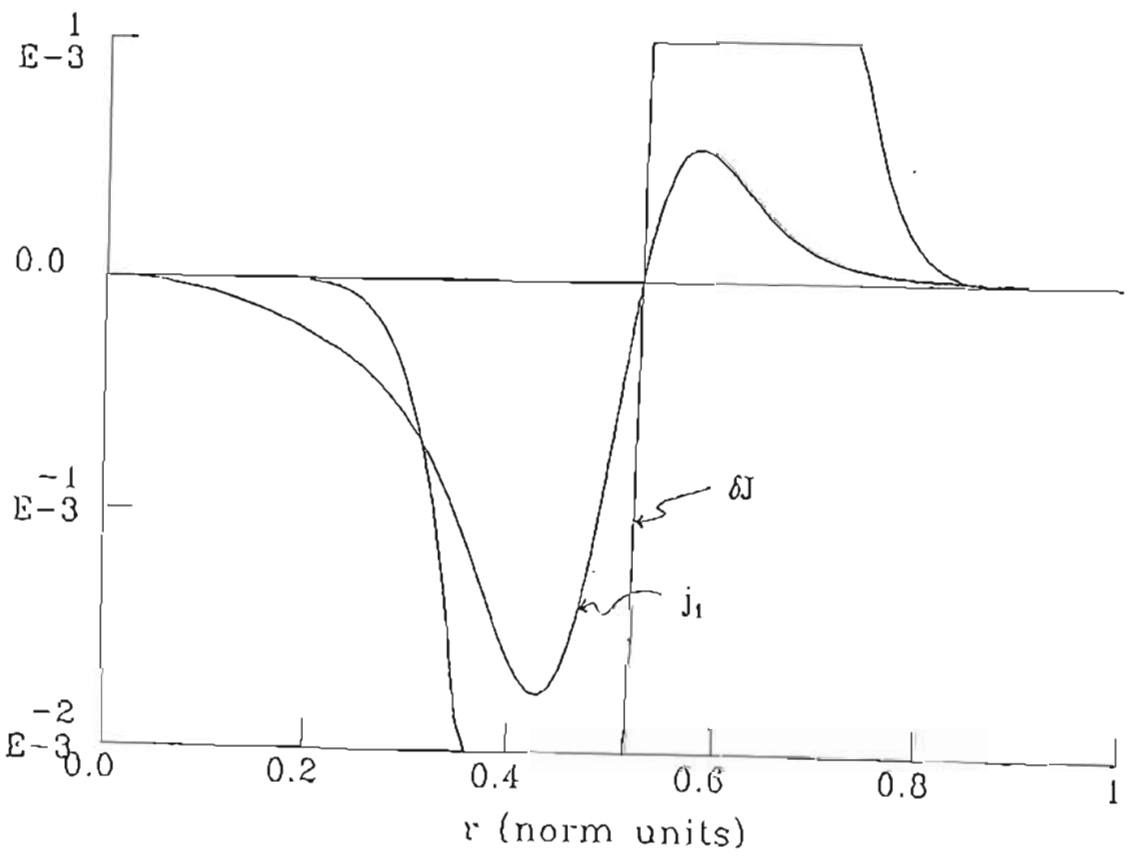

FIGURE 6.24 Both $\delta J(r)$ and $j_1(r)$ are shown for a (2,1) mode.

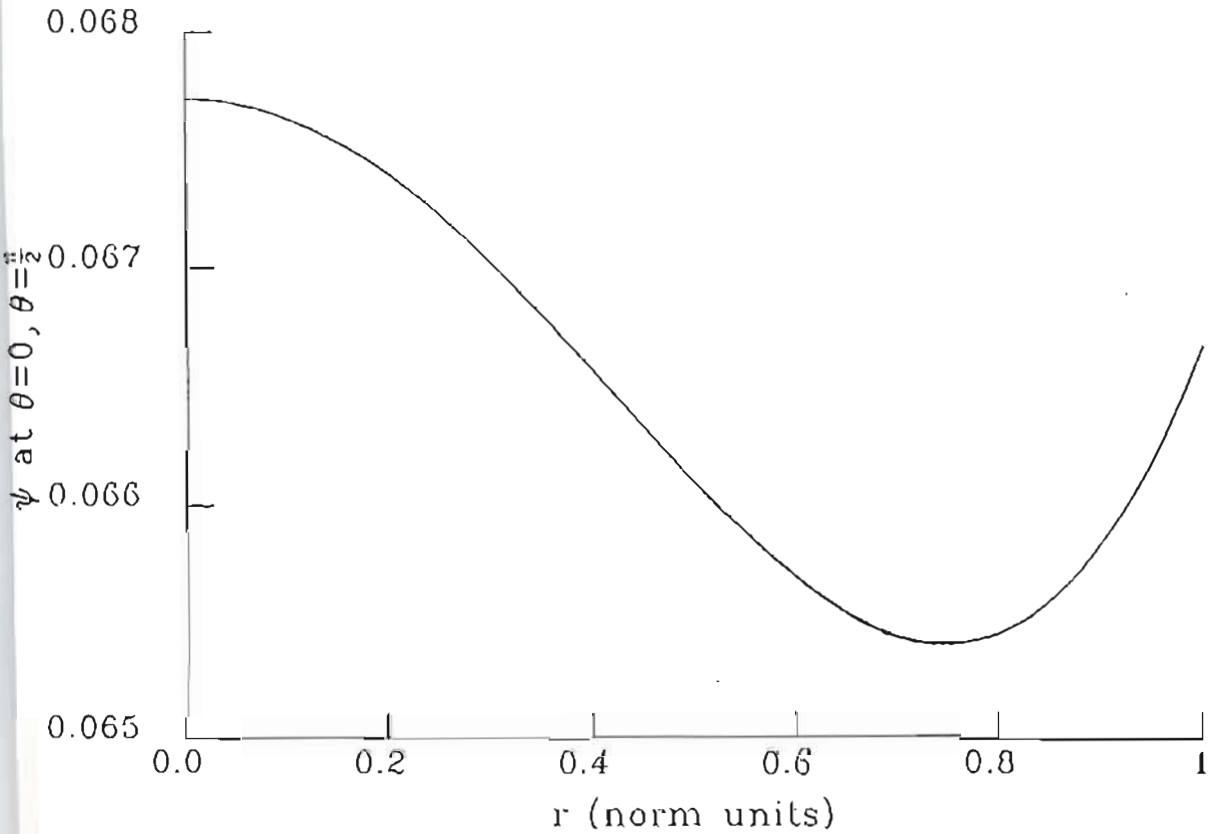

FIGURE 6.25 The graph of $\hat{\psi}$ for both the O and X–points with a (3,1) mode present in the plasma. The difference is negligible.

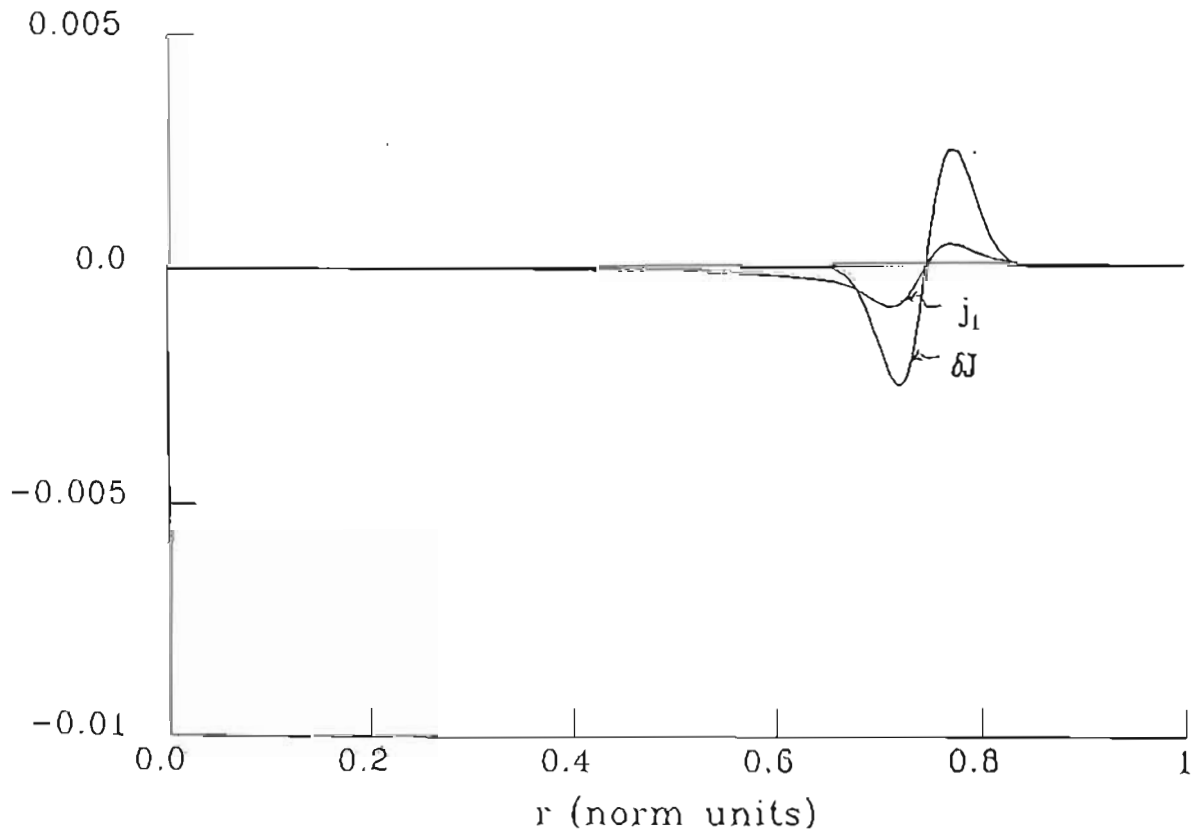

FIGURE 6.26 Both $\delta J(r)$ and $j_1(r)$ are shown for a (3,1) mode.

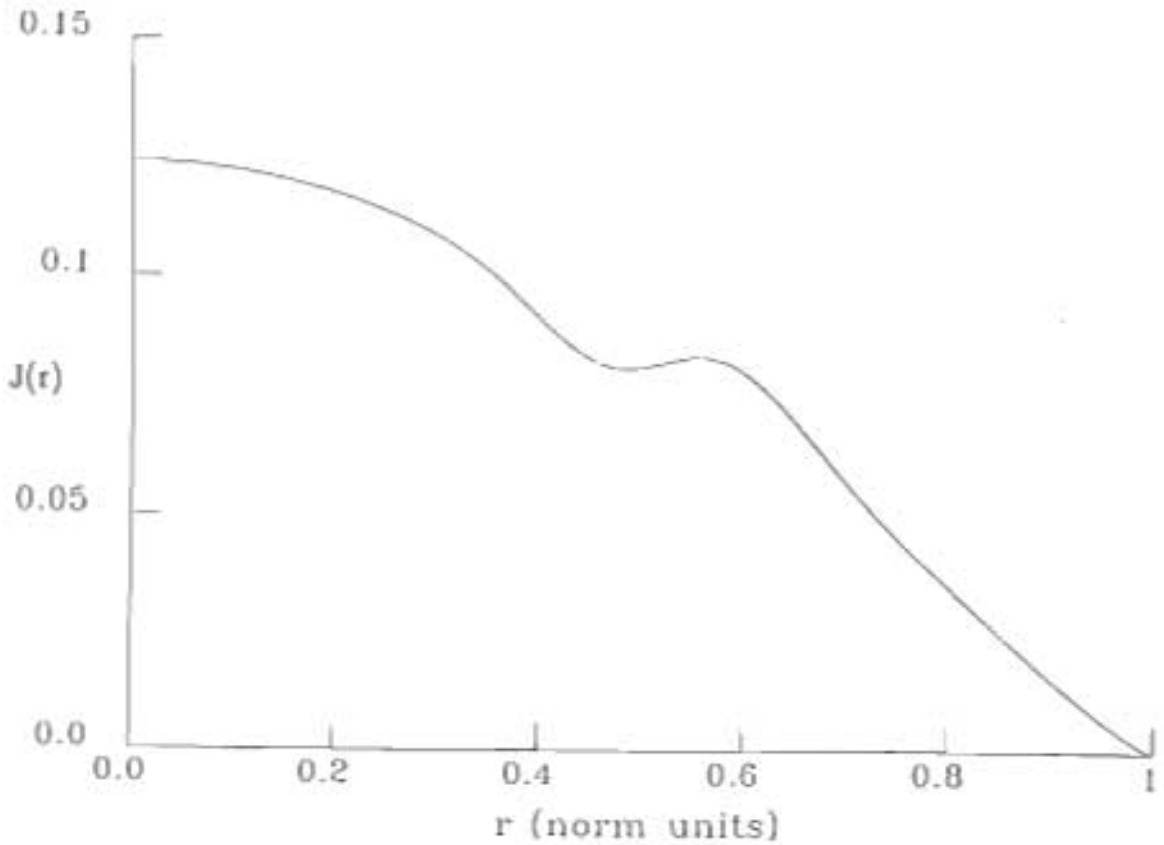

FIGURE 6.27 The current density profile for a (2,1) mode. It is given at the θ–point.

When only first order terms are included in $J(\tilde{\psi})$, an error of $O(\epsilon^2)$ is included:

$$J(\tilde{\psi}) = J(\tilde{\psi}_0) + \tilde{\psi}_1 \frac{dJ(\tilde{\psi}_0)}{d\tilde{\psi}_0} \cos mn + O(\epsilon^2) .$$

The result of this error is that $B.\nabla J \simeq O(\epsilon^2)$. The current will thus not be exactly along flux surface and will thus also not be exactly single valued inside the island. In Figure 6.28 $J(\tilde{\psi})$ is shown as calculated by our model. The error in $J(\tilde{\psi})$ in the island can be detected. If all the terms were to be included in the perturbation expansion, this error would be excluded from the problem.

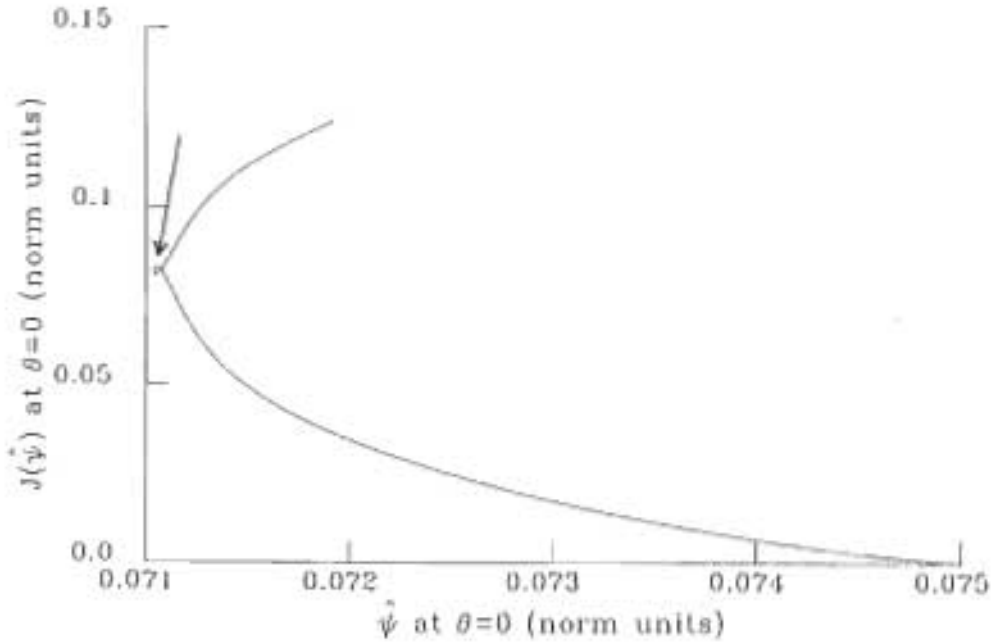

FIGURE 6.28 The graph of total $J(\hat{\psi})$ with an island present. Because of error terms the current is not single valued inside the island. This is indicated with an arrow.

When the position of the sepatrix of the saturated island is calculated at the O–point using the schematic current profile of Figure 6.29, we assume that $r = W_+$ is where $J'(r) = 0$ and $J''(r) > 0$. The value of $r = W_-$ is then found using the fact that $J(W_+) = J(W_-)$. From the form of $J(r)$ as shown in Figure 6.29, it is clear that an error of $0(\epsilon^2)$ would not move $r = W_-$ too far from the correct value calculated using the helical magnetic flux because of the steep slope of $J(r)$ at $r = W_-$. On the other hand, $r = W_+$ can be shifted quite a bit from the correct value if $J(W_+)$ has an error of $0(\epsilon^2)$. From this it is clear that using the current is not a good way to calculate the island width in this model.

It is probably possible to force $B.\nabla J = 0$ with the right choice of δJ consistent with $J''\Big|_{r_s} \neq 0$. To accomplish this a more complicated form of δJ would be needed, which, coupled to some iteration scheme, would make $B.\nabla J = 0$, i.e. $J(\hat{\psi})$ single valued inside the island. We did not investigate this possibility further.

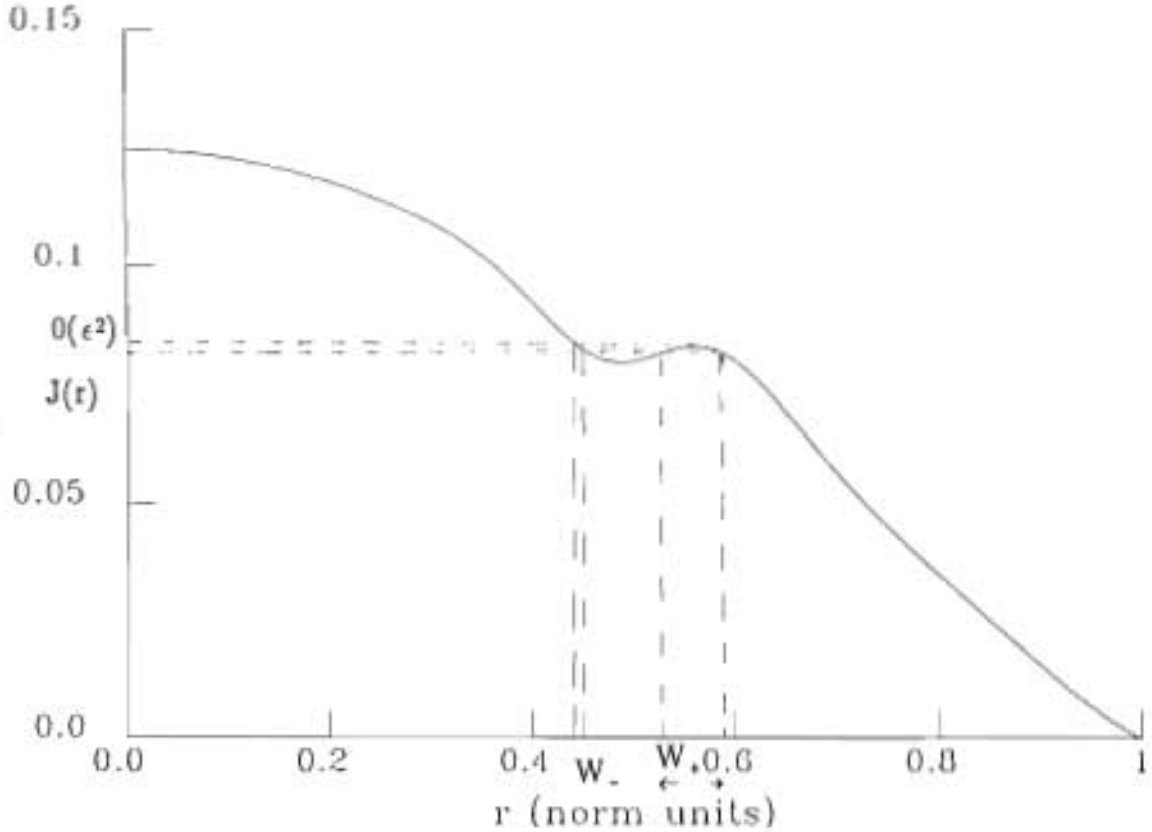

FIGURE 6.29 A schematic diagram of the current density profile. A small error in the value of J(r) can cause a significant error in the calculation of the island size.

6.5.4 The validity of the island width formulae

As was discussed in the beginning of section 6.5.1, the island width formula (given by equation (6.11)) is an approximation to the real island width, which can be calculated accurately as was described in that section. The values calculated from the model are compared below to those calculated using the formula. The % error between these calculations is also presented.

δ	$\sqrt{\delta}$	$7.5\sqrt{\delta}$	W_{model}	$W_{formula}$	% error
0.01	0.1	0.75	0.61	0.77	26
0.005	0.071	0.53	0.48	0.54	13
0.001	0.032	0.24	0.24	0.24	0
0.0005	0.022	0.17	0.17	0.17	0
0.0001	0.01	0.08	0.08	0.08	0

(given for (m,n) = (2,1), $q_0 = 1.3$, $q_1 = 3.6$ with a locked mode).

From the above results it is clear that the island formula is a good approximation when the island width is smaller than about 0.3 of the minor plasma radius.

We also tested a relation of the form $W \sim \sqrt{\delta}$ and found good agreement, especially with the island width formula. The constant of proportionality, calculated to be 7.5 in this case, will change when the profile is changed.

6.6 Calculating Flows

A resistive profile of the form

$$\eta(r) = 1/J_u(r) , \tag{6.16}$$

where $J_u(r)$ is the unperturbed current profile, was included in the model. Such a model is used quite often [3,4]. The motivation for this type of model was discussed in sections 4.5.1 and 4.5.2. This resistive model can be interpreted as an approximation to the resistive profile $\eta(r,\theta,\varphi) = 1/J(r,\theta,\varphi)$ which makes use of Ohm's law where $\underline{V}$ (the velocity) = 0. When the flow is now calculated for a resistive profile of the form given in equation (6.16) (using equation 4.47)), this flow can be interpreted as the flow error involved when the unperturbed current profile is used instead of the perturbed current profile in equation (6.16) i.e. when the resistive profile is not relaxed as is done with the current profile. The flow pattern for the abovementioned resistive profile is shown in Figure 6.30.

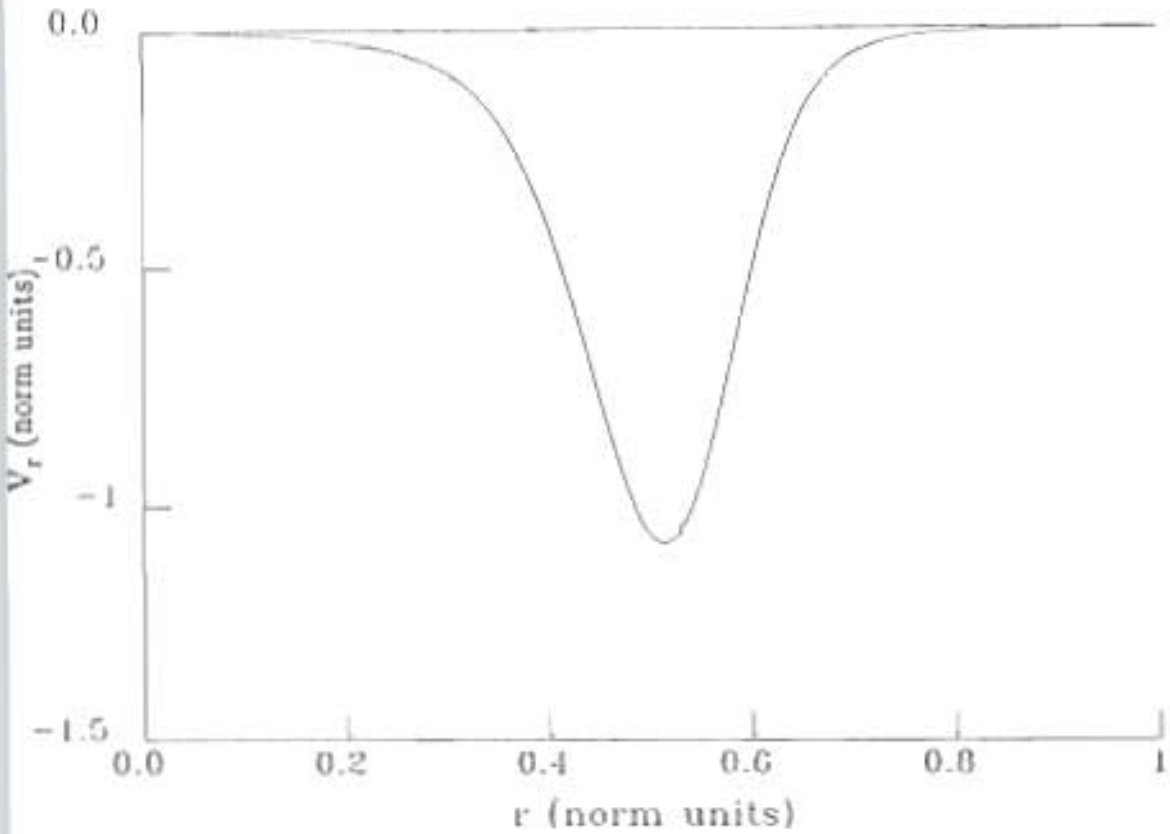

FIGURE 6.30 The flow pattern for a resistive profile of the form $\eta = \eta(r) = {}^{1}/J_0(r)$. The parameters of the model are b = 1.25 and w = 0.1128.

This is not the only way to interpret this flow. When the resistive profile is assumed to be like the one in equation (6.16) then this is what the flow would look like. Using the velocity expression $\underline{V} = \nabla U \Lambda \hat{\varphi}$ (i.e. equation (3.22)), we can see that the flow in Figure 6.30 is the radial flow ($V_r = mb_1$). The poloidal flow changes sign at about r_s, using the fact that $V_\theta \propto -b_1'$.

6.7 Equilibrium Effects

We assume that the equilibrium current profile has the form given in equation (6.3). The value of the safety factor q_0 can now be varied implicitly by changing b (using equation (6.7)), giving rise to a very peaked profile where $q_0 \sim 0.7$, $q_1 = 3.6$ and a more rounded profile with $q_0 \sim 1.3$, $q_1 = 3.6$.

6.7.1 Driving a tearing mode stable situation unstable with mode locking

For both rotation and non–rotation the local flatness of the current density profile at the rational surface with a (2,1) mode present, first increases and then decreases when the on–axis current of the profile increases (q_0 gets smaller). This is shown in Figure 6.31. From this figure it is also clear that the profile is flatter at $r = r_s$ when the plasma is locked than when it is rotating.

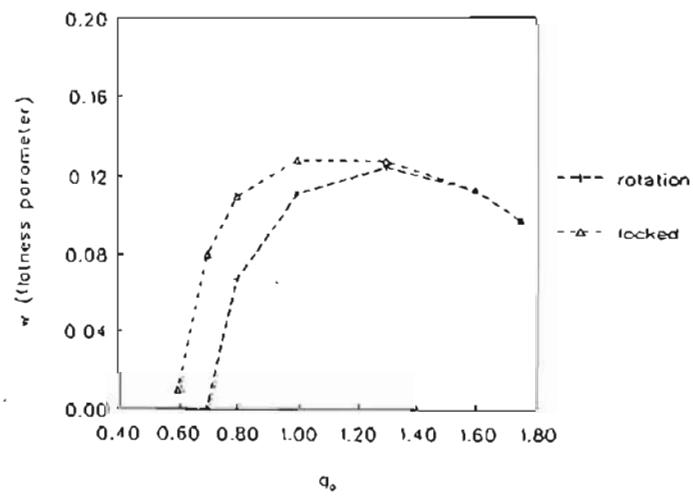

FIGURE 6.31 The graph of the parameter w (i.e. the flattening of the current profile) against the profile type expressed in terms of q_0. When q_0 is small the profile is very peaked. When q_0 is large (i.e. 1.6) the profile is round. Also shown are the values of w for the case of an infinitely fast rotating plasma with a partly conducting wall, and the case when the plasma is locked.

In the next figure a similar graph is shown for the island width. It is immediately clear that there is no real difference between the w (the flatness parameter in equation (6.5)) and W (the island width) behaviour. The relation between W and w is discussed in section 6.7.2.

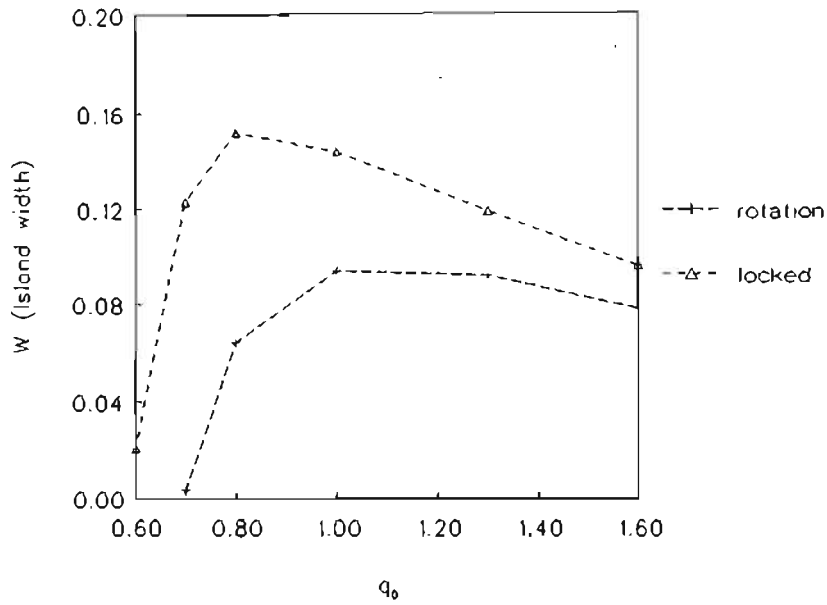

FIGURE 6.32 The graph of the island width against the current profile type. The effect of locking is the largest when $q_0 \simeq 0.8$.

A schematic graph very similar to Figure 6.32 was presented by Reiman [75]. In his approach he specified a profile parameter γ which is related to Δ', i.e. Δ' increases monotonically with γ. For ϵ_1 (i.e. $\hat{\psi}_1\Big|_1$) $= 0$ a bifurcation point is found at $\Delta' = 0$. When $\Delta' < 0$ there is a unique solution, corresponding to a cylindrically stable equilibrium. When $\Delta' > 0$ there are two possible stable solutions agreeing with non–axisymmetric equilibria with islands ($\hat{\psi}_1(r_s)$ can be positive or negative). This is shown in Figure 6.33, taken from his publication.

When $\epsilon_1 \neq 0$, the situation changes. The island width is now not zero at the point $\Delta' = 0$. This is shown in Figure 6.34, also taken from this publication [75].

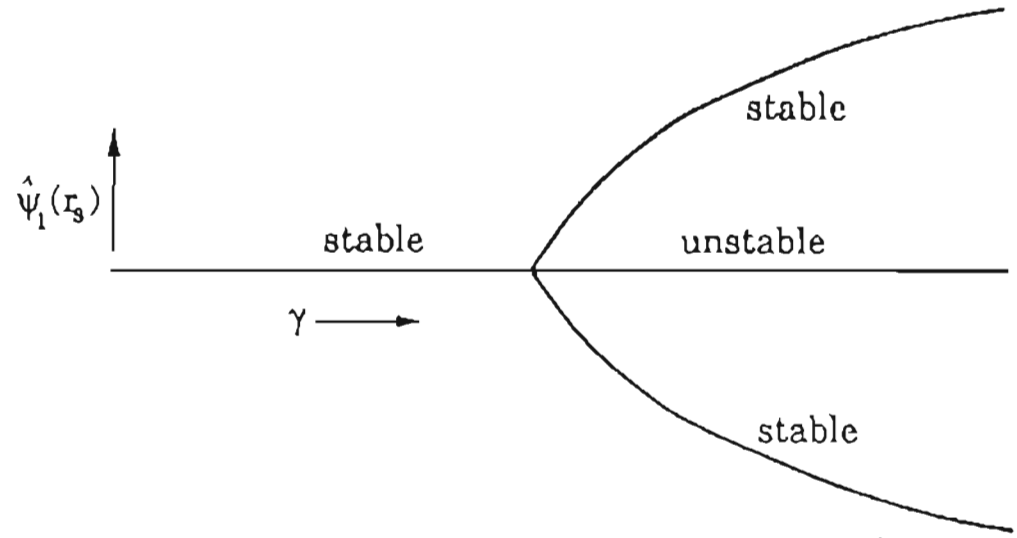

FIGURE 6.33 The graph of $\hat{\psi}_1(r_s)$ against a profile parameter γ which is directly related to Δ'. At $\Delta' = 0$ there is a bifurcation point. To the right of this bifurcation point we find the two possible situations with a saturated island present, i.e. with $\hat{\psi}_1$ negative and positive.

In our approach, the fast rotating case $(\Omega \to \infty)$ agrees with $\epsilon_1 = 0$ and the locked case with $\epsilon_1 \neq 0$. The parameter q_0 is used to change Δ'. As q_0 decreases from $q_0 = 1.0$, Δ' decreases as can be seen from the island width calculations in Figure 6.32. Our q_0 thus relates to his γ. The point where $W \to 0$ for the rotational case agrees with Reiman's $\Delta' = 0$. It is clear from Figure 6.32 that $W \neq 0$ for the locked case at this same q_0 (i.e. $\Delta'_{\epsilon_1} \neq 0$). This is also what Reiman found as was shown in Figure 6.34.

We will now use Figure 6.31 for the rest of the discussion taking the similarity to Figure 6.32 into account.

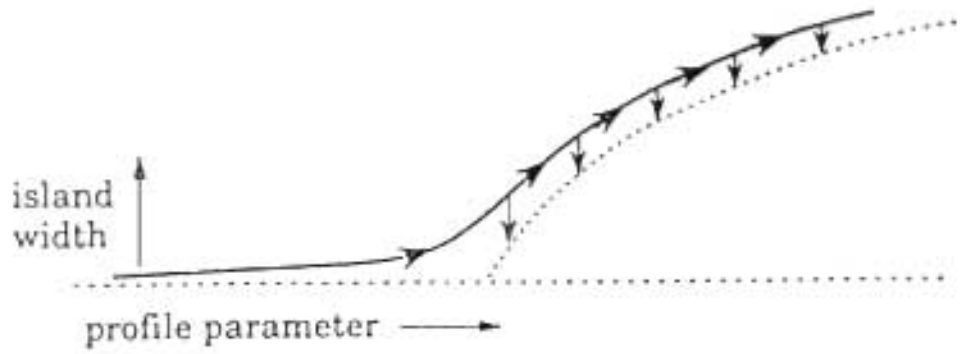

FIGURE 6.34 The graph W against γ. The case of $\epsilon_1 = 0$ is given as the dotted line — agreeing with Figure 6.33. When $\epsilon_1 \neq 0$, the situation changes to the dark line.

When q_0 is about 0.7, the value of w goes to zero in the case of rotation for a (2,1) mode. In the case of a locked mode this happens when q_0 is about 0.6. For a (3,1) mode the value of q_0 where this happens is larger at about 0.8 for a fast rotating mode and 0.7 for a locked mode. Note $w \to 0$ means that there is no flattening of the profile. It also leads to the disappearance of the type I solution in Figure 6.10 — as a result of which there are no tearing mode unstable situations possible. Equilibria with $q_0 \lesssim 0.7$ are thus stable to a fast rotating (2,1) tearing mode. This is qualitatively in agreement with Ellis [31] who found in general that all equilibria with $q_0 \lesssim 0.6$ are stable to (2,1) tearing modes.

Between the graph for an infinitely fast rotating tearing mode and that for a locked one in Figure 6.32, there are lots of possible situations where $B_r\Big|_1$ has penetrated the wall to some extent, but not fully. To each point on this graph we can then associate a rotation frequency.

While the profile is in the process of peaking with q_0 decreasing, it will reach the position where no eigenvalue for a fast rotating mode exists (i.e. $q_0 \lesssim 0.7$). It can then be in some stage of locking with a mode present ($w > 0$) or with no mode present ($w = 0$). This possibility, that a mode can be present for a perturbed boundary although none is possible for a superconducting wall as boundary (or fast rotating mode with a partly conducting wall, i.e. $\Omega \to \infty$), can be seen from Reiman's equation

$$\Delta'_{\epsilon_1}(W) = \Delta'(W) - \epsilon_1 \sigma'(W)/\hat{\psi}_1(r_s) , \qquad (6.15)$$

which was discussed in section 6.5.2.

For $\Delta'(W) = 0$ (i.e. when $\epsilon_1 = 0$) it is still possible to have $\Delta'_{\epsilon_1}(W) > 0$, indicating a tearing mode. It is also in agreement with the work of Gimblett [71] where it was shown that the removal of a superconducting wall can lead to a stable mode becoming unstable.

From Figure 6.32 it is further clear that, although the locking has lead to mode growth, it has not lead to disruptive growth. This is in agreement with other work with parabolic current profiles [86]. What is needed for disruptive growth (i.e. very large islands) is not only profile peaking, but steepening. Generally, steeper profiles result in larger saturated islands.

6.7.2 The relation between flatness of the profile (w) and the island width (W)

The present tearing mode model is only valid when $0.15 \gtrsim w \gtrsim 0.01$. When $w \lesssim 0.01$, the quantities to be measured (like the island width) are smaller than the error bars within which the island can be measured. When w is large, the total

current is not preserved because δJ is non–zero at the boundary. In spite of the fact that it is not possible to calculate the physical quantities, the trends are consistent at the extremes of w.

If an analytic relation between w and the island width could be found, it would be possible to predict an island width outside the region where it can be numerically calculated. If it is assumed that the parameter w (i.e. the local flatness of the profile at $r = r_s$) is directly proportional to the island width, and since W is zero when w is zero, a relationship of the form $W = hw$ can be tested with the data. It was found that

$$W = hw\sqrt{q_0} \qquad (6.16)$$

fits the data quite well if q_1 is kept fixed. The constant h is found to be 1.6 giving $W = 1.6\ w\sqrt{q_0}$ for the (2,1) island. The largest error found with this formula is about 1 % of the minor radius.

6.7.3 The perturbation of the boundary

The perturbation of the boundary (Figure 6.35) follows the change in island width (presented in Figure 6.32) for different current profiles, i.e. different q_0. This means that larger islands will perturb the boundary more than small islands.

In Figure 6.35 we show the change in $B_{\theta 1}\Big|_1$ for fast rotating modes as well as the change in δ for locked modes – both with changing q_0. The results are for a (2,1) mode.

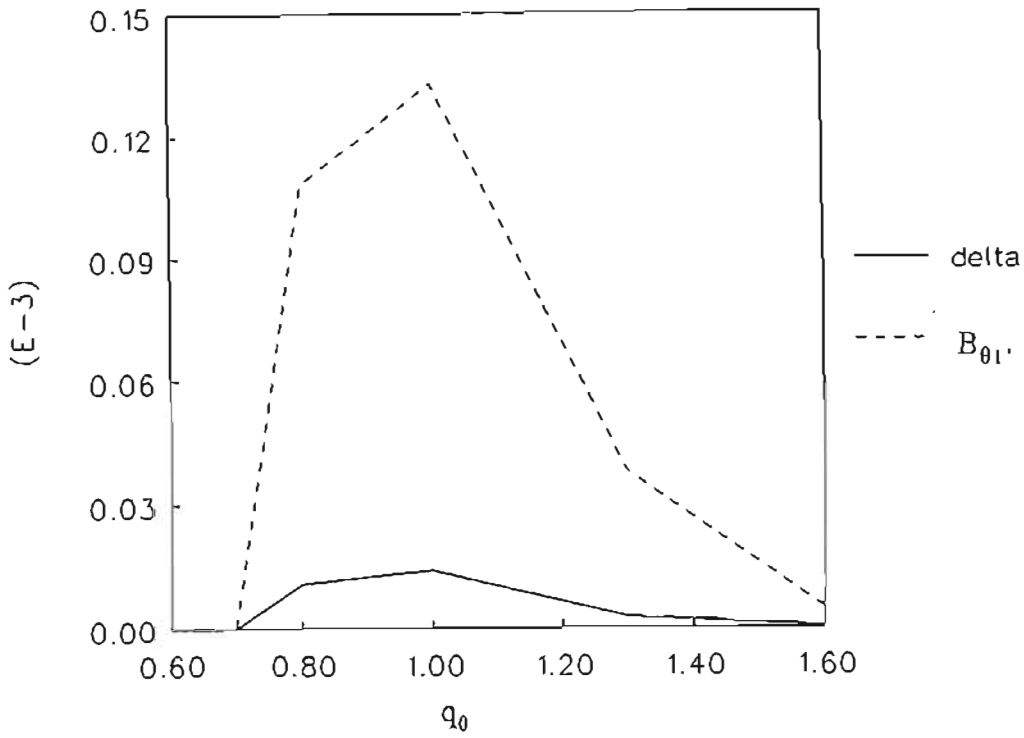

FIGURE 6.35 The graph of D_{θ_1} and δ against current profile parameter q_0. Larger islands perturb the boundary more as is clear when this is compared with Figure 6.32.

The deeper the island is, inside the plasma, the smaller the effect of the boundary perturbation on it. This can be seen from Figure 6.36. In this graph we compare the values of $\left.\frac{a_1}{a_1'}\right|_1$ against w for two profiles where $q_1 = 3.6$ but $q_0 = 1.75$ and 0.8. The rational surface is at $r_s = 0.45$ when $q_0 = 1.75$ and at $r_s = 0.73$ when $q_0 = 0.8$. It can be seen that the eccentricity of the "hyperbole" is much smaller when r_s is deep inside the plasma than when it is more to the outside. This was found to be generally true. This means that the effect of a change in $\left.\frac{a_1}{a_1'}\right|_1$ on w is much smaller when the rational surface is deep inside the plasma. When it is remembered that $\left.\frac{a_1}{a_1'}\right|_1$ is related to the outside physical situation and w to the island width (W), it is clear that the island width becomes rather insensitive to the external situation when the island is deeper inside the plasma. Clearly, this is physically reasonable and was found to be true on Tokoloshe [84].

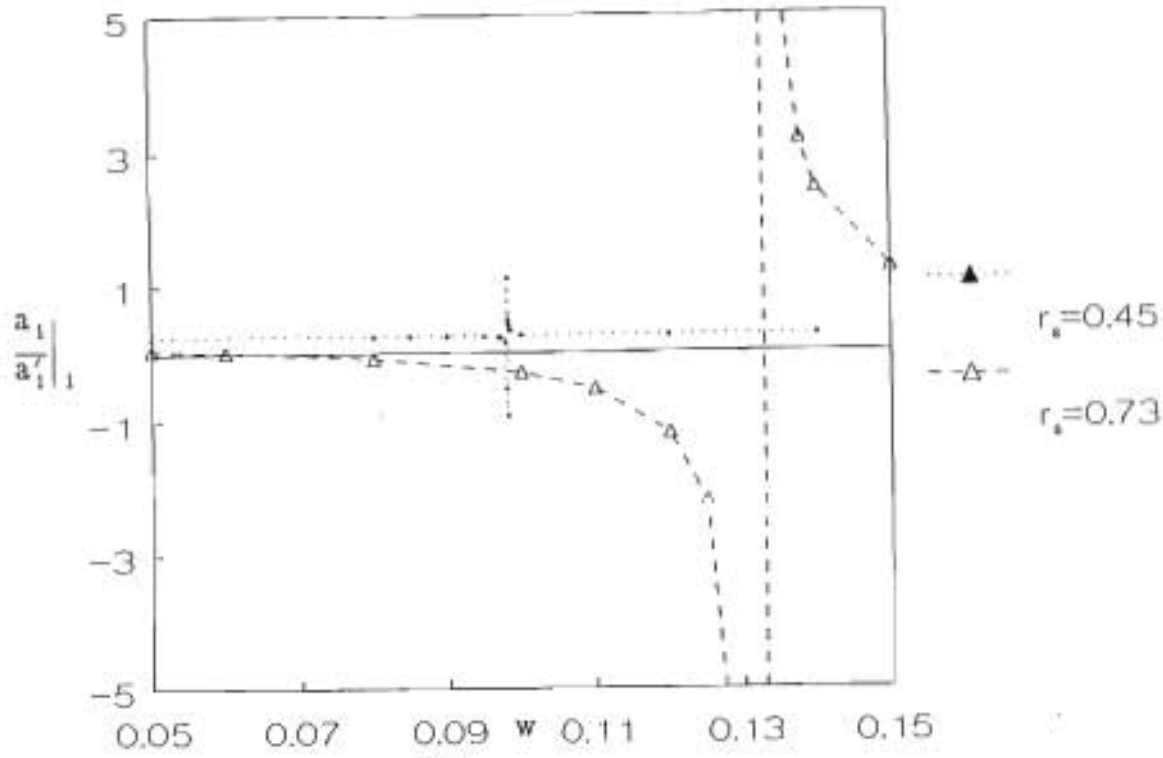

FIGURE 6.36 The graph of $\frac{a_1}{a_1'}\Big|_1$ against w for $q_0 = 1.75$ ($r_s = 0.45$) and $q_0 = 0.8$ ($r_s = 0.73$) with $q_1 = 3.6$. The value of w becomes rather insensitive to $\frac{a_1}{a_1'}\Big|_1$ when r_s get smaller.

6.8 The Effect of Rotation on the Island Width

In chapter 5 the effect of rotation on the parameter $\frac{a_1}{a_1'}\Big|_1$ was discussed. It was shown (in Figure 5.5) how this parameter changes with $\omega\tau_w$. Using the $\Delta'_{\epsilon_1}(W)$ criterion of Reiman, it is now possible to calculate the saturated island width for any value of $0 \le \frac{a_1}{a_1'}\Big|_1 \le \frac{a_1}{a_1'}\Big|_1$ (locked mode), i.e. for any rotational frequency. From this calculation a boundary perturbation δ is immediately known (as was discussed in section 6.5.2) which allows us to calculate $a_1\Big|_1$ i.e. $B_r\Big|_1$, from equation (5.10). We can thus plot figures of $B_r\Big|_1$ and $B_{\theta 1}\Big|_1$ against $\omega\tau_w$. This is done in Figure 6.37 and 6.38 for a (2,1) mode with $r_w = 1.01$. Figure 6.37 is for the high MHD phase ($q_0 = 1.3$, $q_1 = 3.6$) and Figure 6.38 for the low MHD phase ($q_0 = 0.8$, $q_1 = 3.6$). Note that the amplitude of $B_{\theta_1}\Big|_1$ is much larger during the high MHD phase than during the low MHD phase.

The radial magnetic field reduces when the mode frequency increases. The reason is simple and was discussed in section 5.3 – the time for field penetration reduces when the mode frequency increases. The perturbed poloidal magnetic field ($\left|B_{\theta 1}\right|$) does the opposite, increasing with mode frequency.

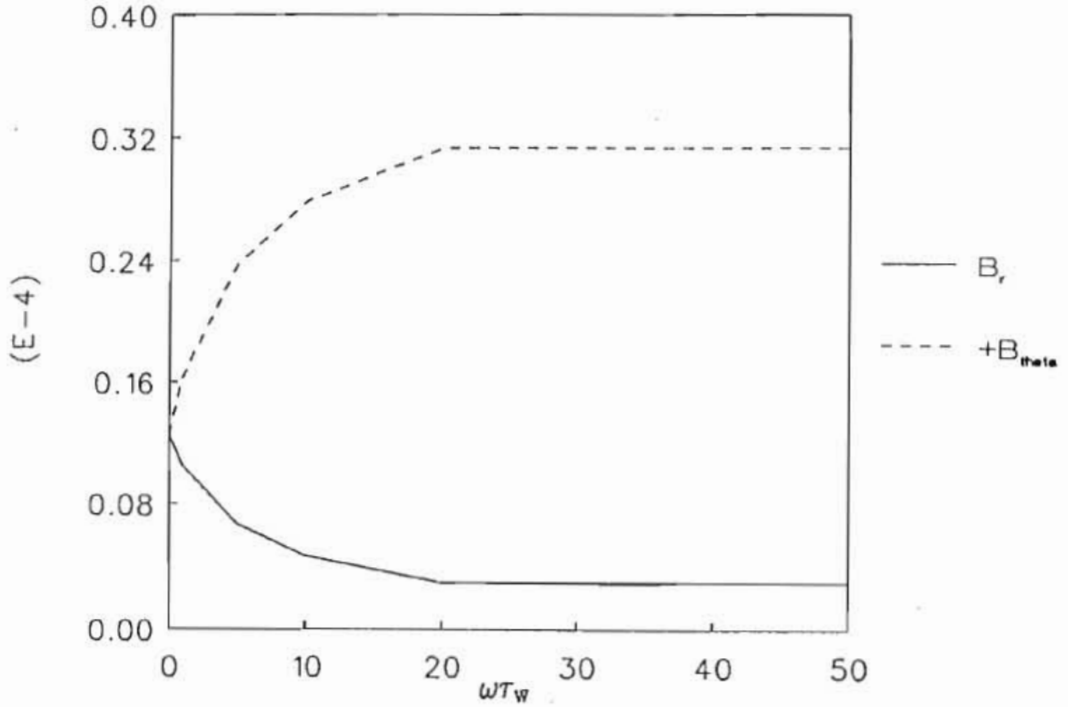

FIGURE 6.37 The graph of B_r and $B_{\theta 1}$ against $\omega\tau_w$. When $\omega\tau_w$ decreases, i.e. the mode slows down, the radial magnetic field increases (as does δ), but the perturbed poloidal magnetic field decreases.

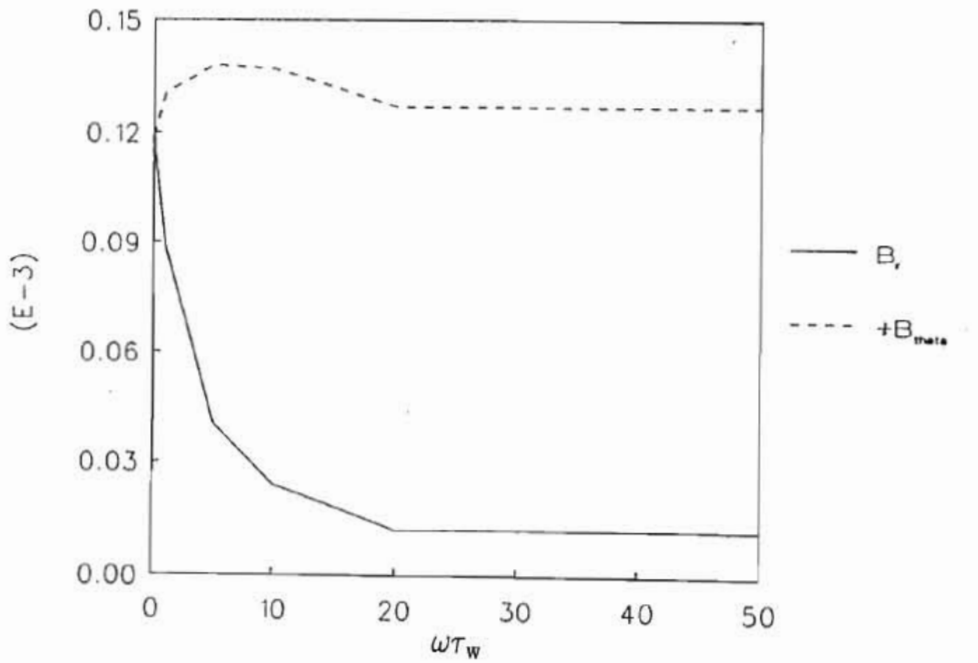

FIGURE 6.38 The behaviour of B_r and $B_{\theta 1}$ when the mode slows down ($\omega\tau_w$ decreases) during the low MHD phase.

In Figure 6.39 we present the island width against $\omega\tau_w$ for the same parameters. It is now possible to see how the island evolves if the rotating mode is locked, assuming adiabatic changes in the equilibrium. The island width increases when the mode frequency decreases for both high and low MHD phases. The effect on the island size is, however, bigger during the low MHD phase (i.e. $q_0 = 0.8$).

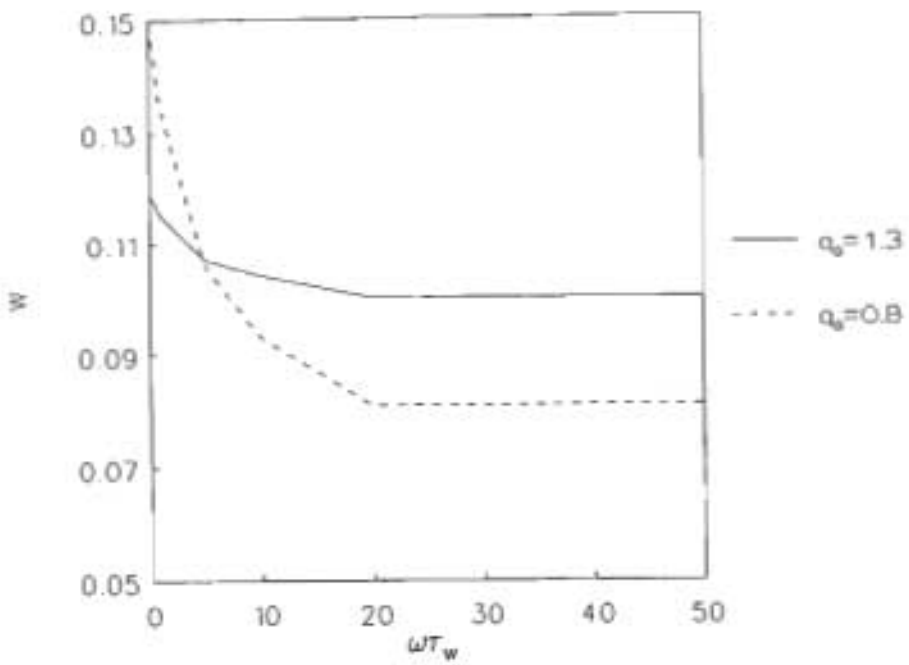

FIGURE 6.39 The island width increases when the mode frequency decreases for both high and low MHD phases.

6.9 The Different $\Delta'(W)$ Criteria Compared

In this section we compare the different $\Delta'(W)$ criteria. We will first discuss the case of $B_r\Big|_1 = 0$. The criteria of Rutherford [2], White et al. [3] and Reiman [75] were discussed in section 6.5.2. It is shown in Figure 6.40 that the criterion of Rutherford predicts a slightly larger island than that of Reiman. This is because the criterion is defined differently as is clear from equations (6.12) and (6.13). The effect of the α parameter in the criterion of White et al. (see section 6.5.2) is to reduce the island size from that predicted by the Rutherford criterion, bringing it more in line with that of Reiman.

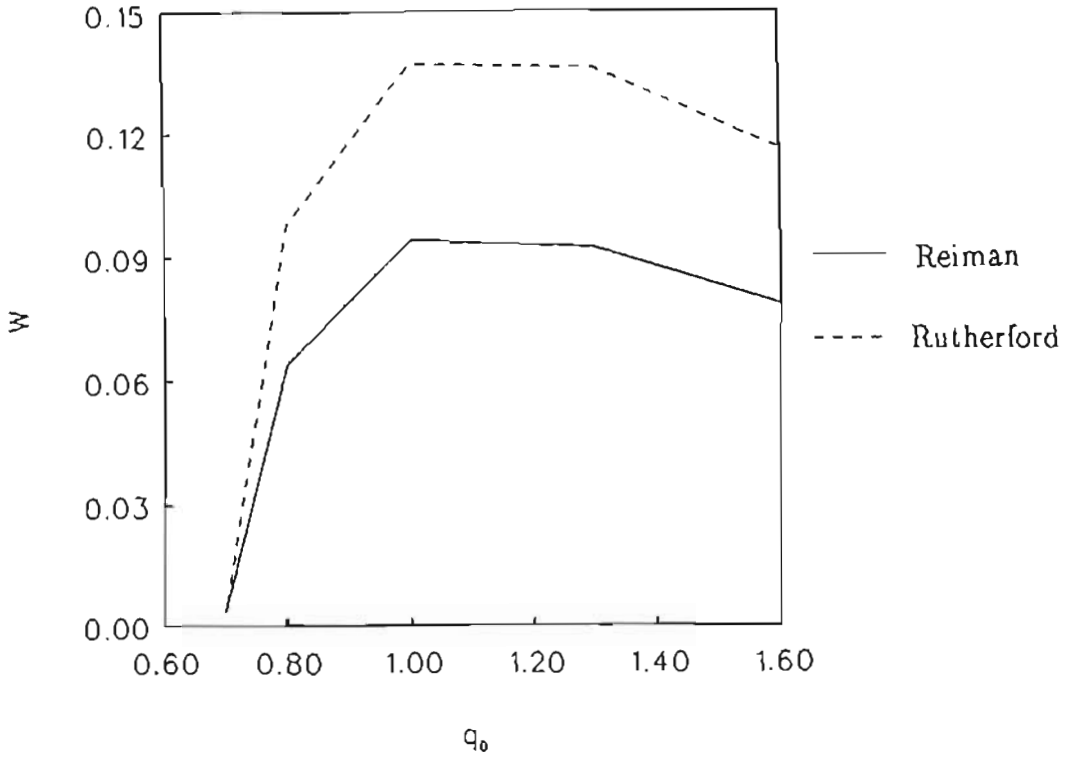

FIGURE 6.40 Comparing the criteria of Rutherford with that of Reiman in the case of a superconducting wall, for varying equilibrium parameter q_0.

When an external perturbation $\left(B_r\Big|_1 \neq 0\right)$ is included in the problem, that is the case with decreasing $\omega\tau_w$ (i.e. Ω), the criteria of Reiman and Rutherford can be compared to determine what error is involved in using Rutherford instead of Reiman for cases where external perturbations are included as has been done by Hansen [79]. This difference in island width is shown in Figure 6.41 for a (2,1) mode. It is clear that, although the island size is larger when the Rutherford criterion is used, the effect of mode locking is qualitatively the same irrespective of the type of criterion used.

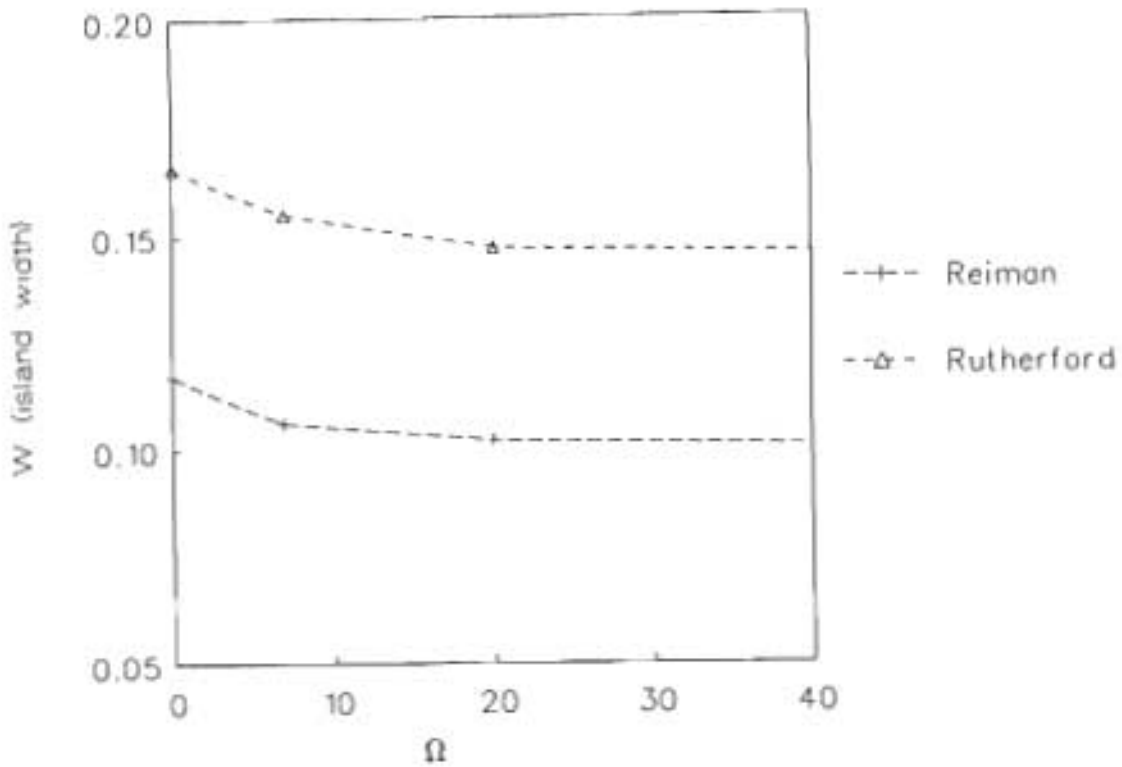

FIGURE 6.41 The island size using the $\Delta'(W)$ criteria of Reiman and Rutherford is compared for different rotational frequencies.

6.10 External Coils

6.10.1 The effect of the external coils on the island size

For this section it is important to remember the plasma current direction shown in Figure 4.1. It is now possible to choose the external coil configuration in line with the plasma current direction (as was done in Figure 5.2), or in opposite direction. When it is chosen in line with the plasma current direction, i.e. $I_\ell > 0$, the radial magnetic field is of the form $B_r(r,\theta,\varphi) = B_r(r) \sin \chi$, with $B_r(r) < 0$.

When the magnetic fields associated with such a configuration ($I_\ell > 0$) are drawn, it is immediately clear where the islands will form. This is shown in Figure 6.42. On the inside of the rational surface the fields are in the anti–clockwise direction. When the poloidal magnetic field at the rational surface is subtracted to give the helical magnetic field, the poloidal field on the outside of the rational surface will be in the clockwise direction. Together with the fields of the coils, it is clear that the islands will form in the positions shown.

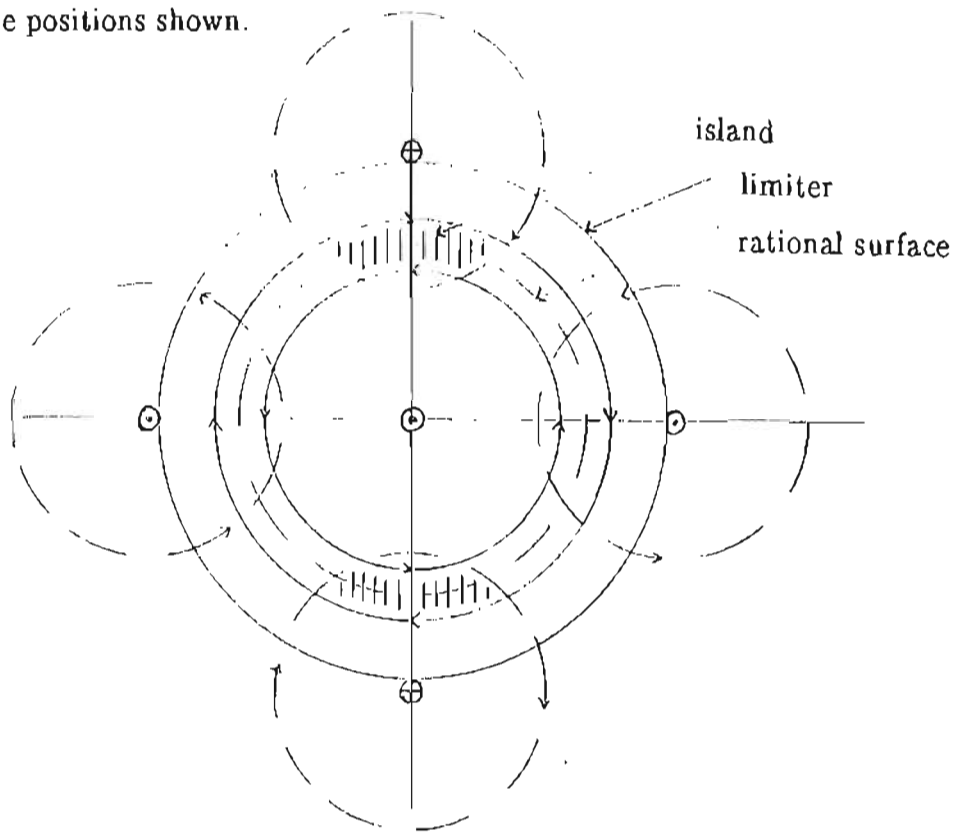

FIGURE 6.42 The formation of islands with $I_\ell > 0$.

For this configuration we have $\delta < 0$, which corresponds to $a_1 > 0$ (from the discussion in section 6.5.1). Thus $B_r(r,\theta,\varphi) = \frac{1}{r}\frac{\partial \psi}{\partial r} = -\frac{m}{r} a_1 \sin\chi$ gives $B_r(r) = -\frac{m}{r} a_1 < 0$ as was discussed earlier in this section.

From equation (5.59) we know that $j_z^{(m,n)} > 0$ when $I_\ell > 0$ for a (2,1) mode. We can now in summary state that

$$I_\ell > 0\,, \qquad j_\chi^{(m,n)} > 0\,, \qquad a_1 > 0\,, \qquad B_r < 0 \qquad (6.17)$$

and

$$I_\ell < 0\,, \qquad j_\chi^{(m,n)} < 0\,, \qquad a_1 < 0 \qquad B_r > 0\,, \qquad (6.18)$$

which is valid if the mode is always in phase with the external coil. When these different configurations are substituted into equation (5.45) we find that an increase in $\left|j_\chi^{(m,n)}\right|$ (either positive or negative) will always change $\left.\frac{a_1}{a_1'}\right|_1$ such that w will increase (keeping Figure 6.10 in mind). This means that when the island is locked in phase with the coil, a DC coil current will always lead to an increase in island size.

We will now look in more depth at this increase in w caused by an in–phase external coil. In the case of $\omega \to \infty$ the equilibrium is at point 1 on Figure 6.43 (which is just the inverse of Figure 6.10). Once it is locked, it is at point 2 with $\left.\frac{a_1}{a_1'}\right|_1 = -0.501$ as was discussed earlier. The effect of a coil current is now to drive $\left.a_1/a_1'\right|_1$ along the arrow on the graph shown in Figure 6.43.

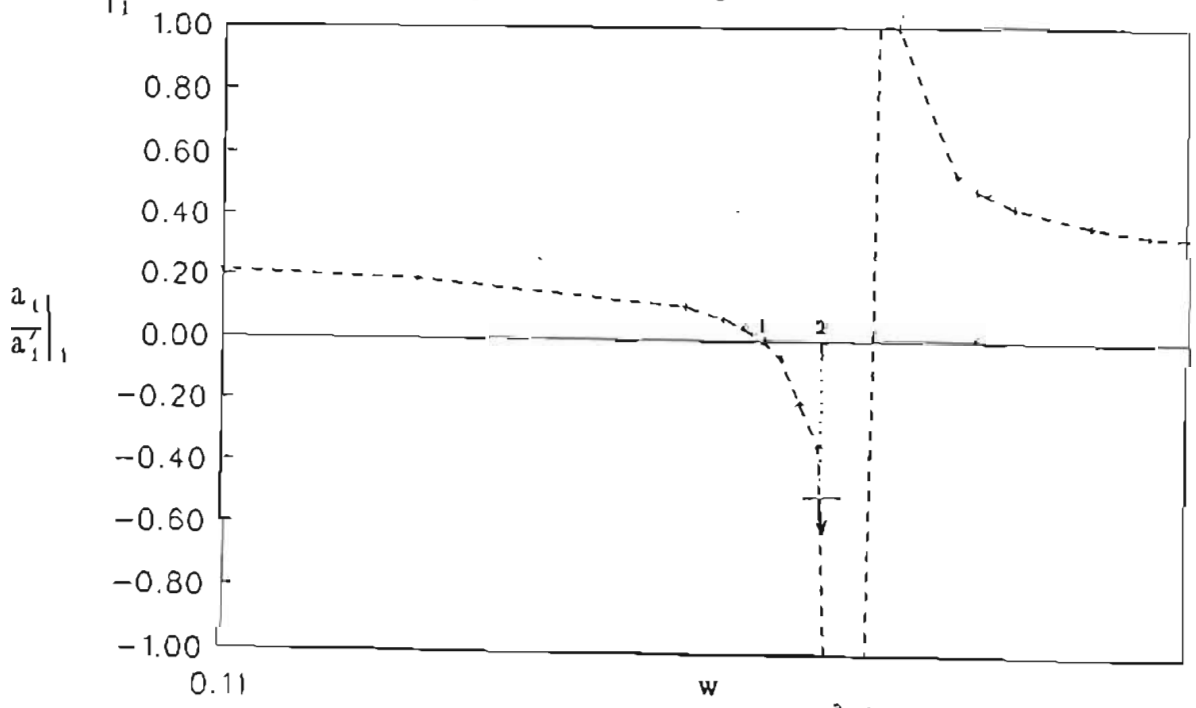

FIGURE 6.43 This graph shows how w will change when $\left.\frac{a_1}{a_1'}\right|_1$ is changed because of an external coil current. The effect of the current is to drive w larger.

Equation (5.45) can also be written as

$$j_z^{(m,n)} = \frac{a_1'\Big|_1}{r_c} \frac{K_m(\epsilon n r_c)}{K_m(\epsilon n)} \frac{L(\epsilon n r_c)}{L(\epsilon n)} \left[\frac{m^2}{\epsilon n} \frac{K_m(\epsilon n)}{K'(\epsilon n)} \frac{a_1}{a_1'}\Big|_1 - 1 \right] . \qquad (6.19)$$

For any $\frac{a_1}{a_1'}\Big|_1$ we can calculate the saturated island width from Reiman's criterion (given in equation (6.13)). Once this is found, both $a_1\Big|_1$ and $a_1'\Big|_1$ are known ($a_1'\Big|_1$ is known because it is the shooting value, and $a_1\Big|_1$ because δ is known – see equations (5.10) and (5.11).). The values of $\frac{a_1}{a_1'}\Big|_1$ and $a_1'\Big|_1$ can now be substituted into equation (6.19) to obtain the coil current which must be associated with that specific $\frac{a_1}{a_1'}\Big|_1$.

In Figure 6.44 the relation of $j_z^{(m,n)}$ to $\frac{a_1}{a_1'}\Big|_1$ is shown for a (2,1) mode with $\epsilon = 0.1$. It is clear, when compared with Figure 6.43, that an increase in coil current leads to an increase in the value of w . Our configuration is such that the coil current is only switched on when the mode is already locked, i.e. $\frac{a_1}{a_1'}\Big|_1 = -0.501$ for the (2,1) mode.

6.10.2 The relation between W and I_ℓ

As was already mentioned, the value of $a_1'\Big|_1$ (and thus $B_{\theta 1}\Big|_1$) and $a_1\Big|_1$ (and thus $B_r\Big|_1$) can be calculated for any $\frac{a_1}{a_1'}\Big|_1$ with a saturated island present. We can now draw $B_r\Big|_1$ and $B_{\theta 1}\Big|_1$ against $j_z^{(m,n)}$ (which is related to $\frac{a_1}{a_1'}\Big|_1$ as was illustrated in Figure 6.44). This is done in Figure 6.45. It is clear that $B_r\Big|_1$ is increasing with increasing $j_z^{(m,n)}$. From section 6.7.3, we know that larger islands perturb the

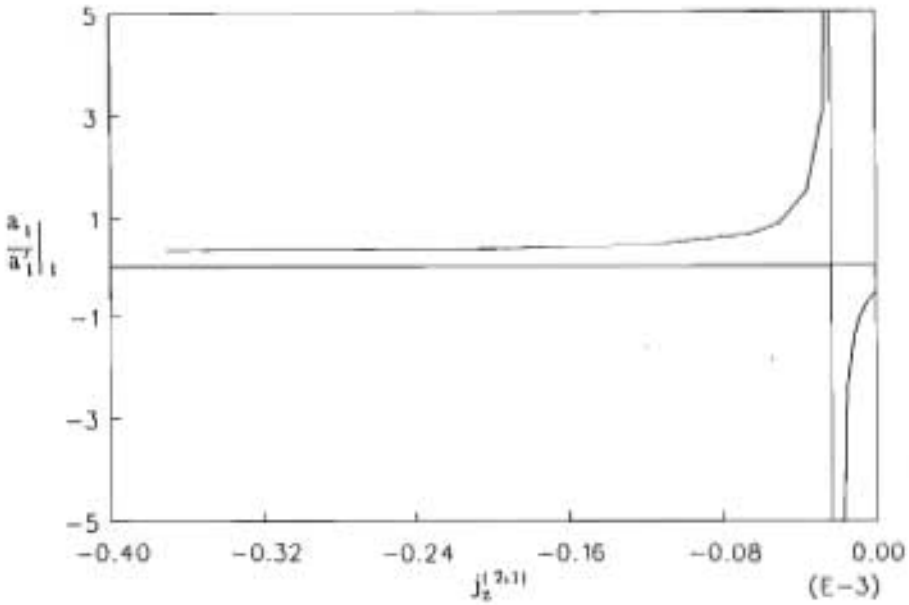

FIGURE 6.44 The effect of $j_z^{(m,n)}$ on the quantity $\left.\frac{a_1}{a_1'}\right|_1$. The values of $j_z^{(m,n)}$ are negative because δ was chosen to be positive.

boundary more, leading to an increase in $B_r\Big|_1$. The increasing coil current will thus lead to an increase in island size. In Figure 6.46 we illustrate this for a (2,1) mode during the high MHD phase ($q_0 = 1.3$, $q_1 = 3.6$) and in Figure 6.47 during the low MHD phase ($q_0 = 0.8$, $q_1 = 3.6$). We used $\epsilon = 0.5$ and $r_c = 1.2$. This was done to be able to relate the results to Tokoloshe where $\epsilon \sim 0.5$. One should remember that the island width W is normalized to the plasma radius.

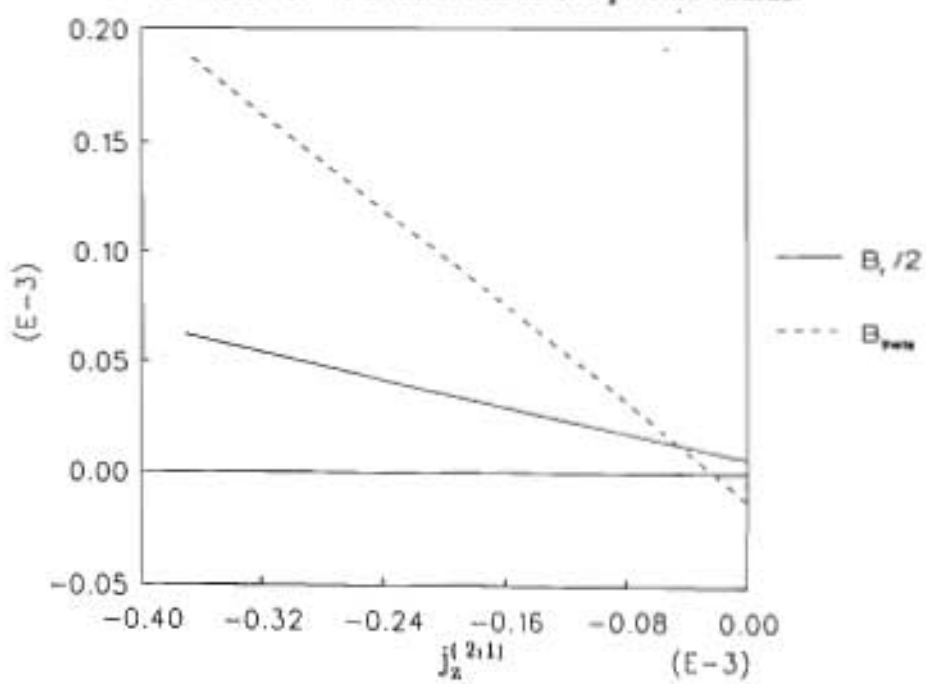

FIGURE 6.45 The graph of B_r and B_{θ_1} against $j_z^{(m,n)}$. The value of B_r increases with current. As the coil current is increased in magnitude (going from right to left) the initially small value of B_{θ_1} decreases, goes through zero and then increases in the opposite sense.

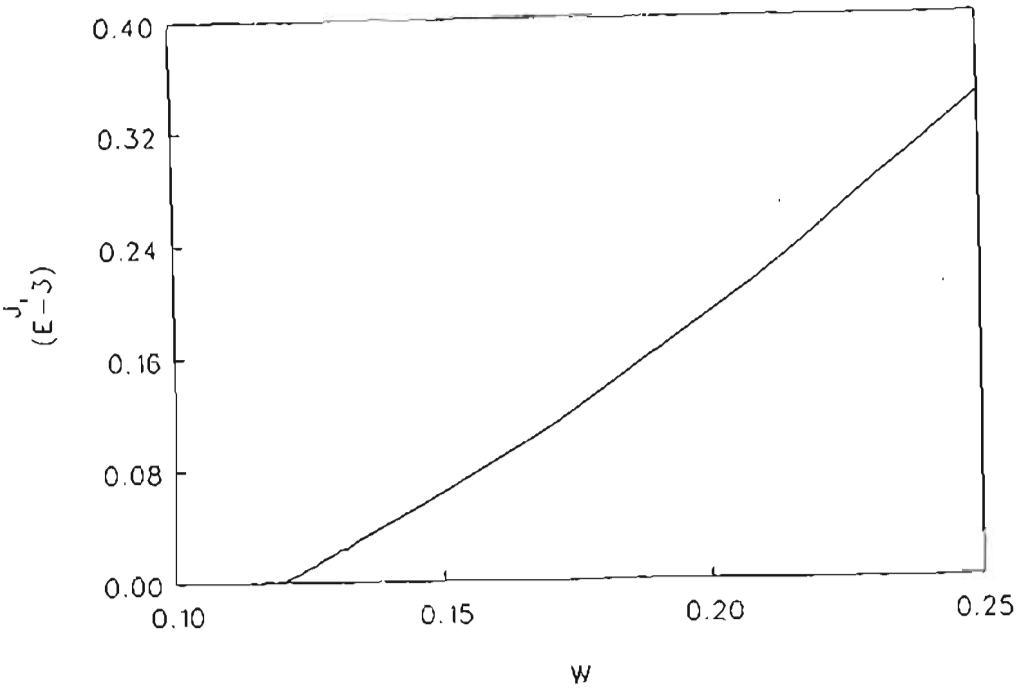

FIGURE 6.46 An increase in coil current leads to island growth. The parameters are $q_1 = 3.6$, $q_0 = 1.3$ and $\epsilon = 0.5$ (high MHD regime). This ϵ is chosen because of the large value on Tokoloshe (~ 0.5).

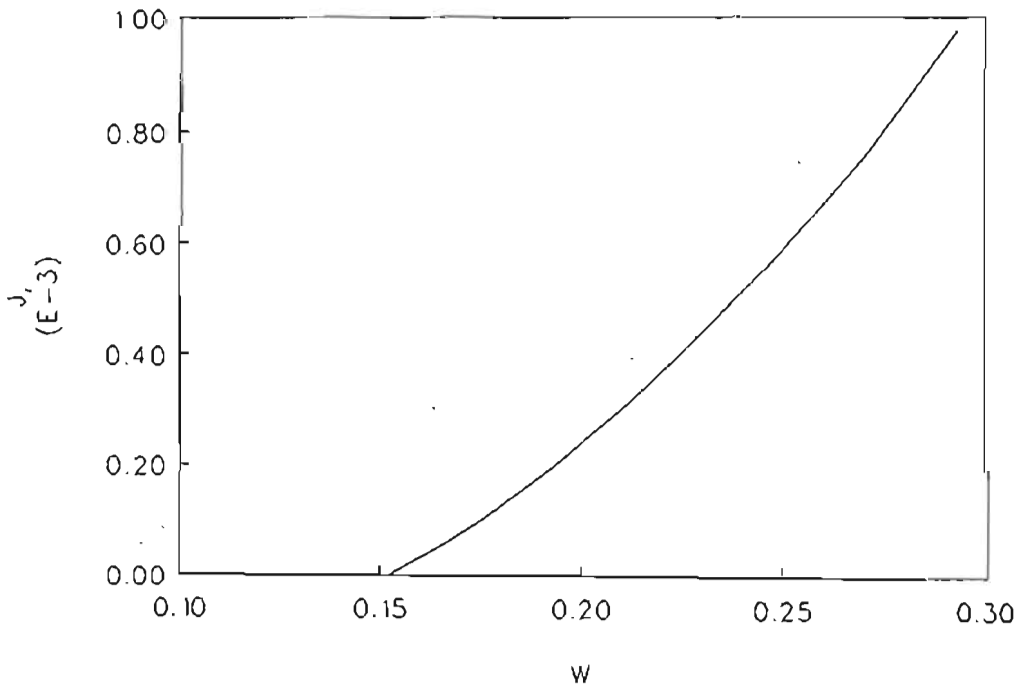

FIGURE 6.47 The island grows with an increase in coil current. The parameters are $q_1 = 3.6$, $q_0 = 0.8$, $\epsilon = 0.5$ (low MHD regime). The islands are, however, smaller than those for the high MHD regime for the same coil current.

The current density $j_z^{(m,n)}$ used in these calculations is in normalized units. We know that (from section 3.7)

$$j_z^{(m,n)} = B_0/a\mu_0 \, \bar{j}_z^{(m,n)} ,$$

with $\bar{j}_z^{(m,n)}$ the normalized current, a the minor radius and B_0 the on–axis toroidal magnetic field. In chapter 3 we used $\mu_0 = 1$, which is not assumed in the above equation. From equation (5.59) we have

$$j_z^{(m,n)} = (-1)^{m-n\ell} I_\ell \left(\frac{1}{\pi r_c}\right) \frac{m}{n} \cdot J_{m-n\ell}(n\ell\Delta_\ell) ,$$

with the quantities **not** normalized. This gives

$$I_\ell = 0.412 \, \frac{\pi r_c}{m} \, n \, \frac{B_0}{a \; \mu_0} \, \bar{j}_z^{(m,n)} .$$

with

$$\Delta_\ell = 0.838 , \text{ and } J_0(1.676) \simeq 0.412.$$

for the (2,1) mode as was observed on Tokoloshe.

A configuration with $B_0 = 0.6$ T, $a = 0.24$ m, $r_c = 0.288$ m and (m,n) = (2.1) gives

$$I_\ell = 370\,800 \, \bar{j}_z^{(m,n)} .$$

As an example we can take $\bar{j}_z^{(m,n)} = 0.001$ which corresponds to a coil current of 370 A.

The same island width variation as shown in Figures 6.46 and 6.47 was also found by Hansen [79] as shown in Figure 6.48. Our model, however, predicts smaller

islands. For 370 A we get an (2,1) island of about 7 cm (Figure 6.47) against his 11 cm. This difference in island size can be due to the fact that Hansen [79] used a non–linear $\Delta'(W)$ criterion, but did not consider profile changes (i.e. flattening) caused by the saturated island.

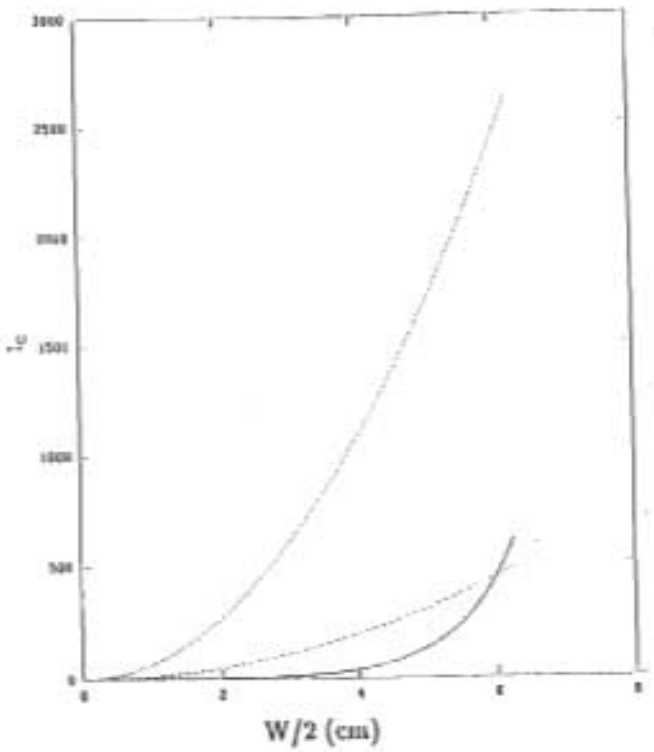

FIGURE 6.48 The variation of island size with coil current as was found by Hansen [79] for the low MHD phase. Solid line — nonlinear, short dashes — vacuum, medium dashes — linear plasma response field.

6.10.3 The effect of rotation frequency

In this section we assume a situation where the plasma is rotating at some frequency, and an external coil current is applied outside. A resistive wall is included between the plasma and the coil with a small vacuum region on the inside of the wall. It is now assumed that this is a time independent situation, i.e. that the rotational frequency of the plasma is constant for each equilibrium. We can thus associate some frequency with a particular equilibrium.

In the previous section we saw that the island size increases with increasing coil current for locked modes, i.e. $\Omega = 0$. This is also true for any given rotational frequency as can be seen in Figure 6.49.

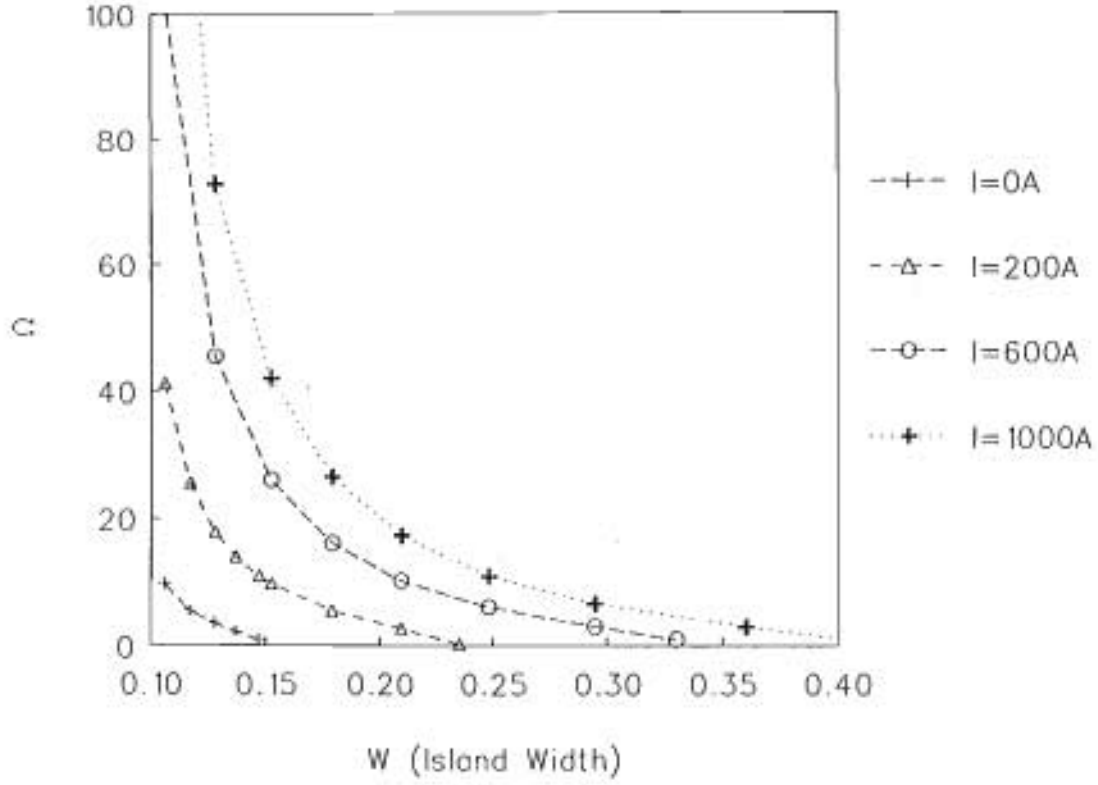

FIGURE 6.49 The effect of rotational frequency on island width for different DC coil currents. The parameters used are $q_L = 3.6$, $q_0 = 0.8$, $\epsilon = 0.1$, $r_W = 1.1$, $r_C = 1.3$ (low MHD regime).

It is interesting to note that changes in Ω do not have any significant effects on the island size when Ω is large. However, when Ω is small, a small change in Ω can have a significant effect on the island size.

The rotational frequency was related to the Δ'–criterion by Hansen [79] without coil current. It was also used in conjunction with an AC coil current by Nave and Wesson [86]. This is however, the first time, as far as we are able to determine, that it is used with a DC current in time independent equilibrium studies.

6.10.4 Equilibrium effects

In Figure 6.32 we showed the difference in island size when the island is locked or rotating infinitely fast for different equilibria. During the high MHD phase

(parameterized by $q_0 = 1.6$) we found no significant differences between locked and fast rotating cases. This changed for the low MHD phase (parameterized by $q_0 = 0.8$), for which the difference is larger.

We now include the effect of an external DC coil current. This is shown in Figure 6.50. It is clear that the effect of a coil current is much larger during the high MHD phase, i.e. when the profile is flat. When the profile gets very flat ($q_0 \simeq 1.6$) it can have a large effect on the island size – leading possibly to island overlap with the limiter. The differences in behaviour of the graphs for high q_0 are probably due to details of the chosen profile.

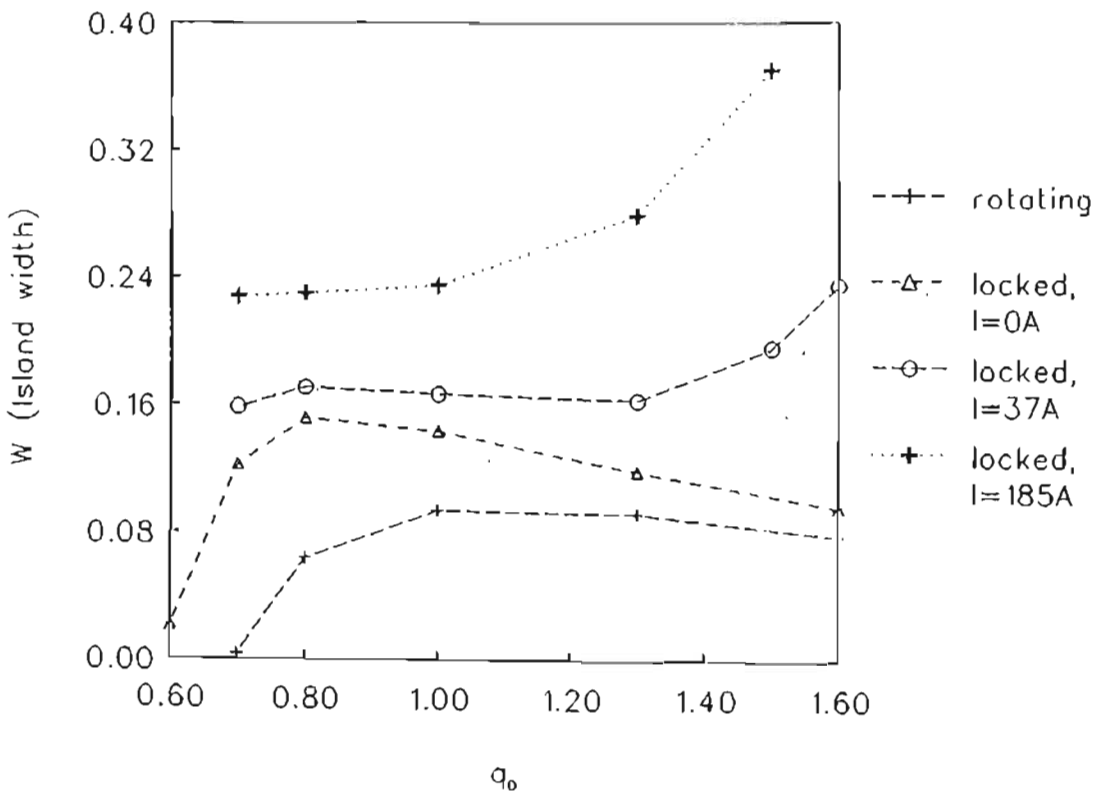

FIGURE 6.50 The island width as a function of profile type (parameterized by q_0) for rotating and locked modes.

It is now possible to take into account the effect of rotational plasma frequency, together with external coils. This is shown in Figure 6.51. In this graph we show the effect of rotational frequency on the island width for different current profiles (i.e. $q_0 = 0.8, 1.3, 1.5$). The island sizes of the high MHD phase ($q_0 = 1.3/1.5$) are consistently larger than those of the low MHD phase ($q_0 = 0.8$). This is the same as to say that island size widens with broadening profiles ($q_0 = 0.8$ – peaked, $q_0 = 1.5$ flat) as was found before (shown in Figure 6.49). It is true for all realistic rotational frequencies ($\omega\tau_w \lesssim 50$).

Figure 6.51 can be used in an interesting way when it is assumed that each equilibrium is associated with a particular rotational frequency. This is in agreement with observations on Tokoloshe. The typical toroidal frequency during the low MHD phase (i.e. a very peaked profile) on Tokoloshe is 15 kHz. For the high MHD phase this changes to 8 kHz (i.e. for a flat current profile). One possible explanation for this can be found in the conservation of angular momentum. When the body of the plasma contracts (i.e. the profile peaks), the rotational frequency speeds up. On the other hand, when the body of the plasma expands (i.e. the profile flattens), the rotational frequency reduces.

$$\text{Let } I_{AA} = \int R_0^2 \, dm$$

$$= \int R_0^2 \, M \, dV$$

with I_{AA} the moment of inertia about the axis of the tokamak, dm the unit element, M the mass density and dV the volume element. For a time independent situation we have

$$A = I_{AA} \, \omega$$

with A the angular momentum and ω the rotational frequency. Let us further propose that the current density profile and the density profile are very similar (preliminary experimental results are in agreement with this) and further that the mass density M_0 does not change. Then we have

$$I_{AA} = 4\pi^2 R_0^3 \int_0^1 M_0(1-r^2)^b \, r \, dr$$

for the profile type given by equation (6.3).

The solution of this integral is just

$$A = 4\pi^2 R_0^3 M_0 \frac{1}{2(b+1)} \omega .$$

Now we get

$$b = 3.5 \quad : \quad A = T \frac{\omega}{4.5}$$

$$b = 2.6 \quad : \quad A = T \frac{\omega}{3.6}$$

$$b = 1.77 \quad : \quad A = T \frac{\omega}{2.77}$$

$$b = 1.25 \quad : \quad A = T \frac{\omega}{2.25} ,$$

with $T = 4\pi^2 R_0^3 M_0$.

The parameter b=3.5 agrees with $q_0 = 0.8$, $q_1 = 3.6$ and the parameter b=1.25 with $q_0 = 1.6$, $q_1 = 3.6$. According to this model the rotational frequency will double when the plasma goes from the high MHD ($q_0 = 1.3$) to the low MHD phase ($q_0 = 0.8$). This is in agreement with observations on Tokoloshe.

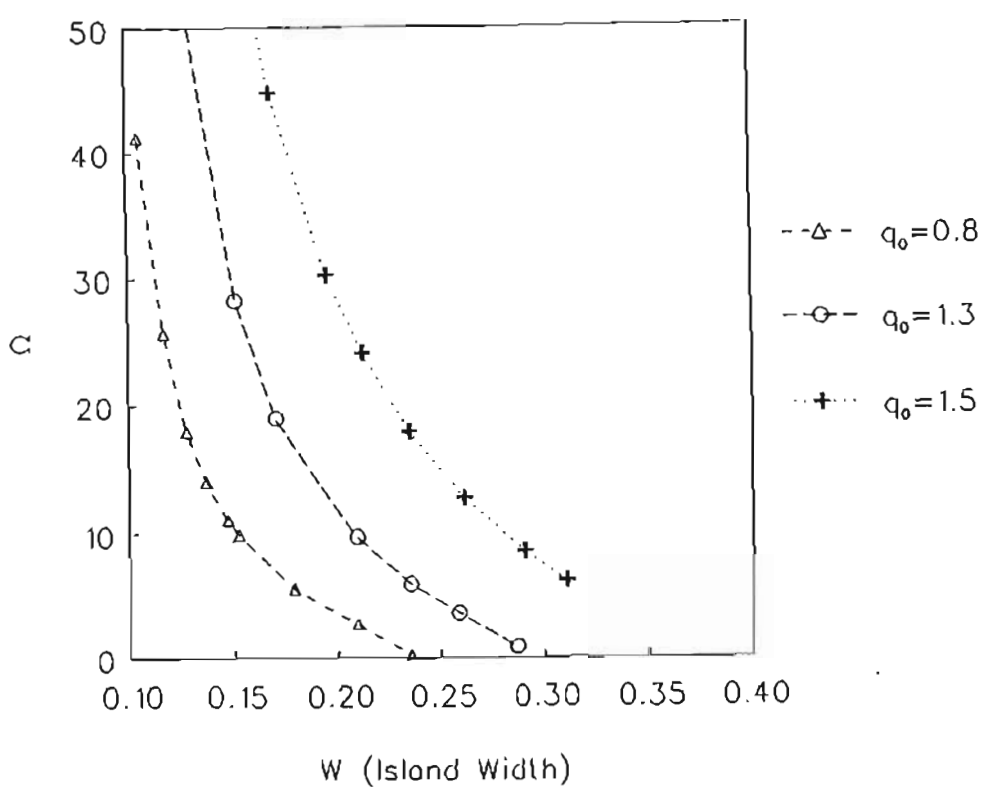

FIGURE 6.51 The effect of rotational frequency on the island size for different profile types in the presence of a small external coil current (200 A).

Let us assume that $\Omega = 20$ during the low MHD phase ($q_0 = 0.8$). If this rotational frequency is halved ($\Omega = 10$) when the plasma moves to the high MHD phase (as is observed on Tokoloshe) when $q_0 = 1.5$, the island size will grow from $W = 0.12$ to 0.29. This is a rather large increase in island size. This is qualitatively in agreement with observations on Tokoloshe [94].

6.10.5 The relation between $B_{\theta 1}$ and Ω

When no external coil currents are applied outside the plasma, the relation between $B_{\theta 1}$ and Ω is of the form $B_{\theta 1} \sim \Omega$ ($\Omega < 20$) as was shown in Figure 6.37. This situation is changed when coil currents are switched on. In Figure 6.52 we show $B_{\theta 1}$ against Ω for $I_\ell = 1000$ A. For small velocities we found a relation of $B_{\theta 1} \sim \frac{1}{\Omega}$, and for larger ones $B_{\theta 1} \sim \Omega$ (see Figure 6.52). On Tokoloshe we found

$B_{\theta l} \sim \frac{1}{V_\varphi}$, where V_φ is now related to Ω [94]. This relation is shown in Figure 6.53. This was true even for no external coil current, suggesting error fields in the ohmic heating and other coils.

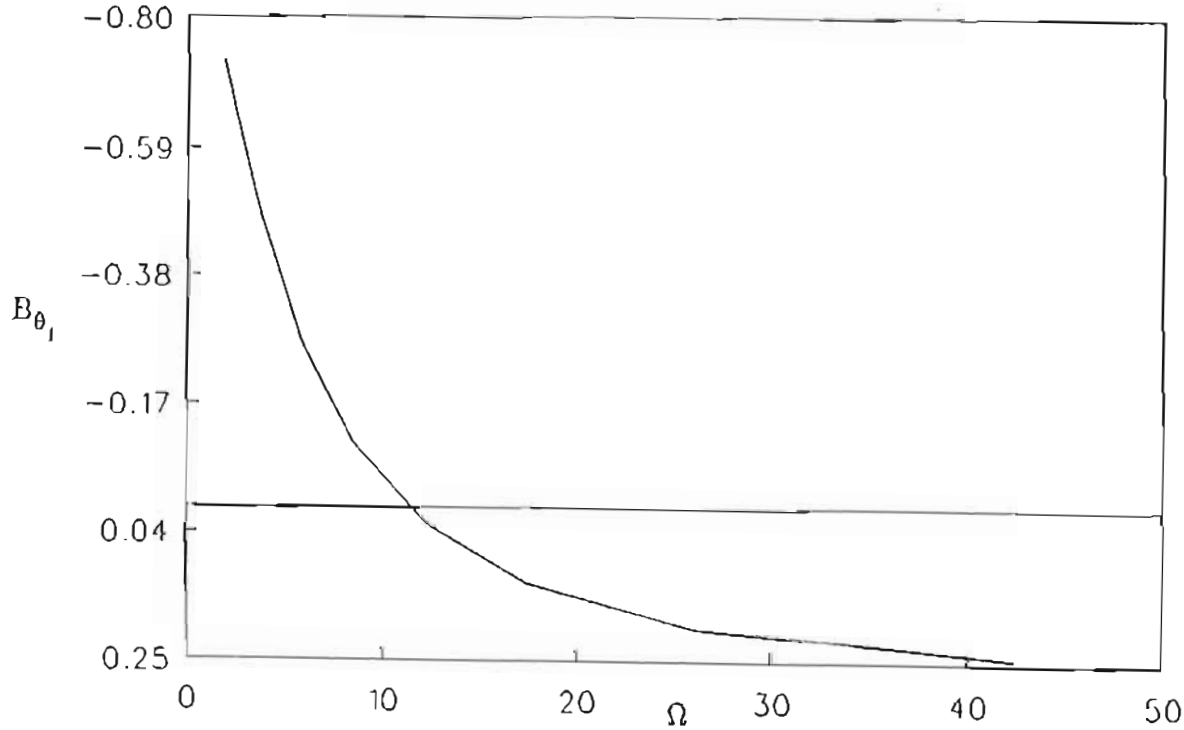

FIGURE 6.52 The relation of $B_{\theta l}$ to Ω for $q_l = 3.6$, $q_0 = 0.8$, b = 3.5.

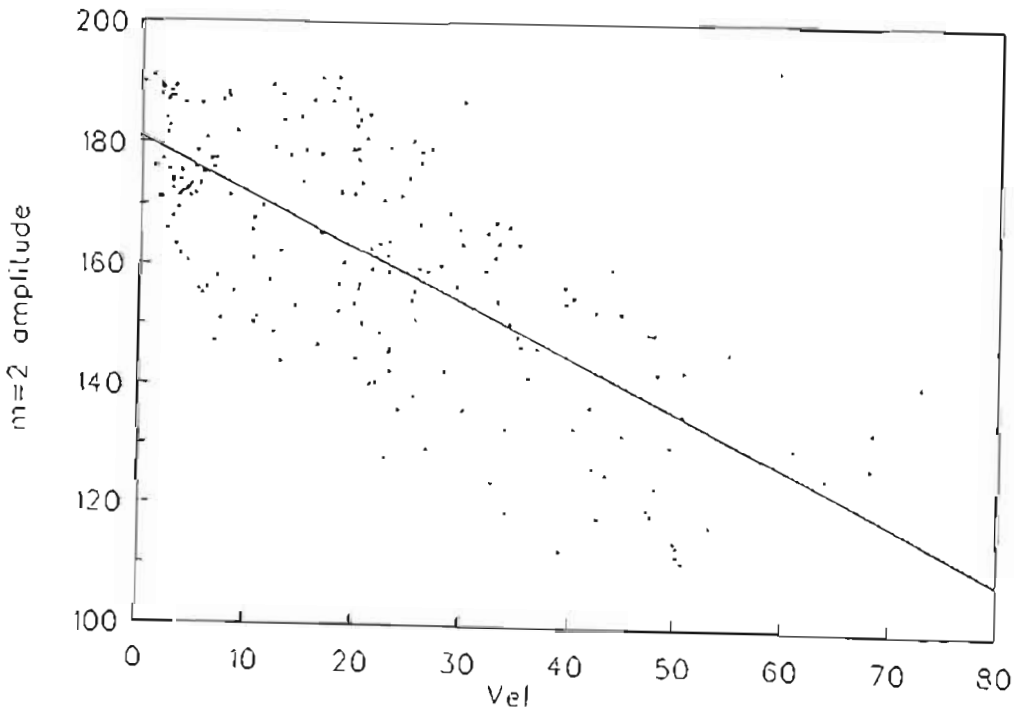

FIGURE 6.53 The relation of $B_{\theta l}$ to V_φ for a typical Tokoloshe shot without external coils. Quantities are in normalized units.

6.10.6 The relation between the Reiman and Rutherford criteria

In this section we explore the relation between the Rutherford and Reiman $\Delta'(W)$ criteria given by equations (6.12) and (6.13). We will first look at the effect of the profile type on the different criteria. In Figure 6.54 we show the effect of rotational frequency on the island size as calculated by both these criteria for a low MHD peaked profile. The lower the rotational frequency (Ω), the closer the island sizes predicted by the different criteria gets.

The difference between the island sizes predicted by the Rutherford and Reiman criteria for high frequencies, are in agreement with the differences found earlier (see Figure 6.41). The differences are caused by the difference in the Rutherford and Reiman expressions for $\Delta'(W)$ as given in equations (6.12) and (6.13). They can possibly be reduced if the α–like terms (see the expression of White et al. [3] before equation (6.12)) are included in the Reiman expression.

In figures 6.55 and 6.56 we show the same situation for $q_0 = 1.3$ and 1.5 i.e. high MHD, broad profiles. As before it can be seen that the island size for $\Omega = 0$ (a locked mode) increases when the profile flattens, i.e. q_0 increases. From these graphs it is clear that the criteria predict islands of similar size as Ω is decreased. For $W > 0.24$ the two criteria do not predict significantly different island sizes.

It is now also possible to look at the effect of the coil current on the predicted island sizes using Rutherford and Reiman's criteria. As in Figure 6.54, we choose the value of $q_0 = 0.8$, but we have changed the coil current to $I_\ell = 1\ 000$ A in Figure 6.57. The effect of increasing coil current is the same as the broadening of the current profile. It leads not only to larger islands when $\Omega = 0$, but also to insignificant differences in the island sizes predicted by both criteria when $W \gtrsim 0.24$.

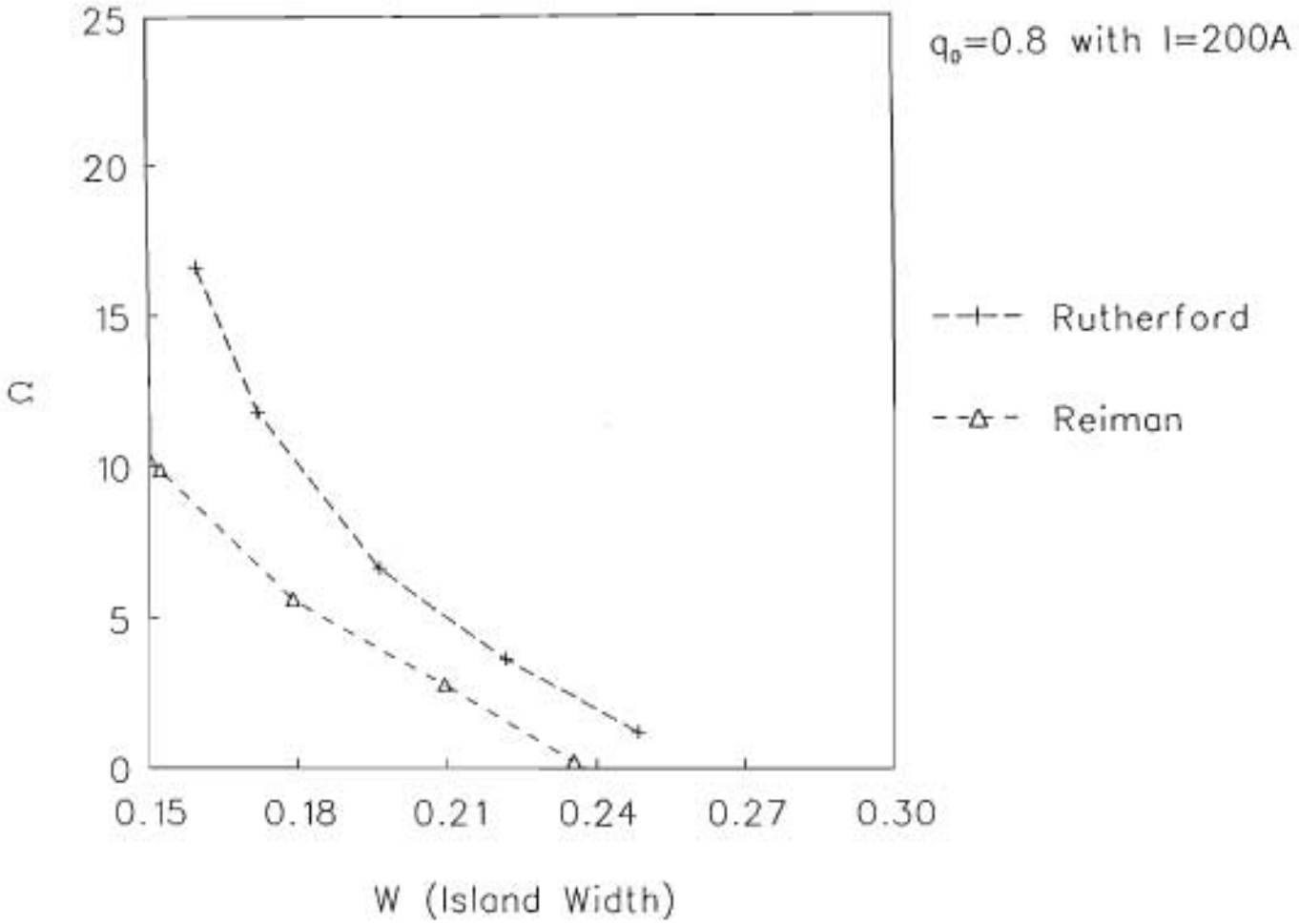

FIGURE 6.54 The effect of rotational frequency on island size as determined by both the Reiman and Rutherford criteria. It is for the low MHD phase ($q_0 = 0.8$, $q_1 = 3.6$) with $I_\ell = 200$ A.

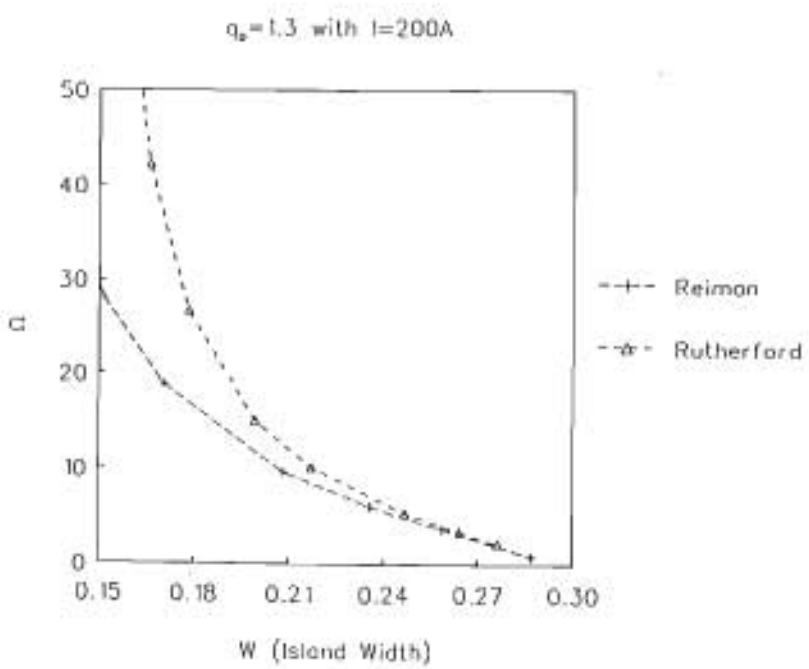

FIGURE 6.55 The difference between the Rutherford and Reiman criteria for $q_0 = 1.3$ and $I_\ell = 200$ A.

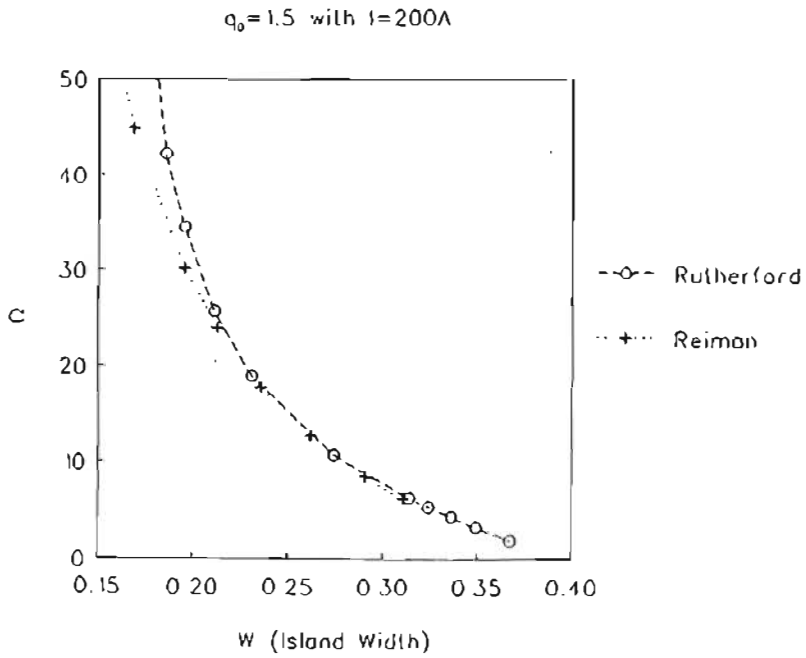

FIGURE 6.56 The difference between the Rutherford and Reiman criteria for $q_0 = 1.5$ and $I_\ell = 200$ A.

We can thus conclude that the different $\Delta'(W)$ criteria will predict different island sizes when $W \lesssim 0.24$ of the minor plasma radius. When δ is large ($W \gtrsim 0.24$), there are no significant differences between the criteria of Rutherford and Reiman. This justifies the use of the Rutherford criterion when the boundary is perturbed as was done by Hansen [75].

These relationships between the Reiman and Rutherford criteria have not been studied before in the presence of an external DC coil current.

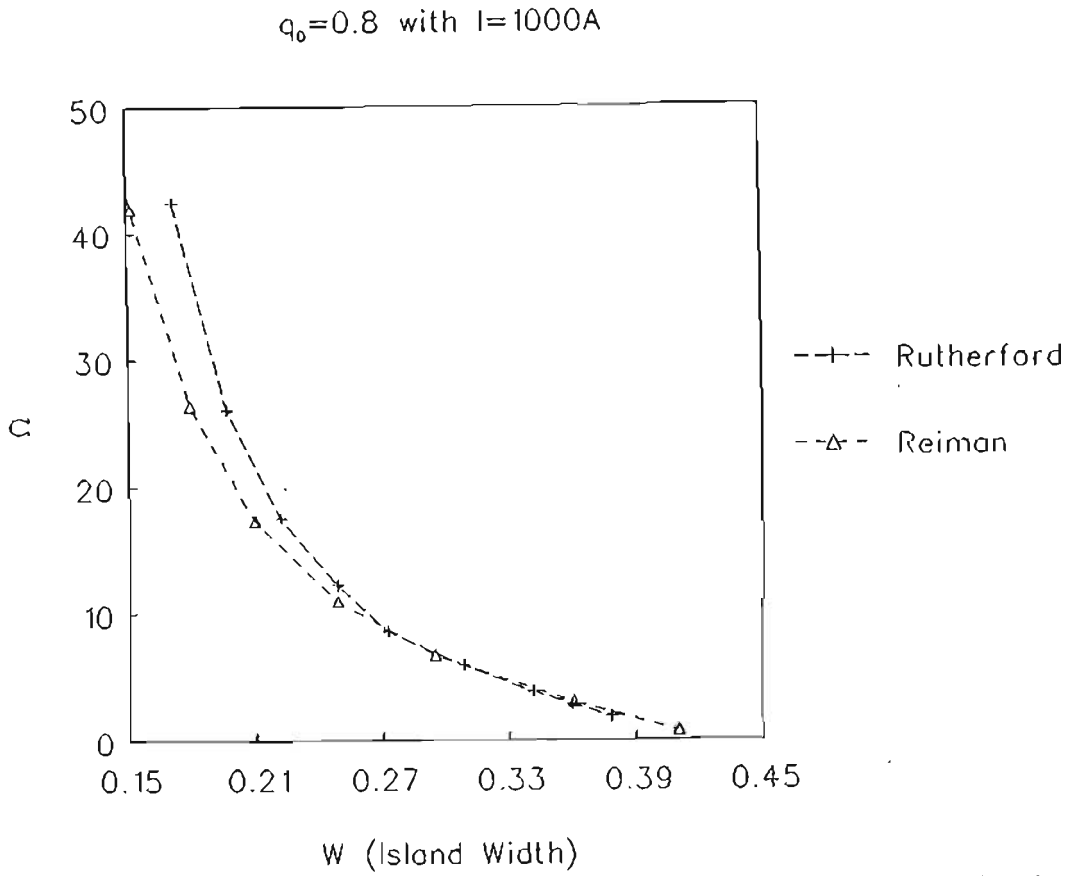

FIGURE 6.57 The relation between island sizes for the Rutherford and Reiman criteria for different rotational frequencies. It is for the low MHD phase ($q_0 = 0.8$) with $I_\ell = 1\,000$ A.

6.11 Out of Phase Situations

All the cases discussed up to now involve a tearing island locked in phase with the external coil, or, when the plasma is rotating, only the in–phase situations. We will now also consider out of phase situations.

The plasma cannot be locked out of phase with the external coil because it is an unstable equilibrium [85]. When the plasma is rotating however, the island moves out of phase with the external coil and this calculation gives an estimate of the minimum island size during rotation. Let us, then, consider such a hypothetical steady–state case where the plasma island is locked out of phase with the coil.

When the island is out of phase with the external coil, we can again evaluate the island behaviour from Figure 6.43. Instead of moving along the arrow to the right as shown in Figure 6.43, an out–of–phase coil current will move along the arrow to the left as shown in Figure 6.58. The effect is that $\left.\frac{a_1}{a_1^{\prime}}\right|_1$ will decrease from –0.501 (for a (2,1) island) to zero and will then start increasing positively as the value of w decreases.

From equation 5.105 the cases of rotation can now be investigated. When the plasma is rotating very fast, which is similar to a superconducting wall, the value of $\Omega \to \infty$. This means that

$$D^2\left(\left.\frac{a_1}{a_1^{\prime}}\right|_1\right)^2 - E^2 = 0 .$$

When the plasma is touching the wall, i.e. $r_w \to 1$, the value of E is just zero as can be seen from the expression for E presented under equation (5.103). Thus $\left.\frac{a_1}{a_1^{\prime}}\right|_1 \to 0$ in the case when $\Omega \to \infty$ and the plasma is touching the resistive wall.

All the intermediate frequencies of Ω will fall between the locked case, and the case when $\Omega \to \infty$. When the coil current is large, and $\left.\frac{a_1}{a_1^{\prime}}\right|_1$ is positive, $\left.\frac{a_1}{a_1^{\prime}}\right|_1$ will decrease with increasing rotation frequency to zero for the case of the plasma touching the resistive wall. When the coil current is small and $\left.\frac{a_1}{a_1^{\prime}}\right|_1$ is negative $\left(\left|\left.\frac{a_1}{a_1^{\prime}}\right|_1\right| \leq 0.501 \text{ for a (2,1) island} \right)$, the value of $\left.\frac{a_1}{a_1^{\prime}}\right|_1$ will also decrease with increasing rotation frequency to zero.

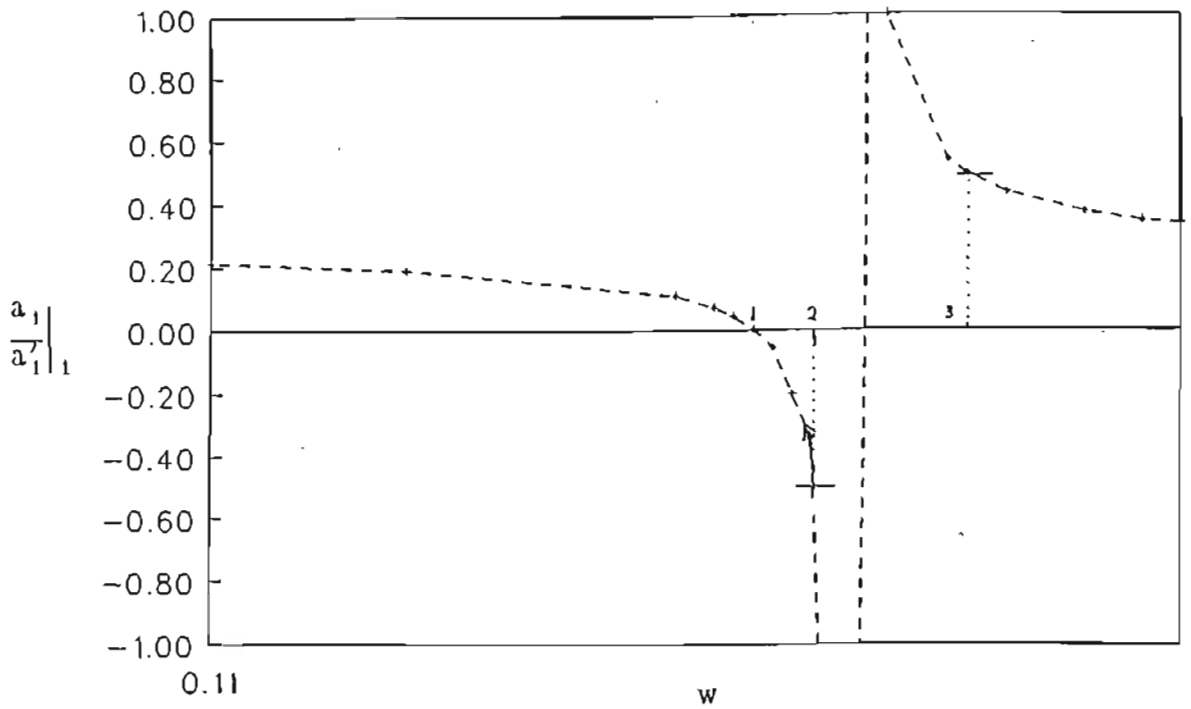

FIGURE 6.58 This graph shows how w will change when $\left.\frac{a_1}{a_1'}\right|_1$ is changed because of an out–of–phase coil current.

When the out–of–phase coil current is increased from zero, we have already shown that the value of $\left.\frac{a_1}{a_1'}\right|_1$ starts decreasing from –0.501 following the arrow on Figure 6.58. Now, the value of a_1 is also decreasing. This means that δ would also decrease. Once $\delta = 0$ is reached, it will again start increasing in magnitude as a_1 increases. However, now the sign of δ would be different and a_1 would thus also change sign. This can be seen from equation (6.19) when the procedure of increasing $j_z^{(2,1)}$ is followed through.

As an example we will now investigate a profile with $q_1 = 3.6$ and $q_0 = 1.6$. In Figure 6.59 we show $j_z^{(2,1)}$ as a function of $\left.\frac{a_1}{a_1'}\right|_1$. It is clear that $j_z^{(2,1)}$ increases as $\left.\frac{a_1}{a_1'}\right|_1$ gets smaller, goes through zero, and then increases positively.

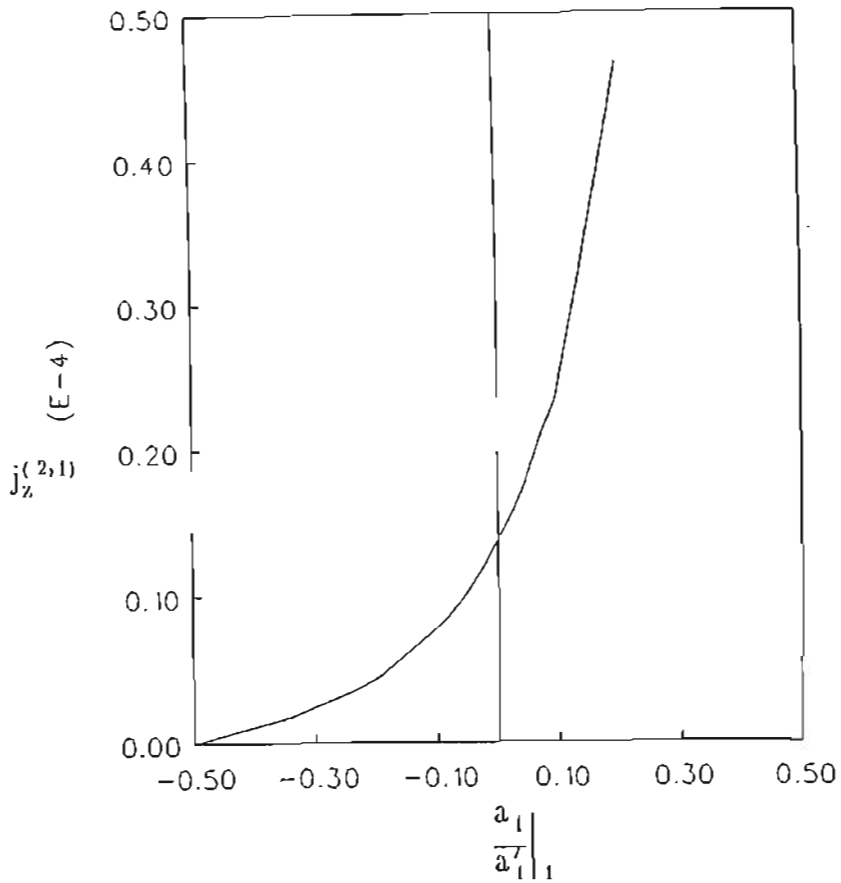

FIGURE 6.59 The graph of $j_z^{(2,1)}$ against $\left.\frac{a_1}{a_1'}\right|_1$. The parameter values of the equilibrium are $q_1 = 3.6$, $q_0 = 1.6$, $r_w = 1.1$, $r_c = 1.3$.

In Figure 6.60 we show the rotational frequency as a function of $\left.\frac{a_1}{a_1'}\right|_1$ for two different coil current densities, one agreeing with $\left.\frac{a_1}{a_1'}\right|_1 < 0$ $(j_z^{(2,1)} = 0.175 \times 10^{-5})$ and one with $\left.\frac{a_1}{a_1'}\right|_1 > 0$ $(j_z^{(2,1)} = 0.466 \times 10^{-4})$. When the rotational frequency increases, both these curves show $\left.\frac{a_1}{a_1'}\right|_1 \to -0.094$ which agrees with $r_w = 1.1$. If $r_w \to 0$, this value of $\left.\frac{a_1}{a_1'}\right|_1$ would also go to zero.

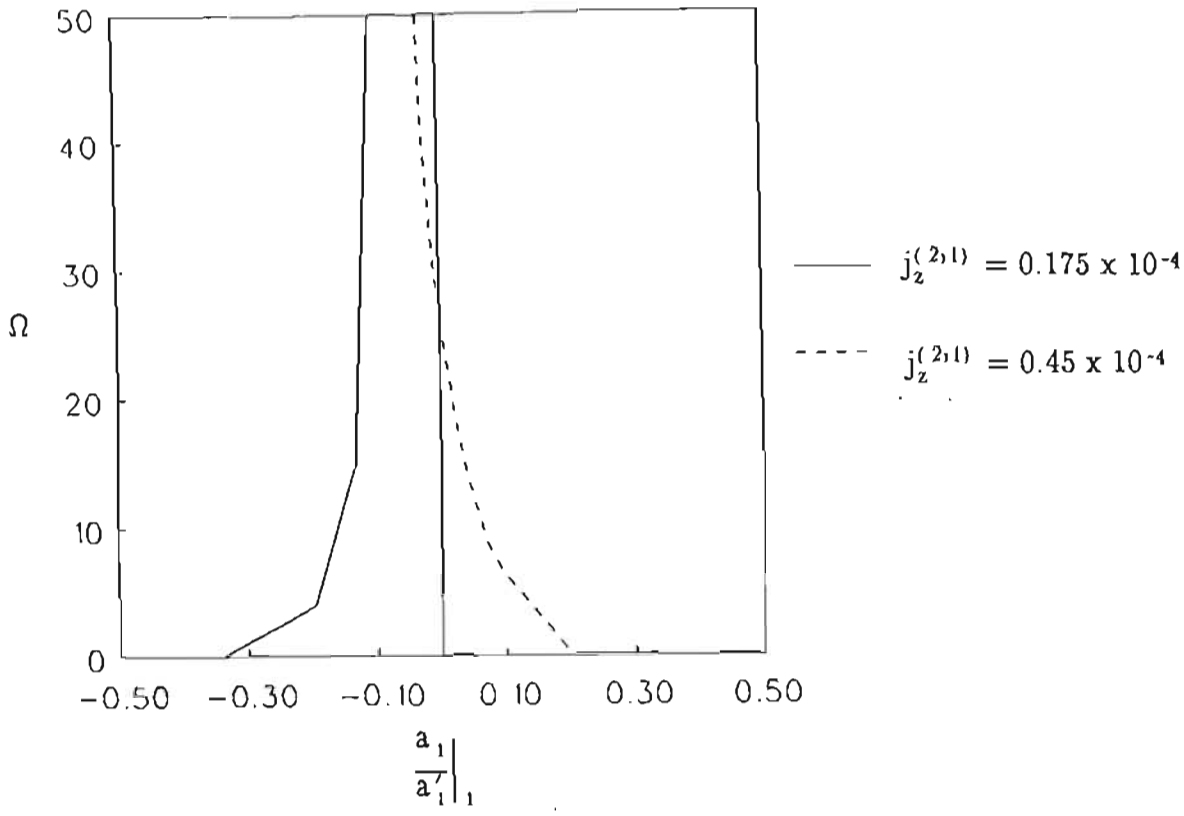

FIGURE 6.60 The graph of Ω against $\frac{a_1}{a_1'}\Big|_1$. The profile parameters are the same as for the previous graph.

We can now plot the island width against current density for both the high ($q_0 = 1.6$) and low ($q_0 = 0.8$) MHD phases (q_1 is 3.6 for both cases). This is done in Figure 6.61. It is immediately clear that the coil current will reduce the (2,1) island much more during the high MHD phase.

Finally, we can combine the results of the in–phase and out–of–phase situations. When the plasma is rotating, and a fixed coil current is applied on the outside, the island will move in and out of phase with the external coil current. This will cause the island to increase (when in–phase) and to decrease (when out–of–phase). A

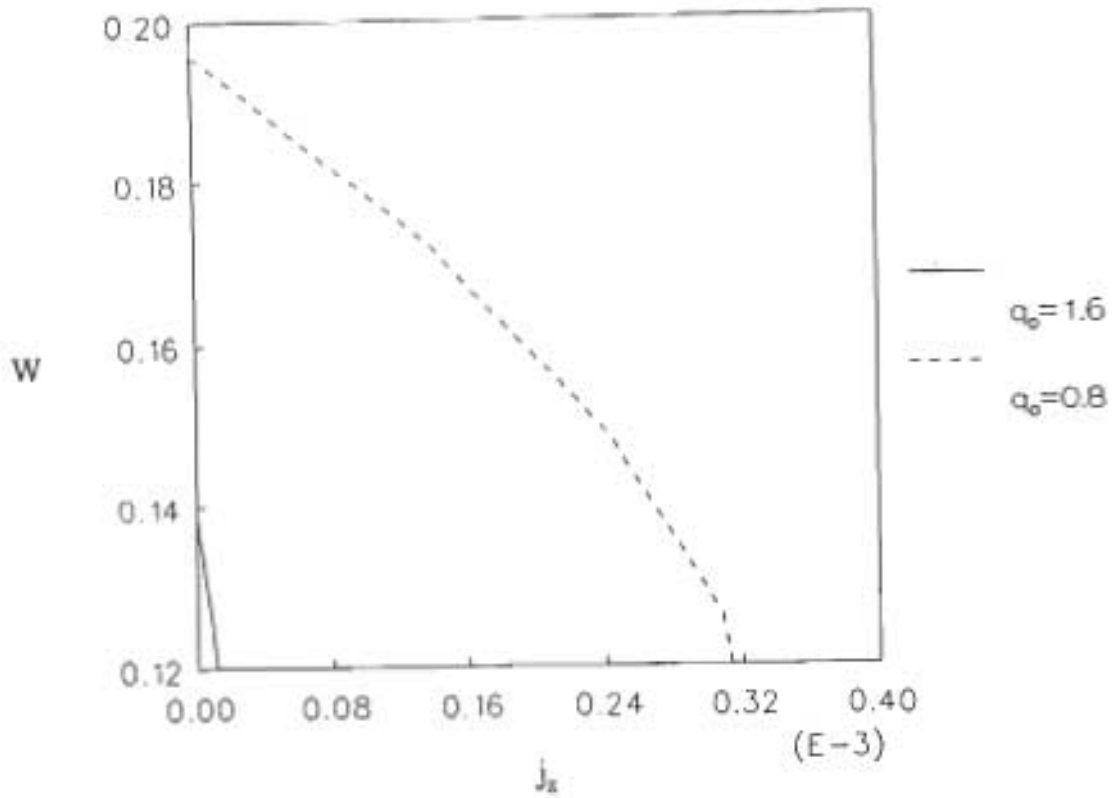

FIGURE 6.61 The graph of W against $j_z^{(2,1)}$ for two profiles with $q_0 = 1.6$ and 0.8. The value of q_1 is 3.6.

time–dependent treatment will thus show the island increasing and decreasing in size at a fixed frequency when the plasma is rotating at a fixed frequency. We however, only considered the in–phase and out–of–phase cases. The island–width will thus vary between these two extreme values (maximum when in phase and minimum when out of phase). In Figure 6.62 we present a graph showing these extreme values for a variety of rotational frequencies for the low MHD case. A coil current density of 0.14 x 10^{-3} is applied to an equilibrium with $q_1 = 3.6$, $q_0 = 0.8$, $b = 3.5$. As before the islands are assumed to be saturated. This assumption will break down when Ω gets too large or when the difference between the minimum and maximum values gets too big.

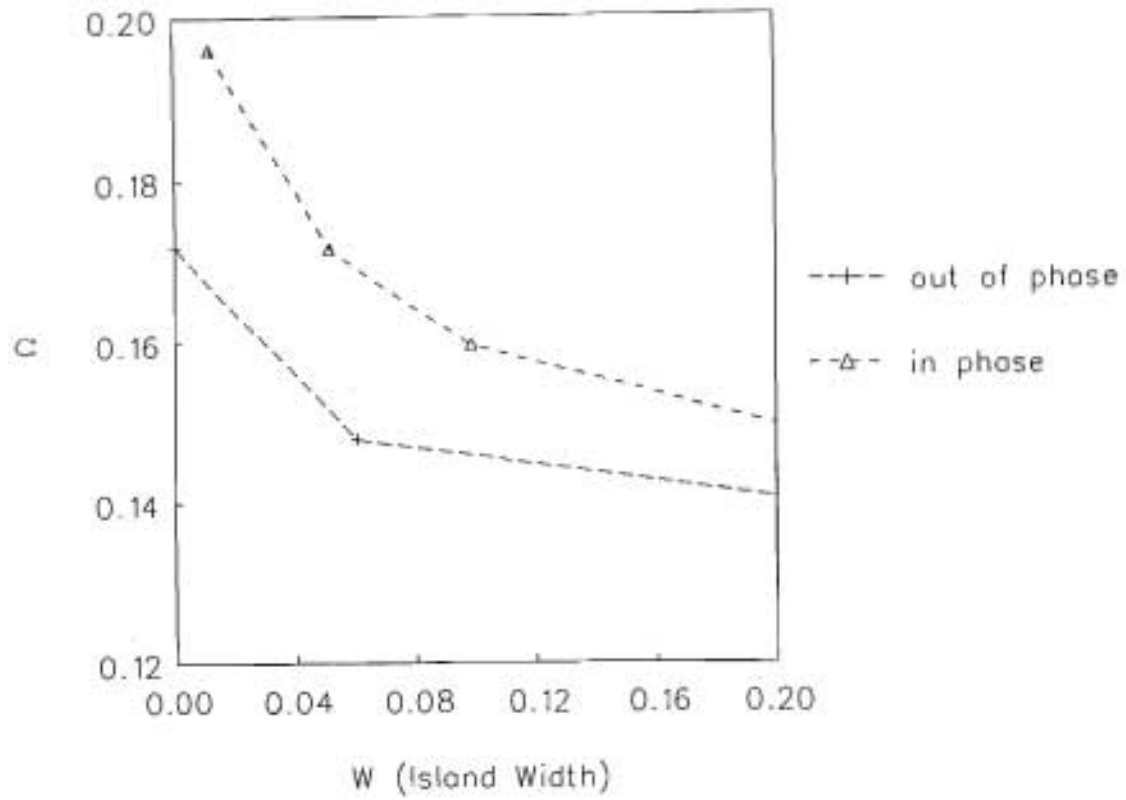

FIGURE 6.62 The in–phase and out–of–phase island widths for different rotational frequencies. The parameters are $q_t = 3.6$, $q_0 = 0.8$, $b = 3.5$, $j_\pi^{(2,1)} = 0.14 \times 10^{-3}$.

6.12 Conclusions

In this chapter the current perturbation δJ has been modelled for a prescribed overall current profile. The eigenvalue w specifies the width of the perturbation δJ. No significant difference was found between the results of the two models used for δJ.

An unperturbed profile similar to the one used with success on Tokoloshe [94] was used in this study. We did, however, not include a second small flat region on the outside of the profile as was done when the profile was used to explain experimental results. This explains why we found that the profile did not predict the (3,1) island behaviour correctly, but only the (2,1) behaviour. The (3,1) island as calculated with the profile we have used, is too small.

We also tried to model the (1,1) mode. Taking into account that $\tilde{\psi}_1 \sim r^m$, i.e. that $B_r\Big|_0 \to 0$, but not $B_{\theta 1}\Big|_0$, we attempted the calculation by shooting with a_1 instead of a_1' as was done for the other modes (i.e. equation (5.11)). In spite of this we were not able to find any eigenvalues. The reason for this may be that the assumed δJ or J_u profiles were not applicable to (1,1) mode modelling.

The model does allow the form of the profile to be changed from peaked to flat when the parameters are changed. It can thus be used to study different situations in the slow time evolution of a shot. It was found that a locked island is larger than the fast rotating one, although the difference is small for certain flat profiles. For certain profiles we found that a superconducting wall (or rotation) can stabilize a tearing mode unstable equilibrium. An external DC coil leads to mode growth.

These results are consistent with other linear and non–linear work that has been done, as was discussed earlier in the chapter. The Reiman Δ'_{ϵ_1} criterion was of importance in this study because non–superconducting walls were included in the problem. It enabled us to apply our model to a wide variety of boundary conditions. The Reiman and Rutherford criteria were also compared in the study. No significant differences were found when $W \gtrsim 0.24$ of the minor plasma radius.

Results that appear to be new include:

- The graph of $\left.\frac{a_1}{a_1^{\gamma}}\right|_1$ (i.e. $\left.{}^{B_r}/_{B_{\theta 1}}\right|_1$) against w giving all possible island widths for any external situation. Only parts of this graph were previously described mathematically by Lazzaro and Nave [92].

- Finding both values of $\left.B_r\right|_1$ and $\left.B_{\theta 1}\right|_1$ for saturated islands with perturbed boundaries.

- Investigating the effect of external coils on rotating plasma for Tokoloshe type profiles.

- The finding that broad profiles have very large islands in the presence of small external coil currents.

- A very simple model of angular momentum conservation coupling profile type to rotational frequency.

- Comparison of the Δ'–criteria of Rutherford and Reiman for perturbed and unperturbed boundaries.

CHAPTER 7

A TOROIDAL MODEL WITH TWO MODES PRESENT

7.1 Introduction

In this chapter the cylindrical one–mode model of chapter 4 is extended to include two modes with toroidal coupling between them. As before, a perturbation expansion is used for a "toroidal current density" (not J_φ but $(1 + \epsilon r \cos\theta)J_\varphi$). The current density profile is flattened at both rational surfaces using two axisymmetric perturbations, parameterized by w_1, w_2 which again form eigenvalues. This makes perturbation theory work and keeps the equations analytic for all values of radius. The boundary is perturbed in phase with the two modes, with amplitude δ_1, δ_2 determined by the Rutherford criterion. The one mode is dominant and the other is assumed smaller.

Our work is related to that of Bateman and Morris [67] in the sense that their quasilinear model considers the asymptotic time limit of the reduced MHD equations as we do. They also consider saturated tearing islands with toroidal coupling. They used a simple approximation for the pressure and current density within a magnetic island. This modifies the background equilibrium and removes the singularity from the linearized MHD equations, as in our case. To find the saturated island width, they used a computer algorithm to find neighboring equilibria. This however, does not solve the problem of island width determination satisfactory as they state: "Since the saturated magnetic island width and even its existence depends to a large extent on the local current density profile, knowledge of the global current density profile may not be sufficient to predict magnetic island behaviour. Unless the current density profile can be measured accurately or

externally controlled, the prediction of the saturated magnetic island width may, by necessity, take on a probabilistic nature" [67]. We overcome this problem using boundary conditions as was discussed in the previous chapter.

Bateman and Morris [67] studied profile related effects predominantly, whereas we concentrate on boundary effects. All the external situations discussed in Chapter 5 are considered. To our knowledge it is the first time that toroidal coupling has been studied with the emphasis on boundary conditions.

7.2 Defining a "current" Density that follows Flux Surfaces

The equations we solve are (3.60), (3.14), (3.10), and are repeated here. Note now that ∇ and Δ^* are the full toroidal operators.

$$\underline{V}.\nabla\nabla^2 U - 2\epsilon \frac{\partial U}{\partial z} \nabla^2 U = (S^2/h)(\nabla\psi \wedge \hat{\varphi} + \hat{\varphi}).\nabla\Delta^*\psi \qquad (7.1)$$

$$J_\varphi = -1/h\ \Delta^*\psi \qquad (7.2)$$

$$\underline{B} = 1/h(\nabla\psi \wedge \hat{\varphi} + \hat{\varphi}) \qquad (7.3)$$

$$h = 1 + \epsilon r \cos\theta\,, \qquad (7.4)$$

with everything normalized according to the normalization of section 3.7. When $S \to \infty$, equation (7.1) can be written as

$$\underline{B}.\nabla K = 0\,, \qquad (7.5)$$

with

$$K = -\Delta^*\psi = hJ_\varphi\,, \qquad (7.6)$$

K a "toroidal current density".

The assumption of $S \to \infty$ is made because of the fact that the role of resistivity is small when saturated islands are considered. (Carreras et al. [46] have shown that the α term of White et al. [3], which contains the details of the resistive profile, can be neglected – see section 6.5.2). Equation (7.5) can now be written as

$$h \frac{\partial \psi}{\partial \theta} \frac{\partial K}{\partial r} - h \frac{\partial \psi}{\partial r} \frac{\partial K}{\partial \theta} + \epsilon r \frac{\partial K}{\partial \varphi} = 0 , \qquad (7.7)$$

where use is made of the expression for $\underline{B}$ in equation (7.3). Let us now assume Fourier expansions for ψ and K i.e.

$$\psi = a_0(r) + a_1(r) \cos (m\theta - n\varphi) + a_2(r) \cos [(m+1)\theta - n\varphi + \chi_1] \qquad (7.8)$$

$$K = K_0(r) + k_1(r) \cos (m\theta - n\varphi) + k_2(r) \cos [(m+1)\theta - n\varphi + \chi_1] , \qquad (7.9)$$

where χ_1 denotes a phase shift between the a_1 and a_2 perturbations which are both of $0(\epsilon)$ smaller than a_0. We only considered two perturbations with poloidal mode numbers m and m+1, but with the same toroidal mode number n. The reason for this was to simplify the model and to model a situation similar to that on Tokoloshe where only the (2,1) and (3,1) modes are dominant during the high MHD phase. When only two modes are included in the problem, those modes are coupled by toroidicity. We ignore non–linear mode–mode coupling as discussed in section 3.9.

When the Fourier expansions (7.8) and (7.9) are substituted into equation (7.7), we get the following equations for the modes and their harmonics:

sin $(m\theta-n\varphi)$:

$$K_0' \left(ma_1 + \tfrac{1}{2}(m+1)\,\epsilon r a_2 \cos\chi_1\right) = a_0'\left(mk_1 + \tfrac{1}{2}(m+1)\,\epsilon r k_2 \cos\chi_1\right) + \epsilon r n k_1 \qquad (7.10)$$

sin $((m+1)\theta-n\varphi+\chi)$:

$$K_0' \left((m+1)a_2 + \tfrac{1}{2}\,m\epsilon r a_1 \cos\chi_1\right) = a_0'\left((m+1)k_2 + \tfrac{1}{2}\,m\epsilon r k_1 \cos\chi_1\right) + \epsilon r n k_2 \qquad (7.11)$$

sin $2(m\theta-n\varphi)$: $$a_1 k_1' = k_1 a_1' \qquad (7.12)$$

sin $2((m+1)\theta-n\varphi+\chi_1)$: $$a_2 k_2' = k_2 a_2' \qquad (7.13)$$

Terms of $0(\epsilon^3)$ have been dropped. Only modes of interest have been included. The $'$ denotes derivatives to r.

7.3 The Magnetic Flux Defined for Two Modes

The flux surfaces $\hat{\psi}$ = constant may again be usefully defined by the equation

$$\underline{B}.\nabla\hat{\psi} = 0\,. \qquad (7.14)$$

When the flux is written as

$$\hat{\psi} = \hat{\psi}_0 + \hat{\psi}_1 \cos(m\theta-n\varphi) + \hat{\psi}_2 \cos((m+1)\theta - n\varphi + \chi_1)\,, \qquad (7.15)$$

and substituted into equation (7.14), we can proceed in exactly the same way as with $\underline{B}.\nabla K = 0$ to get

$$\hat{\psi}_0'\left(ma_1 + \tfrac{1}{2}(m+1)\,\epsilon r a_2 \cos\chi_1\right) = a_0'\left(m\hat{\psi}_1 + \tfrac{1}{2}(m+1)\,\epsilon r\hat{\psi}_2 \cos\chi_1\right) + \epsilon r n\hat{\psi}_1 \qquad (7.16)$$

$$\dot{\psi}_0'((m+1)a_2 + \tfrac{1}{2} m\epsilon r a_1 \cos\chi_1) = a_0'((m+1)\dot{\psi}_2 + \tfrac{1}{2} m\epsilon r \dot{\psi}_1 \cos\chi_1) + \epsilon r n \dot{\psi}_2 \qquad (7.17)$$

$$a_1 \dot{\psi}_1' = \dot{\psi}_1 a_1' \qquad (7.18)$$

$$a_2 \dot{\psi}_2' = \dot{\psi}_2 a_2' . \qquad (7.19)$$

Equations (7.16) and (7.17) can now be written as

$$\dot{\psi}_0^{I'} = \frac{a_0'\dot{\psi}_1 \ (m + \frac{1}{2}(m+1)\ \epsilon r \frac{\dot{\psi}_2}{\dot{\psi}_1} \cos\chi_1) + \epsilon r n \dot{\psi}_1}{(m a_1 + \frac{1}{2}(m+1)\ \epsilon r a_2 \cos\chi_1)} \qquad (7.20)$$

and

$$\dot{\psi}_0^{II'} = \frac{a_0'\dot{\psi}_2 \ (\ (m+1) + \frac{1}{2}\ m\epsilon r \frac{\dot{\psi}_1}{\dot{\psi}_2} \cos\chi_1) + \epsilon r n \dot{\psi}_2}{((m+1)a_2 + \frac{1}{2}\ m\epsilon r a_1 \cos\chi_1)}, \qquad (7.21)$$

where superscripts I and II are used to distinguish between the two equations flowing from the two harmonics.

From equations (7.18) and (7.19) we know that

$$a_1 = \gamma \dot{\psi}_1 \qquad (7.22)$$

$$a_2 = \lambda \dot{\psi}_2 , \qquad (7.23)$$

with γ and λ integration constants.

Let us now assume that $\gamma = \lambda = 1$ for this model. This will be discussed in more detail later in this chapter. Then we have

$$a_1 = \dot{\psi}_1 \qquad (7.24)$$

$$a_2 = \hat{\psi}_2 . \tag{7.25}$$

We can now rewrite equations (7.20) and (7.21) as

$$\hat{\psi}_0^{I} = a_0' + \epsilon r \frac{n}{m}/(1 + \frac{1}{2} \epsilon r \frac{(m+1)}{m} \frac{a_2}{a_1} \cos \chi_1) \tag{7.26}$$

$$\hat{\psi}_0^{II} = a_0' + \epsilon r \frac{n}{(m+1)}/(1 + \frac{1}{2} \epsilon r \frac{m}{(m+1)} \frac{a_1}{a_2} \cos \chi_1) . \tag{7.27}$$

If we assume that $\frac{a_2}{a_1} \sim 0(1)$, expand the denominators and drop terms of $0(\epsilon^2)$, we get

$$\hat{\psi}_0^{I'} = a_0' + \epsilon r \frac{n}{m} \tag{7.28}$$

$$\hat{\psi}_0^{II'} = a_0' + \epsilon r \frac{n}{(m+1)} \tag{7.29}$$

which are just the cylindrical helical magnetic flux functions for the two modes. However, if terms of $0(\epsilon^2)$ are not dropped in the expressions for $\hat{\psi}_0^{I}$ and $\hat{\psi}_0^{II}$ as given by equations (7.26) and (7.27), then each of these expressions also contains the information about the other via the a_1 or a_2 variables respectively. Equations (7.26) and (7.27) can thus be interpreted as functions of $\hat{\psi}_0'$ written either in terms of the m–harmonic parameters $(\hat{\psi}_0^{I'})$ or in terms of the m+1 – harmonic parameters $(\hat{\psi}_0^{II'})$. We will thus drop the superscripts.

Let $\chi = \hat{\psi}_0' - a_0'$. We can now write equations (7.26) and (7.27) as

$$\chi(ma_1 + \frac{1}{2} \epsilon r(m+1)\, a_2 \cos \chi_1) = \epsilon r n a_1 \tag{7.30}$$

$$\chi((m+1)a_2 + \frac{1}{2} \epsilon r n a_1 \cos \chi_1) = \epsilon r n a_2 . \tag{7.31}$$

From equation (7.31) we can get

$$a_2 = \frac{-\frac{1}{2}\ \epsilon r m a_1\ \cos\chi_1\ \chi}{((m+1)\ \chi\ -\ \epsilon r n)}. \tag{7.32}$$

When this expression for a_2 is substituted into equation (7.30), it results in

$$\chi^2 - (\epsilon r \frac{n}{m} + \epsilon r \frac{n}{(m+1)} + \frac{1}{4}(\epsilon r)^2 \cos^2\chi_1)\ \chi + \frac{(\epsilon r n)^2}{m(m+1)} = 0 \tag{7.33}$$

to give

$$\chi = \left[\epsilon r \frac{n}{m} + \epsilon r \frac{n}{(m+1)} + \frac{1}{4}(\epsilon r)^2 \cos^2\chi_1 \pm \sqrt{S} \right] / 2 \tag{7.34}$$

$$\begin{aligned} S &= (\epsilon r \frac{n}{m} + \epsilon r \frac{n}{(m+1)} + \frac{1}{4}(\epsilon r)^2 \cos^2\chi_1)^2 - 4(\epsilon r n)^2 \frac{1}{m(m+1)} \\ &= \left[\epsilon r(\frac{n}{m} - \frac{n}{(m+1)}) \right]^2 \left[1 + \frac{1}{2} \epsilon r \frac{(2m+1)\ m\ (m+1)}{n} \cos^2\chi_1 \right. \\ &\quad \left. + \frac{1}{16}(\epsilon r)^2 (\frac{m(m+1)}{n})^2 \cos^4\chi_1 \right]. \end{aligned} \tag{7.35}$$

We thus have the solutions for χ,

$$\chi^{I} = \frac{1}{2} \epsilon r n \frac{1}{m(m+1)} \left[2\,m+1 + \sqrt{1+R_1} \right] \tag{7.36}$$

and

$$\chi^{II} = \frac{1}{2} \epsilon r n \frac{1}{m(m+1)} \left[2\,m+1 - \sqrt{1+R_1} \right], \tag{7.37}$$

where

$$R_1 = \frac{1}{2} \epsilon r \frac{(2m+1)\ m\ (m+1)}{n} \cos^2\chi_1 \tag{7.38}$$

and the terms of $\sim 0(\epsilon^3)$ have been dropped.

When $\cos\chi_1 = 0$ (i.e. when the modes are $\frac{\pi}{2}$ out of phase), the problem reduces to the pure cylindrical one in that the modes do not interact. This is immediately clear from equations (7.26) and (7.27). We can now also see this in equations (7.36) and (7.37).

When $\cos\chi_1 = 0$ we have $R_1 = 0$ and the equations reduce to

$$\chi^{I} = \epsilon r \frac{n}{m}$$

or

$$\hat{\psi}_0^{I\prime} = a_0' + \epsilon r \frac{n}{m}$$

and

$$\chi^{II} = \epsilon r \frac{n}{(m+1)}$$

or

$$\hat{\psi}_0^{II\prime} = a_0' + \epsilon r \frac{n}{(m+1)},$$

which are just the cylindrical helical magnetic flux equations for the two modes (see equation 4.9). Thus the toroidal mode–coupling corrections play a role if and only if $\cos\chi_1 \neq 0$.

Equations (7.37) and (7.38) can be integrated to give

$$\hat{\psi}_0^{I} = a_0 + \frac{D}{2}(2m+1)r^2 + D\,\frac{2}{C^2}\left[\frac{1}{5}(\sqrt{1+R_1})^5 - \frac{1}{3}(\sqrt{1+R_1})^3\right] \tag{7.39}$$

$$\hat{\psi}_0^{II} = a_0 + \frac{D}{2}(2m+1)r^2 - D\,\frac{2}{C^2}\left[\frac{1}{5}(\sqrt{1+R_1})^5 - \frac{1}{3}(\sqrt{1+R_1})^3\right], \tag{7.40}$$

with

$$C = \frac{1}{2}\epsilon\,\frac{(2m+1)\;m\;(m+1)}{n}\cos^2\chi_1$$

$$D = \frac{1}{2}\epsilon\,\frac{n}{m(m+1)}, \tag{7.41}$$

and the integration constants chosen to be zero.

However, when we attempted to solve the final set of equations (given in section 7.6) we found numerical iteration to be difficult. We then instead of equations (7.39) and (7.40) used the normal cylindrical equations (i.e. $R_1 = 0$). This can be justified because of the small difference between the cylindrical $\hat{\psi}_0$ and the $\hat{\psi}_0$ where toroidal corrections have been included. The only restriction is that the outer island must not be to close too the boundary in which case the effect can become large. Toroidal terms in the first order equations are however retained.

In Figure 7.1 below we compared the cylindrical $\hat{\psi}_0$ with one for which toroidal corrections have been included. It was done for a typical current profile of the type to be discussed in section 7.8.

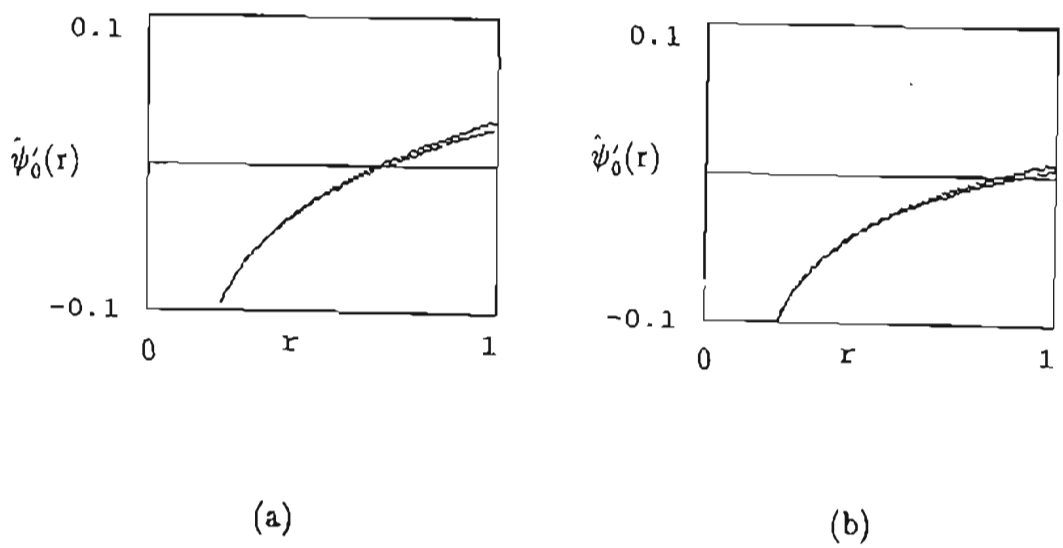

(a) (b)

FIGURE 7.1 The cylindrical $\hat{\psi}_0$ (left graph) compared with the $\hat{\psi}_0$ where toroidal corrections have been included for (a) a (2,1) mode (b) a (3,1) mode.

7.4 A Perturbation Expansion of K

The solutions $\dot{\psi}_0^{I'}$ and $\dot{\psi}_0^{II'}$ as defined in equations (7.20) and (7.21) can now be substituted into the expressions for K_0' in equations (7.10) and (7.11). This gives

$$K_0' = \frac{a_1' k_1 (m + \frac{1}{2}\epsilon r(m+1)\frac{k_2}{k_1}\cos\chi_1) + \epsilon r n k_1}{m a_1 + \frac{1}{2}\epsilon r(m+1) a_2 \cos\chi_1}$$

$$= \frac{k_1\left[a_0'(m + \frac{1}{2}\epsilon r(m+1)\frac{k_2}{k_1}\cos\chi_1) + \epsilon r n \right]\dot{\psi}_0^{I'}}{\dot{\psi}_1\left[a_0'(m + \frac{1}{2}\epsilon r(m+1)\frac{\dot{\psi}_2}{\dot{\psi}_1}\cos\chi_1) + \epsilon r n \right]} \qquad (7.42)$$

and

$$K_0' = \frac{k_2\left[a_0'((m+1) + \frac{1}{2}\epsilon r m\frac{k_1}{k_2}\cos\chi_1) + \epsilon r n \right]\dot{\psi}_0^{II'}}{\dot{\psi}_2\left[a_0'((m+1) + \frac{1}{2}\epsilon r m\frac{\dot{\psi}_1}{\dot{\psi}_2}\cos\chi_1) + \epsilon r n \right]}. \qquad (7.43)$$

We can now write equations (7.12), (7.13), (7.18) and (7.19) as

$$\frac{a_1}{a_1'} = \frac{\dot{\psi}_1}{\dot{\psi}_1'} = \frac{k_1}{k_1'} \qquad (7.44)$$

and

$$\frac{a_2}{a_2'} = \frac{\dot{\psi}_2}{\dot{\psi}_2'} = \frac{k_2}{k_2'}, \qquad (7.45)$$

with solutions

$$\dot{\psi}_1 = \alpha k_1 \qquad (7.46)$$

$$\hat{\psi}_2 = \beta k_2 , \tag{7.47}$$

and α, β integration constants.

For our model we will now choose $\alpha = \beta$ to get

$$\frac{\hat{\psi}_1}{\hat{\psi}_2} = \frac{k_1}{k_2} . \tag{7.48}$$

This modelling will be justified at a later stage.

Equation (7.48) can now be substituted into equations (7.42) and (7.43) to give

$$K_0' = \frac{k_1}{\hat{\psi}_1} \hat{\psi}_0^{I\prime}$$

or

$$k_1 = \hat{\psi}_1 \frac{\partial K_0}{\partial \hat{\psi}_0^I} \tag{7.49}$$

and $K_0' = \frac{k_2}{\hat{\psi}_2} \hat{\psi}_0^{II\prime}$

or

$$k_2 = \hat{\psi}_2 \frac{\partial K_0}{\partial \hat{\psi}_0^{II}} . \tag{7.50}$$

From equations (7.49) and (7.50) it is clear that K_0 is a function of both $\hat{\psi}_0^I$ and $\hat{\psi}_0^{II}$, i.e.

$$K_0 \equiv K_0(\hat{\psi}_0^I , \hat{\psi}_0^{II}) . \tag{7.51}$$

Equation (7.9) can now be written as

$$K = K_0(\hat{\psi}_0^I , \hat{\psi}_0^{II}) + \hat{\psi}_1 \frac{\partial K_0}{\partial \hat{\psi}_0^I} \cos (m\theta - n\varphi) + \hat{\psi}_2 \frac{\partial K_0}{\partial \hat{\psi}_0^{II}} \cos ((m+1)\theta - n\varphi + \chi_1) , \quad (7.52)$$

using equations (7.49) and (7.50). This is just a first order Taylor expansion of two independent variables, i.e.

$$F(P_1 + \Delta P_1, P_2 + \Delta P_2) = F(P_1 , P_2) + \frac{\partial F(P_1, P_2)\ \Delta P_1}{\partial P_1}$$

$$+ \frac{\partial F(P_1 , P_2)\ \Delta P_2}{\partial P_2} + \ldots .$$

It is now clear that, within this model, the equation $\underline{B}.\nabla K = 0$ (i.e. equation (7.5)) can be represented by

$$K \equiv K(\hat{\psi}^I , \hat{\psi}^{II}) , \quad (7.53)$$

with

$$\hat{\psi}^I = \hat{\psi}_0^I + \hat{\psi}_1 \cos (m\theta - n\varphi) \quad (7.54)$$

$$\hat{\psi}^{II} = \hat{\psi}_0^{II} + \hat{\psi}_2 \cos ((m+1)\theta - n\varphi + \chi_1) . \quad (7.55)$$

7.5 Solving $K = -\Delta^* \psi$

We will now investigate equation (7.6). This equation can be written as

$$\epsilon \cos\theta \frac{\partial \psi}{\partial r} - \frac{\epsilon}{r} \sin\theta \frac{\partial \psi}{\partial \theta} - \frac{h}{r} \frac{\partial \psi}{\partial r} - h \frac{\partial^2 \psi}{\partial r^2} - h \frac{1}{r^2} \frac{\partial^2 \psi}{\partial \theta^2} = hK . \tag{7.56}$$

When the Fourier expansions for ψ and K have been substituted into equation (7.56), we get

$$a_0'' + \frac{1}{r} a_0' = -K_0 \tag{7.57}$$

$$a_1'' + \frac{1}{r} a_1' - \frac{m^2}{r^2} a_1 - \frac{1}{2} \epsilon a_2' \cos\chi_1 - \frac{(m+1)^2}{r^2} a_2 \cos\chi_1$$

$$+ \frac{1}{2} \epsilon r \cos\chi_1 \left(a_2'' + \frac{1}{r} a_2' - \frac{(m+1)^2}{r^2} a_2\right)$$

$$= -\hat{\psi}_1 \frac{\partial K_0}{\partial \hat{\psi}_0^I} - \frac{1}{2} \epsilon r \hat{\psi}_2 \frac{\partial K_0}{\partial \hat{\psi}_0^{II}} \cos\chi_1 \tag{7.58}$$

$$a_2'' + \frac{1}{r} a_2' - \frac{(m+1)^2}{r^2} a_2 - \frac{1}{2} \epsilon a_1' \cos\chi_1 + \frac{1}{2} \frac{\epsilon}{r} m a_1 \cos\chi_1$$

$$+ \frac{1}{2} \epsilon r \cos\chi_1 \left(a_1'' + \frac{1}{r} a_1' - \frac{m^2}{r^2} a_1\right)$$

$$= -\hat{\psi}_2 \frac{\partial K_0}{\partial \hat{\psi}_0^{II}} - \frac{1}{2} \epsilon r \hat{\psi}_1 \frac{\partial K_0}{\partial \hat{\psi}_0^I} \cos\chi_1 . \tag{7.59}$$

When equation (7.59) is substituted into equation (7.58), it results in

$$a_1'' + \frac{1}{r} a_1' - \frac{m^2}{r^2} a_1 - \frac{1}{2} \epsilon a_2' \cos\chi_1 - \frac{1}{2} \frac{\epsilon}{r} (m+1) a_2 \cos\chi_1$$

$$= \hat{\psi}_1 \frac{\partial K_0}{\partial \hat{\psi}_0^I} \tag{7.60}$$

when terms of $0(\epsilon^3)$ are neglected. In the same way equation (7.59) can be written as

$$a_2'' + \frac{1}{r} a_2' - \frac{(m+1)^2}{r^2} a_2 - \frac{1}{2} \epsilon a_1' \cos \chi_1 + \frac{1}{2} \frac{\epsilon}{r} m a_1 \cos \chi_1$$

$$= - \dot{\psi}_2 \frac{\partial K_0}{\partial \dot{\psi}_0^{II}} \tag{7.61}$$

7.6 A Closed Set of Toroidal Equations

Finally the equations in the toroidal approximation can be written down as

$$a_0'' + \frac{1}{r} a_0' = - K_0 \tag{7.62}$$

$$a_1'' + \frac{1}{r} a_1' - \frac{m^2}{r^2} a_1 - \frac{1}{2} \epsilon a_2' \cos \chi_1 - \frac{1}{2} \frac{\epsilon}{r} (m+1) a_2 \cos \chi_1$$

$$= - \dot{\psi}_1 \frac{\partial K_0}{\partial \dot{\psi}_0^{I}} \tag{7.63}$$

$$a_2'' + \frac{1}{r} a_2' - \frac{(m+1)^2}{r^2} a_2 - \frac{1}{2} \epsilon a_1' \cos \chi_1 + \frac{1}{2} \frac{\epsilon}{r} m a_1 \cos \chi_1$$

$$= - \dot{\psi}_1 \frac{\partial K_0}{\partial \dot{\psi}_0^{II}} \tag{7.64}$$

$$\dot{\psi}_0^{I'} = a_0' + \frac{1}{2} \epsilon r n \frac{1}{m(m+1)} \left[2m+1 + \sqrt{1+R_1} \right] \tag{7.65}$$

$$\dot{\psi}_0^{II'} = a_0 + \frac{1}{2} \epsilon r n \frac{1}{m(m+1)} \left[2m+1 - \sqrt{1+R_1} \right] \tag{7.66}$$

$$R_1 = \frac{1}{2} \epsilon r \frac{(2m+1)\ m\ (m+1)}{n} \cos^2 \chi_1 .$$

(where a_1 and a_2 clearly coupled by toroidicity).

The rationale behind putting $\gamma = \lambda = 1$ and $\alpha = \beta$ may now be examined.

(i) $\alpha = \beta$: When this assumption is made, we get

$$K = K_0 + k_1 \cos(m\theta - n\varphi) + k_2 \cos((m+1)\theta - n\varphi + \chi_i)$$

$$= K_0 + \dot{\psi}_1 \cos(m\theta - n\varphi) \frac{\partial K_0}{\partial \dot{\psi}_0^I} + \dot{\psi}_2 \cos((m+1)\theta - n\varphi + \chi_i) \frac{\partial K_0}{\partial \dot{\psi}_0^{II}},$$

which means that the Fourier expansion of K is compatible with the perturbation expansion of K in terms of the functions $\dot{\psi}^I$ and $\dot{\psi}^{II}$ as defined in equations (7.36) and (7.37).

(ii) $\gamma = \lambda = 1$: This assumption leads to

$$\dot{\psi}_0' = a_0' + \epsilon r \frac{n}{m_s} + 0(\epsilon^2)$$

where $\dot{\psi}_0'$ signifies any of $\dot{\psi}_0^{I'}$ or $\dot{\psi}_0^{II'}$ and m_s the particular poloidal mode number (m or m+1). This reduces to the cylindrical helical magnetic flux when terms of $0(\epsilon^2)$ are dropped and equations (7.26) and (7.27) are decoupled.

Thus each of these assumptions contributes to the self–consistency of the model.

7.7 The Toroidal Safety Factor

The safety factor (q) can now also be defined for this case where toroidal coupling is included in the model. From the fieldline equation for (r,θ,φ) coordinates

$$\frac{r\,d\theta}{B_{\theta_0}} = \frac{R d\varphi}{B_\varphi}$$

and the toroidal quantities B_{θ_0} and B_φ (given by equations (3.8) and (3.7)), we get

$$\int d\theta(1 + \epsilon r \cos\theta)^{-1} = -\frac{\partial\psi}{\partial r}\frac{1}{\epsilon r}\int d\varphi .$$

Define

$$\omega_L = \int \frac{d\theta}{1 + \epsilon r \cos\theta}$$

to get

$$\omega_L = -\frac{a_0'}{\epsilon r}\varphi + \omega_{LC} . \tag{7.67}$$

with ω_{LC} an integration constant,

in the absence of no non–axisymmetric perturbations. A new safety factor can now be defined as

$$q = \frac{\Delta\omega_L}{\Delta\varphi} = \frac{a_0'}{\epsilon r} . \tag{7.68}$$

When this is substituted into equations (7.65) and (7.66), it is immediately clear that $\dot{\psi}_0^{I'} = 0$ defines the rational surface at $r = r_{sI}$ and $\dot{\psi}_0^{II'} = 0$ defines the rational surface at $r = r_{sII}$.

7.8 The Model for $K_0(r)$

Closer inspection of equations (7.49) and (7.50) shows that

$$\frac{\partial K_0}{\partial \dot{\psi}_0^I} = K_0'/\dot{\psi}_0^{I'} \to \infty \text{ if } K_0' \neq 0 \text{ at } r = r_{sI} \tag{7.69}$$

$$\frac{\partial K_0}{\partial \dot{\psi}_0^{II}} = K_0'/\dot{\psi}_0^{II'} \to \infty \text{ if } K_0' \neq 0 \text{ at } r = r_{sII} . \tag{7.70}$$

We will now proceed in exactly the same way as in the cylindrical case to prescribe K_0 in equations (7.62) to (7.66). From its definition we know that K_0 is a function of r. We must also demand that $K_0'\Big|_{r_{sI}} = 0$ and $K_0'\Big|_{r_{sII}} = 0$ (from equations (7.69) and (7.70). We will thus model two axisymmetric perturbations δK_1 and δK_2 to flatten the profile of $K_0(r)$ at both $r_{sI}(r_{s1})$ and $r_{sII}(r_{s2})$.

The function $K(\hat{\psi}^I,\hat{\psi}^{II})$ is similar to the cylindrical $J(\hat{\psi})$. In chapter 6 we used a parabolic current density profile with only one free variable as was specified in equation 6.3. We will now use a two parameter model for $K_0(r)$ of the form

$$K_{u0}(r) = g_0(1-r^f)^b . \tag{7.71}$$

It is now easy to show from equation (7.62) that

$$g_0 = \frac{\epsilon}{q_1}\frac{f}{B(b+1,\frac{2}{f})} \tag{7.72}$$

and

$$q_0 = \frac{2\epsilon}{g_0}, \tag{7.73}$$

where $B(b+1,\frac{2}{f})$ denotes the Beta function with parameters $b+1$ and $\frac{2}{f}$, and q the safety factor as specified by equation (7.68) using the normal notation as was discussed after equation (6.8).

For any choice of the parameters b and f in the expression for $K_{u0}(r)$ (i.e. equation (7.71)), it is thus possible to find g_0 and q_0 when q_1 is specified.

Equation (7.71) specifies the unperturbed equilibrium profile. We will now proceed to include two axisymmetric perturbations δK_1 and δK_2 at the two rational surfaces.

Let

$$\delta K_1(r) = -g_0[(1-r^f)^b - (1-r_{s1}^f)^b]\, e^{-\left(\frac{r-r_{s1}}{w_1}\right)^2} \qquad (7.74)$$

and

$$\delta K_2(r) = -j_2[(1-r_{s2}+d_2)\, e^{-\left(\frac{r-r_{s2}+d_2}{w_2}\right)^2}. \qquad (7.75)$$

We assume that the one island is dominant and is located at r_{s1}. The other island located at r_{s2} is smaller. The larger island will thus affect the flatness of the smaller island at r_{s2} but not the other way round. The variable j_2 can now be specified in such a way that, when the effect of $\delta K_1(r)$ is included, $K_0'\Big|_{r_{s2}}$ is zero, where

$$K_0(r) = K_{u0}(r) + \delta K_1(r) + \delta K_2(r). \qquad (7.76)$$

As before (see constraints (a) and (b) in section 6.2) we force

$$K_0'\Big|_{r_{s2}} = 0 \qquad (7.77)$$

and

$$K_0''(r)\Big|_{r_{s2}} = 0. \qquad (7.78)$$

The constraints $K_0'\Big|_{r_{s1}} = 0$ and $K_0''\Big|_{r_{s1}} = 0$ will automatically be satisfied if the effect of δK_2 is negligible at $r = r_{s1}$.

Equation (7.77) results in

$$j_2 = -\Big[-bg_0(1-r_{s2}^f)^{b-1} f\, r_{s2}^{f-1}\left(1-e^{-\left(\frac{r-r_{s2}-r_{s1}}{w_1}\right)^2}\right)$$

$$+\ 2g_0(r_{s2}-r_{s1})\frac{1}{w_1^2}\left[(1-r_{s2}^f)^b-(1-r_{s1}^f)^b\right] e^{-\left(\frac{r_{s2}-r_{s1}}{w_1}\right)^2}\Big]$$

$$\frac{}{e^{-\left(\frac{d_2}{w_2}\right)^2}\ \left(1-2\left(\frac{d_2}{w_2}\right)^2\right)}. \qquad (7.79)$$

Equation (7.78) gives

$$a_3 + a_2 d_2 + a_1 d_2^2 + d_2^3 = 0 \qquad (7.80)$$

with

$$a_3 = B\, w_2^3/(4A)$$

$$a_2 = -6\, w_2^2/4$$

$$a_1 = -2\, B\, w_2^2/(4A)$$

$$A = bg_0(1-r_{s2}^f)^{b-1} f\, r_{s2}^{f-1}\left(1-e^{-\left(\frac{r_{s2}-r_{s1}}{w_1}\right)^2}\right)$$

$$-2\, g_0(r_{s2}-r_{s1})\frac{1}{w_1^2}\left[(1-r_{s2}^f)^b-(1-r_{s1}^f)^b\right] e^{-\left(\frac{r_{s2}-r_{s1}}{w_1}\right)^2}$$

$$B = b(b-1)\, g_0(1-r_{s2}^f)^{b-2}\,(f\, r_{s2}^{f-1})^2\left(1-e^{-\left(\frac{r_{s2}-r_{s1}}{w_1}\right)^2}\right)$$

$$-\ bg_0(1-r_{s2}^f)^{b-1} f\,(f-1)\, r_{s2}^{f-2}\left(1-e^{-\left(\frac{r_{s2}-r_{s1}}{w_1}\right)^2}\right)$$

$$- \quad 4\, g_0\, (r_{s2} - r_{s1})\, \frac{1}{w_1^2}\, b(1 - r_{s2}^f)^{b-1} f\, r_{s2}^{f-1}\, e^{-\left(\frac{r_{s2}-r_{s1}}{w_1}\right)^2}$$

$$+ \quad 2\, g_0\, \frac{1}{w_1^2} \left[(1 - r_{s2}^f)^b - (1 - r_{s1}^f)^b \right] e^{-\left(\frac{r_{s2}-r_{s1}}{w_1}\right)^2} \left(1 - 2\left(\frac{r_{s2}-r_{s1}}{w_1}\right)^2\right) .$$

As before (section 6.2) we can now solve for d_2. Now, with j_2 and d_2 known, we can substitute the expression for $K_0(r)$ (equation (7.76)) into equation (7.62) and solve for the equilibrium values of a_0 and a_0' as well as $\hat{\psi}_0^{I\prime}$ and $\hat{\psi}_0^{II\prime}$. As before (in the cylindrical case) the value of g_0 will change slightly when the perturbations δK_1 and δK_2 are included in $K_0(r)$. The real value of g_0 can be found by forcing $B_{\theta_0}\Big|_0 = -\,a_0'\Big|_0 = 0$. The rational surfaces r_{s1} and r_{s2} can be found iteratively from the expressions $\hat{\psi}_0^{I\prime}\Big|_{r_{s1}} = 0$ and $\hat{\psi}_0^{II\prime}\Big|_{r_{s1}} = 0$.

Equations (7.63) and (7.64) can now also be solved because $\frac{\partial K_0}{\partial \hat{\psi}_0^I}$ as well as $\frac{\partial K_0}{\partial \hat{\psi}_0^{II}}$ are analytic for all r.

7.9 Boundary Conditions for the Toroidal Equations

We know that $K = K(\hat{\psi}_0^I, \hat{\psi}_0^{II})$. Now assume as before that the boundary has the same form as $\hat{\psi}_0^I$ or $\hat{\psi}_0^{II}$, i.e.

$$r^{\partial} = r_0 + \delta_1 \cos(m\theta - n\varphi) + \delta_2 \cos((m+1)\theta - n\varphi + \chi_1) . \qquad (7.81)$$

Therefore K will follow the boundary such that

$$K^{\partial} = 0 . \qquad (7.82)$$

If we make a perturbation expansion of $K(r)$ about the boundary, we get

$$\begin{aligned} K^{\partial} &= K_0(r^{\partial}) + k_1(r^{\partial}) \cos(m\theta - n\varphi) + k_2(r^{\partial}) \cos((m+1)\theta - n\varphi + \chi_1) \\ &= K_0(r_0) + K_0'(r_0)\left[\delta_1 \cos(m\theta - n\varphi) + \delta_2 \cos((m+1)\theta - n\varphi + \chi_1)\right] \\ &+ k_1(r_0) \cos(m\theta - n\varphi) + k_2(r_0) \cos((m+1)\theta - n\varphi + \chi_1) \\ &+ k_1'(r_0) \cos(m\theta - n\varphi)\left[\delta_1 \cos(m+1)\theta + \delta_2 \cos((m+1)\theta - n\varphi + \chi_1)\right] \\ &+ k_2'(r_0) \cos((m+1)\theta - n\varphi + \chi_1)\left[\delta_1 \cos(m\theta - n\varphi) + \delta_2 \cos((m+1)\theta - n\varphi + \chi_1)\right] \\ &= 0 . \end{aligned}$$

From the Fourier components $\cos(m\theta - n\varphi)$ and $\cos((m+1)\theta - n\varphi + \chi_1)$ we get

$$k_1(r_0) = -\delta_1 K_0'(r_0) \tag{7.83}$$

$$k_2(r_0) = -\delta_2 K_0'(r_0) . \tag{7.84}$$

The expression for $k_1'(r_0)$ and $k_2'(r_0)$ in equations (7.49) and (7.50) can now be substituted into the above equations to give

$$k_1(r_0) = -\delta_1 k_1 \dot{\psi}_0^{I'} / \dot{\psi}_1 \Big|_{r_0}$$

or

$$\dot{\psi}_1(r_0) = -\delta_1 \dot{\psi}_0^{I'}(r_0) \tag{7.85}$$

and

$$k_2(r_0) = -\delta_2 k_2 \hat{\psi}_0^{II\prime}/\hat{\psi}_2\Big|_{r_0}$$

or

$$\hat{\psi}_2(r_0) = -\delta_2 \hat{\psi}_0^{II\prime}(r_0)\,. \tag{7.86}$$

As before (section 5.2) we may set $r_0 = 1$ because of the normalization with regard to the plasma boundary $a = r_0$. The value of $a_0\Big|_1$ may be chosen freely because $\underline{B}_\perp = (^1/h)\,(\nabla\psi \wedge \hat{\varphi})$, which allows us to add any constant to $\psi = a_0$. The values of $\hat{\psi}_0^I\Big|_1$ and $\hat{\psi}_0^{II}\Big|_1$ are now known from equations (7.36) and (7.37).

The value of $a_0'\Big|_1$ can be found from equation (7.68), i.e.

$$a_0'\Big|_1 = {}^{\epsilon}/q_1\,.$$

Finally the values of $a_1'\Big|_1$ and $a_2'\Big|_1$ will be chosen such that $-a_1'\Big|_0 = B_{\theta_1}\Big|_0 = 0$ and $-a_2'\Big|_0 = B_{\theta_2}\Big|_0 = 0$.

All the boundary conditions that are needed to solve equations (7.62) – (7.66), i.e. $a_0\Big|_1$, $\hat{\psi}_0^I\Big|_1$, $\hat{\psi}_0^{II}\Big|_1$, $a_0'\Big|_1$, $a_1\Big|_1$, $a_2\Big|_1$, $a_1'\Big|_1$, $a_2'\Big|_1$, are now known or are to be determined in the numerical procedure. We thus have

$$a_0\Big|_1 = k_1 \text{ (free constant)} \tag{7.87}$$

$$\dot{\psi}_0^{I}\Big|_1 = k_1 + \frac{D}{2}(2m+1) + D\,\frac{2}{C^2}\left(\frac{1}{5}(\sqrt{1+R_1})^5 - \frac{1}{3}(\sqrt{1+R_1})^3\right) \tag{7.88}$$

$$\dot{\psi}_0^{II}\Big|_1 = k_1 + \frac{D}{2}(2m+1) - D\,\frac{2}{C^2}\left(\frac{1}{5}(\sqrt{1+R_1})^5 - \frac{1}{3}(\sqrt{1+R_1})^3\right) \tag{7.89}$$

$$a_0'\Big|_1 = \epsilon/q_1 \tag{7.90}$$

$$a_1\Big|_1 = -\delta_1\,\dot{\psi}_0^{I}\Big|_1 \tag{7.91}$$

$$a_2\Big|_1 = -\delta_2\,\dot{\psi}_0^{II}\Big|_1 \tag{7.92}$$

$$a_1'\Big|_1 = \text{shooting value} \tag{7.93}$$

$$a_2'\Big|_1 = \text{shooting value} \tag{7.94}$$

$$D = \frac{1}{2}\epsilon\,\frac{(2m+1)\;m\;(m+1)}{n}\cos^2\chi_1$$

$$C = \frac{1}{2}\epsilon\,\frac{n}{m(m+1)}$$

$$R_1 = D\,,$$

using the fact that $a_i' = \dot{\psi}_i'$, $i = 1,2$.

7.10 The Vacuum Equations

When the plasma equations ((7.62) – (7.66)) are coupled to vacuum on the outside, the toroidal vacuum equations are needed. We know that $\nabla\wedge\underline{B}_1 = 0$ and $\nabla.\underline{B}_1 = 0$ in vacuum, with

$$\underline{B}_1 = (B^A_{1r}\,\hat{r} + B^A_{1\theta}\,\hat{\theta} + B^A_{1\varphi}\,\hat{\varphi})e^{i(m\theta-n\varphi)}$$

$$+ (B^B_{1r}\,\hat{r} + B^B_{1\theta}\,\hat{\theta} + B^B_{1\varphi}\,\hat{\varphi})e^{i(m_2\theta-n\varphi+\chi_1)} \qquad (7.95)$$

the perturbed magnetic field with $m_2 = m+1$ and the superscripts A and B denoting the phase. When this is substituted into the toroidal expressions for $\nabla\wedge\underline{B}_1 = 0$ and $\nabla.\underline{B}_1 = 0$, and terms of $0(\epsilon^3)$ are dropped, we get

$$mB^A_{1\varphi} + \epsilon rn\, B^A_{1\theta} = 0 \qquad (7.96)$$

$$B^{A'}_{1\varphi} + i\epsilon n\, B^A_{1r} = 0 \qquad (7.97)$$

$$B^A_{1\theta} + r\, B^{A'}_{1\theta} - im\, B^A_{1r} = 0 \qquad (7.98)$$

$$B^A_{1r} + r\, B^{A'}_{1r} + im\, B^A_{1\theta} - in\epsilon r\, B^A_{1\varphi} = 0 \qquad (7.99)$$

and

$$m_2B^B_{1\varphi} + \epsilon rn\, B^B_{1\theta} = 0 \qquad (7.100)$$

$$B^{B'}_{1\varphi} + i\epsilon n\, B^B_{1r} = 0 \qquad (7.101)$$

$$B^B_{1\theta} + r\, B^{B'}_{1\theta} - im_2\, B^B_{1r} = 0 \qquad (7.102)$$

$$B^B_{1r} + r\, B^{B'}_{1r} + im_2\, B^B_{1\theta} - in\epsilon r\, B^B_{1\varphi} = 0\,, \qquad (7.103)$$

which are exactly the same as in the pure cylindrical case where the two perturbed modes are decoupled. It is thus now possible to use all the expressions that were derived for one mode in a cylinder with various external situations and to apply them directly to the present model.

7.11 External Coils

The external coils on Tokoloshe have the winding laws $q\varphi = \theta - \Delta_{\#} \sin \theta + (p-1)^{\pi}/\#$, $p = 1,2 \ldots$. The Fourier expansion of this current at $r = r_c$ (the coil radius) allows many $j_z^{(m,n)}$ components to be non–zero. The effects have been included in equation (5.59), with the values of $\Delta_{\#}$ computed for Tokoloshe and given just below equation (5.59).

For the I_2–coil, we get

$$j_z^{(2,1)} = \frac{0.824\ I_2}{\pi r_c} \text{ with } J_0(1.676) = 0.412$$

$$j_z^{(3,1)} = -\frac{1.725\ I_2}{\pi r_c} \text{ with } J_1(1.676) = 0.575$$

and for the I_3–coil

$$j_z^{(2,1)} = 0$$

$$j_z^{(3,1)} = \frac{3}{\pi r_c} I_3 \text{ with } J_0(0) = 1 .$$

When both the I_2 and I_3 coils are on, we get

$$j_z^{(2,1)} = \frac{0.824}{\pi r_c} I_2$$

$$j_z^{(3,1)} = \frac{1}{\pi r_c} (3\ I_3 - 1.725\ I_2) .$$

Another thing to remember is that the coupling at the radius where the coil current is found (i.e. equation (5.28)), is actually

$$(B^{R}_{\theta_1} - B^{L}_{\theta_1})\Big|_{r_c} e^{i(m\theta - n\varphi + \chi_1)} = j_z^{(m,n)} e^{i(m\theta - n\varphi + \chi_1)}$$

with R denoting the outside and L the inside of the boundary. When $j_z^{(m,n)}$ is found, using equations (5.45) or (5.104), it gives the amplitude of $e^{i(m\theta - n\varphi + \chi_1)}$. We need the corresponding $j_z^{(m,n)}$ at $\chi_1 = 0$, $\theta = 0$, $\varphi = 0$ to know the coil current direction. For

$$j_z^{(m,n)} \ (\theta = 0, \varphi = 0, \chi_1 = 0) > 0$$

the coil current is positive and for

$$j_z^{(m,n)} \ (\theta = 0, \varphi = 0, \chi_1 = 0) < 0 \ ,$$

the coil current is negative.

7.12 Conclusions

The one mode cylindrical model of chapter 4 was extended to include two modes with toroidal coupling between them. This agrees with work done by Bateman and Morris [67] but is extended here to allow for non–axisymmetric boundaries.

The model developed in this chapter will now be used in conjunction with the various boundary conditions of chapter 5. This is the first time that toroidally coupled modes have been studied with specific attention to the boundary conditions. The results are presented in the next chapter.

CHAPTER 8

RESULTS OF THE TWO MODE MODEL

8.1 Introduction

The results for the two mode toroidal model will now be presented.

This chapter is divided into three parts. First we present some results on the equilibrium quantities, i.e. the form of $K_0(r)$ as well as other quantities. Contour plots of (2,1) and (3,1) toroidally coupled saturated islands are also presented.

Then we consider the case of a peaked parabolic (f=2) profile for $K_{u0}(r)$, i.e. representing the low MHD phase on Tokoloshe. Locking of the modes, rotation, locking with external coils and external coils with in–phase locking are considered. Lastly, we examine the relation of the natural uncoupled (3,1) mode to the coupled one. In this part we investigate the effect of coupling on a natural (3,1) mode.

8.2 The equilibrium quantities

As was discussed in the previous chapter, the unperturbed "toroidal current profile" $K_{u0}(r)$ is flattened at both rational surfaces when two islands are included. This is shown in Figure 8.1 where toroidally coupled (2,1) and (3,1) modes have been included in the plasma. The value of the safety factor at the boundary (q_1) is 4.5. We did not use the value of 3.6 as was mostly done in the cylindrical case, because the (3,1) island had to lie deeper in the plasma for the theory to be valid (i.e. with $R_1 = 0$ as discussed at the end of section 7.3).

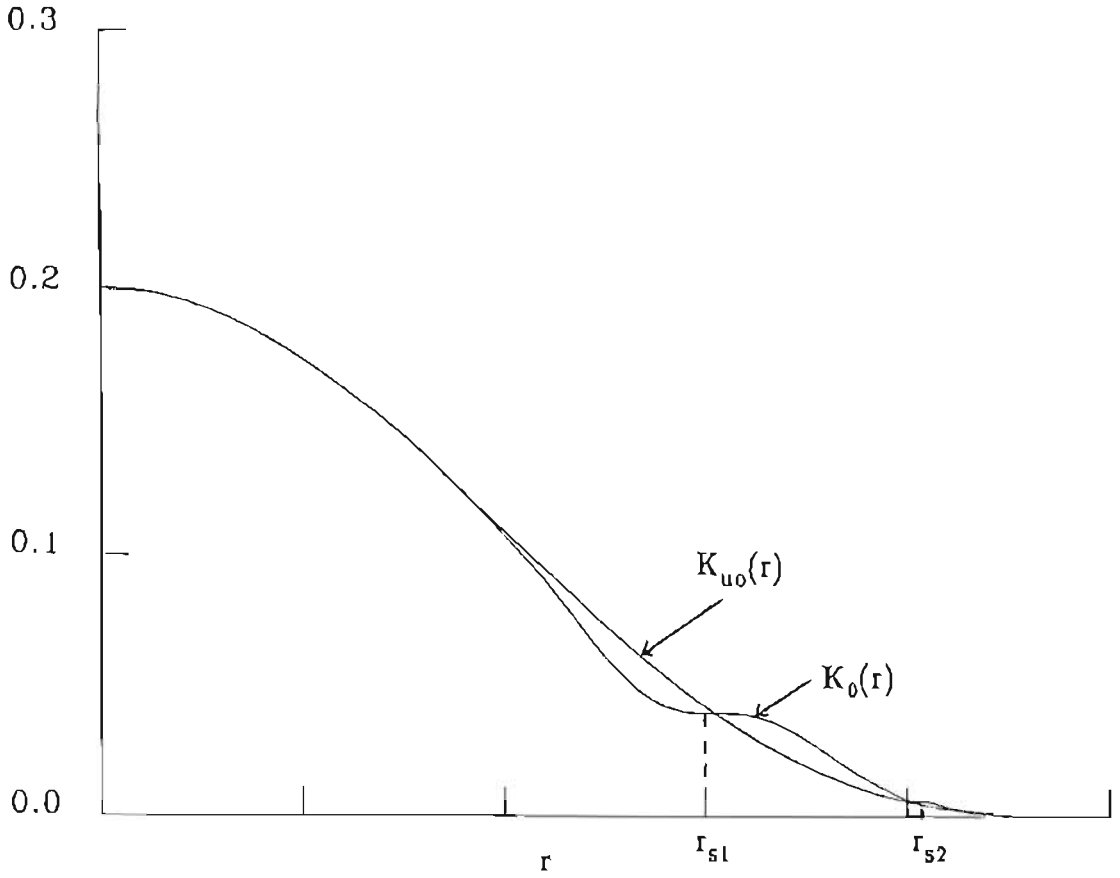

FIGURE 8.1 The graph of $K_{u0}(r)$ and $K_0(r)$ for a peaked profile with $q_1 = 4.5$, $q_0 = 1.0$, $f = 2$, $b = 3.5$.

The form of $\delta K = \delta K_1 + \delta K_2$ that was used to flatten the current profile of Figure 8.1, is shown in Figure 8.2. Both δK_1 and δK_2 are similar to the δJ used in the cylindrical case (Figure 6.3), changing sign at $r = r_{s1}$ and $r = r_{s2}$ respectively. When both are, however, included simultaneously, and the (2,1) island is dominant ($\delta K_1 > \delta K_2$), the effect of δK_1 on δK_2 can be significant as is shown in Figure 8.2. The δK_1 curve prevents the δK curve from changing sign at $r = r_{s2}$.

Also shown are k_1 and k_2. Both change sign at the particular rational surface, i.e. k_1 at r_{s1} and k_2 at r_{s2}. Note that k_1 is zero at r_{s2} and k_2 at r_{s1}. This will be discussed later in this section.

The amplitude of k_2 is much smaller than k_1 because the (3,1) mode is only 22 % of the (2,1) mode for this case in which the modes were locked.

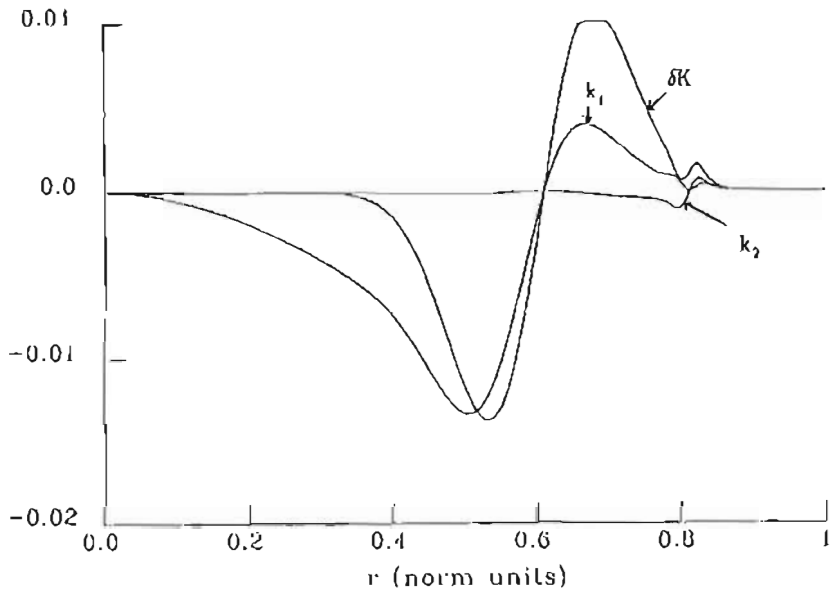

FIGURE 8.2 The forms of $\delta K = \delta K_1 + \delta K_2$, k_1 and k_2 for the same profile as in Figure 8.1.

The last equilibrium quantity to be discussed is $\hat{\psi}_0$, the helical magnetic flux. There are two expressions for $\hat{\psi}_0$, i.e. $\hat{\psi}_0^I$ which agrees with the helicity of a (2,1) mode in our work, and $\hat{\psi}_0^{II}$ which agrees with the helicity of a (3,1) mode in our case. The functional form of $\hat{\psi}_0^I$ has a minimum at $r = r_{s1}$ (the rational surface of the (2,1) mode) and that of $\hat{\psi}_0^{II}$ has a minimum at $r = r_{s2}$ (the rational surface of the (3,1) mode). This is shown in Figure 8.3.

Other important quantities to be calculated are $\partial K_0/\partial\hat{\psi}_0^I$ and $\partial K_0/\partial\hat{\psi}_0^{II}$. These are needed to calculate a_1 and a_2 from equations (7.63) and (7.64). Both these quantities ($\partial K_0/\partial\hat{\psi}_0^I$ and $\partial K_0/\partial\hat{\psi}_0^{II}$) are shown in Figure 8.4. The quantity $\partial K_0/\partial\hat{\psi}_0^I = K_0'/\hat{\psi}_0^{I'}$ changes sign at $r = r_{s1}$ because $\hat{\psi}_0^{I'}$ changes sign at that point ($\hat{\psi}_0^I$ has a minimum at $r = r_{s1}$ as was discussed in the previous paragraph). This is also true of $\partial K_0/\partial\hat{\psi}_0^{II} = K_0'/\hat{\psi}_0^{II'}$ which changes sign at $r = r_{s2}$. Also note that both these quantities are zero at the rational surface other than the one where they change sign. This happens because K_0' is zero at both rational surfaces.

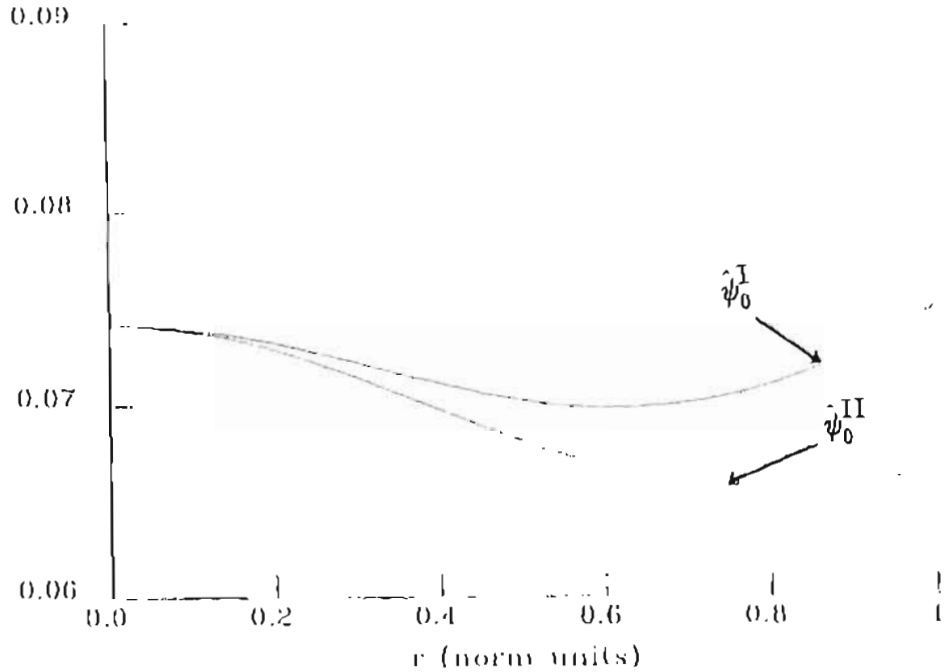

FIGURE 8.3 The form of $\hat{\psi}_0^I$ and $\hat{\psi}_0^{II}$ for a (2,1) and (3,1) island respectively. The equilibrium specified in Figure 8.1 is used.

This also explains the behaviour of k_1 and k_2 which is just

$$k_1 = \hat{\psi}_1 K_0'/\hat{\psi}_0^{I'}$$

$$k_2 = \hat{\psi}_1 K_0'/\hat{\psi}_0^{II'} .$$

Finally, being able to calculate all the equilibrium and perturbed quantities for this particular profile ($q_1 = 4.5$, $q_0 = 1.0$, $f = 2$, $b = 3.5$), we can calculate the total perturbed values of

$$\hat{\psi}^I = \hat{\psi}_0^I + \hat{\psi}_1 \cos(m\theta - n\varphi)$$

$$\hat{\psi}^{II} = \hat{\psi}_0^{II} + \hat{\psi}_2 \cos((m+1)\theta - n\varphi)$$

$$K(\hat{\psi}^I, \hat{\psi}^{II}) = K_0(r) + k_1 \cos(m\theta - n\varphi) + k_2 \cos((m+1)\theta - n\varphi) ,$$

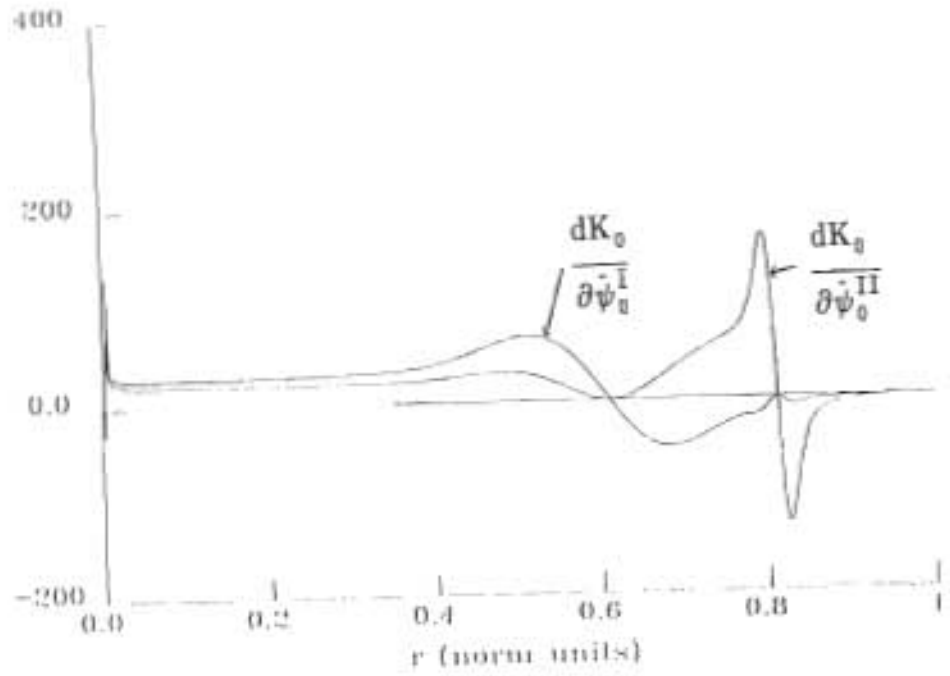

FIGURE 8.4 The graphs of $K_0'/\tilde{\psi}_0^{I\prime}$ and $K_0'/\tilde{\psi}_0^{II\prime}$. The equilibrium specified in Figure 8.1 is used.

with $k_1 = 0$, $m = 2$, $n = 1$. The contour plot of $\tilde{\psi}^I$ is shown in Figure 8.5, that of $\tilde{\psi}_0^{II}$ in Figure 8.6 and that of $K(\tilde{\psi}^I, \tilde{\psi}^{II})$ in Figure 8.7. Only on the graph of $K(\tilde{\psi}^I, \tilde{\psi}^{II})$ are both islands visible as can be expected.

8.3 The eigenvalues of both modes

Instead of one eigenvalue as before, the problem now has two eigenvalues, w_1 and w_2. These parameters are defined in equations (7.74) and (7.75). The graphs of $\left.\frac{a_i}{a_i'}\right|_1$ against w_i, $i = 1, 2$, have exactly the same form as before. The only difference is that in the case of only one mode present, the graph was independent of both δ and ϵ. It was thus possible to find the functional form of the graph and only afterwards to solve for δ when the saturated island width is determined using some $\Delta'(W)$ criterion. Now, the form of the graph can only be found at the same

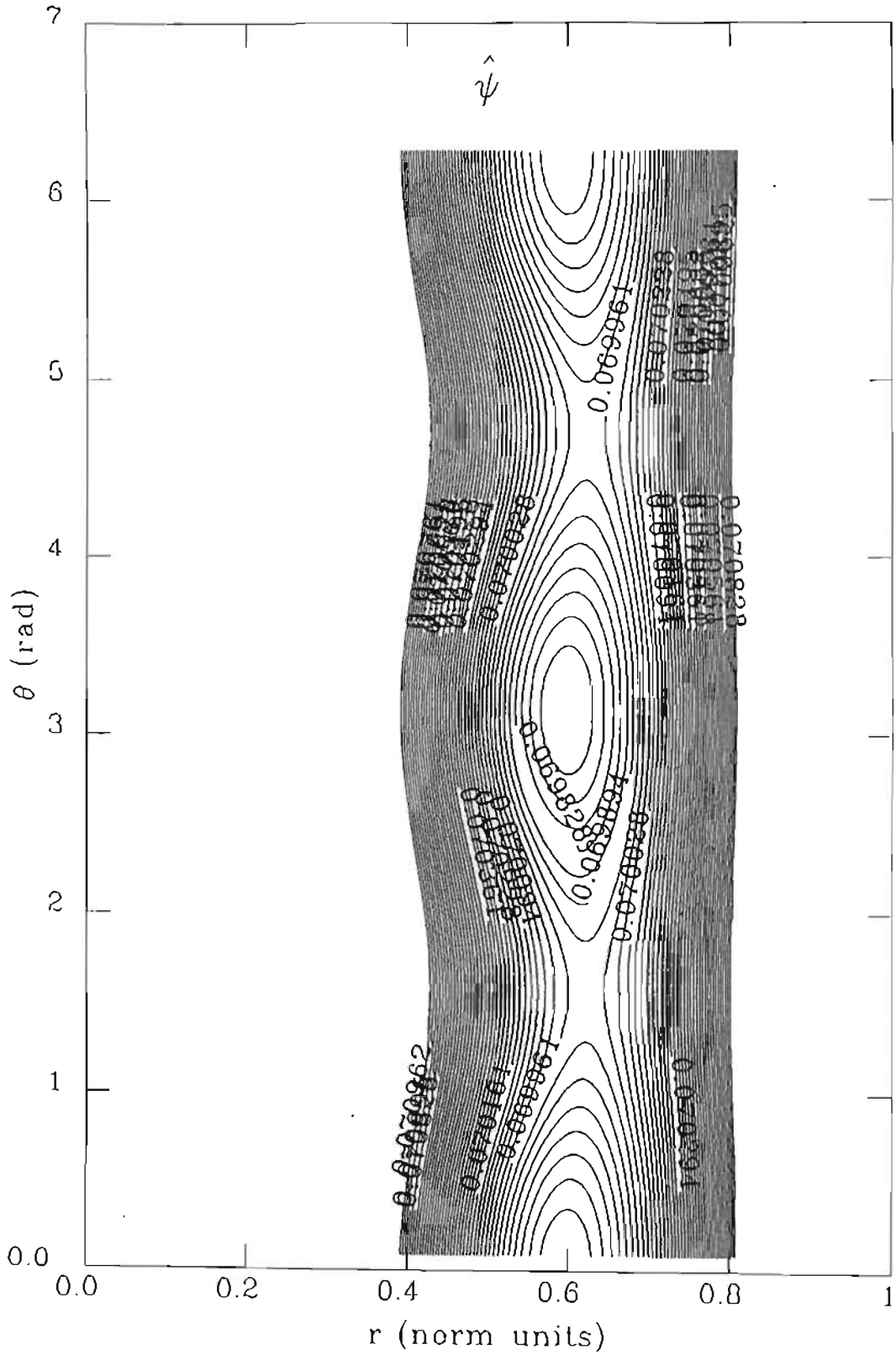

FIGURE 8.5 The (2,1) mode with b = 3.5, f = 2, q_1 = 4.5 and q_0 = 1.0.

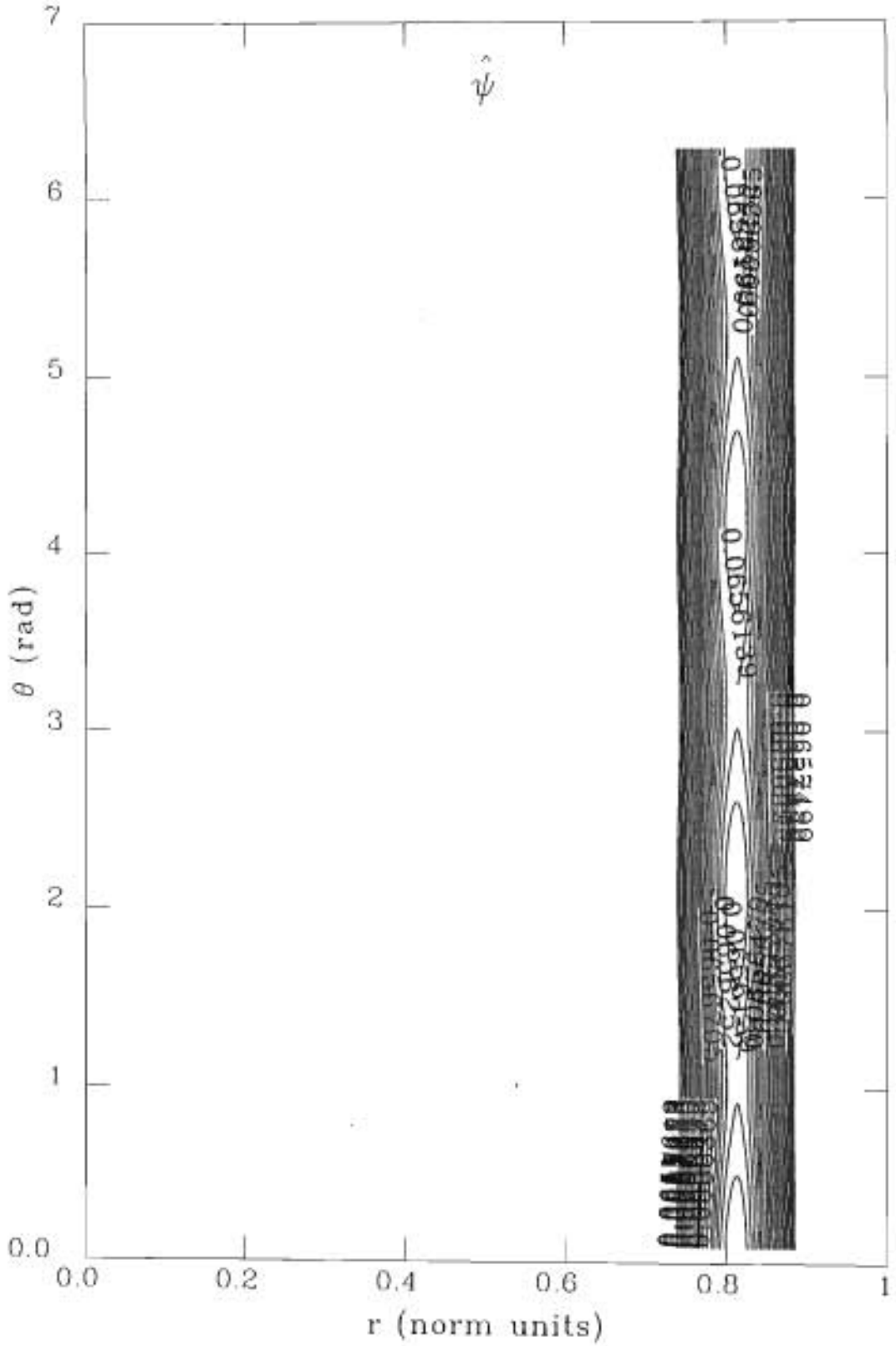

FIGURE 8.6 The (3,1) mode with the same equilibrium as in Figure 8.5.

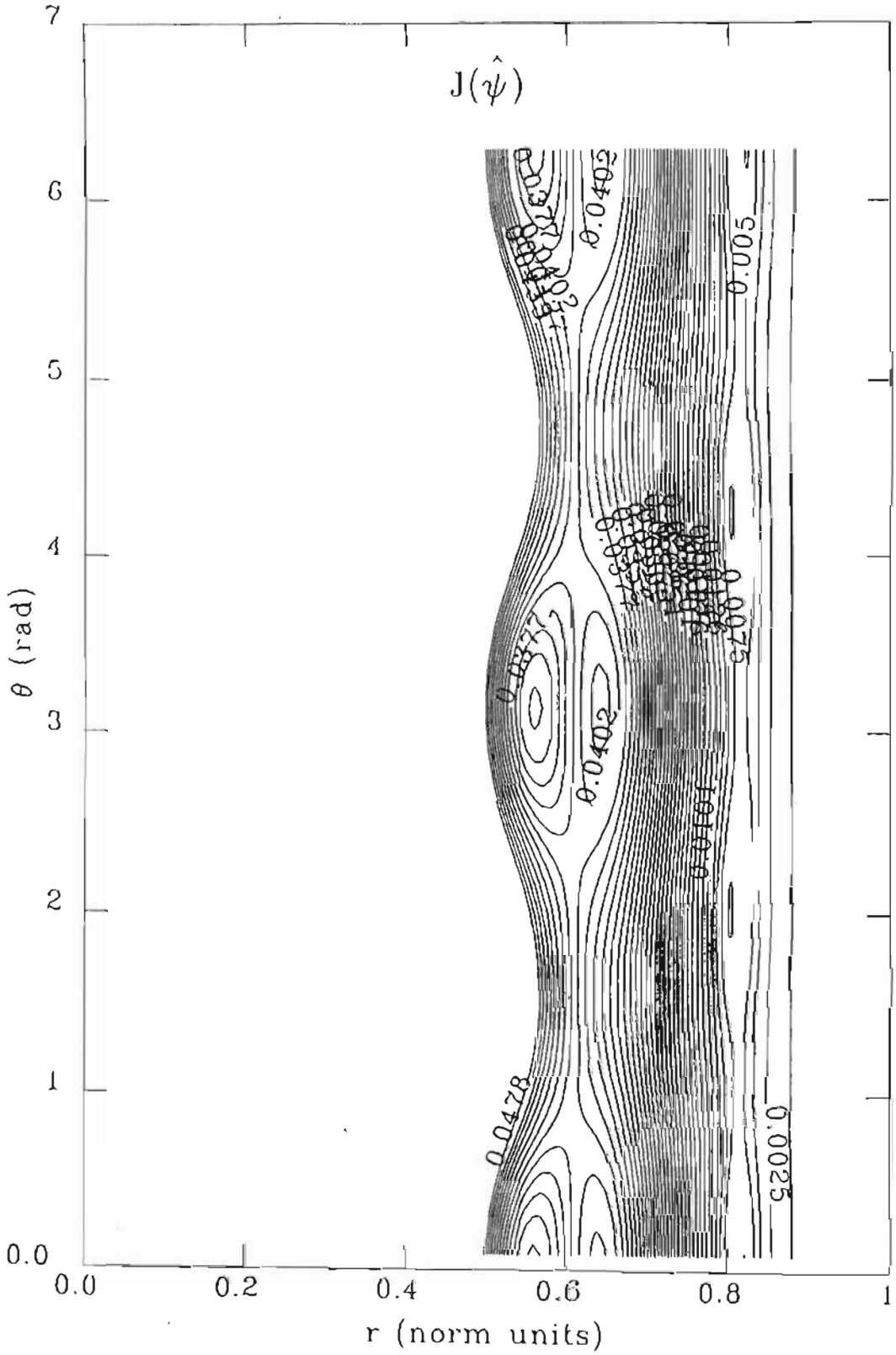

FIGURE 8.7 Both the (2,1) and (3,1) islands are visible on the contour plot of $K(\hat{\psi}^{I}, \hat{\psi}^{II})$. The equilibrium is the same as in Figure 8.5.

time that δ_i, $i = 1, 2$, are determined. For every value of w_i, the correct value of $\left.\frac{a_i}{a_i'}\right|_1$ is only known once the saturated island width, and thus also δ_i, has been determined. This increases the computing time considerably (up to a 100 times because both the starting shooting values must also be chosen correctly). In the following graph we present $\left.\frac{a_i}{a_i'}\right|_1$ against w_i for both modes in the case of a peaked parabolic profile for $K_0(r)$ ($b = 3.5$, $f = 2$, $q_1 = 4.5$, $q_0 = 1.0$). It is clear that the profile is flattened much more at the (2,1) rational surface than at the (3,1) surface, i.e. $w_1 > w_2$ for the same $\left.\frac{a_i}{a_i'}\right|_1$. This implies a (2,1) island that is considerably larger than the (3,1) island. It is consistent with our present model, which is only valid if the (3,1) island is not very large.

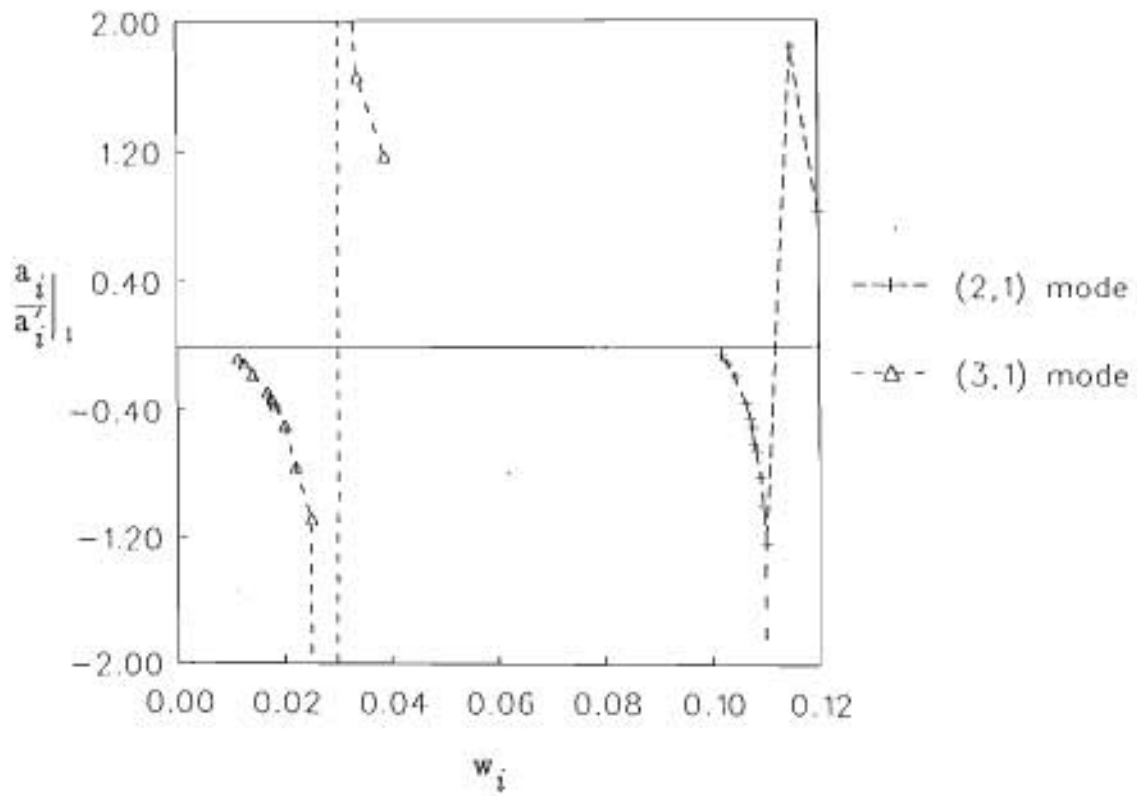

FIGURE 8.8 The graph of $\left.\frac{a_i}{a_i'}\right|_1$ against w_i, $i = 1,2$ for coupled (2,1) ($i=1$) and (3,1) ($i=2$) modes.

8.4 Mode Rotation without External Coils

As was discussed in chapter 5, we will now assume a configuration where the plasma is rotating. Between the plasma and the resistive wall a small vacuum region is allowed for, and vacuum is also assumed outside the wall. The form of $\left.\frac{a_i}{a_i'}\right|_1$ for such a configuration is given by equation (5.73). From this equation we can tabulate Ω against $\left.\frac{a_i}{a_i'}\right|_1$ for both modes. This is done in Table 8.1 for $\epsilon = 0.1$ and r_w, the wall radius, at 1.01, i.e. the wall is very close to the plasma edge.

Ω	$\left.\frac{a_1}{a_1'}\right\|_1$	$\left.\frac{a_2}{a_2'}\right\|_1$
0	–0.501	–0.33
1	–0.447	–0.316
2	–0.353	–0.283
5	–0.185	–0.171
10	–0.104	–0.105
20	–0.05	–0.055
∞	–0.01	–0.011

Table 8.1

In Figure 8.9 we show the island width as a function of rotational frequency Ω. The (2,1) island increases by 16 % when it is locked (from a very fast rotating situation), and the (3,1) island by 36 %. The effect of mode locking is thus much larger on the (3,1) island. The islands are considered to be coupled together and rotating at the same frequency.

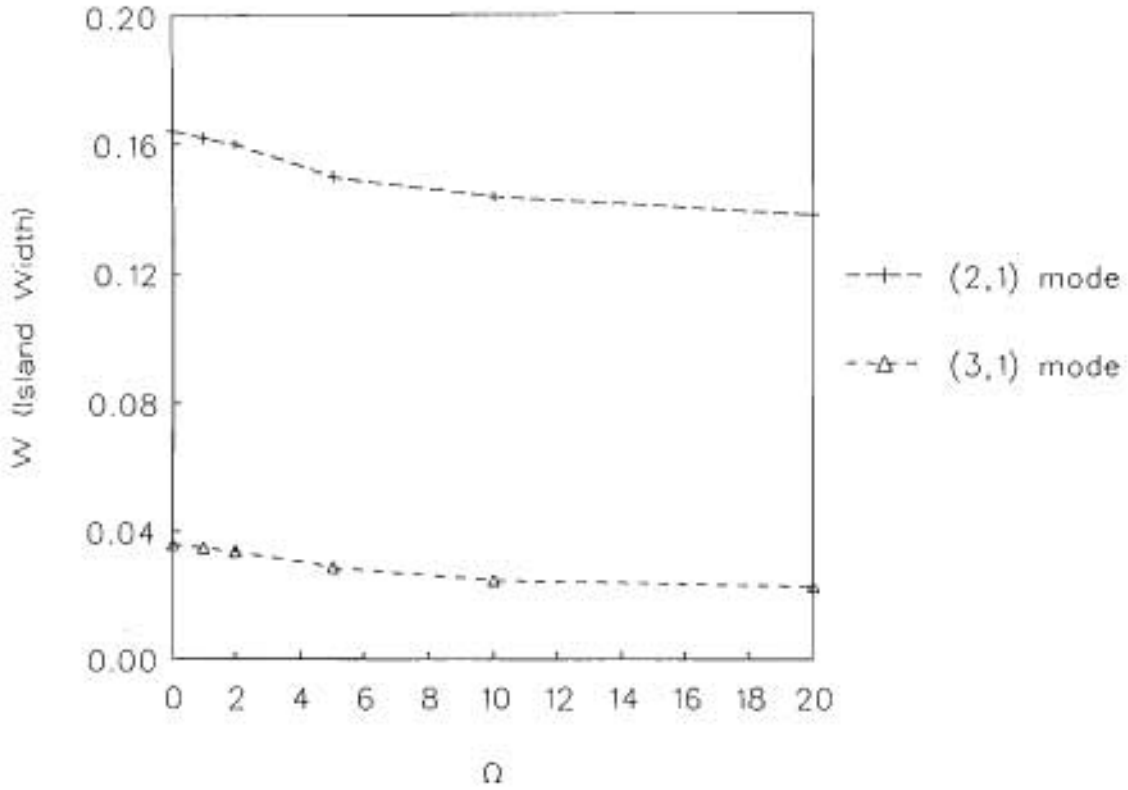

FIGURE 8.9 The island widths of the (2,1) and (3,1) islands for different rotational frequencies. The equilibrium parameters are $q_1 = 4.5$, $q_0 = 1.0$, $b = 3.5$, $f = 2.0$.

8.5 External Coils

Equation (5.45) gives $\left.\frac{a_i}{a_i'}\right|_1$ when an external coil is included in the vacuum outside the plasma. When $r_w = 1$ and $r_c = 1.1$, we get

$$j_z^{(3,1)} = \left(\left.\frac{a_2}{a_2'}\right|_1 / 0.3336 + 1 \right) \frac{\left.a_2'\right|_1}{0.8264}$$

$$j_z^{(2,1)} = \left(\left.\frac{a_1}{a_1'}\right|_1 / 0.501 + 1 \right) \frac{\left.a_1'\right|_1}{0.9094} .$$

We will now consider three situations, i.e. when only the I_3 coil is switched on, when both I_2 and I_3 coils are switched on such that $j_z^{(3,1)} = 0$, and when both the I_2 and I_3 coils are on with $j_z^{(2,1)} = j_z^{(3,1)}$. In Figure 8.10 the case of I_3 alone is shown, in Figure 8.11 we show the second case where $j_z^{(3,1)} = 0$, and in Figure 8.12 the third case where $j_z^{(2,1)} = j_z^{(3,1)}$. The same profile as before is used, i.e. with parameters $q_1 = 4.5$, $q_0 = 1.0$, $b = 3.5$, $f = 2$. In all the cases the islands are locked in phase with the external coil.

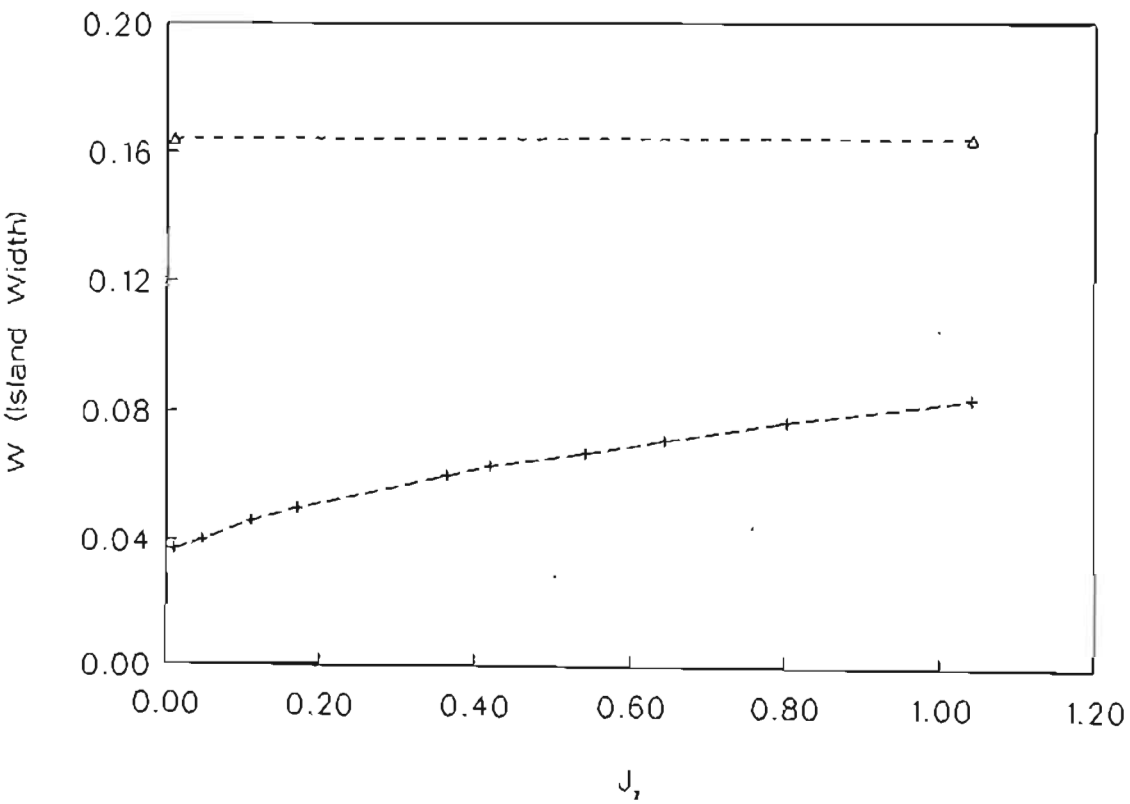

FIGURE 8.10 The width of the (3,1) island for the I_3 coil. The (2,1) island width stays unchanged on 0.164.

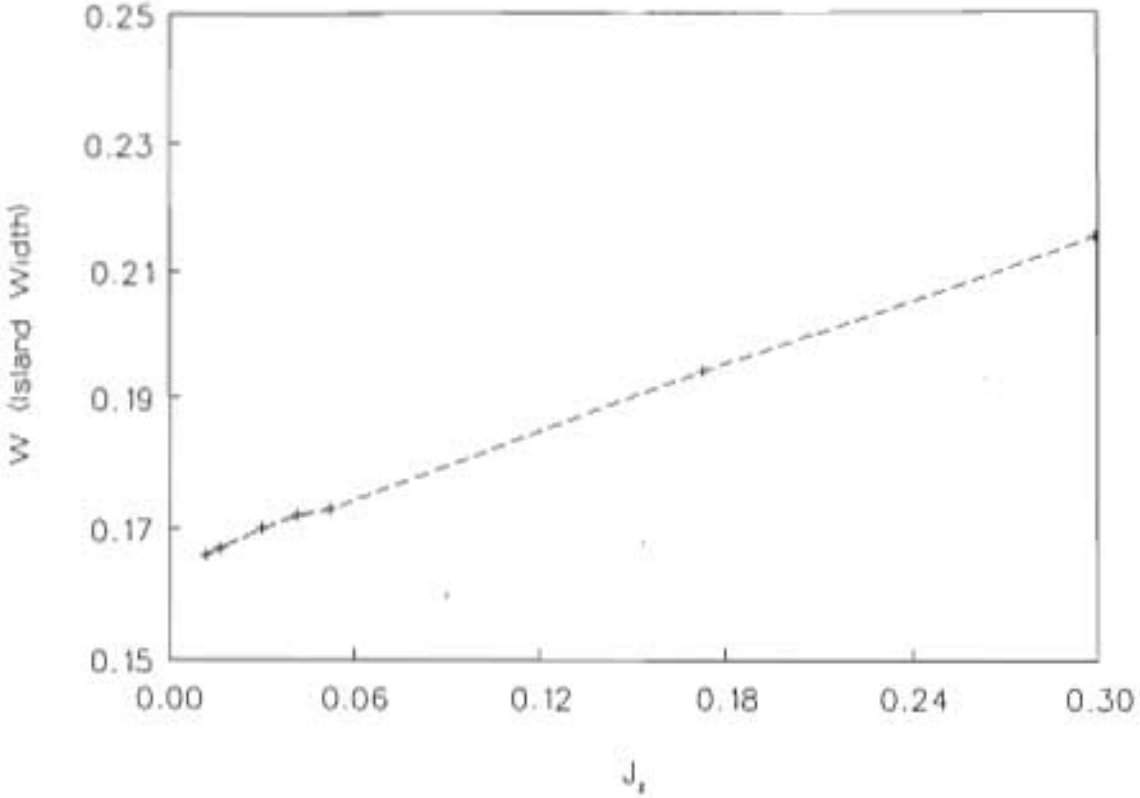

FIGURE 8.11 The width of the (2,1) island when $j_z^{(2,1)} \neq 0$, $j_z^{(3,1)} = 0$. The width of the (3,1) island stays unchanged at 0.036.

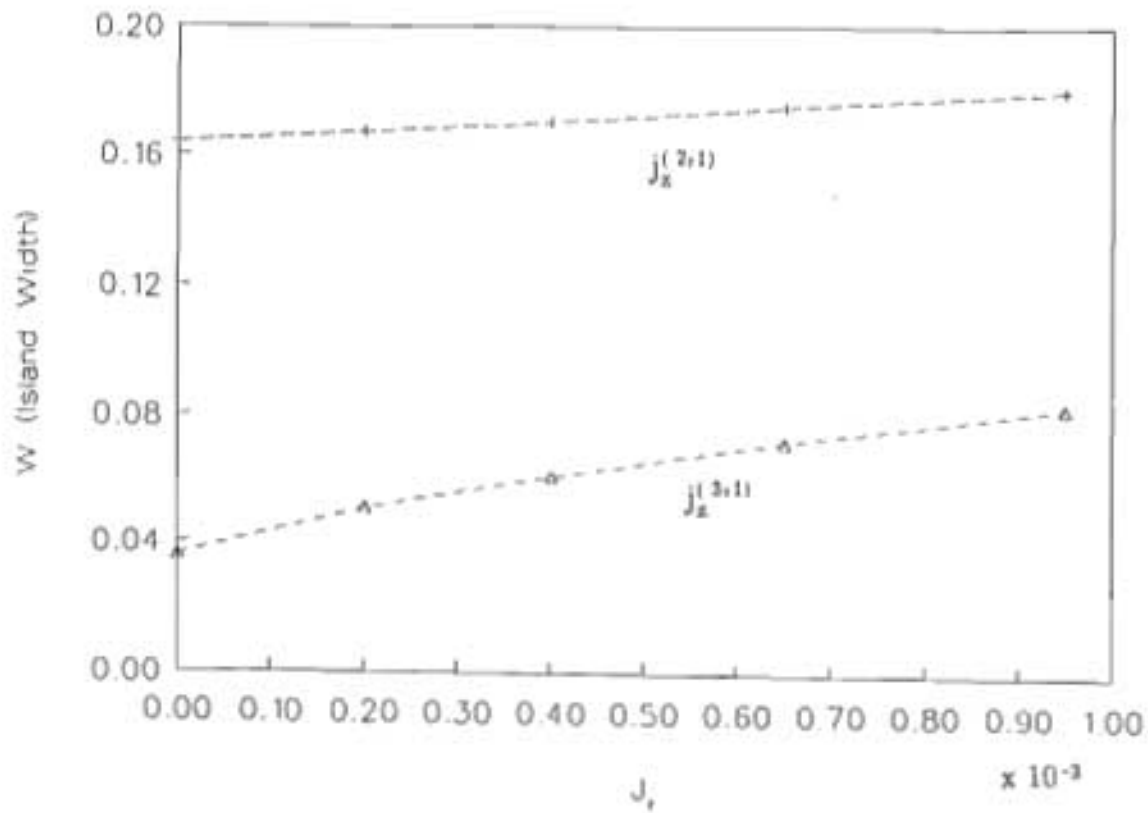

FIGURE 8.12 The island widths when $j_z^{(2,1)} = j_z^{(3,1)}$.

Important conclusions can be drawn from these graphs:

- The island size does not change if the boundary condition for that mode is not changed. When $\left.\frac{a_1}{a_1}\right|_1$ is kept at –0.5 (i.e. locked but no external coil current), but $\left.\frac{a_2}{a_2}\right|_1$ is increased consistently with increasing I_3 (Figure 8.10), the (2,1) island stays unchanged on 0.164 but the (3,1) island is increased. On the other hand, when $\left.\frac{a_2}{a_2}\right|_1$ is kept at –0.33 (i.e. locked but no external current density of similar helicity), but $\left.\frac{a_1}{a_1}\right|_1$ is increased consistently with increasing $j_z^{(2,1)}$ (Figure 8.11), the (3,1) island stays unchanged on 0.036 but the (2,1) island is increased in size. This may have implications for experimental mode suppression.

- The effect of a similar current density is much larger on the (3,1) island than on the (2,1) island. The (2,1) island width increased by 10 % and the (3,1) island width by 131 % for $j_z^{(2,1)} = j_z^{(3,1)} = 0.1 \times 10^{-3}$. From this we observe that the (3,1) island is much more sensitive to the boundary conditions than the (2,1) island. The reason for this is probably due to the proximity of the (3,1) island to the surface.

8.6 External Coils with Rotation

We will now consider the case where an external coil is included with a rotating plasma. Only "in–phase" cases are considered. The parameters are $r_w = 1.1$, $r_c = 1.3$, $q_0 = 1.0$, $q_1 = 4.5$, $b = 3.5$, $f = 2.0$.

In Figure 8.13 we present the case when $j_z^{(2,1)} = j_z^{(3,1)} = 0.1 \times 10^{-3}$ and in Figure 8.14 when $j_z^{(2,1)} = 0$ and $j_z^{(3,1)} = 0.1 \times 10^{-3}$. As before we note that the (3,1) island is much more sensitive to the boundary conditions than the (2,1) mode.

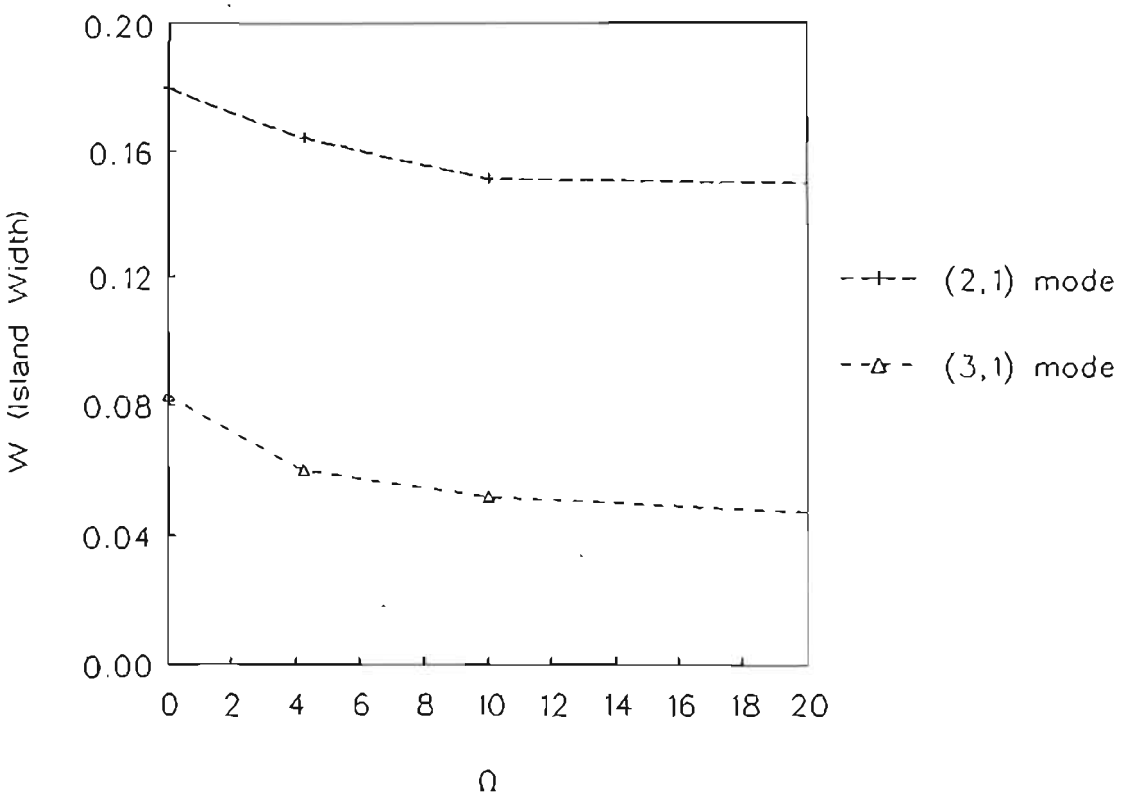

FIGURE 8.13 The variation of island size (W) with rotational frequency (Ω) for both modes present and $j_z^{(2,1)} = j_z^{(3,1)} = 0.1 \times 10^{-3}$

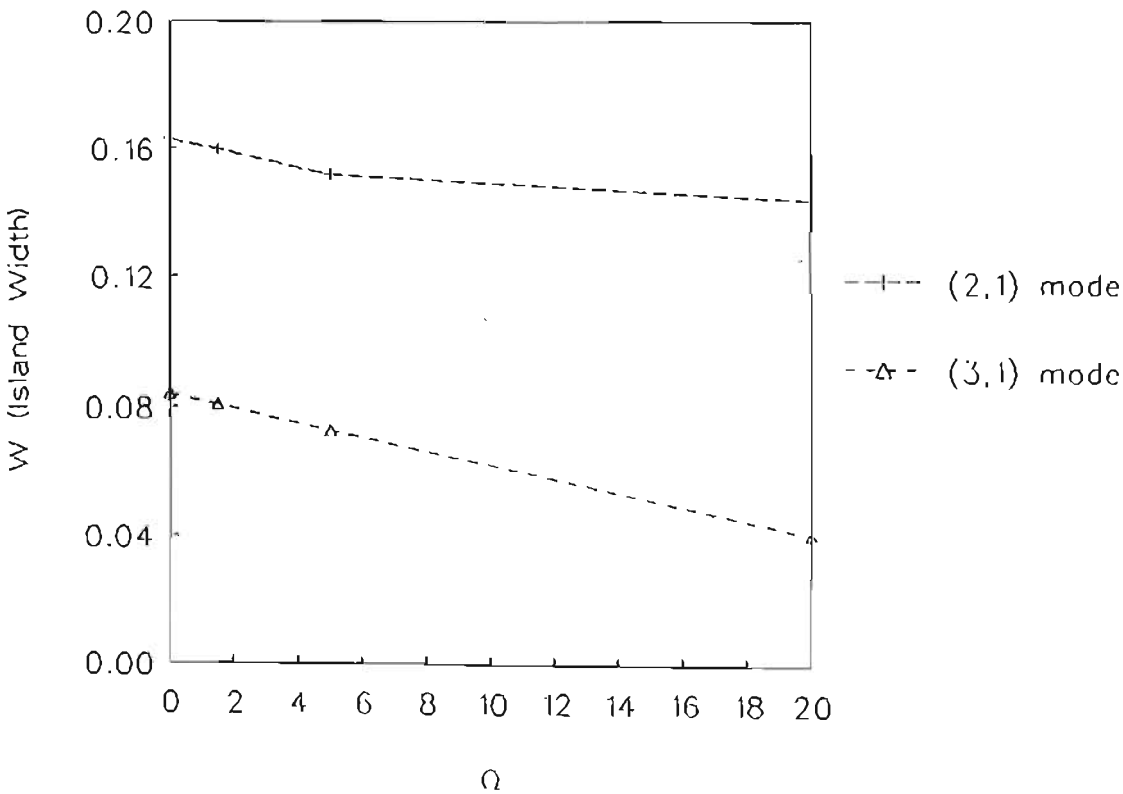

FIGURE 8.14 Island size variation with frequency for both the (2,1) and (3,1) modes when $j_z^{(2,1)} = 0$ and $j_z^{(3,1)} = 0.1 \times 10^{-3}$

As before the modes are considered to be coupled and rotating at the same frequency.

8.7 The Effect of the Aspect Ratio

On Tokoloshe we do not have an inverse aspect ratio of $\epsilon = 0.1$ as was used in the calculations up to now, but of ~ 0.5. It is thus important to examine the effect of ϵ.

In the following graph we show the effect of inverse aspect ratio on island size. As ϵ increases, the ratio of the (3,1) island size to the (2,1) island size increases. This means that the toroidal sideband increases in size when ϵ is increased. This could be due to the proximity of the (3,1) island to the plasma edge. Note that the (2,1) mode is not affected significantly by the change in ϵ.

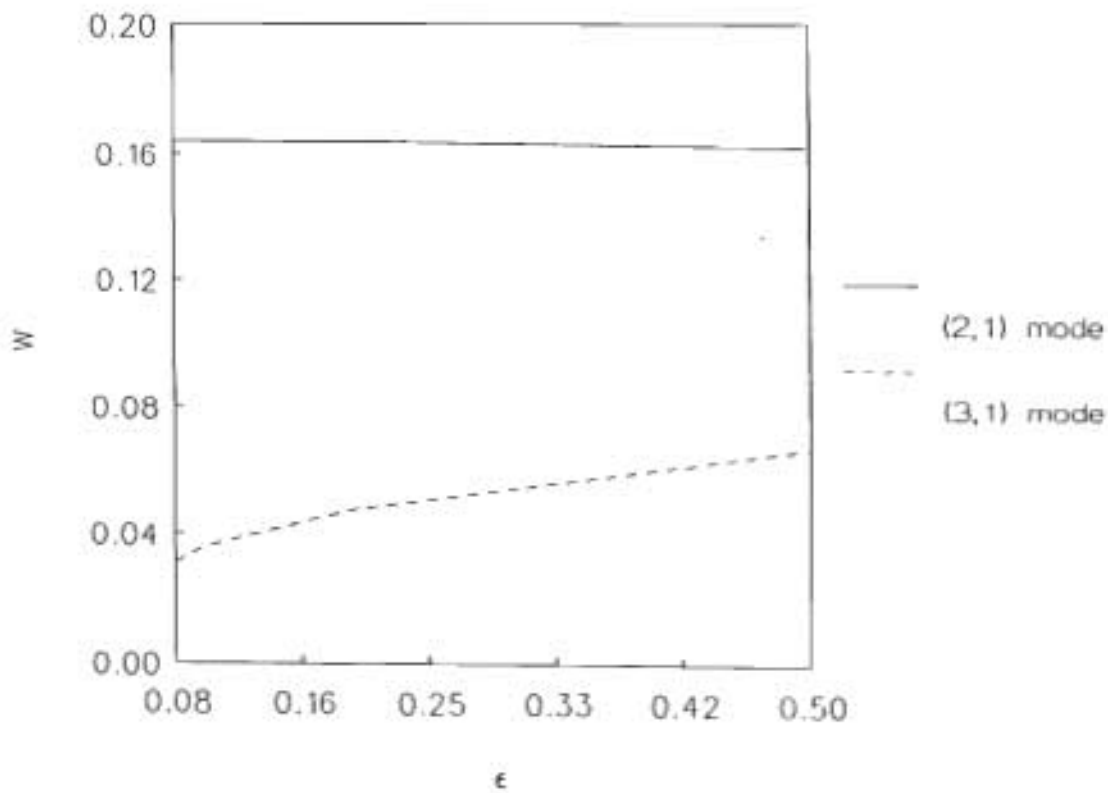

FIGURE 8.15 The effect of inverse aspect ratio (ϵ) on mode coupling. The equilibrium parameters were $q_1 = 4.5$, $q_0 = 1.0$, $b = 3.5$, $f = 2.0$.

8.8 Equilibrium Effects

The effect of equilibrium changes can also be looked into. In Figure 8.16 we show how the island width of the (2,1) and (3,1) islands changes with profile. The (2,1) island varies in exactly the same way as in the cylindrical case (see Figure 6.32). The (3,1) island width is the largest for a profile with $q_1 = 4.5$, $q_0 = 1.3$, b = 2.46, f = 2.0 and profiles with $q_0 = 1.0$ and $q_0 = 1.5$ having smaller sideband islands. We are not sure why the pronounced maximum for the (3,1) island width occurs. This may be due to the effects of the chosen profile.

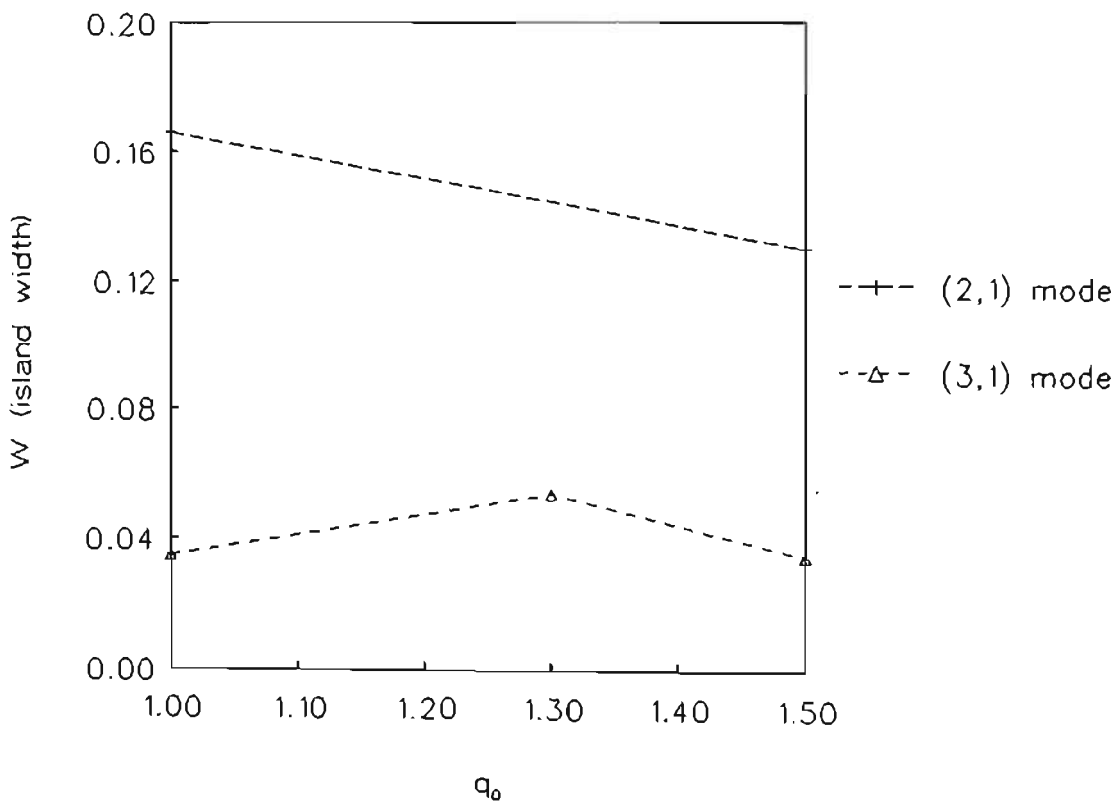

FIGURE 8.16 Island width variation with equilibrium parameter q_0. The other parameters are $q_1 = 4.5$ and f = 2.0. The value of b can be calculated from equation (6.7).

8.9 Other Effects

8.9.1 Boundary perturbation

We found that the (3,1) island perturbs the boundary much more than the (2,1) island. This is shown in Figure 8.17. A boundary perturbation of $\delta_i = 0.19 \times 10^{-2}$ corresponds to a (3,1) island width of 0.08 and a (2,1) island width of 0.16. This may also be the reason why the (3,1) island is much more sensitive to the boundary conditions than the (2,1) island as was discussed earlier.

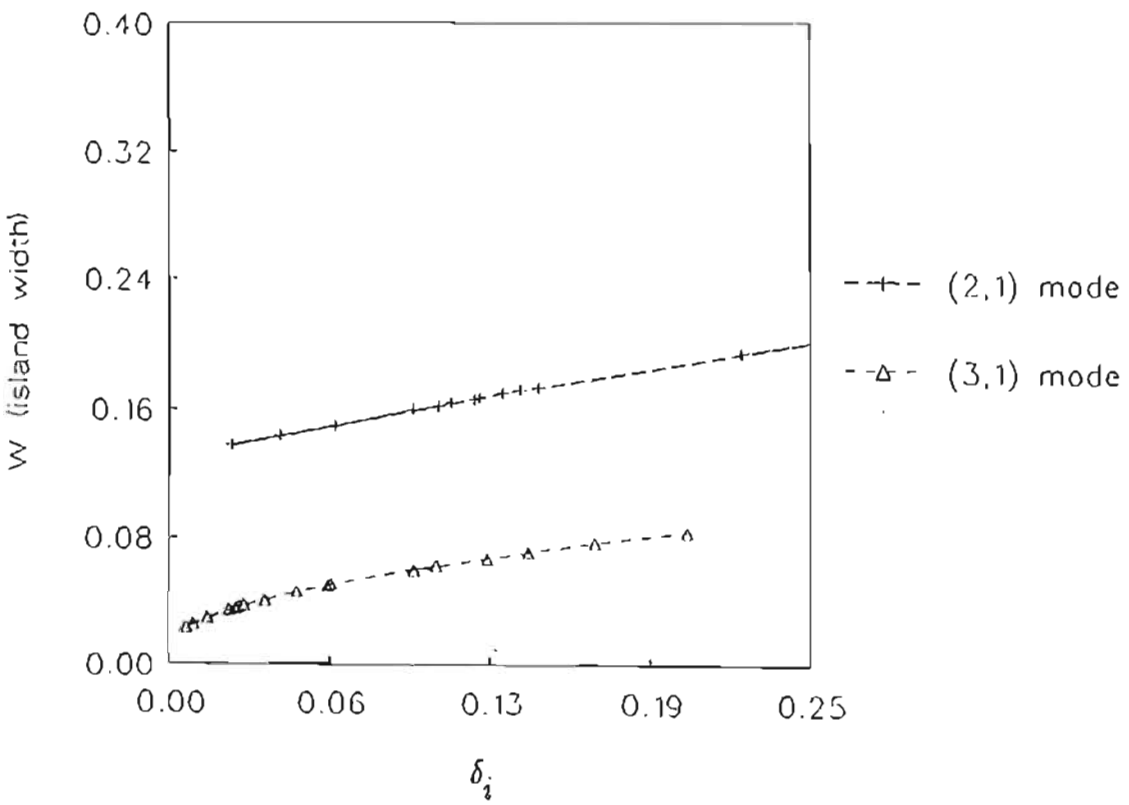

FIGURE 8.17 The (2,1) and (3,1) island widths are related to the boundary perturbation δ_i, $i = 1,2$.

8.9.2 "Coupling" of islands through the background current density profile

When the unperturbed equilibrium profile is flattened locally at the rational surfaces, the surrounding regions are also affected. This happens because the current density on the inside of the rational surface is redistributed to the region just on the outside of the inner rational surface. Such a change in the form of the profile can affect the nearby islands, increasing or decreasing the steepness of the profile at those islands. Although other authors found this effect to be significant [67], we found it to be small. The main reason why these effects are small in our model is that the islands are not positioned close to each other in the plasma. This coupling would also be present in a two–mode cylindrical model.

8.9.3 Toroidal effects in the helical flux

As was discussed earlier, we used a simplified form for the helical flux expression to enhance iteration of the model at the end of section 7.3. Instead of using the toroidal helical flux expressions, we used the cylindrical ones. The effect of this toroidal modification is to move the islands to the outside (when coupled in–phase i.e. $\chi_1 = 0$) or to move them to the inside (when coupled out of phase i.e. $\chi_1 = \pi$). This will clearly have an effect on the island size. For an equilibrium profile with parameters $q_1 = 4.5$, $q_0 = 1.0$, $b = 3.5$, $f = 2.0$, we found that the locked (2,1) mode was reduced from 0.164 (cylindrical flux function) to 0.142 (toroidal flux function). This is a reduction of 13 %. Other authors also found a reduction in island size [4,67].

8.10 The relation of a natural tearing mode to a toroidally induced one

The profile that was used up to now ($q_1 = 4.5$, $q_0 = 1.0$, $b = 3.5$, $f = 2.0$) does not have a natural (3,1) island present. The (3,1) island was included in the plasma as

a pure toroidal sideband of the (2,1) island. It is thus clear that a (3,1) island of nearly the same size as the (2,1) island (for certain values of ϵ and equilibria) can be introduced into the plasma when toroidicity is included, even if no natural (3,1) tearing mode exists. This effect of a (3,1) tearing stable profile having a (3,1) toroidally induced mode present, was also found by Bateman and Morris [67].

To study the relation between a natural tearing island (i.e. an island which exists when no toroidal coupling is allowed for) and a sideband island, we proceeded as follows: We took two equilibria with very similar parameters (profile 1 – $q_1 = 3.99$, $q_0 = 1.43$, b = 1.4, f = 1.6 and Profile 2 – $q_1 = 4.11$, $q_0 = 1.33$, b = 1.4, f = 1.4), the first being tearing mode unstable and the other tearing mode stable. The island sizes of the natural and the sideband islands of the tearing unstable profile and the island size of the sideband in the tearing stable equilibrium were then compared. This is tabled in Table 8.2 and shown graphically in Figure 8.18. The profile we have used up to now is also included in Table 8.2. The – means island size is zero, "tor" means the (3,1) island is a toroidally coupled sideband and "nat" means that a natural (3,1) island exists in the case of no toroidal coupling.

An interesting result from Figure 8.18 is that the island sizes of the natural and sideband islands are the same for $W \gtrsim 0.05$. It is probable that the sideband island takes the value of the natural island when the latter is larger.

$J_\varphi = g_0(1-r^f)^b$	Superconducting Wall			Locked			$j_z^{(2,1)} = 0$ $j_z^{(3,1)} = 0.1 \times 10^{-4}$			$j_z^{(2,1)} = 0$ $j_z^{(3,1)} = 0.5 \times 10^{-4}$		
	(2,1)	tor (3,1)	nat (3,1)	(2,1)	tor (3,1)	nat (3,1)	(2,1)	tor (3,1)	nat (3,1)	(2,1)	tor (3,1)	nat (3,1)
$g_0 = 0.14$ $f = 1.6$ $b = 1.4$ $q_1 = 3.99$	0.121	0.021	---	0.130	0.042	0.015	0.130	0.052	0.054	0.130	0.08	0.082
$g_0 = 0.15$ $f = 1.4$ $b = 1.4$ $q_1 = 4.11$	0.121	0.018	---	0.125	0.023	---	0.125	0.047	---	0.125	0.075	---
$g_0 = 0.2$ $f = 2.0$ $b = 3.5$ $q_1 = 4.5$	0.138	0.023	---	0.164	0.036	---	0.164	0.046	---	0.164	0.066	---

Table 8.2

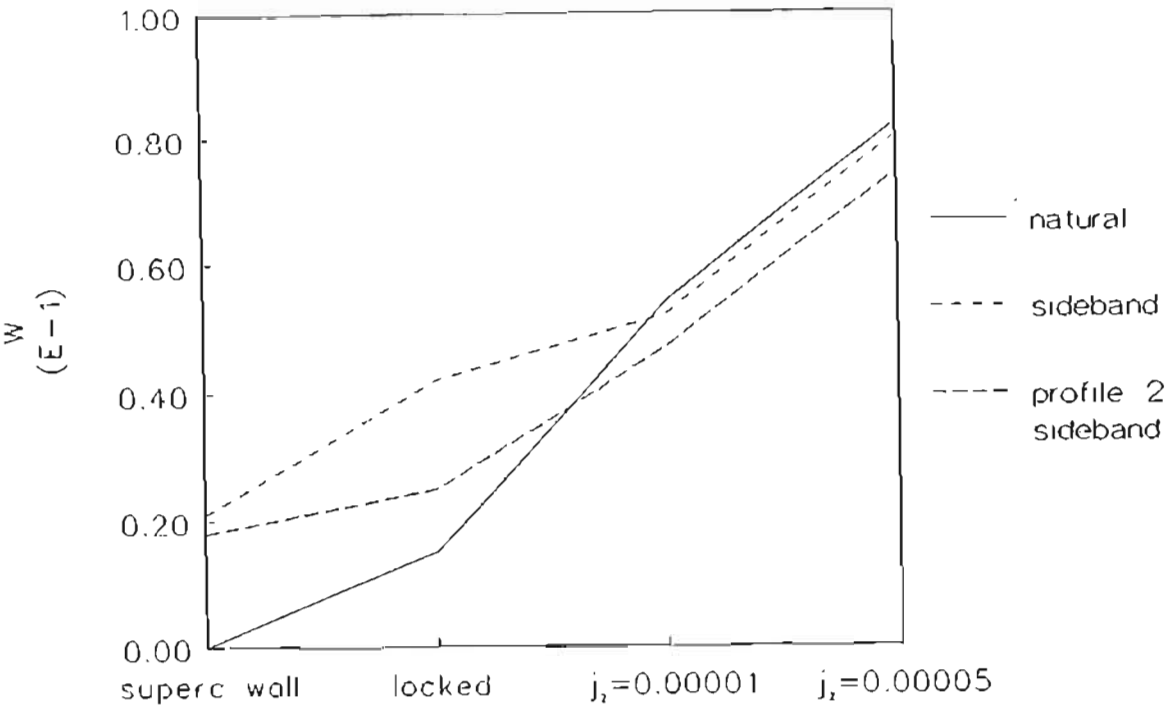

FIGURE 8.18 The island width of natural and toroidal sideband islands for profile 1 and of toroidal sideband islands for profile 2. These are compared for a super conducting wall situation, a locked one, and locked with $j_z^{(3,1)} = 0.1 \times 10^{-4}$ and 0.5×10^{-4}.

On Tokoloshe we observed a situation where the (3,1) island is comparable in size with the (2,1) island before the minor disruption. Thereafter it is much smaller. We can tentatively conclude that this can be because of profile changes at the edge. It is possible that a large natural (3,1) island exists before the minor disruption, and that we only observe the toroidal sideband afterwards. It is also possible that both before and after the minor disruption the (3,1) island is due to toroidal coupling. In such a case the profile change can be the reason for the island size changes. We, however, did not find pure toroidal sideband islands of that size for the profiles used.

8.11 Conclusions

We modelled a situation of two toroidally coupled modes in a Tokamak. The effect of external situations on these modes is of particular interest as it is the first time that such a study had been undertaken.

The main findings of this model for the specific current density profiles studied, include:

- Toroidal sidebands can be introduced although no natural island is present. This was also found by Bateman and Morris [67].

- Island sizes are not affected if the boundary conditions are not changed. If a current density of a particular helicity is applied at the coil position, it will only affect that particular mode of the same helicity.

- The (3,1) island is much more sensitive to the boundary conditions.

- When a large natural island is present, the toroidal sideband island will be of the same size. Toroidicity will not increase the size of such an island.

- Large inverse aspect ratios can give rize to large sideband islands.

CHAPTER 9

CONCLUSIONS

9.1 General Conclusions

In this thesis cylindrical and toroidal models were developed to study the behaviour of saturated tearing mode behaviour on Tokamaks. Some of the interesting features of the cylindrical model that appear to be new include:

- A graph of $^{a_1}/_{a_1'}\,(^{B_r}/_{B_{\theta 1}})\Big|_1$ against w giving all possible boundary conditions the plasma can be coupled to. The island width as well as boundary perturbation can be calculated on every point on this graph using some $\Delta'(W)$ criterion.

- The values of both $B_r\Big|_1$ and $B_{\theta 1}\Big|_1$ can be calculated for any boundary condition.

- The relation of $B_{\theta 1}\Big|_1$ to toroidal rotational frequency with external coils resembles that of Tokoloshe for a natural shot. From this it follows that error fields play a role on Tokoloshe even if the external coils are switched off.

- Broad flat profiles have very large islands in the presence of small external coil currents.

- A simple model of angular momentum conservation, which couples profile type to rotational frequency, describes the Tokoloshe situation quite accurately.

- A comparison of the Δ' criteria of Rutherford and Reiman. Although the Rutherford criterion is only applicable when the boundary is circular, it agrees very well with the Reiman criterion (which is valid for perturbed boundaries) in the case of perturbed boundaries. The criteria do differ for circular boundaries because of the difference in their formulation and because the White et al. [3] α–terms do not appear in the Reiman criterion.

The toroidal model enabled us to include two toroidally coupled modes in the plasma. The effect of external coils as well as plasma rotation on toroidally coupled modes appears to be new. We also looked at the relation between a natural (3,1) tearing mode and a toroidally induced one which is of particular interest for Tokoloshe. The effect of aspect ratio on the findings was also investigated.

Some of the findings are:

- Large inverse aspect ratios can give rize to large sideband islands.

- The toroidally coupled (3,1) mode grows much faster than the (2,1) mode with the same current density applied at the boundary. Both modes reduce when the rotational frequency is increased (assuming rigid body rotation, i.e. modes rotating at the same frequency). However, the (3,1) mode reduces much more as a percentage of original width. This will probably also be true for two uncoupled cylindrical modes.

- None of the island widths change if the boundary condition of that mode is not changed. This can easily be observed in the case when a current density of only one mode number (i.e. (2,1) or (3,1)) is applied to the boundary. In that case only the one island grows, but the other remains unchanged.

- The problem that Bateman and Morris [67] mention with regard to the determination of the island width (as was discussed in the introduction to chapter 7) is overcome by using the boundary conditions as is described in section 8.3.

- The (3,1) island is toroidally induced in many profiles studied. When the aspect ratio is changed, the (2,1) island remains unchanged, but the (3,1) increases with aspect ratio.

- When the natural tearing island is small, the toroidally induced one can be much larger. However, when the natural tearing island is large, the toroidally induced one is of the same size. This is contrary to a possible expectation that the effect of both the natural instability and the coupling would give an even larger island.

9.2 Shortcomings of the Models

The models have certain shortcomings which include:

- The effect of the axisymmetric current density perturbations used in the model can influence the results. The inclusion of two possible models for δJ in the cylindrical case was an effort to determine the effect of this variable (δJ). The fact that no significant difference was found in the results is not particularly revealing because of the similarities of the models. However, it can be argued that the eigenvalue will force any axisymmetric perturbation to flatten the unperturbed profile to the same extent, and that this can be the reason for the agreement between the two models used.

- The fact that only terms of $0(\epsilon)$ were included in the expansion for $J(\hat{\psi})$ has as side effect the result that the current density is not single valued inside the island. The error of $0(\epsilon^2)$ in $B.\nabla J = 0$ can be observed in Figure 6.28. An iteration scheme can possibly be used to eliminate this problem as was discussed at the end of section 6.5.4.

- The rotational frequency (with external coils) was not included in a fully satisfactory way since we actually modelled a set of coils rotating with the plasma, which is not the situation on Tokoloshe. Assuming that the islands will be saturated all the time during the rotation, allows the model to be applied to Tokoloshe. In the cylindrical case we considered both in–phase and out–of–phase situations, and in the toroidal case only in–phase situations. For low frequencies the model also breaks down.

- In the toroidal model we used the cylindrical helical magnetic flux expressions assuming small differences. This had as an effect that the (2,1) island sizes were not affected which is not fully true as was discussed. This simplification, however, enables us to get easier iteration for the system of equations.

- In this model we did not allow for overlapping of islands because of the restriction that the (3,1) mode be small (section 7.8). This is consistent with the theoretical modelling where non–linear mode coupling has been ignored (section 3.9).

9.3 Recommendations for Future Work

As it was not possible to consider all interesting situations in this thesis, the following cases seem to be of interest in case of future work:

- The consideration of AC coil currents in conjunction with toroidally coupled modes.

- More complete investigation of the case where the tearing mode is out of phase with the external coil current direction.

- The effect of profile changes with toroidally coupled modes in the case of rotation or external coils.

- The inclusion of more modes, including secondary modes, in the toroidal model, and coupling it to the various boundary conditions.

- The analytic model of section 6.4.2 provides a relatively direct way of obtaining analytic estimates for stability and should be persued in the future.

REFERENCES

1. H.P. Furth, J. Killeen, M.N. Rosenbluth, *Phys. Fluids 6*, 459 (1963).

2. P.H. Rutherford, *Phys. Fluids 16*, 1903 (1973).

3. R.B. White, D.A. Monticello, M.N. Rosenbluth, B.V. Waddell, *Phys. Fluids* 20(5), 800 (1977).

4. R. Izzo, D.A. Monticello, W. Park, J. Manickam, H.R. Strauss, R. Grimm and K. McGuire, *Phys. Fluids 26(8)2240* (1983).

5. A. Sykes and J.A. Wesson, *in Plasma Physics and Controlled Nuclear Fusion Research 1980*, Vol 1, p237, IAEA, Vienna (1981).

6. I.B. Bernstein, E.A. Friedman, M.D. Kruskal and R.M. Kulsrud, *Proc. Roy. Soc.* A244,17 (1958).

7. W.A. Newcomb, *Ann. of Phys.* 10, 232–267 (1969).

8. B .R. Suydam, *TID–7558* (*Papers presented at the Controlled Thermonuclear Conference* held at Washington, D.C., Feb. 3–5, 1958).

9. G. Bateman, *MHD Instabilities*, MIT Press, Cambridge, England, 1978.

10. G. Bateman, R.N. Morris, DOE/ET/5205/15, Department of Energy of the USA, 1980. (Later published in Ref. 67).

11. R.B. White, *Handbook of Plasma Physics*, Eds. M.N. Rosenbluth and R.Z. Sagdeev, North–Holland Publishing Company (1983).

12. P.A. Sweet, *Nuovo Cim. Suppl.* 8, Ser. X, 188 (1958).

13. E.N. Parker, *Astrophys. J. Suppl.* Sr. 77(8)177 (1963).

14. H.E. Petschek, *AAS–NASA Symp. on Phys. Solar Flares.* SP–50, Ed. W.N. Hess (1964).

15. W. Park, D.A. Monticello, R.B. White, *Phys. Fluids 27*, 119 (1984).

16. T.S. Hahm, R.M. Kulsrud, *Phys. Fluids 28(8)* 2412 (1985).

17. J.W. Dungey, *Cosmic Electrodynamics*, Cambridge University Press, New York. p98–102, 1958.

18. G.S. Murty, *Arkiv Fysik 19*, 499 (1961).

19. K. Aitken, R. Bickerton, S. Cockroft, J. Jukes, P. Reynolds, *Bull. Am. Phys. Soc. 6*, 204 (1961).

20. B.B. Kadomtsev, A.V. Nedospasov, *J. Nuclear Energy*, Part C, 1, 230 (1960).

21. W.M. Manheimer, C.N. Lashmore–Davies, *MHD and Microinstabilities in Confined Plasmas*, Adam Hilger, NY, 1989.

22. B. Coppi, J.M. Greene, J.L. Johnson, *Nuclear Fusion*, 6, 101 (1966).

23. H.P. Furth, *Nucl. Fusion Supp.* Pt 1, 169 (1961).

24. B. Coppi, *Phys. Fluids 8*, 2273 (1965).

25. G. van Hoven, M.A. Cross, *Phys. Rev. Letters*, 30, 642 (1973).

26. B. Coppi, *Phys. Fluids 7*, 1501 (1964).

27. R.D. Hazeltine, D. Dobrott, T.S. Wang, *Phys. Fluids 16*, 1778 (1975).

28. J.F. Drake, Y.C. Lee, *Phys. Fluids 20*, (8) 1341 (1977).

29. H.P. Furth, P.H. Rutherford, H. Selberg, *Phys. Fluids*, 16(7), 1054 (1973).

30. D.C. Robinson, J.A. Dibiase, A.S. Furzer, J. Killeen, J.E. Nunn Price, *The growth of resistive instabilities in a diffuse pinch*, Culham pre–print CLM–P710, United Kingdom Atomic Energy Authority (UKAEA), 1983.

31. J.J. Ellis, *The Control of Resistive Instabilities in Pinches*, Oxford, 1985.

32. R.B. White, *Rev. Mod. Phys.*, 58(1), 183 (1986).

33. J.D. Callen, B.C. Waddell, B. Carreras, M. Azumi, P.J. Catto, H.R. Hicks, J.A. Holmes, D.K. Lee, S.J. Lynch, J. Smith, M. Soler, K.T. Tsang, J.C. Whitson, *in Plasma Physics and Controlled Nuclear Fusion Research, Innsbruck 1978*, Vol 1, p415–431, IAEA, Vienna (1979).

34. V.A. Kutvitshii, E.I. Yurchenko, *Sov. J. Plasma Phys.* 12(7), 449 (1986).

35. A.H. Glasser, J.M. Greene, J.L. Johnson, *Phys. Fluids 19*, 567 (1976).

36. M. Kotshenreuther, R.D. Hazeltine, P.J. Morrison, *Phys. Fluids* 28 (1), 294 (1985).

37. A.S. Furzer, D.C. Robinson, *in Controlled Fusion and Plasma Physics*, Proc. 7th Eur. Conf. Lausanne, 1, 113 (1975).

38. D. Dobrott, S.C. Prager, J.B. Taylor, *Phys. Fluids 20*, 1850 (1977).

39. J.A. Dibiase, *Numerical Studies of Resistive Instabilities in Diffuse Pinches*, Rep. UCRL–51591, Lawrence Livermore Laboratory, University of California, 1974. (Later published in Ref. 78).

40. X.L. Chen, P.J. Morrison, *Phys. Fluids B2(3)*, 495 (1990).

41. D.A. Monticello, R.B. White, M.N. Rosenbluth, *in Plasma Physics and Controlled Nuclear Fusion Research 1978: Proceedings of the 7th International Conference, Innsbruck* (IAEA, Vienna), Vol 1, 605 (1979).

42. D.A. Monticello, R.B. White, *Phys. Fluids 23*, 366 (1980).

43. H. Grad, H. Rubin, *Proceedings of the 2nd UN International Conference on the Peaceful Uses of Atomic Energy, Geneva 1958*, Vol 31, p190–197, UN (1958).

44. V.D. Shafranov, *Reviews of Plasma Physics*, 2, p103–151, Consultants Bureau, New York, 1966.

45. R. Lüst and A. Schlüter. *Axialsymmetrische magnetohydrodynamische Gleichgewichtskonfigurationen.* Zeitschrift für Naturforschung 12A,850 (1957).

46. B. Carreras, B.V. Waddell and H.R. Hicks, *Nuclear Fusion 19(11)1423* (1979).

47. D. Schnack, J. Killeen, *J. Comput. Phys. 35*, 110 (1980).

48. T.C. Hender, D.C. Robinson, *Comp. Phys. Commun. 24*, 413 (1981).

49. A. Aydemir, D.C. Barnes, *Proceedings of the US–Japan Theory Workshop on 3–D MHD Studies for Toroidal Devices*, ONRL, Oak Ridge, Tennessee, ONF–8110101, 187, 1981.

50. R. White, D. Monticello, M.N. Rosenbluth, H. Strauss, B.B. Kadomtsev, *in Plasma Physics and Controlled Nuclear Fusion Research*, Tokyo, IAEA, Vienna, CN–33/A13–3, 1975.

51. M.N. Rosenbluth, D.A. Monticello, H.R. Strauss, R.B. White, *Phys. Fluids 19(12)*, 1987 (1976).

52. H.R. Strauss, *Phys. Fluids 19(1)*, 134, (1976).

53. T.A. Holmes, B.A. Carreras, T.C. Hender, H.R. Hicks, V.E. Lynch, B.F. Masden, *Phys. Fluids 26(9)*, 2569 (1983).

54. B.B. Kadomtsev, O.P. Pogutse, *Sov. Phys. JETP*, 38(2) 283 (1974).

55. J.F. Drake, R.G Kleva, *Phys. Rev. Letters*, 53(15) 1465) (1984).

56. J.W. Eastwood, W. Arter, *Phys. Fluids 30(9)* 2774, (1987).

57. B.V. Waddell, B. Carreras, H.R. Hicks, J.A. Holmes, *Phys. Fluids 22(5)* 896 (1979).

58. R.G. Kleva, J.F. Drake, D.A. Boyd, *Phys. Fluids 29(2)* 475 (1986).

59. R.G. Kleva, J.F. Drake, A. Bondeson, *Phys. Fluids 27(4)* 769 (1984).

60. S. van Goeler, W. Stodiek, N. Sauthoff, *Phys. Rev. Lett. 33*, 1201 (1974).

61. B.B. Kadomtsev, *Fizika Plazmy 1*, 710 (1975).

62. B.V. Waddell, M.N. Rosenbluth, D.A. Monticello, R.B. White, *Nuclear Fusion 16(3)* 528 (1976).

63. G. Kurita, M. Azumi, T. Tsunematsu, T. Takeda, *Plasma Physics 25(10)* 1097 (1983).

64. H.R. Strauss, *Phys. Fluids 20(8)*, 1354 (1977).

65. J.K. Lee, *Plasma Physics and Controlled Fusion 30(4)* 415 (1988).

66. B. Carreras, B.V. Waddell, H.R. Hicks, S.J. Lynch, *Physical Review A 18(6)* 2732 (1978).

67. G. Bateman and R.N. Morris. *Phys. Fluids* 29(3)753, 1986.

68. J.W. Connor, S.C. Cowley, R.J. Hastie, T.C. Hender, A. Hood, T.J. Martin. *Phys. Fluids* 31(3)577, 1988.

69. L.E. Zakkarov, A.A. Subbotin, N.V. Chudin. K. Atanasiu. *in Plasma Physics and Controlled Nuclear Fusion Research, Washington 1990*, Vol 2, p117–119, IAEA (1991).

70. J.W. Connor, R.J. Hastie, J.B. Taylor, *Phys. Fluids* B3(7)1532, 1991.

71. C.G. Gimblett, *Nuclear Fusion, 26(5)617* (1986).

72. M. Persson and A. Bondeson, *Nuclear Fusion, Vol 29 (6) 989* (1989).

73. A. Bondeson, R.D. Parker, M. Hugon, P. Smeulders, *Nuclear Fusion 31(9)1695* (1991).

74. A. Bondeson and M. Persson, *Nuclear Fusion 28(10)1887* (1988).

75. A.H. Reiman, *Phys. Fluids B3(9)2617* (1991).

76. J.K. Lee, H. Ikezi, F.W. McClain, N. Ohyabu, *Nuclear Fusion 23(1)* 63 (1983).

77. F. Karger, *Private Communication.*

78. J.A. Dibiase, *Numerical Studies of Resistive Instabilities in Diffuse Pinches*, PhD thesis, University of California/Livermore, 1974.

79. B.M.S. Hansen, M.A. Hellberg, D. Sherwell, D.E. Roberts, W.S. McLoud, *International Conference on Plasma Physics, Innsbruck 1992*, Vol II, p1397 (1992).

80. H. Yamada, Z. Yoshida, *Journal of the Physical Society of Japan*, 56(7) 2241–2244 (1987).

81. F. Karger, W. Feneberg and J. Gernhardt, et al., in *Controlled Fusion and Plasma Physics* (Proc. 8th Eur. Conf. Prague), European Physical Society, Vol 1, 3 (1977).

82. S.C. McCool et. al., *Nuclear Fusion 29(4)* 547 (1989).

83. D.E. Roberts, D. Sherwell, J.D. Fletcher, G. Nothnagel, J.A.M. de Villiers, *Major disruptions induced by helical coils on the Tokoloshe Tokamak*, Nuclear Fusion 31(2)319 (1991).

84. D.E. Roberts, J.D. Fletcher, G. Nothnagel, D. Sherwell, J.A.M. de Villiers and W.S. McLoud, *Physical Review Letters 66(22)2875* (1991).

85. T.C. Hender, C.G. Gimblett and D.C. Robinson. *Proceedings of the 15th European Conference on Controlled Fusion and Plasma Heating, Dubrovnik, 1988*, Vol 12B, Part 1, p437–440, Europpean Physical Society (1988).

86. M.F.F. Nave and J.A. Wesson. *Controlled Fusion and Plasma Physics, 11D(III)1103* (1987).

87. N.N. Speranskii, *Sov. J. Plasma Phys. 15(9)* 646 (1989).

88. T.C. Hender, K.S. Riedel, K. Grassie, *Stabilization of the m=2 tearing mode with applied helical fields*, IPP 5/21, Max Planck Institut für Plasmaphysik, 1988.

89. A.H. Reiman, *Phys. Fluids 26(5)* 1338 (1983).

90. J.D. Neethling, *Lecture Notes on Theoretical Plasma Physics*, PER–157, Pretoria, 1988.

91. R.B. White, D.A. Monticello, M.N. Rosenbluth, *Physical Review Letters 39(25)1618* (1977).

92. E. Lazzaro and M.F.F. Nave, *Phys. Fluids 31(6)1623* (1988).

93. G.J.P. Goedbloed, D. Pfirsch, H. Tasso, *Nucl. Fusion 12,649* (1972).

94. D.E. Roberts, *Private Communication.*

95. K. Miyamoto, *Plasma Physics for Nuclear Fusion.* MIT Press, Cambridge, 1980.

APPENDIX A

Term A in equation (3.27) can be written as

$$R^2\hat{\varphi}.\nabla\wedge\rho\frac{dv}{dt} = R^2\rho\left[\frac{\partial}{\partial z}\frac{dV_R}{dt} - \frac{\partial}{\partial R}\frac{dV_z}{dt}\right]$$

$$= R^2\rho\left[\frac{\partial}{\partial z}\left(\frac{dV_R}{dt} + V.\nabla V_R\right) - \frac{\partial}{\partial R}\left[\frac{dV_z}{dt} + V.\nabla V_R\right]\right]$$

$$R^2\rho\left[\frac{\partial}{\partial z}\frac{\partial}{dt}\left[-R/R_0\frac{\partial U}{\partial z}\right] + \frac{\partial}{\partial z}\left[\left[-R/R_0\frac{\partial U}{\partial z}\right]\frac{\partial}{\partial R}\left[-R/R_0\frac{\partial U}{\partial z}\right]\right]\right.$$

$$\left. + \frac{\partial}{\partial z}\left[\left[R/R_0\frac{\partial U}{\partial R}\right]\frac{\partial}{\partial R}\left[-R/R_0\frac{\partial U}{\partial z}\right]\right]\right.$$

$$\left. - \frac{\partial}{\partial R}\frac{\partial}{\partial t}\left[R/R_0\frac{\partial U}{\partial R}\right] - \frac{\partial U}{\partial R}\left[\left[-R/R_0\frac{\partial U}{\partial z}\right]\frac{\partial U}{\partial R}\left[R/R_0\frac{\partial U}{\partial R}\right]\right]\right.$$

$$\left. - \frac{\partial}{\partial R}\left[\left[R/R_0\frac{\partial U}{\partial R}\right]\frac{\partial}{\partial z}\left[R/R_0\frac{\partial U}{\partial R}\right]\right]\right]$$

$$= R^2\rho\left[\left[-R/R_0\frac{\partial U}{\partial t}\frac{\partial^2 U}{\partial z^2} + \frac{\partial}{\partial z}\left[R/R_0\frac{\partial U}{\partial z}\left[1/R_0\frac{\partial U}{\partial z} + R/R_0\frac{\partial}{\partial R}\frac{\partial U}{\partial z}\right]\right]\right]\right.$$

$$\left. + \frac{\partial}{\partial z}\left[\left[-R^2/R_0^2\frac{\partial U}{\partial r}\frac{\partial^2 U}{\partial z^2}\right] - \frac{\partial}{\partial t}\left[1/R_0\frac{\partial U}{\partial R} + R/R_0\frac{\partial^2 U}{\partial z^2}\right]\right]\right.$$

$$\left. - \frac{\partial}{\partial R}\left[-R/R_0\frac{\partial U}{\partial z}\left[1/R_0\frac{\partial U}{\partial R} + R/R_0\frac{\partial^2 U}{\partial z^2}\right]\right]\right.$$

$$\left. - \frac{\partial}{\partial R}\left[R^2/R_0^2\frac{\partial U}{\partial R}\frac{\partial}{\partial z}\left[\frac{\partial U}{\partial R}\right]\right]\right]$$

$$= R^2\rho\left[-R/R_0\frac{\partial}{\partial t}\frac{\partial^2 U}{\partial z^2} + 2R/R_0^2\frac{\partial U}{\partial z}\frac{\partial^2 U}{\partial z^2} + R^2/R_0^2\frac{\partial^2 U}{\partial z^2}\frac{\partial}{\partial R}\left[\frac{\partial U}{\partial z}\right]\right.$$

$$\left. + R^2/R_0^2\frac{\partial U}{\partial z}\frac{\partial U}{\partial R}\left[\frac{\partial^2 U}{\partial z^2}\right] - R^2/R_0^2\frac{\partial}{\partial z}\left[\frac{\partial U}{\partial R}\right]\frac{\partial^2 U}{\partial z^2} - R^2/R_0^2\frac{\partial U}{\partial R}\frac{\partial}{\partial z}\left[\frac{\partial^2 U}{\partial z^2}\right]\right.$$

$$\left. - 1/R_0\frac{\partial}{\partial t}\frac{\partial U}{\partial R} - R/R_0\frac{\partial}{\partial t}\frac{\partial^2 U}{\partial R^2} + 1/R_0^2\frac{\partial U}{\partial z}\frac{\partial U}{\partial R}\right.$$

$$+ {}^{R}/R_0^2 \frac{\partial}{\partial R}\left[\frac{\partial U}{\partial z}\right]\frac{\partial U}{\partial R} + {}^{R}/R_0^2 \frac{\partial U}{\partial z}\frac{\partial^2 U}{\partial R^2} + {}^{2R}/R_0^2 \frac{\partial U}{\partial z}\frac{\partial^2 U}{\partial R^2}$$

$$+ {}^{R^2}/R_0^2 \frac{\partial^2 U}{\partial R^2}\frac{\partial}{\partial R}\left[\frac{\partial U}{\partial z}\right] + {}^{R^2}/R_0^2 \frac{\partial U}{\partial z}\frac{\partial}{\partial R}\left[\frac{\partial^2 U}{\partial R^2}\right]$$

$$- {}^{2R}/R_0^2 \frac{\partial U}{\partial R}\frac{\partial}{\partial z}\left[\frac{\partial U}{\partial R}\right] - {}^{R^2}/R_0^2 \frac{\partial^2 U}{\partial R^2}\frac{\partial}{\partial z}\left[\frac{\partial U}{\partial R}\right]$$

$$- {}^{R^2}/R_0^2 \frac{\partial U}{\partial R}\frac{\partial}{\partial z}\left[\frac{\partial^2 U}{\partial R^2}\right]\Big]$$

$$= -R^2\rho\Big[{}^{1}/R_0 \frac{\partial}{\partial t}\frac{\partial U}{\partial R} + {}^{R}/R_0 \frac{\partial}{\partial t}\frac{\partial^2 U}{\partial R^2} + {}^{R}/R_0 \frac{\partial}{\partial t}\frac{\partial^2 U}{\partial z^2}$$

$$+ {}^{R}/R_0^2 \frac{\partial U}{\partial R}\frac{\partial}{\partial z}\left[\frac{\partial U}{\partial R}\right] + {}^{R^2}/R_0^2 \frac{\partial U}{\partial R}\frac{\partial}{\partial z}\left[\frac{\partial^2 U}{\partial R^2}\right]$$

$$+ {}^{R^2}/R_0^2 \frac{\partial U}{\partial R}\frac{\partial}{\partial z}\left[\frac{\partial^2 U}{\partial R^2}\right] + {}^{1}/R_0^2 \frac{\partial U}{\partial z}\frac{\partial U}{\partial R} - {}^{R}/R_0^2 \frac{\partial U}{\partial z}\frac{\partial^2 U}{\partial R^2}$$

$$- {}^{R^2}/R_0^2 \frac{\partial U}{\partial z}\frac{\partial}{\partial R}\left[\frac{\partial^2 U}{\partial R^2}\right] - {}^{R^2}/R_0^2 \frac{\partial U}{\partial z}\frac{\partial}{\partial R}\left[\frac{\partial^2 U}{\partial R^2}\right]\Big]$$

$$+ R^2\rho\Big[{}^{2}/R_0^2 \frac{\partial U}{\partial z}\frac{\partial U}{\partial R} + {}^{R}/R_0^2 \frac{\partial U}{\partial z}\frac{\partial^2 U}{\partial R^2} + {}^{2R}/R_0^2 \frac{\partial U}{\partial z}\frac{\partial^2 U}{\partial z^2}$$

$$+ {}^{R}/R_0^2 \frac{\partial U}{\partial z}\frac{\partial^2 U}{\partial R^2}\Big]$$

$$= -\rho R^2\Big[\ {}^{R}/R_0\ {}^{D}/dt\ \nabla^2 U - 2\ {}^{R}/R_0^2 \frac{\partial U}{\partial z}\nabla^2 U\Big]$$

$$= -\rho R^2\Big[{}^{R}/R_0\Big]\Big[\frac{D}{dt}\nabla^2 U - 2\ {}^{R}/R_0 \frac{\partial U}{\partial z}\nabla^2 U\Big]$$

APPENDIX B

DERIVING AN ENERGY INTEGRAL IN THE TOROIDAL SYSTEM

In this section we derive the energy integral given by Izzo et al. [4] . We recall equation (3.32), i.e.,

$$\rho_0\left(\frac{D}{dt}\nabla^2 U - 2/R_0\,\frac{\partial U}{\partial z}\nabla^2 U\right) = \frac{2\nabla R \wedge \nabla P}{R_0}\cdot\hat{\varphi} + \underline{B}.\nabla\,\Delta^*\psi\,.$$

If this equation is multiplied with U, we get

$$U\rho_0\,\frac{\partial}{\partial t}\nabla^2 U + U\rho_0\,\underline{V}_\perp.\nabla(\nabla^2 U) - U\rho_0\,2/R_0\,\frac{\partial U}{\partial z}\nabla^2 U$$

$$= \quad 2U\,\frac{\nabla R \wedge \nabla P}{R_0}\cdot\hat{\varphi} + U\,\underline{B}.\nabla\Delta^*\psi\,. \qquad \text{(B.1)}$$

We know, from vector analysis, that

$$\begin{aligned}
&\underline{\nabla}.(U\Delta^*\psi\underline{B} - U\nabla^2 U\underline{V}) \\
&= \nabla(U\Delta^*\psi).\underline{B} + U\Delta^*\psi(\nabla.\underline{B}) - \nabla(U\nabla^2 U).\underline{V} - U\nabla^2 U(\nabla.\underline{V}) \\
&= \nabla(U\Delta^*\psi).\underline{B} - \nabla(U\nabla^2 U).\underline{V} \\
&= U\nabla\Delta^*\psi\underline{B} + \Delta^*\psi\nabla U.\underline{B} - U\nabla(\nabla^2 U).\underline{V} - \nabla^2 U(\nabla(\nabla U.\underline{V})\,. \qquad \text{(B.2)}
\end{aligned}$$

In the derivation of equation (B.2) we used the fact that

$$\begin{aligned}
U &\sim 0(\epsilon) \\
U\nabla^2 U(\nabla.\underline{V}) &\sim 0(\epsilon^3) \\
\nabla.\underline{B} &= 0\,.
\end{aligned}$$

But

$$\underline{B} = {}^{R_0}/_{R}\,\nabla\psi \wedge \hat{\varphi} + ({}^{I_0}/_{R} + {}^{\tilde{I}}/_{R})\hat{\varphi} .$$

Thus,

$$\nabla U.\underline{B} = {}^{R_0}/_{R}\,(\nabla\psi \wedge \hat{\varphi} + B_0\hat{\varphi}).\nabla U \quad , \quad {}^{\tilde{I}}/_{R} \sim O(\epsilon^2)$$

$$= {}^{R_0}/_{R}\,[(\nabla\psi \wedge \hat{\varphi}\nabla)U + \frac{1}{R} B_0 \frac{\partial U}{\partial \varphi}]$$

$$= ({}^{R_0}/_{R})^2 \frac{\partial \psi}{\partial t} + {}^{R_0}/_{R}\,\eta J_\varphi . \qquad \text{(B.3)}$$

(from equations (3.34) and (3.14))

This can be substituted into equation (B.2).

We now have

$$\nabla.(U\Delta^*\psi\underline{B} - U\nabla^2 U\underline{V})$$

$$= U\underline{B}.\nabla\Delta^*\psi + \Delta^*\psi({}^{R_0}/_{R})^2 \frac{\partial \psi}{\partial t} + \Delta^*\psi\,{}^{R_0}/_{R}\,\eta J_\varphi - U\nabla(\nabla^2 U).\underline{V} - \nabla^2 U(\nabla U.\underline{V}) . \qquad \text{(B.4)}$$

Neglecting higher order terms, we know that

$$\nabla^2 U(\nabla U.\underline{V}) \sim \nabla^2 U(\nabla U.\underline{V}_\perp) .$$

Substituting $\underline{V}_\perp = {}^{R}/_{R_0}\,\nabla U \wedge \hat{\varphi}$ in $\nabla U.\underline{V}_\perp$, we get

$$\nabla U.{}^{R}/_{R_0}\,\nabla U \wedge \hat{\varphi} = -\frac{\partial U}{\partial R}\,{}^{R}/_{R_0}\,\frac{\partial U}{\partial z} + \frac{\partial U}{\partial z}\,{}^{R}/_{R_0}\,\frac{\partial U}{\partial R} = 0 \quad ,$$

eliminating the last term in equation (B.4).

Equation (B.4) can now be substituted into equation (B.1). Using

$$U\,(2/R_0)\,\frac{\partial U}{\partial z}\,\nabla^2 U \sim 0(\epsilon^4)\,.$$

and

$$\rho_0 \sim 1\,,$$

we get

$$U\,\frac{\partial}{\partial t}\nabla^2 U + U\underline{V}_\perp.\nabla(\nabla^2 U) = 2U\,\frac{\nabla R \wedge \nabla P}{R_0}\,.\,\hat{\varphi} + \nabla.(U\Delta^*\psi\underline{B} - U\nabla^2 U\underline{V})$$

$$- \Delta^*\psi(R_0/R)^2\,\frac{\partial\psi}{\partial t} - \Delta^*\psi\,(R_0/R)\eta J_\varphi + U\underline{V}_\perp.\nabla(\nabla^2 U)\,. \qquad \text{(B.5)}$$

This immediately reduces to

$$U\,\frac{\partial}{\partial t}\nabla^2 U = \nabla.(U\Delta^*\psi\underline{B} - U\nabla^2 U\underline{V}) - \Delta^*\psi(R_0/R)^2\,\frac{\partial\psi}{\partial t}$$

$$+ 2U\,\frac{\nabla R \wedge \nabla P}{R_0}\,.\,\hat{\varphi} - \Delta^*\psi\,R_0/R\,\eta\,J_\varphi\,. \qquad \text{(B.6)}$$

To simplify this equation further we proceed as follows: Let

$$\frac{dP}{dt} = \frac{\partial P}{\partial t} + \underline{V}_\perp.\nabla P$$

$$= \frac{\partial P}{\partial t} + R/R_0\,\nabla U\wedge\hat{\varphi}.\nabla P \sim 0(\epsilon^4)\,.$$

This gives

$$\frac{\partial P}{\partial t} = -R/R_0 \, \nabla U \wedge \hat{\varphi}.\nabla P \, .$$

From vector analysis we get

$$\nabla \wedge \frac{UR^2}{R_0} \nabla P = \nabla\left(\frac{UR^2}{R_0}\right) \wedge \nabla P + \frac{UR^2}{R_0} (\nabla \wedge \nabla P)$$

$$= \left[\left(\frac{R^2 \nabla U}{R_0}\right) + 2R \frac{U \nabla R}{R_0}\right] \wedge \nabla P \, .$$

Taking the $\hat{\varphi}$-component, gives

$$\nabla\varphi.\nabla \wedge \frac{UR^2}{R_0} \nabla P = {}^{R}/_{R_0} \, \nabla U \wedge \nabla P.\hat{\varphi} + \frac{2U}{R_0} \nabla R \wedge \nabla P.\hat{\varphi}$$

$$= -{}^{R}/_{R_0} \, \nabla U \wedge \hat{\varphi}.\nabla P + \frac{2U}{R_0} \nabla R \wedge \nabla P.\hat{\varphi}$$

$$= \frac{\partial P}{\partial t} + \frac{2U}{R_0} \nabla R \wedge \nabla P.\hat{\varphi} \, . \qquad \text{(B.7)}$$

Now, using this in equation (B.6), we get

$$U \frac{\partial}{\partial t} \nabla^2 U = \nabla.(U\Delta^* \psi \underline{B} - U\nabla^2 U \underline{V}) - \Delta^* \psi \left({}^{R_0}/_{R}\right)^2 \frac{\partial \psi}{\partial t}$$

$$+ \nabla\varphi.\nabla \wedge \frac{UR^2}{R_0} \nabla P - \frac{\partial P}{\partial t} - \Delta^* \psi \, {}^{R_0}/_{R} \, \eta J_\varphi \, . \qquad \text{(B.8)}$$

We also know from $\underline{B}_\perp = {}^{R_0}/_{R} \, \nabla\psi \wedge \hat{\varphi} \sim 0(\epsilon)$

and from

$$\Delta^* \sim 0(\epsilon^0) \text{ and } \eta \sim 0(\epsilon) \text{ that } \eta(\Delta^*\psi)^2 \sim 0(\epsilon^3) .$$

The resulting equation is

$$U \frac{\partial}{\partial t} \nabla^2 U = \nabla.(U\Delta^*\psi \underline{B} - U\nabla^2 U \underline{V}) - \Delta^*\psi (R_0/R)^2 \frac{\partial \psi}{\partial t}$$

$$+ \nabla\varphi.\nabla \wedge \frac{UR^2}{R_0} \nabla P - \frac{\partial P}{\partial t} . \qquad \text{(B.9)}$$

Taking the integral of equation (B.9) gives

$$\int U \frac{\partial}{\partial t} \nabla^2 U \, d\gamma = \int \nabla.(U\Delta^*\psi \underline{B} - U\nabla^2 U \underline{V}) - \Delta^*\psi (R_0/R)^2 \frac{\partial \psi}{\partial t}$$

$$+ \nabla\varphi.\nabla \wedge \frac{UR^2}{R_0} \nabla P - \frac{\partial p}{\partial t}) \, d\gamma \qquad \text{(B.10)}$$

with $d\gamma \equiv dV_{\text{toroidal}}$.

We can now proceed to analyse each term in equation (B.10). Thus

$$\int \nabla.(U\Delta^*\psi \underline{B} - U\nabla^2 U \underline{V}) d\gamma = \int (U\Delta^*\psi \underline{B} - U\nabla^2 U \underline{V}) dS_{tor}$$

$$= 0 \text{ because } U(a) = 0 .$$

Now

$$\int (\nabla\varphi.\nabla \wedge \frac{UR^2}{R_0} \nabla P) d\gamma$$

$$= \int \frac{1}{R} (\nabla \wedge \frac{UR^2}{R_0} \nabla P)_\varphi \, d\gamma$$

$$= -\int \left(\frac{1}{R}\frac{UR^2}{R_0}\nabla P \wedge dA\right)_\varphi = 0 \text{ because } U(a) = 0 ,$$

using

$$\int (\nabla\wedge\underline{F})dV = -\int \underline{F}\wedge d\underline{A} .$$

The right hand side of equation (B.10) can also be simplified:

$$\int U \frac{\partial}{\partial t}\nabla^2 U \, d\gamma = \int U \nabla^2 \frac{\partial U}{\partial t} d\gamma$$

$$= \int U (\nabla \frac{\partial U}{\partial t}).d\underline{A} - \int \nabla \frac{\partial U}{\partial t}.\nabla U \, d\gamma$$

$$= -\int (\frac{\partial U}{\partial t}\nabla U).\nabla U \, d\gamma = -\tfrac{1}{2}\int \frac{\partial U}{\partial t}(\nabla U)^2 d\gamma ,$$

using

$$\int (\nabla\varphi).(\nabla\psi)dV = \int \varphi(\nabla\psi).d\underline{A} - \int \varphi\nabla^2\psi \, dV .$$

and $(\nabla U)^2 = \nabla U.\nabla U$.

We also have

$$\int \Delta^*\psi(R_0/R)^2 \frac{\partial\psi}{\partial t} d\gamma = \int \nabla.(R_0^2/R^2\,\nabla\psi)\frac{\partial\psi}{\partial t} d\gamma$$

$$= \int \frac{\partial\psi}{\partial t}(R_0^2/R^2\,\nabla\psi).d\underline{A} - \int \nabla\frac{\partial\psi}{\partial t}.(R_0^2/R^2\,\nabla\psi)\, d\gamma .$$

Finally,

$$\int \frac{\partial \psi}{\partial t} \left(R_0^2 / R^2 \nabla \psi\right) . d\underline{A} = 0 \quad \text{because} \quad \psi = \text{constant on the boundary.}$$

Thus

$$\int \Delta^* \psi \left(R_0/R\right)^2 \frac{\partial \psi}{\partial t} \, d\gamma = - \int \nabla \frac{\partial \psi}{\partial t} \left(R_0^2 / R^2 \nabla \psi\right) d\gamma$$

$$= - \tfrac{1}{4} \int \frac{\partial}{\partial t} \left(R_0 / R \nabla \psi\right)^2 d\gamma - \int (\nabla \psi)^2 R_0^2 \frac{\partial}{\partial t} \left(\frac{1}{R^2}\right) d\gamma$$

$$= - \tfrac{1}{4} \int \frac{\partial}{\partial t} R_0^2 / R^2 \left(\nabla \psi\right)^2 d\gamma$$

The final energy integral is

$$\frac{\partial}{\partial t} \int \tfrac{1}{4} \left[\left(R_0 / R \nabla \psi\right)^2 + \left(\nabla U\right)^2 - 2P \right] d\gamma = 0 . \qquad \text{(B.11)}$$

APPENDIX C

THE COEFFICIENTS FOR ψ AND U

We define ψ and U as follows:

$$\psi = \frac{1}{2}\sum_{mn}\left(a_{mn}e^{i(m\theta-n\varphi)} + a^{*}_{mn}e^{i(m\theta-n\varphi)}\right)$$

$$U = \frac{1}{2}\sum_{mn}\left(b_{mn}e^{i(m\theta-n\varphi)} + b^{*}_{mn}e^{i(m\theta-n\varphi)}\right).$$

Let

$$a_{mn} = \alpha_{mn} + i\beta_{mn}\,,\quad b_{mn} = \delta_{mn} + i\gamma_{mn}\,.$$

Thus

$$\psi = \sum_{mn}\left(\alpha_{mn}\cos\left(m\theta-n\varphi\right) - \beta_{mn}\sin\left(m\theta-n\varphi\right)\right)$$

$$U = \sum_{mn}\left(\delta_{mn}\cos\left(m\theta-n\varphi\right) - \gamma_{mn}\sin\left(m\theta-n\varphi\right)\right).$$

We know from the equations that

$$\psi(\theta,\varphi) = \psi(-\theta,-\varphi))$$

and

$$U(\theta,\varphi) \quad = \quad -U(-\theta,-\varphi) \, .$$

Now

$$\psi(\theta,\varphi) - \psi(-\theta,-\varphi) \quad = \quad \sum_{mn} (\alpha_{mn} \cos(m\theta - n\varphi) - \beta_{mn} \sin(m\theta - n\varphi))$$

$$- \alpha_{mn} \cos(m\theta - n\varphi) - \beta_{mn} \sin(m\theta - n\varphi)$$

$$= 2 \sum_{mn} -\beta_{mn} \sin(m\theta - n\varphi) \, .$$

This implies that $\beta_{mn} = 0$ for all m,n.

In the same way we can show that $\delta_{mn} = 0$ for all m,n.

From the symmetry it is clear that

$$\sum_{\substack{mn \\ -\infty}}^{\infty} \alpha_{mn} \cos(m\theta - n\varphi) \quad = \quad \sum_{\substack{mn \\ \infty}}^{-\infty} \alpha_{-m,-n} \cos(m\theta - n\varphi)$$

giving

$$\alpha_{mn} = \alpha_{-m,-n} \, .$$

In the same way we can get

$$\gamma_{mn} = -\gamma_{-m,-n} \, .$$

Now

$$\psi = \sum_{\substack{m \\ n \\ -\infty}}^{\infty} \alpha_{mn} \cos (m\theta - n\varphi)$$

and

$$U = \sum_{\substack{m \\ n \\ -\infty}}^{\infty} \gamma_{mn} \sin (m\theta - n\varphi) .$$

APPENDIX D

FOURIER ANALYZING THE REDUCED MHD EQUATIONS

When $\nabla^2 U$ and $\Delta^* \psi$ are substituted into equations (3.75) and (3.76), (using equations (3.74) and (3.69), it is possible to see from inspection that

$$U(\theta,\varphi) = -U(-\theta,-\varphi)$$
$$\psi(\theta,\varphi) = \psi(-\theta,-\varphi) .$$

We now choose

$$\psi = \sum_{mn} a_{mn} e^{i(m\theta - n\varphi)}$$

$$U = \sum_{mn} i\, b_{mn} e^{i(m\theta - n\varphi)}$$

where a Fourier expansion is done in θ and φ and the r–derivatives will be discretized later on.

Substituting this in equation (3.76) gives

$$\sum_{mnkl} \left(\frac{h}{r}\, im a_{mn}\, ib_{kl} - \frac{h}{r}\, a'_{mn}\, ikb_{kl}\right) e^{i[(m+k)\theta - (n+\ell)\varphi]}$$

$$+ \sum_{kl} \left(\epsilon(-i\ell) ib_{kl} + \eta \frac{1}{r}\, a'_{kl} + \eta\, a''_{kl} + (ik)^2 \frac{\eta}{r^2}\, a_{kl}\right.$$

$$\left. - \eta\epsilon/h \cos\theta\, a'_{kl} + \epsilon/h\, \frac{\eta}{r} \sin\theta (ik)\, a_{kl}\right) e^{i(k\theta - \ell\varphi)} = 0$$

or

$$\sum_{mnkl} \left(-\frac{h}{r} m a_{mn} b'_{kl} + \frac{h}{r} k\, a'_{mn}\, b_{kl}\right) \cos\left[(m+k)\theta - (n+\ell)\varphi\right]$$

$$+ \sum_{kl} \left(\epsilon \ell\, b_{kl} + {}^{\eta}/_{r}\, a'_{kl} + \eta a''_{kl} - {}^{k^2}/_{r^2}\, \eta\, a_{kl}\right.$$

$$\left. - {}^{\eta\epsilon}/_{h} \cos\theta\, a'_{kl}\right) \cos\left(k\theta - \ell\varphi\right)$$

$$+ \sum_{kl} \left(- {}^{\epsilon}/_{h}\, {}^{\eta}/_{r}\, k \sin\theta\, a_{kl}\right) \sin\left(k\theta - \ell\varphi\right) = 0 \ .$$

Let

$$A = -\frac{h}{r} m a_{mn} b'_{kl} + \left({}^{h}/_{r}\right) k a'_{mn}\, b_{kl}$$

$$B = \epsilon \ell\, b_{kl} + \left({}^{\eta}/_{r}\right) a'_{kl} + \eta a''_{kl} - \frac{k^2}{r^2}\, \eta a_{kl} - \eta\left({}^{\epsilon}/_{h}\right) \cos\theta\, a'_{kl}$$

$$C = - {}^{\epsilon}/_{h}\, \left({}^{\eta}/_{r}\right) k \sin\theta\, a_{kl}$$

to give

$$\sum_{mnkl} A \cos\left[(m+k)\theta - (n+\ell)\varphi\right]$$

$$+ \sum_{kl} \left[B \cos\left(k\theta - \ell\varphi\right) + C \sin\left(k\theta - \ell\varphi\right)\right] = 0 \ . \qquad \text{(D.1)}$$

If the same procedure is followed for equation (3.75), we get

$$\sum_{mnkl} \{A \cos [(m+k)\theta - (n+\ell)\varphi] + D \sin [(m+k)\theta - (n+\ell)\varphi]\}$$

$$+ \sum_{kl} \{B \cos (k\theta - \ell\varphi) + E \sin (k\theta - \ell\varphi)\} + C = 0 \qquad (D.2)$$

with

$$A = \frac{h}{r}\frac{\epsilon}{h} m \frac{k}{r^2} \sin\theta\, b_{mn}\, b_{kl} + \frac{\epsilon^2}{rh} mk \cos\theta \sin\theta\, b_{mn}\, b_{kl}$$

$$- \frac{\epsilon^2}{r^2} mk \sin\theta\, b_{mn}\, b'_{kl} - \frac{2\epsilon^3}{h^2} \ell^2 \sin\theta\, b'_{mn}\, b_{kl}$$

$$+ \frac{\epsilon^2}{h} \sin\theta \cos\theta\, b'_{mn}\, b'_{kl} - \frac{\epsilon}{r} \sin\theta\, b'_{mn}\, b'_{kl} + \frac{\epsilon}{r^2} k^2 \sin\theta\, b'_{mn}\, b_{kl}$$

$$+ \frac{2\epsilon}{r} \sin\theta\, b'_{mn}\, b'_{kl} + 2\epsilon \sin\theta\, b'_{mn}\, b''_{kl} - \frac{2\epsilon}{r^2} k^2 \sin\theta\, b'_{mn}\, b_{kl}$$

$$- \frac{2\epsilon}{h^2} \ell^2 \sin\theta\, b'_{mn}\, b_{kl} + \frac{2\epsilon^2}{h} \sin\theta \cos\theta\, b'_{mn}\, b'_{kl} + \frac{2\epsilon^2}{r^2 h} mk \cos\theta \sin\theta\, b_{mn}\, b_{kl}$$

$$+ \frac{\epsilon S^3}{h^2 r^2} mk \sin\theta\, a_{mn}\, a'_{kl} - \frac{\epsilon S^2}{h^2 r^3} mk \sin\theta\, a_{mn}\, a_{kl}$$

$$- \frac{\epsilon^2 S^2}{h^3 r^2} mk \cos\theta \sin\theta\, a_{mn}\, a_{kl} + \frac{\epsilon S^2}{h^2 r} \sin\theta\, a'_{mn}\, a'_{kl}$$

$$- \frac{\epsilon^2 S^2}{h^3} \sin\theta \cos\theta\, a'_{mn}\, a'_{kl} - \frac{\epsilon S^2}{h^2 r^2} k^2 \sin\theta\, a'_{mn}\, a_{kl}$$

$$B = - \frac{\epsilon^2 S^2}{h^3 r} \ell k \sin\theta\, a_{kl}$$

$$C = \epsilon S^2 \sin\theta \frac{\partial P}{\partial r} + \epsilon S^2 \frac{1}{r} \cos\theta \frac{\partial P}{\partial \theta}$$

$$D = \frac{h}{r^2} m\, b_{mn}\, b''_{kl} - \frac{h}{r^3} m\, b_{mn}\, b'_{kl} + \frac{h}{r} m\, b_{mn}\, b''_{kl} - \frac{h}{r^3} mk^2\, b_{mn}\, b'_{kl}$$

$$+ \frac{2h}{r^4} mk^2\, b_{mn}\, b_{kl} + \frac{2\epsilon^3}{h^3}\frac{h}{r} m\ell^2\, b_{mn}\, b_{kl} - \frac{\epsilon^2}{rh} m\ell^2\, b_{mn}\, b'_{kl}$$

$$- \frac{\epsilon^2}{rh} m \cos^2\theta\, b_{mn}\, b'_{kl} + \frac{\epsilon}{r} m \cos\theta\, b_{mn}\, b''_{kl} - \frac{h}{r^2} k\, b'_{mn}\, b'_{kl}$$

$$- \frac{h}{r} k\, b'_{mn}\, b''_{kl} + \frac{h}{r^3} k^3\, b'_{mn}\, b_{kl} + \frac{\epsilon^2}{hr} k\ell^2\, b'_{mn}\, b_{kl}$$

$$- \frac{\epsilon}{r} k \cos\theta\, b'_{mn}\, b'_{kl} + \frac{\epsilon^2}{rh} k \sin^2\theta\, b'_{mn}\, b_{kl} - \frac{\epsilon}{r^2} k \cos\theta\, b'_{mn}\, b_{kl}$$

$$+ \frac{\epsilon^2}{rh} k \sin^2\theta\, b'_{mn}\, b_{kl} - \frac{2\epsilon}{r^2} m \cos\theta\, b_{mn}\, b'_{kl} - \frac{2\epsilon}{r} m \cos\theta\, b_{mn}\, b''_{kl}$$

$$+ \frac{2\epsilon}{r^3} mk^2 \cos\theta\, b_{mn}\, b_{kl} + \frac{2\epsilon^3}{rh^2} m\ell^2 \cos\theta\, b_{mn}\, b_{kl}$$

$$- \frac{2\epsilon^2}{rh} m \cos\theta\, b_{mn}\, b'_{kl} + \frac{S^2}{r^2 h} m\, a_{mn}\, a''_{kl} - \frac{S^2}{hr^3} m\, a_{mn}\, a'_{kl}$$

$$+ \frac{S^2}{hr} m\, a_{mn}\, a''_{kl} - \frac{S^2}{hr^3} m\, k^2\, a_{mn}\, a'_{kl} + \frac{2S^2}{hr^4} m\, k^2\, a_{mn}\, a_{kl}$$

$$- \frac{\epsilon S^2}{rh^2} m \cos\theta\, a_{mn}\, a''_{kl} + \frac{\epsilon^2 S^2}{h^3 r} m \cos^2\theta\, a_{mn}\, a'_{kl} - \frac{S^2}{hr^2} k\, a'_{mn}\, a'_{kl}$$

$$- \frac{S^2}{hr} k\, a'_{mn}\, a''_{kl} + \frac{S^2}{hr^3} k^3\, a'_{mn}\, a_{kl} + \frac{S^2\epsilon}{h^2 r} k \cos\theta\, a'_{mn}\, a'_{kl}$$

$$- \frac{\epsilon^2 S^2}{rh^3} k \sin^2\theta\, a'_{mn}\, a_{kl} + \frac{\epsilon S^2}{h^2 r^2} k \cos\theta\, a'_{mn}\, a_{kl}$$

$$E = -\frac{\epsilon S^2}{rh^2} \ell\, a'_{kl} - \frac{\epsilon S^2}{h^2} \ell\, a''_{kl} + \frac{\epsilon S^2}{h^2 r^2} \ell\, k^2\, a_{kl} + \frac{\epsilon^2 S^2}{h^3} \ell \cos\theta\, a'_{kl}\,.$$

If terms of $0(\epsilon^4)$ are neglected, we finally get an expression for the momentum equation (D.2):

$$\sum_{mn} \left[\sum_{kl} \left[D + E + F \right] + A + B + C \right] \sin(m\theta - n\varphi) = 0 , \tag{D.3}$$

$$A = -\frac{\epsilon^2 S^2}{r} n\, a'_{mn} - \epsilon^2 S^2\, n\, a''_{mn} + \epsilon^2 \frac{S^2}{r^2} n m^2\, a_{mn}$$

$$B = \frac{\epsilon^3}{2}\frac{S^2}{r} n(m+1)\, a_{m+1,n} + \frac{1}{2}\epsilon^3 \frac{S^2}{r} n(m+1)^2\, a_{m+1,n} - \frac{1}{2}\epsilon^3\, r\, S^2\, n a''_{m+1,n}$$

$$C = -\frac{\epsilon^3}{2}\frac{S^2}{r} n(m-1)\, a_{m-1,n} + \frac{1}{2}\epsilon^3 \frac{S^2}{r} n(m-1)^2\, a_{m-1,n} - \frac{1}{2}\epsilon^3\, r\, S^2\, n a''_{m-1,n}$$

$$D = \frac{m-k}{r^2}\epsilon^2\, b_{m-k,n-1}\, b''_{kl} - \frac{m-k}{r^3}\epsilon^2\, b_{m-k,n-1}\, b'_{kl} + \frac{m-k}{r}\epsilon^2\, b_{m-k,n-1}\, b''_{kl}$$

$$- \frac{(m-k)}{r^3} k^2 \epsilon^2\, b_{m-k,n-1}\, b'_{kl} + \frac{2(m-k)k^2}{r^4}\epsilon^2\, b_{m-k,n-1}\, b_{kl} - \frac{k}{r^2}\epsilon^2\, b'_{m-k,n-1}\, b'_{kl}$$

$$- \frac{k}{r}\epsilon^2\, b'_{m-k,n-1}\, b''_{kl} + \frac{k^3}{r^3}\epsilon^2\, b'_{m-k,n-1}\, b_{kl} + \frac{S^2}{r^2}(m-k)\epsilon^2\, a'_{m-k,n-1}\, a''_{kl}$$

$$- \frac{S^2}{r^3}(m-k)\epsilon^2\, a_{m-k,n-1}\, a'_{kl} + \frac{\epsilon^2 S^2}{r}(m-k)\, a_{m-k,n-1}\, a''_{kl} - \frac{S^2}{r^3}(m-k)\, k^2\epsilon^2\, a_{m-k,n-1}\, a'_{kl}$$

$$+ \frac{2S^2}{r^4}(m-k)\, k^2\epsilon^2\, a_{m-k,n-1}\, a_{kl} - \frac{\epsilon^2 S^2}{r^2} k\, a'_{m-k,n-1}\, a'_{kl} - \frac{S^2}{r} k\epsilon^2\, a'_{m-k,n-1}\, a''_{kl}$$

$$+ \frac{S^2}{r^3} k^3 \epsilon^2\, a'_{m-k,n-1}\, a_{kl}$$

$$E = \frac{1}{2}\frac{\epsilon^3}{r^3}(m-k-1)\,k\,b_{m-k-1,n-1}\,b_{kl} - \frac{1}{2}\frac{\epsilon^3}{r^2}(m-k-1)\,k\,b_{m-k-1,n-1}\,b'_{kl}$$

$$+ \frac{1}{2}\frac{\epsilon^3}{r}\,b'_{m-k-1,n-1}\,b'_{kl} + \epsilon^3\,b'_{m-k-1,n-1}\,b''_{kl} - \frac{1}{2}\frac{\epsilon^3}{r^2}\,k^2\,b'_{m-k-1,n-1}\,b_{kl}$$

$$+ \frac{1}{2}\frac{\epsilon^3 S^2}{r^2}(m-k-1)\,k\,a_{m-k-1,n-1}\,a'_{kl} - \frac{1}{2}\frac{\epsilon^3 S^2}{r^3}(m-k-1)\,k\,a_{m-k-1,n-1}\,a_{kl}$$

$$+ \frac{1}{2}\frac{\epsilon^3 S^2}{r}\,a'_{m-k-1,n-1}\,a'_{kl} - \frac{1}{2}\frac{\epsilon^3 S^2}{r^2}\,k^2\,a'_{m-k-1,n-1}\,a_{kl}$$

$$+ \frac{3}{2}\frac{\epsilon^3}{r}(m-k-1)\,b_{m-k-1,n-1}\,b''_{kl} - \frac{3\epsilon^3}{r^2}(m-k-1)\,b_{m-k-1,n-1}\,b'_{kl}$$

$$+ 2\epsilon^3(m-k-1)\,b_{m-k-1,n-1}\,b''_{kl} - \frac{2\epsilon^3}{r^2}\,k^2(m-k-1)\,b_{m-k-1,n-1}\,b'_{kl}$$

$$+ \frac{5\epsilon^3}{r^3}\,k^2(m-k-1)\,b_{m-k-1,n-1}\,b_{kl} - \frac{5}{2}\frac{\epsilon^3}{r}\,k\,b'_{m-k-1,n-1}\,b'_{kl} - 2\epsilon^3 k\,b'_{m-k-1,n-1}\,b''_{kl}$$

$$+ 2\frac{\epsilon^3}{r^2}\,k^3\,b'_{m-k-1,n-1}\,b_{kl} + \frac{1}{2}\frac{\epsilon^3}{r^2}\,k\,b'_{m-k-1,n-1}\,b_{kl} + \frac{1}{2}\frac{S^2\epsilon^3}{r}(m-k-1)\,a_{m-k-1,n-1}\,a''_{kl}$$

$$- \frac{S^2\epsilon^3}{r^2}(m-k-1)\,a_{m-k-1,n-1}\,a'_{kl} + \epsilon^3 S^2(m-k-1)\,a_{m-k-1,n-1}\,a''_{kl}$$

$$- \frac{\epsilon^3 S^2}{r^2}\,k^2\,(m-k-1)\,a_{m-k-1,n-1}\,a'_{kl} + \frac{2\epsilon^3 S^2}{r^3}\,k^2(m-k-1)\,a_{m-k-1,n-1}\,a_{kl}$$

$$- \frac{1}{2}\frac{\epsilon^3 S^2}{r}\,k a'_{m-k-1,n-1}\,a'_{kl} - \epsilon^3 S^2\,k\,a'_{m-k-1,n-1}\,a''_{kl} + \frac{\epsilon^3}{r^2}\,S^2\,k^3\,a'_{m-k-1,n-1}\,a_{kl}$$

$$- \frac{1}{2}\frac{\epsilon^3 S^2}{r^2}\,k\,a'_{m-k-1,n-1}\,a_{kl}$$

$$F = \frac{-1}{2}\frac{\epsilon^3}{r^3}(m-k+1)\,k\,b_{m-k+1,n-1}\,b_{kl} + \frac{1}{2}\frac{\epsilon^3}{r^2}(m-k+1)\,k\,b_{m-k+1,n-1}\,b'_{kl}$$

$$-\frac{1}{2}\frac{\epsilon^3}{r}\,b'_{m-k+1,n-1}\,b'_{kl} - \epsilon^3\,b'_{m-k+1,n-1}\,b''_{kl} + \frac{1}{2}\frac{\epsilon^3}{r^2}\,k^2\,b'_{m-k+1,n-1}\,b_{kl}$$

$$-\frac{1}{2}\frac{\epsilon^3 S^2}{r^2}(m-k+1)\,k\,a_{m-k+1,n-1}\,a'_{kl} + \frac{1}{2}\frac{\epsilon^3 S^2}{r^3}(m-k+1)\,k\,a_{m-k+1,n-1}\,a_{kl}$$

$$-\frac{1}{2}\frac{\epsilon^3 S^2}{r}\,a'_{m-k+1,n-1}\,a'_{kl} + \frac{1}{2}\frac{\epsilon^3 S^2}{r^2}\,k^2\,a'_{m-k+1,n-1}\,a_{kl}$$

$$+\frac{3}{2}\frac{\epsilon^3}{r}(m-k+1)\,b_{m-k+1,n-1}\,b''_{kl} - \frac{3\epsilon^3}{r^2}(m-k+1)\,b_{m-k+1,n-1}\,b'_{kl}$$

$$+2\epsilon^3(m-k+1)\,b_{m-k+1,n-1}\,b''_{kl} - \frac{2\epsilon^3 k^2}{r^2}(m-k+1)\,b_{m-k+1,n-1}\,b'_{kl}$$

$$+\frac{5\epsilon^3}{r^3}\,k^2\,(m-k+1)\,b_{m-k+1,n-1}\,b_{kl} - \frac{5}{2}\frac{\epsilon^3}{r}\,k\,b'_{m-k+1,n-1}\,b'_{kl} - 2\epsilon^3\,k\,b'_{m-k+1,n-1}\,b''_{kl}$$

$$+2\frac{\epsilon^3}{r^2}\,k^3\,b'_{m-k+1,n-1}\,b_{kl} + \frac{1}{2}\frac{\epsilon^3}{r^2}\,k\,b'_{m-k+1,n-1}\,b_{kl} + \frac{1}{2}\frac{S^2\epsilon^3}{r}(m-k+1)\,a_{m-k+1,n-1}\,a''_{kl}$$

$$-\frac{S^2\epsilon^3}{r^2}(m-k+1)\,a_{m-k+1,n-1}\,a'_{kl} + \epsilon^3 S^2(m-k+1)\,a_{m-k+1,n-1}\,a''_{kl}$$

$$-\frac{\epsilon^3 S^2}{r^2}\,k^2\,(m-k+1)\,a_{m-k+1,n-1}\,a'_{kl} + \frac{2\epsilon^3 S^2}{r^3}\,k^2\,(m-k+1)\,a_{m-k+1,n-1}\,a_{kl}$$

$$-\frac{1}{2}\frac{\epsilon^3 S^2}{r}\,k\,(m-k+1)\,a'_{m-k+1,n-1}\,a'_{kl} - \epsilon^3 S^2\,k a'_{m-k+1,n-1}\,a''_{kl} + \frac{\epsilon^3}{r^2}\,S^2 k^3 a'_{m-k+1,n-1}\,a_{kl}$$

$$-\frac{1}{2}\frac{\epsilon^3 S^2}{r^2}\,k\,a'_{m-k+1,n-1}\,a_{kl} \quad .$$

In these coefficients, as well as those below, the ϵ has been made explicit. The equation for the magnetic flux, equation (D.1), can also finally be written as

$$\sum_{mn}\left[\left[\sum_{kl} D + E_+ + E_-\right] + A + B + C\right]\cos(m\theta - n\varphi) = 0\,, \tag{D.4}$$

with

$$A = \epsilon^2 n\, b_{mn} + \epsilon\frac{f}{r}a'_{mn} + \epsilon f a''_{mn} - \frac{\epsilon m^2}{r^2} f a_{mn}$$

$$B = \epsilon^3 nr b_{m+1,n} + \frac{\epsilon^2}{2} r f a''_{m+1,n} - \frac{\epsilon^2}{2}\frac{(m+1)^2}{r} f a_{m+1,n} - \frac{\epsilon^2}{2}\frac{f(m+1)}{r} a_{m+1,n}$$

$$C = \epsilon^3 nr b_{m-1,n} + \frac{\epsilon^2}{2} r f a''_{m-1,n} - \frac{\epsilon^2}{2}\frac{(m-1)^2}{r} f a_{m-1,n} + \frac{\epsilon^2}{2}\frac{f(m-1)}{r} a_{m-1,n}$$

$$D = -\frac{\epsilon^2(m-k)}{r} a_{m-k,n-1} b'_{kl} + \frac{\epsilon^2 k}{r} a'_{m-k,n-1} b_{kl}$$

$$E_+ = -\frac{3}{2}\epsilon^3(m-k+1)\, a_{m-k+1,n-1} b'_{kl} + \frac{3}{2}\epsilon^3 k a'_{m-k+1,n-1} b_{kl}$$

$$E_- = -\frac{3}{2}\epsilon^3(m-k-1)\, a_{m-k-1,n-1} b'_{kl} + \frac{3}{2}\epsilon^3 k a'_{m-k-1,n-1} b_{kl}$$

where

$$\eta = C/\Delta^*\psi = -R_0/R\, C/J_\varphi(r)$$

$$= 1/h\, f(r)\ (f(r) = -C/J_\varphi(r))\,.$$

APPENDIX E

ANOTHER WAY OF DERIVING THE EXPRESSION FOR THE HELICAL FLUX

The expressions for the helical flux can also be derived in another way. Instead of using the Fourier expansions where the first harmonic is included, ordering of terms could also have been used. Using the expression for $\underline{B}$ in the equation for the magnetic flux, that is equation (4.5), we get

$$(\frac{1}{r}\frac{\partial\psi}{\partial\theta}, -\frac{\partial\psi}{\partial r}, 1) \cdot (\frac{\partial\hat{\psi}}{\partial r}, \frac{1}{r}\frac{\partial\hat{\psi}}{\partial\theta}, \epsilon\frac{\partial\hat{\psi}}{\partial\varphi}) = 0,$$

written in another form as

$$\frac{1}{r}\frac{\partial\psi}{\partial\theta}\frac{\partial\hat{\psi}}{\partial r} - \frac{1}{r}\frac{\partial\psi}{\partial r}\frac{\partial\hat{\psi}}{\partial\theta} + \epsilon\frac{\partial\hat{\psi}}{\partial\varphi} = 0.$$

Do the following substitutions:

$$\frac{\partial}{\partial\varphi} = \frac{\partial\chi}{\partial\varphi}\frac{\partial}{\partial\chi} = -n\frac{\partial}{\partial\chi}$$

$$\frac{\partial}{\partial\theta} = \frac{\partial\chi}{\partial\theta}\frac{\partial}{\partial\chi} = m\frac{\partial}{\partial\chi}$$

where $\chi = m\theta - n\varphi$ is a helical coordinate which can be used in the case of one mode.

Now we have

$$\frac{\partial\psi}{\partial\chi}\frac{\partial\hat{\psi}}{\partial r} - \frac{\partial\psi}{\partial r}\frac{\partial\hat{\psi}}{\partial\chi} - \epsilon r\frac{\partial\hat{\psi}}{\partial\chi} = 0$$

or

$$\frac{\partial\psi}{\partial\chi}\frac{\partial\hat{\psi}}{\partial r} - \frac{\partial\hat{\psi}}{\partial\chi}\left(\frac{\partial\psi}{\partial r} + \epsilon r\,\frac{n}{m}\right) = 0 .$$

The general solution of this differential equation is

$$\hat{\psi}' = f\left(\psi' + \epsilon r\,\frac{n}{m}\right) .$$

A particular solution is

$$\hat{\psi}' = \psi' + \epsilon r\,\frac{n}{m} .$$

If this solution is ordered, using the expressions

$$\hat{\psi} = \hat{\psi}_0 + \hat{\psi}_1 \cos mn$$
$$\psi = a_0 + a_1 \cos mn ,$$

we get

$$\hat{\psi}_0' = a_0' + \epsilon r\,\frac{n}{m}$$
$$\hat{\psi}_1 = a_1$$

just as was derived in equation (4.9) for $\alpha = 1$.

APPENDIX F

DERIVING THE COIL CURRENT IN TOROIDAL CONFIGURATION

The magnetic field in a toroid is given by

$$B_\theta = B_{\theta_0}(1 + \epsilon \Lambda \cos\theta)$$

$$\epsilon = {}^{a}/R_0 \text{ (a the minor radius)}$$

$$\Lambda = \beta_p + \ell_i/2 - 1$$

$$\beta_p = {}^{P}/(B_{\theta_0}^2/2\mu_0)$$

$$\ell_i = \int \frac{B_\theta^2 \ \rho \ dp \ d\theta}{\pi \ a^2 \ B_{\theta_0}} \ , \ \rho = {}^{r}/a \text{ [95, p185]} .$$

The equations for a magnetic field line are given by

$$\frac{r\,d\theta}{B_\theta} = \frac{R_0 \ d\psi}{B_\varphi}$$

or

$$\frac{d\theta}{d\varphi} = \frac{R_0}{r}\frac{B_\theta}{B_\varphi} = \frac{R_0}{r}\frac{B_{\theta_0}}{B_\varphi}(1 + \epsilon \Lambda \cos\theta) .$$

Thus

$$\frac{d\theta}{1 + \epsilon \Lambda \cos\theta} = \frac{d\varphi}{q} \ , \ q = {}^{r}/R_0 \frac{B_\varphi}{B_\theta} .$$

This gives

$$d\theta\,(1-\epsilon\wedge\cos\theta)\;\simeq\;\frac{d\varphi}{q}\;.$$

Now

$$\int_0^\theta d\theta-\int_0^\theta \epsilon\wedge\cos\,d\theta\;\simeq\;\int_0^\varphi\frac{1}{q}\,d\varphi$$

or

$$\theta-\epsilon\wedge\sin\theta\;\simeq\;\frac{1}{q}\,\varphi\,.$$

It can also be written as

$$\varphi\;\simeq\;q\theta+\delta\sin\theta\,,\;\delta=q\,\epsilon\wedge\,.$$

Now we want a current density of the form

$$\underline{J}\;\;=\;\;\underline{f}\,(r,\theta,\varphi)\;\delta\,(r-a)\;\delta\,(\varphi-q\theta-\delta\sin\theta-k).$$

To calculate f we proceed in the same way as in the cylindrical case:

Let

$$I_\ell\;\;=\;\;\int\underline{J}\,.\,d\underline{S}\,.$$

Thus

$$I_\ell\;\;=\;\;\int J_\varphi\,r\,dr\,d\theta$$

$$= \int f_\varphi \, \delta(r-b) \, \delta(\varphi - q\theta - \delta \sin\theta - k) \, r \, dr \, d\theta$$

$$= \int f_\varphi \, \delta(r-b) \, \delta(\varphi - g(\theta)) \, r \, dr \, d\theta \, ,$$

$$\left[g(\theta) = q\theta + \delta \sin\theta + k = y \right]$$

$$= b \int f_\varphi(b,\theta,\varphi) \, \delta(\varphi - y) \, \frac{1}{\partial g / \partial \theta} \, dy$$

from $\frac{\partial g}{\partial \theta} \, d\theta = dy$.

Now

$$I_\ell = b \int f_\varphi(b,\theta,\varphi) \, \delta(y - \varphi) \, \frac{1}{\partial g / \partial \theta} \, dy \, , \quad \delta(x) = \delta(-x)$$

$$= \frac{b}{\partial g / \partial \theta} \, f_\varphi(b, \theta(y), \varphi = y) \, .$$

We can also write

$$I_\ell = \int J_\theta \, R \, dr \, d\varphi$$

$$= \int f_\theta \, \delta(r-b) \, \delta(\varphi - q\theta - \delta \sin\theta - k) \, R \, dr \, d\varphi$$

$$= R \int f_\theta(b,\theta,\varphi) \, \delta(\varphi - g(\theta)) \, d\varphi$$

$$= R \, f_\varphi(b,\theta,\varphi = g(\theta)) \, .$$

Now we have $f_\varphi = 1/b \, \frac{\partial g}{\partial \theta} \, I_\ell$, $f_\theta = 1/R \, I_\ell$ and the current density can be written as

$$\underline{J} = I_\ell (0, {}^1/R, ({}^1/b)(q + \delta \cos \theta))\, \delta (r-b)\, \delta (\varphi - q\theta - \delta \sin \theta - k) \ .$$

It is important that $\nabla.\underline{J} = 0$. This can be tested:

$$\nabla.\underline{J} = \frac{1}{r}\frac{\partial}{\partial r}(r\, J_r) + \frac{1}{r}\frac{\partial}{\partial \theta} J_\theta + \frac{1}{R}\frac{\partial}{\partial \varphi} J_z$$

$$= \frac{1}{r}\frac{\partial}{\partial \theta}({}^I\ell/R\ \delta (r-b)\, \delta (\varphi - q\theta - \delta \sin \theta - k))$$

$$+ {}^1/R\ \frac{\partial}{\partial \varphi}({}^I\ell/b\ (q + \delta \cos \theta)\, \delta (r-b)\, \delta (\varphi - q\theta - \delta \sin \theta - k))$$

$$= \frac{1}{r}\, {}^I\ell/R\ \delta (r-b)\, \frac{\partial}{\partial \theta}(\delta - q\theta - \delta \sin \theta - k)\Big|_{r=b}$$

$$+ {}^1/R\ {}^I\ell/b\ (q + \delta \cos \theta)\, \delta (r-b)\, \frac{\partial}{\partial \varphi}(\delta (\varphi - q\theta - \delta \sin \theta - k)) \ .$$

Let

$$u = \varphi - q\theta - \delta \sin \theta \ .$$

We thus have

$$\frac{\partial}{\partial \theta} = \frac{\partial}{\partial u}\frac{\partial u}{\partial \theta} = -(q + \delta \cos \theta)\frac{\partial}{\partial u}$$

$$\frac{\partial}{\partial \varphi} = \frac{\partial}{\partial u}\frac{\partial u}{\partial \varphi} = \frac{\partial}{\partial u}$$

to get

$$\nabla.\underline{J} = 0.$$